AUBURN

SAMUEL GINN
COLLEGE OF ENGINEERING

Research Report for ALDOT Project 930-858

LOAD RATING
OF
BIBB GRAVES CONCRETE ARCH BRIDGE

Submitted to

The Alabama Department of Transportation

Prepared by

Travis H. Le
J. Michael Stallings

October 2014

Highway Research Center
Harbert Engineering Center
Auburn, Alabama 36849

www.eng.auburn.edu/research/centers/hrc.html

1. Report No. ALDOT 930-858	**2. Government Accession No.**	**3. Recipient Catalog No.**
4. Title and Subtitle Load Rating of Bibb Graves Concrete Arch Bridge		**5. Report Date** July 2014
		6. Performing Organization Code
7. Author(s) Travis H. Le, J. Michael Stallings		**8. Performing Organization Report No.** ALDOT 930-858
9. Performing Organization Name and Address Highway Research Center Department of Civil Engineering 238 Harbert Engineering Center Auburn, AL 36849		**10. Work Unit No. (TRAIS)** **11. Contract or Grant No.**
12. Sponsoring Agency Name and Address Highway Research Center Department of Civil Engineering 238 Harbert Engineering Center Auburn, AL 36849		**13. Type of Report and Period Covered** Technical Report **14. Sponsoring Agency Code**

15. Supplementary Notes
Project performed in cooperation with the Alabama Department of Transportation

16. Abstract

To assess the strength of the Bibb Graves Concrete Arch Bridge, the Alabama Department of Transportation sponsored an investigation by Auburn University. In one of the spans, the arches are experiencing severe longitudinal cracking from Alkali-Silica Reactivity (ASR). The significance of ASR on the load carrying capacity of the bridge is unknown for two reasons. First, the effects of ASR on cross section capacity are not well understood. Second, a load rating for the bridge has never been performed. As an initial step for planning maintenance activities for the bridge, a load rating is performed in this project. Ratings are provided for the vertical columns, vertical tension hangers, transverse floor beams, and arch ribs. Rating factors were calculated for components of the bridge based on the as-designed condition. Ratings were provided for eight standard trucks and the AASHTO lane load. Evaluation of the impact of ASR on the ratings was outside the scope of the project.

An operating rating factor significantly less than 1.0 was calculated in preliminary ratings of one arch. The low rating was attributed primarily to slenderness effects calculated using the moment magnifier from AASHTO Standard Specifications for Highway Bridges (2002). An investigation was conducted to identify a more accurate method for including slenderness effects in the arch rating calculations. An analysis that combines an elastic second-order analysis for dead loads and a linear analysis for moving live loads was found to be very practical and sufficiently accurate. This combined analysis approach resulted in significant increases in the arch ratings beyond those found by using the AASHTO moment magnifier method.

Sensitivity analyses were performed to assess the effects of ASR-expansion on the bridge components' internal forces and arch vertical deflection. Effects of changes in concrete strength and modulus of elasticity on member forces, deflection, and ratings were examined.

Load ratings of the Bibb Graves Concrete Arch Bridge resulted in multiple operating rating factors less than 1.0. The lowest operating rating based on the as-designed condition is 0.86 for shear in an arch rib. This rating factor was increased to be greater than 1.0 by using a higher concrete compressive strength that was justified by concrete core test results. The final load ratings are controlled by the positive bending capacity of the transverse floor beams. The controlling operating rating factors are 0.93 and 0.97 for the standard tri-axle truck and concrete truck, respectively.

17. Key Words Load ratings, Bibb Graves Bridge, SAP2000, load-moment interaction, slenderness, reinforced concrete, arch		**18. Distribution Statement** No restriction.	
19. Security Classification (of this report) Unclassified	**20. Security Classification (of this page)** Unclassified	**21. No. of Pages** 253	**22. Price** None.

Research Report

ALDOT Research Project 930-858

LOAD RATING
OF
BIBB GRAVES CONCRETE ARCH BRIDGE

Prepared by

Travis H. Le

J. Michael Stallings

Highway Research Center

and

Department of Civil Engineering

at

Auburn University

July 2014

DISCLAIMERS

The contents of this report reflect the views of the authors who are responsible for the facts and accuracy of the data presented herein. The contents do not necessarily reflect the official views or policies of Alabama Department of Transportation, Auburn University, or the Highway Research Center. This report does not constitute a standard, specification, or regulation.

NOT INTENDED FOR CONSTRUCTION, BIDDING, OR PERMIT PURPOSES

J. Michael Stallings, Ph. D.
Research Supervisor

ACKNOWLEDGEMENTS

The authors would like to acknowledge the financial support provided by the Alabama Department of Transportation that made this project possible. Also, the authors would like to acknowledge the efforts of many in the Alabama Department of Transportation who provided guidance and assistance that were essential to ensure that this project concluded in a useful and practical result.

ABSTRACT

To assess the strength of the Bibb Graves Concrete Arch Bridge, the Alabama Department of Transportation sponsored an investigation by Auburn University. In one of the spans, the arches are experiencing severe longitudinal cracking from Alkali-Silica Reactivity (ASR). The significance of ASR on the load carrying capacity of the bridge is unknown for two reasons. First, the effects of ASR on cross section capacity are not well understood. Second, a load rating for the bridge has never been performed. As an initial step for planning maintenance activities for the bridge, a load rating is performed in this project. Ratings are provided for the vertical columns, vertical tension hangers, transverse floor beams, and arch ribs. Rating factors were calculated for components of the bridge based on the as-designed condition. Ratings were provided for eight standard trucks and the AASHTO lane load. Evaluation of the impact of ASR on the ratings was outside the scope of the project.

An operating rating factor significantly less than 1.0 was calculated in preliminary ratings of one arch. The low rating was attributed primarily to slenderness effects calculated using the moment magnifier from AASHTO Standard Specifications for Highway Bridges (2002). An investigation was conducted to identify a more accurate method for including slenderness effects in the arch rating calculations. An analysis that combines an elastic second-order analysis for dead loads and a linear analysis for moving live loads was found to be very practical and sufficiently accurate. This combined analysis approach resulted in significant increases in the arch ratings beyond those found by using the AASHTO moment magnifier method.

Sensitivity analyses were performed to assess the effects of ASR-expansion on the bridge components' internal forces and arch vertical deflection. Effects of changes in concrete strength and modulus of elasticity on member forces, deflection, and ratings were examined.

Load ratings of the Bibb Graves Concrete Arch Bridge resulted in multiple operating rating factors less than 1.0. The lowest operating rating based on the as-designed condition is 0.86 for shear in an arch rib. This rating factor was increased to be greater than 1.0 by using a higher concrete compressive strength that was justified by concrete core test results. The final load ratings are controlled by the positive bending capacity of the transverse floor beams. The controlling operating rating factors are 0.93 and 0.97 for the standard tri-axle truck and concrete truck, respectively.

TABLE OF CONTENTS

List of Tables

List of Figures

Chapter 1

INTRODUCTION

1.1 BACKGROUND

A load rating of the historic seven-span Bibb Graves Bridge, pictured in Figure 1, was performed and is reported herein. The Bibb Graves Bridge is located in Wetumpka, Alabama, as shown in Figure 2. The bridge is on AL Route 111 and crosses the Coosa River in Elmore County. The bridge was constructed from 1929 to 1931.

Figure 1: Bibb Graves Bridge in Wetumpka, Alabama

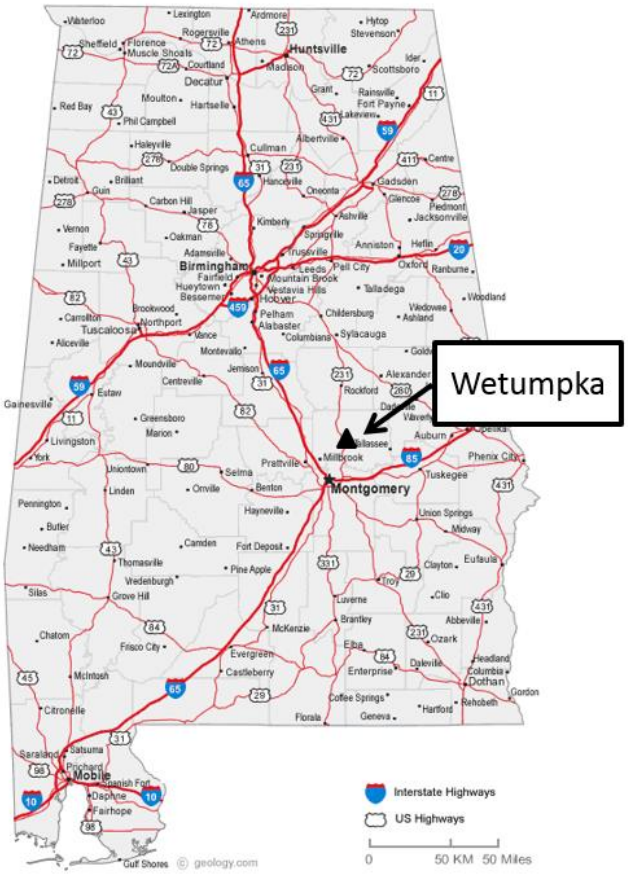

Figure 2: Alabama Map with a Triangular Marker at Wetumpka (Geoscience News and Information 2005)

Figure 3 shows an elevation and a plan view of the bridge along with the directional orientation. It is 44 feet wide by approximately 800 feet long and comprised of seven parabolic arches. The arches at each end are completely under the deck, with the center five being through arches. The bridge is essentially symmetrical about the center arch span (Span IV). The center arch is the longest with a clear span of 132 feet. In each longitudinal direction from the center span, the clear spans are 128 feet, 117 feet, and 40 feet, respectively. The arches are integral at the base with massive concrete piers that have average dimensions of ten feet wide by 40 feet long. The pier names are as labeled in Figure 3. Providing for two travel lanes, the roadway width is 27 feet. The roadway slab is supported on transverse beams that are connected to the arches by hangers and columns. As described by Taylor (1930), the roadway slab is suspended from the through arches above the pier at an elevation of half the height of the arch.

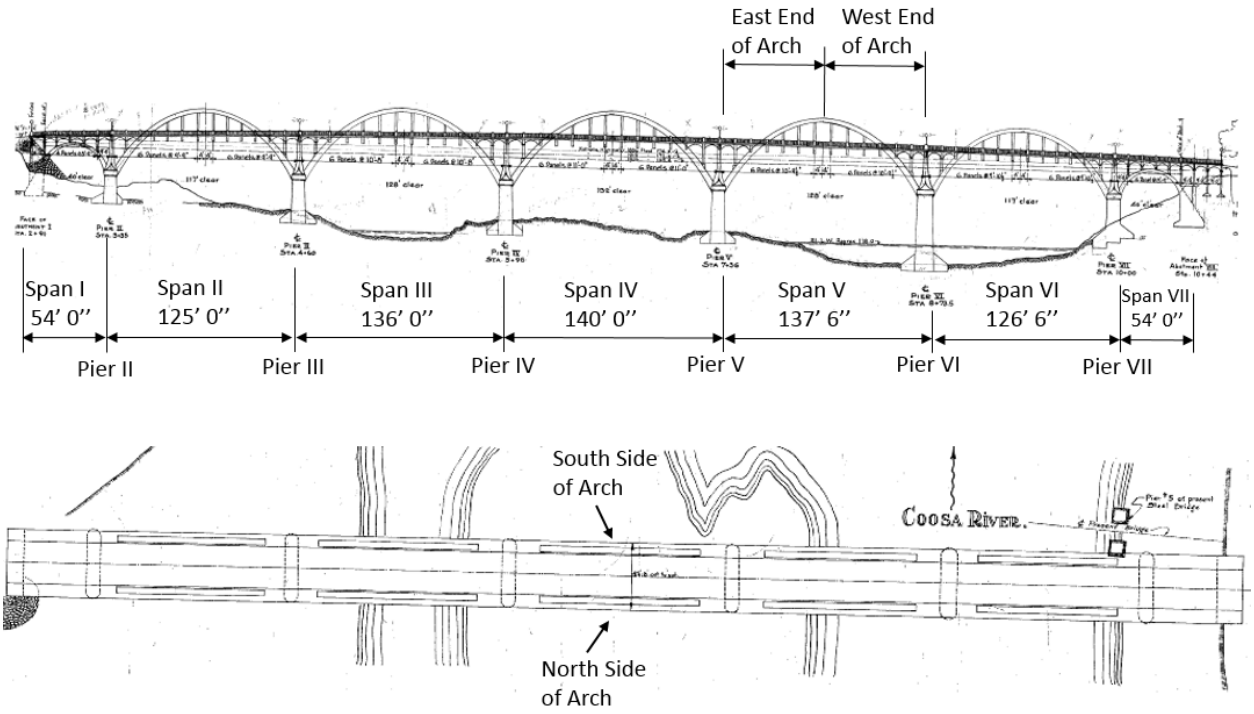

Figure 3: Elevation and Plan Views (AHD 1929)

The load rating reported here is based on the best available information provided by the Alabama Department of Transportation (ALDOT). AHD (1929) drawings from 1929 were provided. Taylor (1930) provided key insights to some construction variances into building the bridge. In addition, TranSystems (2009) provided an evaluation report on the bridge that gives information on concrete cores taken from the existing bridge structure.

1.2 MOTIVATION

Over the years, alkali-silica reactivity (ASR) has resulted in deterioration of the reinforced concrete arches on the Bibb Graves Bridge. Observable signs of ASR include significant longitudinal cracks in the arch ribs along with efflorescence as shown in Figure 4. For unknown reasons, the deterioration is most prominent in Span V. The significance of the effects of ASR on the load carrying capacity of the bridge is unknown for two reasons. First, the effects of ASR on cross section capacity are not well understood. Second, a load rating for the bridge has never been performed; thus, the capacity of the bridge is unknown prior to any deterioration. The

uncertainty surrounding the structural significance of ASR has led to speculation for schemes to strengthen the bridge without clear proof that structural strengthening is necessary. As an initial step to plan and to prepare maintenance activities for the bridge, a load rating is performed in this project. The structural elements for ratings include the vertical columns, vertical tension hangers, transverse floor beams, and arch ribs.

Figure 4: Arch Rib with ASR-Induced Longitudinal Cracks

1.3 REPORT ORGANIZATION

Chapter 2 presents the bridge geometry for the bridge components along with defining the naming convention. Dimensions of cross sections are defined. The method of establishing the arch geometry is discussed in details. Assumptions in defining the geometry are explained.

Chapter 3 provides a detailed overview of the rating procedure. The process of obtaining the rating factor from the axial load-moment interaction diagram is discussed. The member capacity for each component is obtained for the rating process. Dead and live loads are calculated and the location of application are presented. Transverse frame and arch modeling

process is explained. In addition, slenderness effects for the columns and arch rib are evaluated in Chapter 3.

Chapter 4 explains and compares the different approaches that are available to account for in-plane slenderness effects on the bending moments that must be resisted by the arches. Moment magnifiers are calculated using the procedures defined in AASHTO (2002) and AASHTO (2012) and from the results of elastic buckling analyses performed using SAP2000. Magnified moments are compared to bending moments calculated by elastic second-order analysis.

Chapter 5 lists the load factor ratings for Spans IV, V, VI, and VII of the bridge. Components including columns, hangers, transverse beams, and arch ribs were rated. Ratings are listed for the operating and inventory level for the eight ALDOT trucks and the AASHTO lane load.

Chapter 6 provides sensitivity analyses. This Chapter assesses the effects of ASR-expansion on the arch internal forces and vertical deflection. In addition, the effects of changes in the concrete modulus of elasticity and concrete strength for the transverse frames and arches on the member's internal forces and vertical deflection are examined. Effects of these changes on rating factors are listed.

Chapter 7 summarizes what was performed in this project for the Bibb Graves Bridge and points out components where the rating factor is less than 1.0.

Chapter 2

BRIDGE GEOMETRY

The geometry was taken from drawings provided from ALDOT in a PDF file. Full elevation and plan views of the bridge are shown in Figure 3. The span lengths measured from centerline-to-centerline of piers are listed in Table 1. Since the bridge is essentially symmetric, ratings are provided for Spans IV, V, VI, and VII only. The geometry of the bridge was divided up into columns, hangers, transverse floor beams, transverse deep beams, and arches. Before the geometry is discussed any further, the naming convention for the spans and various bridge components is presented.

Table 1: Span Lengths

Span I	54 ft 0 in.
Span II	125 ft 0 in.
Span III	136 ft 0 in.
Span IV	140 ft 0 in.
Span V	137 ft 6 in.
Span VI	126 ft 6 in.
Span VII	54 ft 0 in.

2.1 NAMING CONVENTION

Names along with identification numbers are assigned to components of interest for referencing purposes. Spans IV, V, and VI have the same names since the configuration of components is identical. Span VII's components have their own names, and the order of the numbering is a continuation from Span VI's west end.

2.1.1 Span IV, V, and VI

In Spans IV, V, and VI, the vertical components are hangers and columns. There is also a transverse deep beam. A naming convention is shown in Figure 5 for the hangers, columns, and transverse deep beam for the east half Spans IV, V and VI. The naming convention for the east end applies to the west end since the spans are symmetric about midspan. The transverse deep beam is called a deep beam mainly to distinguish this particular transverse beam from other transverse beams in the bridge. This transverse deep beam is unique in that it is directly supported onto the arch rib with no column or hanger. The transverse deep beam appears as a column in Figure 5 because of the distance between the centerline of the arch rib and centerline of the slab.

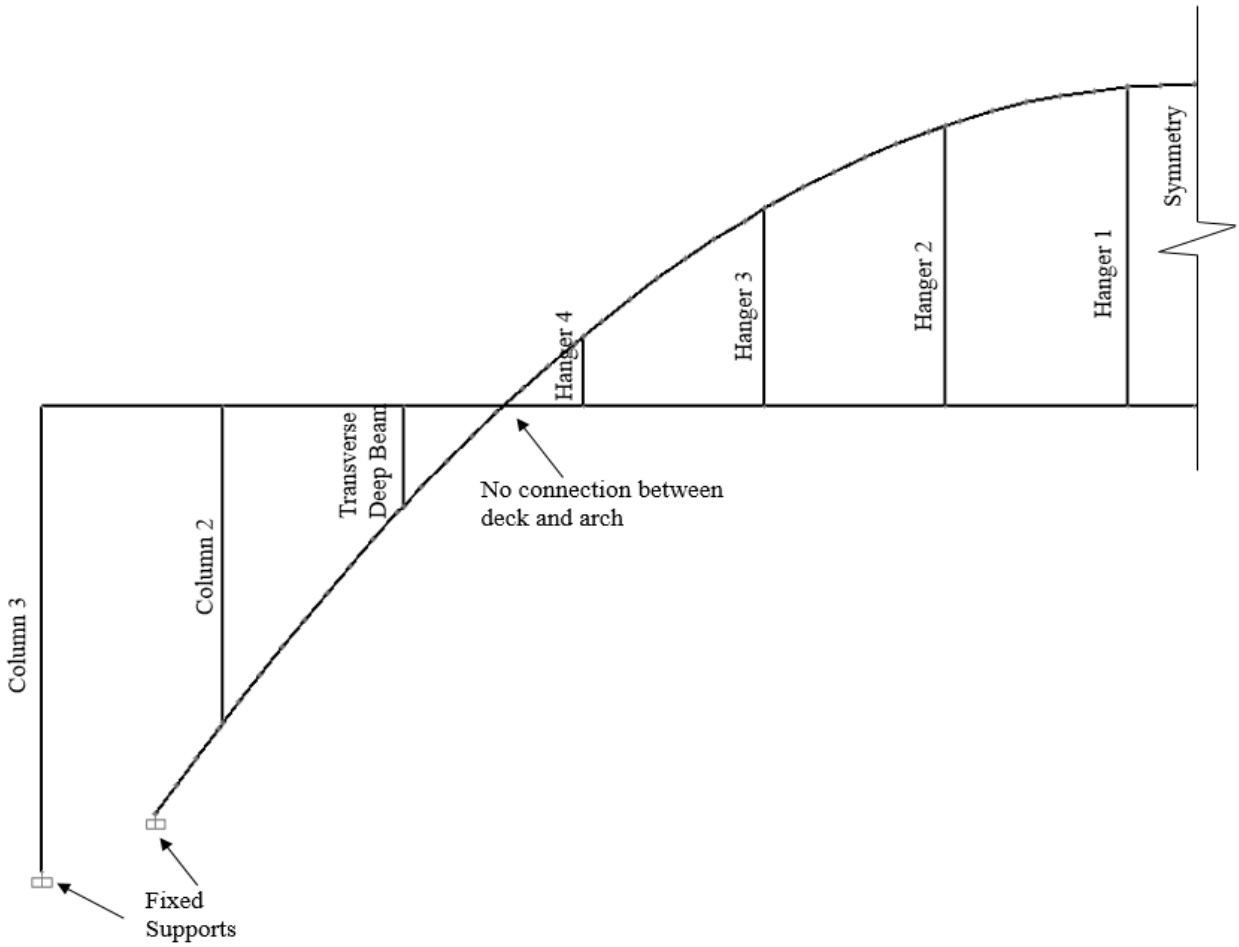

Figure 5: Spans IV, V, and VI East End Naming Convention (SAP 2013)

2.1.2 Span VII

The convention for naming Span VII, which is comprised of columns only, is shown in Figure 6.

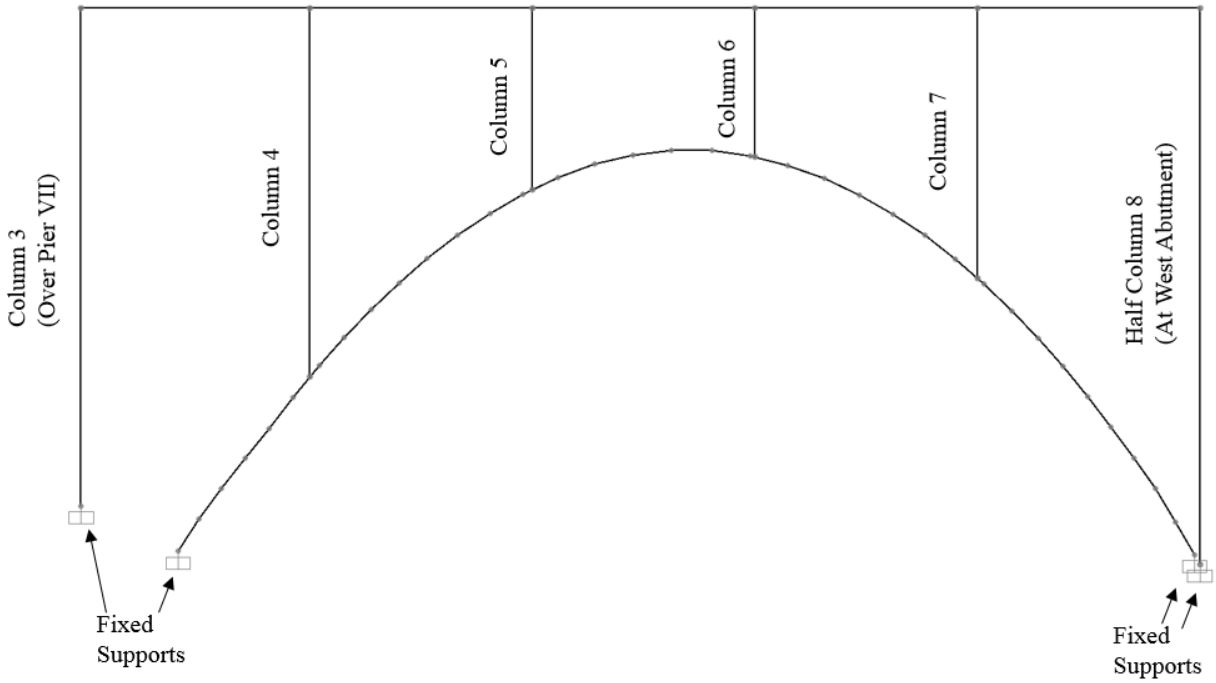

Figure 6: Span VII Naming Convention (SAP 2013)

2.2 ARCHES

2.2.1 Span IV, V, and VI

The geometry of the bridge was defined using the to scale drawings provided by AHD (1929) and Autodesk, Inc. AutoCAD (2014). The original elevation drawings of each span were saved as a JPEG file. Each image file was inserted into AutoCAD as an attachment. The base point of the inserted file was defined to be at the origin of the drawing sheet with a default scale factor of 1.0. Drawing layers were created and defined as necessary for drawing and viewing enhancements. Two perfectly vertical lines were drawn in for reference for each arch. One line was a vertical line through the centerline of the east or left pier, and another one was a vertical line through the arch midspan. Using the linear dimension between these two vertical lines and the longest true horizontal dimension given, which is between these two vertical lines, a scale

factor was inserted to establish the true scale of each drawing.

The deck is sloped in the longitudinal direction. The highest elevation is at midspan of Span IV, the center span. The lowest elevations are at either abutment. To prevent analysis result anomalies, the deck of each span was defined to have zero slope, and the deck was located at the average elevation of the mid-thickness of the deck in that span. These locations are at the quarter span for Span IV and at midspan for Spans V and VI.

All column and hanger centerlines were offset from the two reference vertical lines using the transverse beam spacing shown on the drawings. The lengths of the columns and hangers were bounded by the arch centerline and the mid-thickness of the deck slab. For the column above the pier, its length was defined to extend from the extrados curve of the arch to the mid-thickness of the deck slab.

Being thinnest at midspan and thickest at the base, the thickness of the arch varied along the length. To define the geometry, the arch was discretized at approximately every two feet along the length, which was conveniently located at each hoop location. Each hoop was drawn in at its prescribed location with its ends extending to the intrados and extrados curves of the arch to define the thickness of the cross section at each hoop location. Then, the intrados and extrados were drawn in as straight lines between each cross section. The arch centerline or mid-thickness was drawn in for each section at the midpoint of each hoop. All boundary lines were drawn in with high accuracy and precision as their nodes were either at the center of the originally marked lines or bounded by the edges of the originally marked lines.

At the base of each arch and near the top of the pier, the cross section height increased rapidly. This increase resulted from transitions in the extrados and intrados curves of the arch along circular arcs that provided smooth transitions at the pier supports. To avoid anomalies in the structural analysis results near the arch base, the arch shape and cross section thickness were manually adjusted. These adjustments included extrapolating the curved, concave-down shape of the arch to a point near the top of the pier and neglecting some of the concrete cross section to provide a smooth increase in the arch cross section height that was consistent with the remainder of the arch. To maintain uniformity, the arch base sections were discretized at every two feet using the orientation of the last provided hoop in the elevation drawing. Each cross section height beyond the last shown hoop was increased by 0.10 feet from the previous one to be consistent with the rate of increase of the arch sections near the base. These sections were then

shifted in the plane to line up with the intrados curve as the main reinforcements followed this curve more closely than the extrados curve. The arch base ended at the location of the last extrapolated hoop near the face of the pier.

Once the geometry of each half span was established, the drawing was saved as a DXF file for ease of import into the structural analysis software SAP2000 version 15 by Computers and Structures, Inc. With the structural analysis program running, the AutoCAD DXF file was imported. The global up direction from AutoCAD was selected to the positive Y direction with the units being kips and feet. Then, each layer of the drawing was selected to be imported as frame members. The process was repeated until all necessary layers were imported.

The arches are parabolic. Rise and span length information for each span is provided in Table 2. A cross section of the arch rib for Spans IV – VI is shown in Figure 7. All arch ribs are 4 ft 0 in. wide and are doubly reinforced with eight bars in each layer. All reinforcing bars are square bars unless noted. The overall height, h; distance from extreme top fiber to centroid of top bar group, d_T; distance from extreme top fiber to centroid of bottom bar group, d_B; area of steel in the top layer, $A_{s\,T}$; and area of steel in the bottom layer, $A_{s\,B,}$ are shown in Table 3 through Table 5 for Spans IV through VI. Properties are shown for the arch rib section at the peak, base, and at all hanger and column locations.

Table 2: Spans IV through VI - Arch Rise and Span Length

	Span IV	Span V	Span VI
Arch Rise (ft)	45.58	44.57	40.44
Arch Span (ft)	130.2	128.3	116.5

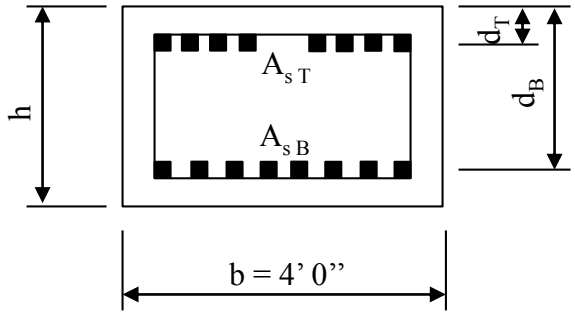

Figure 7: Typical Arch Rib Section for Spans IV – V

Table 3: Arch Rib Section Properties for Span IV

	h (in.)	d_T (in.)	d_B (in.)	$A_{s\,T}$ (in.^{2})	$A_{s\,B}$ (in.^{2})
Arch Rib at Peak	28.0	3.00	25.0	8.00	8.00
Arch Rib at Hanger 1	28.0	3.00	25.0	8.00	8.00
Arch Rib at Hanger 2	29.0	3.00	26.0	8.00	8.00
Arch Rib at Hanger 3	29.6	3.00	26.6	8.00	8.00
Arch Rib at Hanger 4	30.5	3.13	26.9	10.0	9.00
Arch Rib at Transverse Deep Beam	33.7	3.13	30.6	10.0	10.0
Arch Rib at Column 2	41.4	3.13	38.3	10.0	10.0
Arch Rib at Base	47.8	3.13	44.6	10.0	10.0

Table 4: Arch Rib Section Properties for Span V

	h (in.)	d_T (in.)	d_B (in.)	$A_{s\,T}$ (in.^{2})	$A_{s\,B}$ (in.^{2})
Arch Rib at Peak	27.0	3.00	24.0	8.00	8.00
Arch Rib at Hanger 1	27.1	3.00	24.1	8.00	8.00
Arch Rib at Hanger 2	28.0	3.00	25.0	8.00	8.00
Arch Rib at Hanger 3	28.3	3.00	25.3	8.00	8.00
Arch Rib at Hanger 4	29.3	3.13	26.2	10.0	9.0
Arch Rib at Transverse Deep Beam	32.4	3.13	29.3	10.0	10.0
Arch Rib at Column 2	40.4	3.13	37.3	10.0	10.0
Arch Rib at Base	46.6	3.13	43.4	10.0	10.0

Table 5: Arch Rib Section Properties for Span VI

	h (in.)	d_T (in.)	d_B (in.)	$A_{s\,T}$ (in.^{2})	$A_{s\,B}$ (in.^{2})
Arch Rib at Peak	26.0	3.00	23.0	6.28 (round)	6.28 (round)
Arch Rib at Hanger 1	26.8	3.00	23.8	6.28 (round)	6.28 (round)
Arch Rib at Hanger 2	27.4	3.00	24.4	6.28 (round)	6.28 (round)
Arch Rib at Hanger 3	28.2	3.00	25.2	6.28 (round)	6.28 (round)
Arch Rib at Hanger 4	29.0	3.10	26.0	9.00	9.00
Arch Rib at Transverse Deep Beam	32.2	3.10	29.2	9.00	9.00
Arch Rib at Column 2	38.9	3.10	35.9	9.00	9.00
Arch Rib at Base	44.0	3.10	41.0	9.00	9.00

2.2.2 Span VII

A full elevation view of Span I was provided in the original drawings. The full geometry of it was defined in AutoCAD. The deck elevation was defined at the average elevation of the mid-thickness of the slab, which is at the midspan. In Span VII, the arch was discretized at each hoop spacing, which is 1 ft 6 in. On the abutment side, the arch ended at the hoop location at which its centerline was directly below the centerline of the column. The arch base on the pier side ended at the last extrapolated hoop spacing just before the pier cap. The height of the extrapolated arch section was based off the rate of increase of the previous section which was 0.20 ft. Then, each extrapolated hoop was shifted in the plane in such a way that the arch centerline was a smooth transition from one section to the next that was consistent with the remainder of the arch. Once the drawing of Span I was imported into SAP2000, it was mirrored about the vertical axis to match the orientation of Span VII.

The arch in Span VII is parabolic. Rise and span length information is provided in Table 6. A cross section of the arch rib for Span VII is shown in Figure 8. All longitudinal reinforcement in the arch rib is round bars. The properties of the arch rib at both ends and at all columns are shown in Table 7 for Span VII.

Table 6: Span VII - Arch Rise and Span Length

	Span VII
Arch Rise (ft)	15.79
Arch Span (ft)	39.99

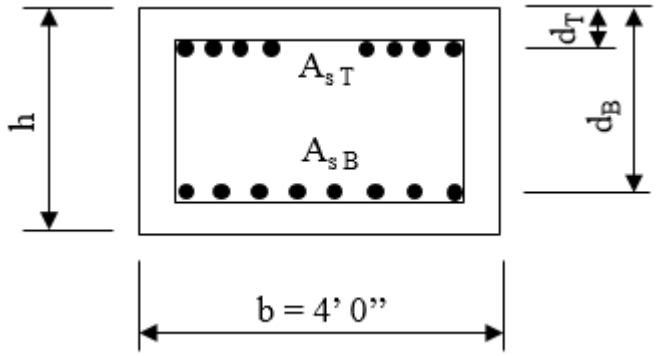

Figure 8: Typical Arch Rib Section for Span VII

Table 7: Arch Rib Section Properties for Span VII

	h (in.)	d_T (in.)	d_B (in.)	$A_{s\,T}$ (in.^{2})	$A_{s\,B}$ (in.^{2})
Arch Rib at East Base	31.1	2.94	28.1	4.81	4.81
Arch Rib at Column 4	20.8	2.94	17.8	4.81	4.81
Arch Rib at Column 5	16.4	2.88	13.5	3.53	4.81
Arch Rib at Column 6	16.8	2.88	13.9	3.53	4.81
Arch Rib at Column 7	17.4	2.94	14.5	3.53	4.81
Arch Rib at West Base	27.4	2.94	24.4	4.81	4.81

2.3 TRANSVERSE FLOOR BEAMS

For the part of the arch ribs that are below the roadway, the deck is supported on a beam and column system. The beam was discretized into three parts shown in Figure 9 because of changes in geometry. Those parts are roadway, curb, and bracket. The curb and bracket are part of the sidewalk slabs on either side. The roadway and curbs on either side are part of the transverse beam length.

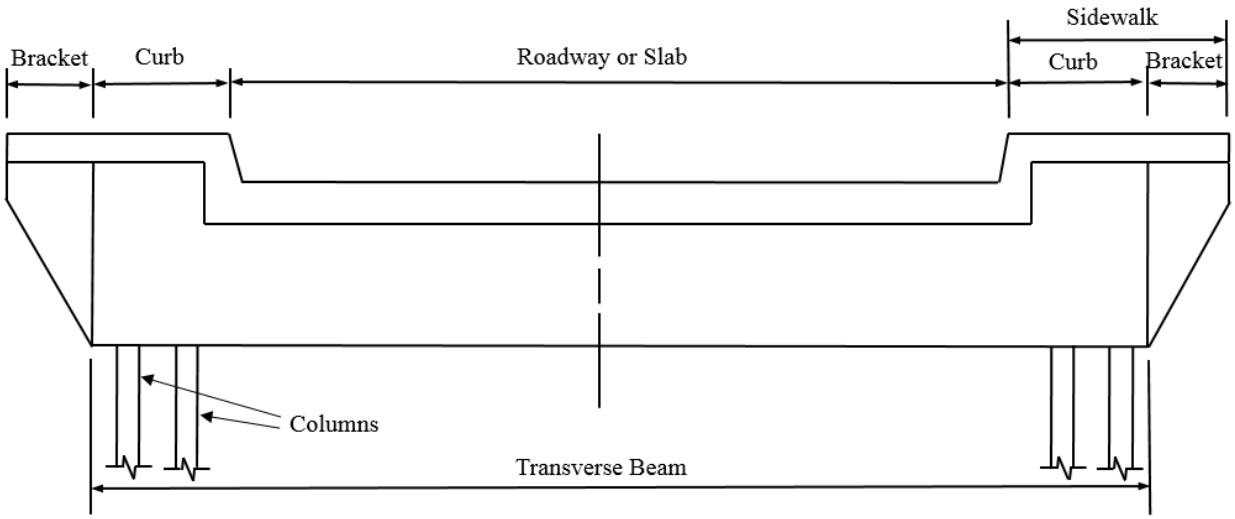

Figure 9: Typical Transverse Beam for all Spans

The dimensions of the transverse beam for Spans IV and V are shown in Figure 10. The dimensions of the transverse beam Spans VI and VII are shown in Figure 11. For all transverse beams, the width of the transverse beam is 1 ft 6 in., and the width of the bracket is 1 ft 0 in.

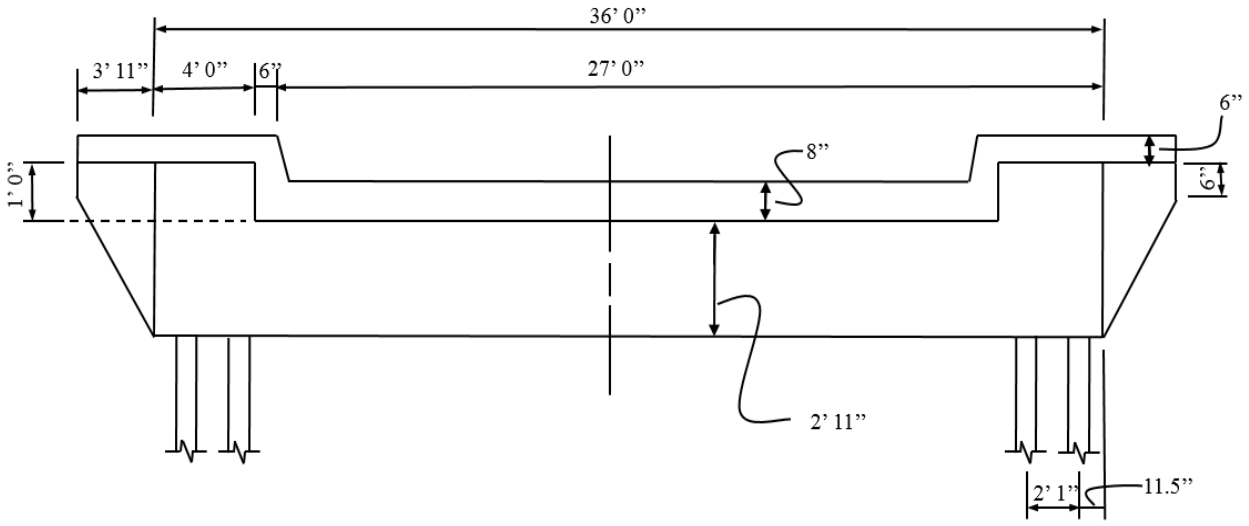

Figure 10: Typical Transverse Beam Dimensions for Spans IV and V

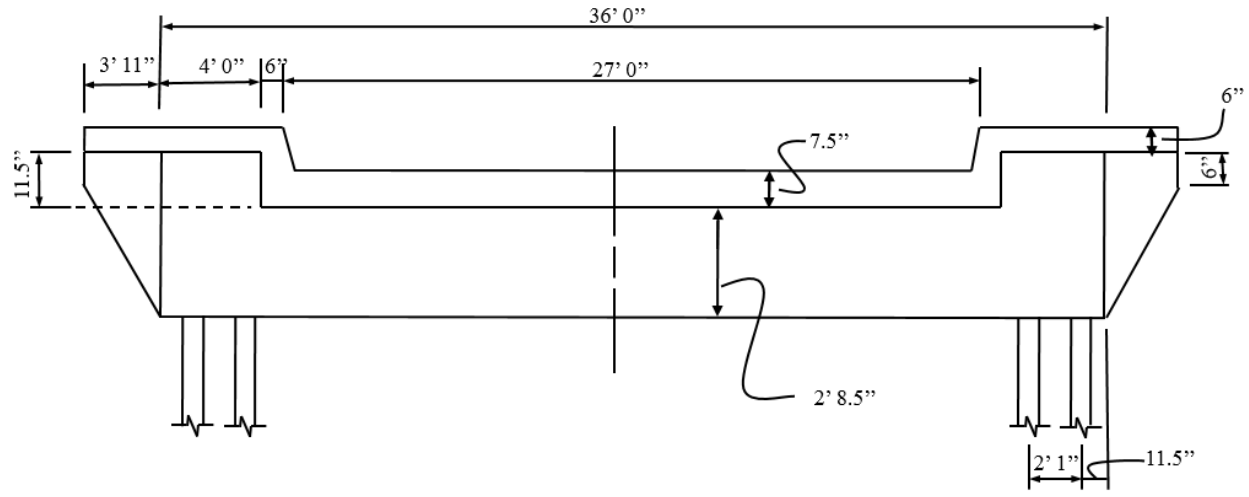

Figure 11: Typical Transverse Beam Dimensions for Spans VI and VII

A typical cross section of the roadway, curb, and bracket is shown in Figure 12. The dimensions for these cross sections for all spans are listed in Table 8. The effective flange width of T-shaped cross sections was determined from AASHTO (2002) Section 8.10.

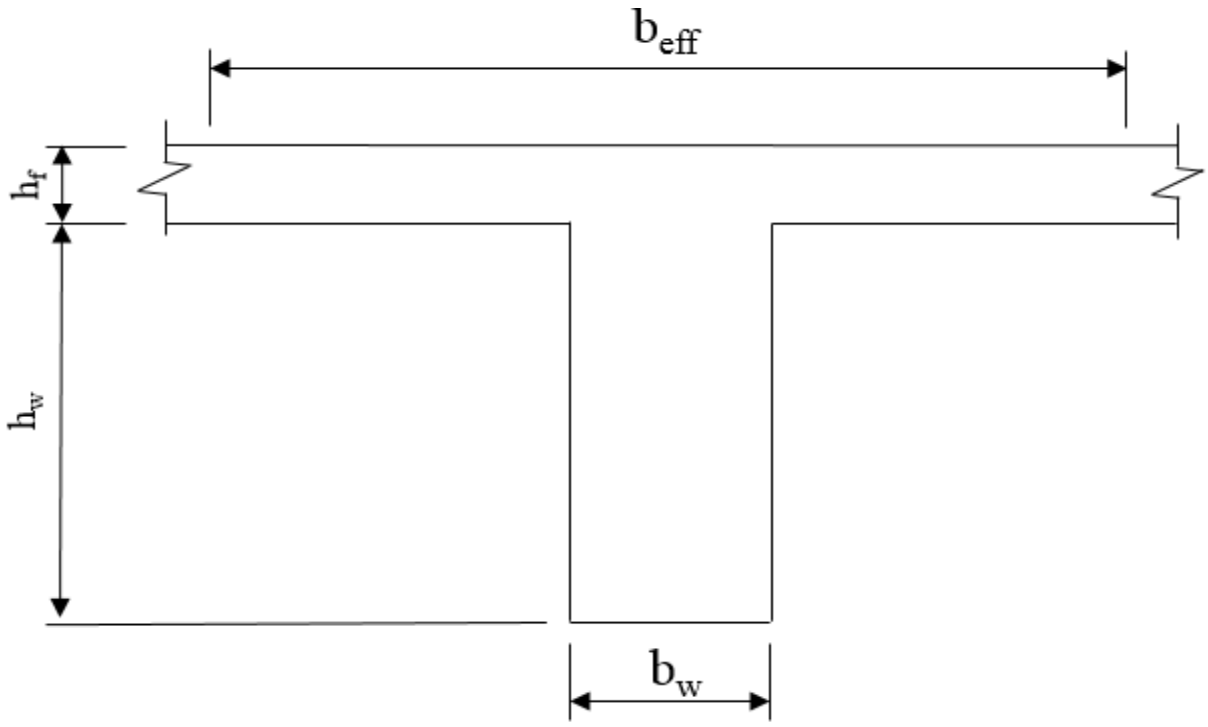

Figure 12: Typical Roadway, Curb, and Bracket Cross Section

Table 8: Transverse Beam Dimensions

		b_{eff}	h_f	h_w	b_w
Spans IV and V	Roadway	8 ft 0 in.	0 ft 8 in.	2 ft 11 in.	1 ft 6 in.
	Curb	7 ft 6 in.	0 ft 6 in.	3 ft 11 in.	1 ft 6 in.
	Bracket	7 ft 0 in.	0 ft 6 in.	2 ft 2.5 in.	1 ft 0 in.
Spans VI and VII	Roadway	8 ft 0 in.	0 ft 7.5 in.	2 ft 8.5 in.	1 ft 6 in.
	Curb	7 ft 6 in.	0 ft 6 in.	3 ft 8 in.	1 ft 6 in.
	Bracket	7 ft 0 in.	0 ft 6 in.	2 ft 1 in.	1 ft 0 in.

2.4 COLUMNS

Two types of column cross section are present in the bridge. All columns not at pier locations have the same cross section. These columns are labeled column followed by an identification number other than three in the naming convention. The other column cross section is for columns over all piers. These columns are all labeled Column 3 in the naming convention.

2.4.1 Column 2s

For all columns except the columns over the piers, the cross section is shown in Figure 13. For Spans IV, V, and VI, columns not at a pier are called Column 2. Traffic flows parallel to the x-x axis or weak axis. Each column is 14 in. x 15 in. and reinforced by four 1-in.-square reinforcing bars. The centerline-to-centerline spacing of the columns is two feet one inch. For Spans IV, V, and VI, the stirrups are 3/8-in. diameter round bars spaced at 12 in. center-to-center.

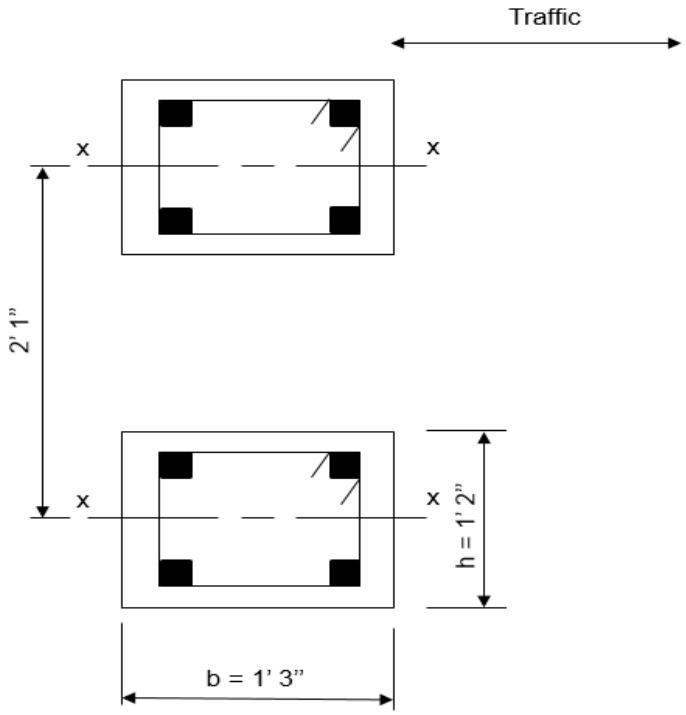

Figure 13: Typical Column 2 Cross Section

For Span VII, the reinforcing bars consist of round and square bars (AHD 1929). Figure 6 shows the naming convention for Span VII. Column 4 has 1-in. square reinforcing bars. Columns 5 and 6 have 3/4-in. round diameter bars. Column 7 has 1-in. round diameter bars. The stirrup spacings are 10 in. and 12 in. center-to-center.

2.4.2 Column 3s

For all columns at a pier, a typical elevation view taken from AHD (1929) is shown in Figure 14. All columns at a pier are also referred to as Column 3. The Column 3 cross section is shown in Figure 15. Traffic flows parallel to the x-x axis or weak axis. The interior Column 3 is 14 in. x 18 in. and reinforced by four 1-in.-diameter reinforcing bars. No information is provided about the stirrup size and spacing. The exterior column is T-shaped with the web facing inward. The exterior column is intentionally shown without any reinforcement in Figure 15 because no information is available. For all exterior Column 3s, the web width, web height, and flange height are as labeled. However, the flange width varies from pier to pier.

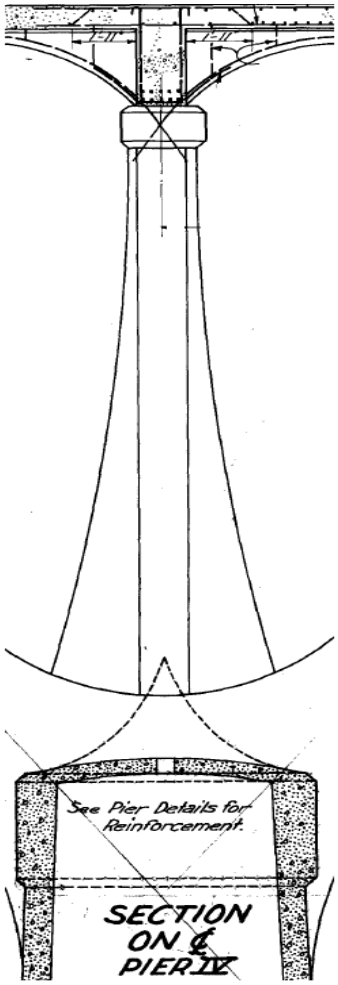

Figure 14: Typical Elevation of Column 3 at Pier IV (AHD 1929)

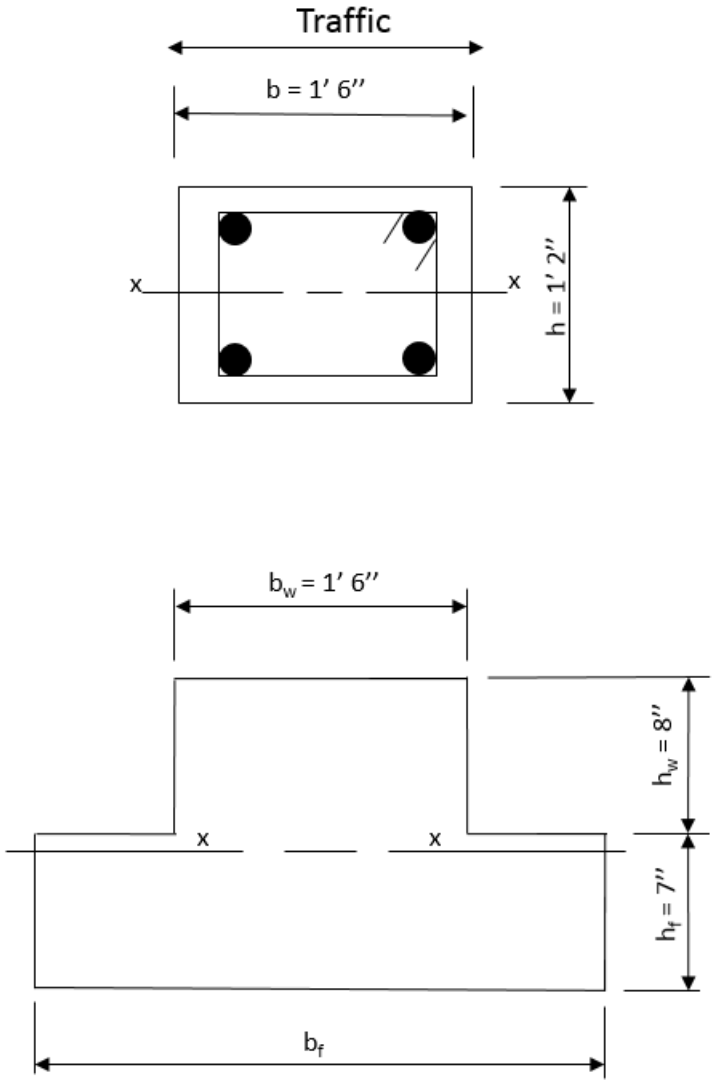

Figure 15: Column 3 Cross Section

Figure 16 shows that the flange edges of the exterior Column 3 are curved. The flange width is thinnest at the top and thickest at the base. To define the geometry, the exterior Column 3 was divided into a top and a bottom section at the mid-height of the column. For each section, the flange width is taken as the average width for that section. The flange width for the exterior Column 3s for the top and bottom sections is shown in Table 9.

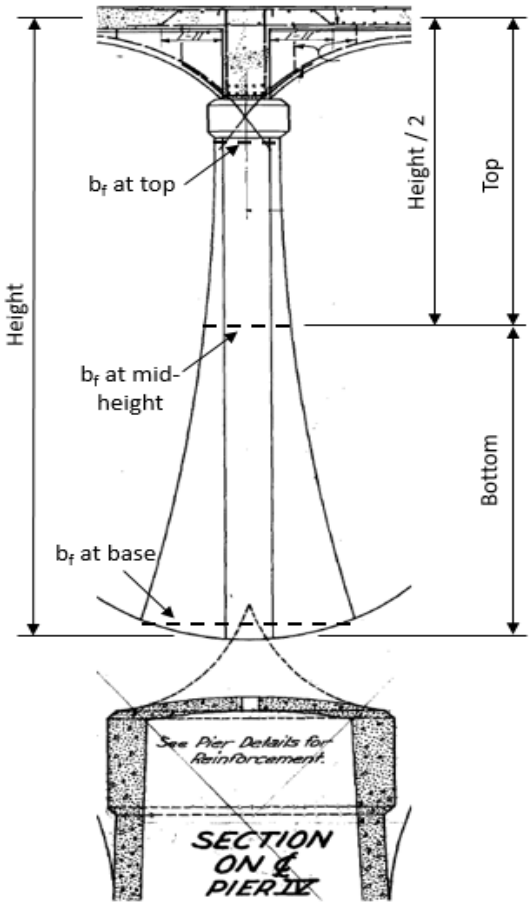

Figure 16: Elevation of Column 3 with Labels (AHD 1929)

Table 9: Exterior Column 3s Flange Width Dimensions

Exterior Column 3		b_f (in)
At Pier V	Top	28.8
	Bottom	56.4
At Pier VI	Top	29.1
	Bottom	55.1
At Pier VII	Top	27.8
	Bottom	55.6

2.5 HANGERS

Each reinforced concrete hanger, as shown in Figure 17, connects the arch rib and transverse floor beam which supports the deck slab. All hangers consist of a pair of 12 in. by 14 in. concrete cross sections reinforced with four 1-in.-square reinforcing bars as shown in Figure 18.

Figure 17: Concrete Hangers

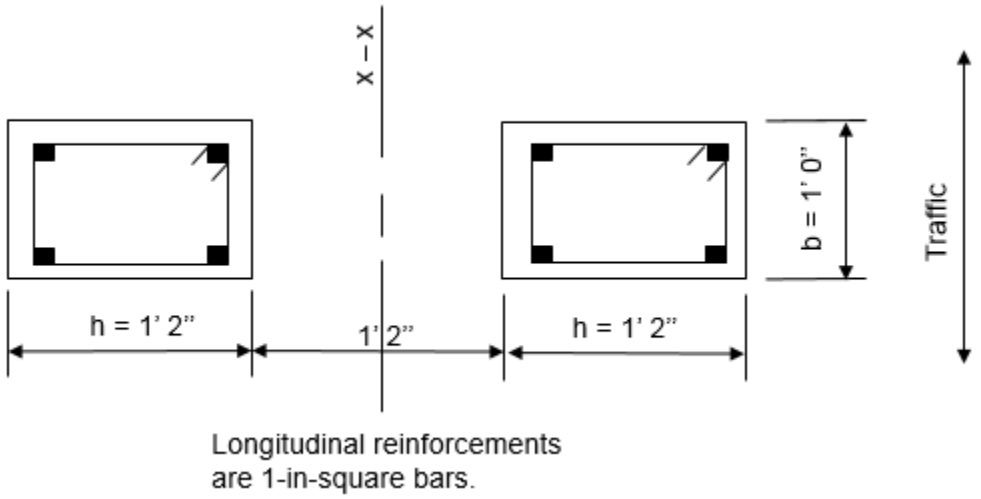

Figure 18: Hanger Cross Section

2.6 TRANSVERSE DEEP BEAMS

The transverse deep beam is directly supported on the arch with no hanger or column as shown in Figure 19. The transverse deep beams are only present in spans with through arches. There is an expansion joint in the deck slab above each transverse deep beam so that the beam is not composite with the slab. The transverse deep beams are rectangular in cross section with dimensions shown in Table 10. The height of the beam was determined by scaling the drawings in AutoCAD. The width is the same as the width of other transverse beams.

Figure 19: Transverse Deep Beam

Table 10: Transverse Deep Beam Dimensions

Span No.	Height (ft)	Width (ft)
IV	6.26	1.50
V	5.63	1.50
VI	5.09	1.50

Chapter 3

RATING METHODOLOGY

The goal of the project is to provide load ratings for the bridge components for the eight ALDOT trucks and the AASHTO lane load. The specifications and ALDOT requirements for the ratings are presented in this Chapter along with a description of the rating methodology used. The process for determining the member capacities is described along with the computer models used for the transverse frames and arches.

3.1 SPECIFICATIONS AND ALDOT REQUIREMENTS

The load ratings were performed in accordance with the Load Factor Rating (LFR) method defined in the 2011 second edition of The Manual for Bridge Evaluation or The MBE by the American Association of State Highway and Transportation Officials' (AASHTO). AASHTO (2011) references AASHTO's 2002 seventeenth edition of the Standard Specifications for Highway Bridges.

As required by the Alabama Department of Transportation (ALDOT), all structural analysis was performed with Computer and Structures, Inc. software SAP2000 version 15. Rating factors were determined for eight standard truck loadings routinely used by ALDOT and a lane loading prescribed by AASHTO as shown in Figure 20. These trucks are the H-truck, two-axle, tri-axle, concrete, 18-wheeler, 6-axle, school bus, and HS-truck. In addition, rating factors were determined for the AASHTO lane load consisting of a uniformly distributed load with concentrated loads positioned for maximum shear and moment. Additional information about the truck loadings is provided in Figure 34.

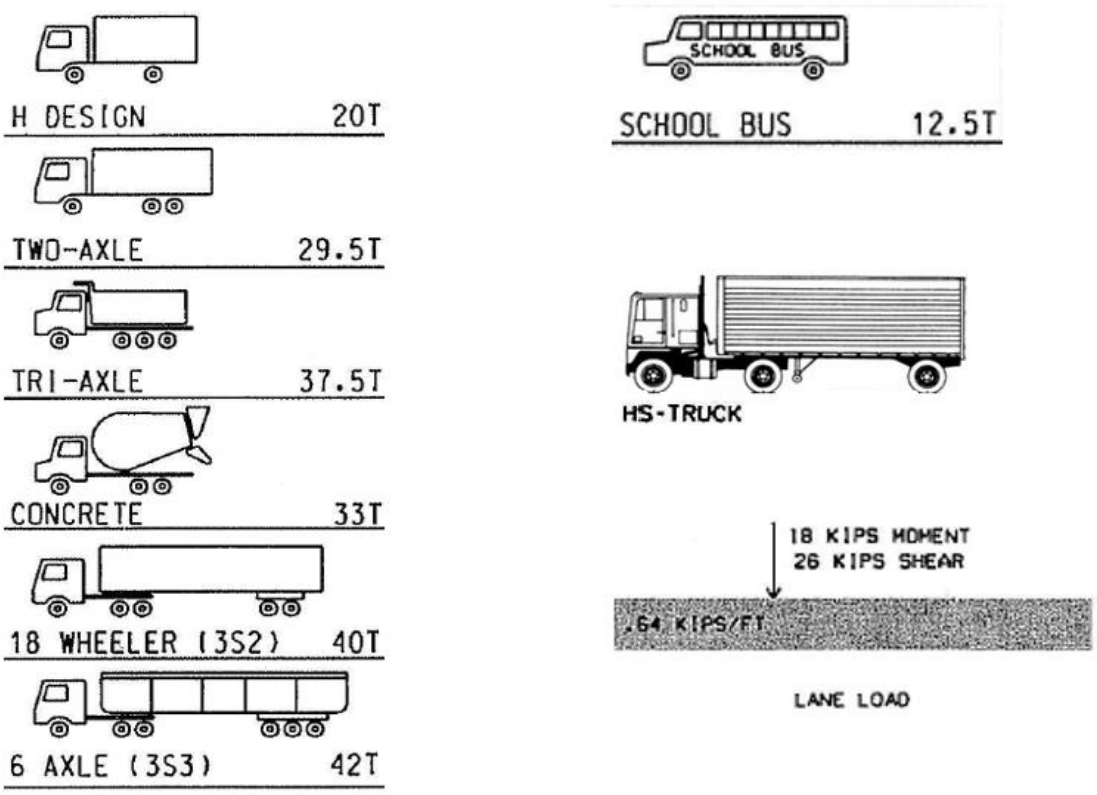

Figure 20: ALDOT Trucks and AASHTO (2002) Lane Load

3.2 MATERIAL PROPERTIES

Rating calculations for the various bridge elements requires the use of a concrete compressive strength and yield strength of the steel reinforcement. There are no ALDOT records of the specified strengths of the concrete and steel reinforcement. Based on an article by Taylor (1930), the specified compressive strengths of the concrete in the arches are known to range from 2,000 psi to 4,000 psi as shown in Figure 21, but the locations of these concrete strengths cannot be accurately determined. Construction joint locations are identified in the AHD (1929) drawings, and many of these joint locations are visible on the side faces of the arches. The casting order of the segments of the arches appears to be identified by a system of letters on the drawings. Unfortunately, the number of arch segments nor the order of casting matches the information in Figure 21. Therefore, there is no reliable way to match the concrete strengths shown in Figure 21 with specific locations along the arches. Also, the drawings provide no information about the concrete strength.

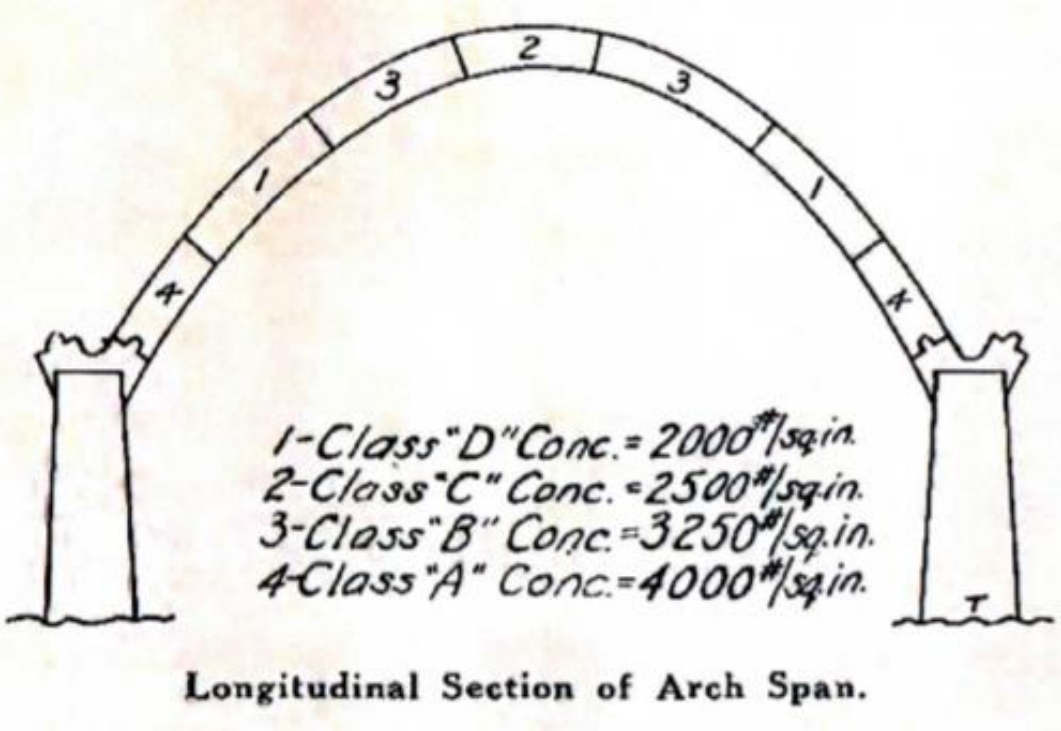

Figure 21: Concrete Strengths Used Along Arch (Taylor 1930)

AASHTO (2011) recommends the use of a reinforcing steel yield strength of 33,000 psi and concrete compressive strength of 2,500 psi for unknown reinforcing steel and concrete in a structure of the age of the Bibb Graves Bridge. Core test results reported by TranSystems (2009) as shown in Table 11 indicate that the measured concrete compressive strength in 14 of the 15 locations sampled exceeded the value recommended in AASHTO (2011). A goal of this project is to determine ratings that are representative of the bridge as designed without regard to damage or deterioration and to not penalize unnecessarily a structure which is known to have safely carried unrestricted traffic for many years. So, the core test results were analyzed to determine whether those results supported the use of a concrete compressive strength greater than 2,500 psi in the rating calculations.

Table 11: Equivalent Concrete Compressive Strength from Core Samples

	Core Sample Location					
	Deck	**Deck minus one**	**Arches**	**Arches Span I and VII**	**Columns**	**Substructure**
Core Compressive Strength, f_c (psi)	7250	7250	10040	4940	9070	6690
	3460	3460	10300	5400	6960	7230
	3830	3830	4940		7890	
	5600	5600	5400		9250	
	2300					
Average (psi)	4490	5040	7670	5170	8290	6960
V	0.434	0.347	0.377	0.0629	0.129	0.0551
n	5	4	4	2	4	2
k_c	1.20	1.28	1.28	2.40	1.28	2.40
f_{ceq} (psi)	2820	3220	4740	3980	6590	5450

A procedure from ACI Committee 562 Code Requirements for Evaluation, Repair, and Rehabilitation of Concrete Buildings (ACI 562-13) and Commentary (2013), Section 6.4.3 was used to estimate an equivalent specified compressive strength from the core test results. The procedure is the best available method to account for the number of core samples and the variability in the core test results; even though, the procedure assumes some facts about the sampling, testing, and adjustments of the raw core test strengths that cannot be verified from the details provided in the TranSystems (2009) report.

Columns 2 and 3 in Table 11 provide results for the concrete in the deck. The individual core test results are shown along with the average, coefficient of variation of the core strengths (V), number of samples (n), coefficient of variation modification factor (k_c) value from Table 6.4.3 in ACI Committee 562 (2013), and the equivalent specified compressive strength (f_{ceq}). The equation for f_{ceq} is as follow.

$$f_{ceq} = 0.9\bar{f}_c\left[1 - 1.28\sqrt{\frac{(k_c V)^2}{n} + 0.0015}\right] \quad (1)$$

Where:

$\bar{f}_c$ = average core strength (psi)

k_c = coefficient of variation modification factor

V = coefficient of variation of the core strengths

n = number of cores taken

Locations for five core samples taken from the deck were selected by TranSystems with the assistance of ground penetrating radar test results. One of the core samples was taken from Span I in an area of potential deterioration, and the compressive strength determined for that core was 2,300 psi. The remaining four core samples were taken from areas "which are representative of the remainder of the bridge deck" (TranSystems 2009, page 19 of 24). The equivalent specified concrete compressive strength determined from the four deck core samples of greatest strength is 3,220 psi. Equivalent specified concrete compressive strengths determined from cores taken from other structural elements are also listed in Table 11, and all exceed the value of 2,500 psi recommended by AASHTO (2011).

Columns 4 and 5 of Table 11 list core strength results for samples taken from the arches as reported by TranSystems (2009). Column 4 lists all four of the available core test results. Each of the core samples was taken from a different arch span as follows: 10,040 from Span II, 10,300 psi from Span V, 4,940 psi from Span VII, and 5,400 psi from Span I. The specific location of these core samples is not reported by TranSystems (2009), and the concrete that was sampled cannot be reliably linked to any particular value of specified concrete strength shown in Figure 21. So, the equivalent specified compressive strength of 4,740 psi in Column 4 of Table 11 provides an indication of the overall quality of the concrete in the arches, but it is not an accurate prediction of the concrete strength at any specific cross section in the arches.

Section 5.4.5 of this report shows that the shear strength of the arch rib in Span I and Span 7 potentially controls the bridge rating. So, the core strengths from those spans are analyzed separately in Column 5 of Table 7. The result is an equivalent specified compressive strength of 3,980 psi. Because the actual specified concrete strengths are known to vary as shown by Figure 21, it is impossible to state with a high level of confidence that the equivalent specified compressive strength of 3,980 psi is representative of the critical cross section in Span I and Span VII. However, all the core test results in Columns 4 and 5 of Table 7 support the use of a concrete strength greater than 2,500 psi in the rating calculation.

Load ratings reported here were determined using a concrete compressive strength of 3,000 psi unless otherwise noted. This choice is supported by the analysis of the core test results

presented in Table 11. The use of higher compressive strengths can be justified for the current condition of the structure. Since the deterioration of the structure due to ASR is expected in the future, having ratings at a lower bound on the concrete strength will be useful. If the ratings are determined at the upper bound of the concrete strength, an additional evaluation of the structure will be required after only a small decrease in concrete strength occurs due to ASR.

For structural analysis models built in SAP2000, the material properties for concrete and steel are listed in Table 12for all cases except those noted.

Table 12: Material Properties for SAP2000

Concrete			Reinforcing Steel		
Unit Weight (pcf)	f'_c (psi)	$57000\sqrt{f'_c}$ (psi)	Unit Weight (pcf)	f_y (ksi)	E_s (ksi)
150	3,000	3,122,000	490	33	29,000

3.3 LOAD FACTOR RATING METHOD

The purpose of the project was to provide a load rating of the Bibb Graves Bridge. The load rating procedure required by AASHTO (2011) Section 6B.4.3 is the Load Factor Rating (LFR) method. This method provides two ratings; an inventory and an operating rating. Table 13 lists the load factors associated with each.

Table 13: Load Factors for LFR Method

	Operating	Inventory
A_1	1.3	1.3
A_2	1.3	2.17

The inventory rating corresponds to design loading cases and always result in a lower rating factor and a higher factor of safety. The operating rating is used by ALDOT for load postings. A_1 is the factor for dead loads, and A_2 is the factor for live loads. According to AASHTO (2011) Section 6B.4.1, the rating factor is defined as

$$RF = \frac{C - A_1 D}{A_2 L(1 + I)} \tag{2}$$

Where:

C = the capacity of the member

D = the dead load effect on the member

L = the live load effect on the member

I = the impact fraction to be used with the live load effect

3.4 MEMBER CAPACITY

In order to obtain a rating factor, the capacities of each of the components were assessed. The general expression of the rating factor is given in Eq. (2). For the transverse floor beams and transverse deep beams, flexural and shear capacities were determined. For the hangers, tension capacity was determined. For the columns and arch ribs, which are beam-column members, capacity was determined for the axial load and bending moment combination. In addition, shear capacity was determined for the arch ribs.

3.4.1 Flexure

Flexural capacity was determined for the transverse floor beams and transverse deep beams as described below.

3.4.1.1 Transverse Floor Beams

The singly reinforced cross section utilized for positive bending moment for the transverse floor beams for Spans IV and V, taken at midspan, is shown in Figure 22. The reinforcing bars are 1-1/8-in.-square bars in the top layer and 1-1/4-in.-square bars in the bottom layer. For Spans VI and VII, the reinforcement is the same, but the height of the flange is 7-1/2 in. and the height of the web is 2 ft 8-1/2 in as listed in Table 8. The positive bending moment capacity was used to rate the transverse floor beams at the hanger and column locations. Table 14 lists the positive bending moment capacity for all spans.

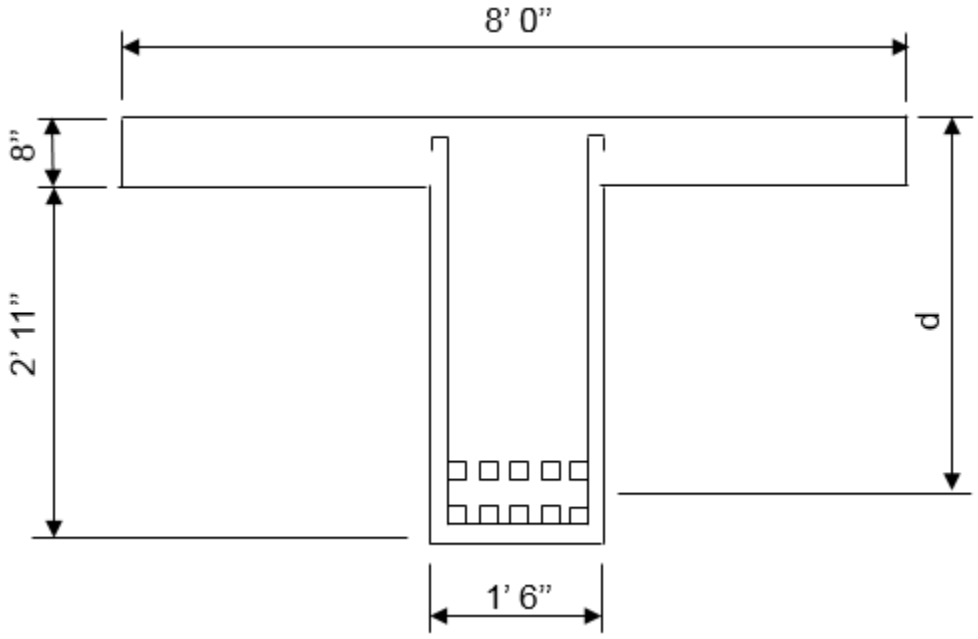

Figure 22: Positive Bending Moment Cross Section (Spans IV and V)

The doubly reinforced cross section utilized for negative bending moment for the transverse floor beams for Spans IV and V, taken at the interior face of the interior column, is shown in Figure 23. For negative bending moment, there is a single layer of tension steel

consisting of three 1-1/8-in.-square bars and two ¾-in.-diameter round bars. At the bottom of the beam, there is a single layer of five 1-1/4-in.-square bars that were not included in determining the negative bending moment resistance. For Spans VI and VII, the reinforcement is the same, but the height of the web is 3 ft 8 in as listed in Table 8. The negative bending moment capacity was used to rate the transverse floor beams at the column locations. The transverse floor beams at the hanger locations have no negative bending moment as discussed Section 3.5.6.1. Table 14 lists the negative bending moment capacity for all spans.

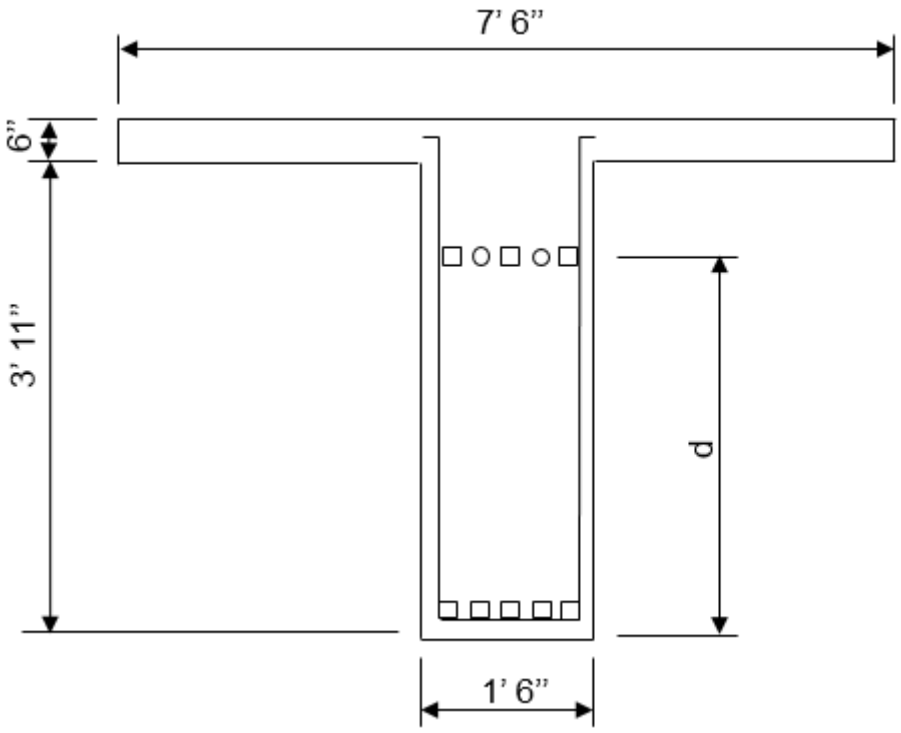

Figure 23: Negative Bending Moment Cross Section (Spans IV and V)

According to Section 8.16.3 in the AASHTO (2002), the factored flexural capacity or factored nominal moment strength is as followed:

$$\phi M_n = \phi\left[A_s f_y\left(d - \frac{a}{2}\right)\right] \quad (3)$$

And:

$$a = \frac{A_s f_y}{0.85 f'_c b} \quad (4)$$

Where:

- a = depth of equivalent rectangular stress block (in.)
- A_s = area of tension reinforcement (in.^{2})
- b = width of compression face of member (in.)
- d = distance from extreme compression fiber to centroid of tension reinforcement (in.)
- f'_c = specified concrete compressive strength (psi)
- f_y = specified yield strength of reinforcement (psi)
- ϕ = strength reduction factor, 0.9

Table 14: Transverse Floor Beam Factored Moment Capacity

Span No.	Factored Positive Bending Moment (k-ft)	Factored Negative Bending Moment (k-ft)
IV and V	1320	449
VI and VII	1220	414

3.4.1.2 Transverse Deep Beams

The singly reinforced cross section at midspan utilized for positive bending moment for the transverse deep beams for Spans IV, V, and VI is shown in Figure 24. The dimensions of the transverse deep beams were presented in Table 10. Two layers of reinforcing bars were used for flexural reinforcement for all transverse deep beams. In the top layer, there are five 1-in.-diameter bars. In the bottom layers, there are two 1-in.-diameter round bars and three 1-in.-square bars. Bending moment capacities are showing in Table 15.

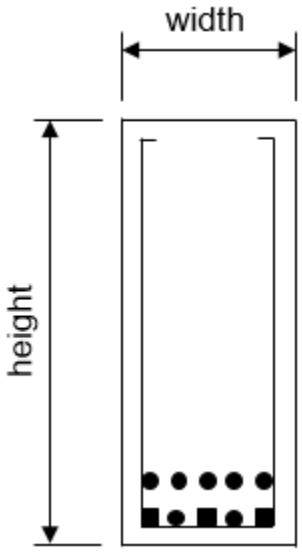

Figure 24: Transverse Deep Beam Cross Section

Table 15: Transverse Deep Beam Factored Bending Moment Capacities

Span No.	Factored Bending Moment Capacity (k-ft)
IV	1430
V	1270
VI	1130

3.4.2 Shear

Shear capacity was determined for the transverse deep beams, transverse floor beams, and arch ribs.

3.4.2.1 Transverse Deep Beams

All transverse deep beams have stirrups that are ¾ inch diameter round bars spaced at 12 in. center-to-center. Thus, the shear capacity was constant along the length of the transverse deep beam. All transverse deep beam factored shear capacities are listed in Table 16.

Section 8.16.6 of AASHTO (2002) defines the factored nominal shear strength, or shear capacity, as

$$\phi V_n = \phi_v \left(V_c + V_s \right) \tag{5}$$

Where the nominal shear strength provided by concrete and steel are defined as

$$V_c = 2\sqrt{f'_c} b_w d \tag{6}$$

$$V_s = \frac{A_v f_y d}{s} \tag{7}$$

Where:

A_v = area of shear reinforcement within a distance s (in.^{2})

b_w = web width (in.)

d = distance from extreme compression fiber to centroid of tension reinforcement (in.)

f'_c = specified concrete compressive strength (psi)

f_y = specified yield strength of reinforcement (psi)

s = spacing of shear reinforcement (in.)

ϕ = strength reduction factor, 0.85

According to Section 8.19.3 of AASHTO (2002), the shear strength provided from the steel reinforcement, V_s, was included into Eq. (5) only if the spacing of the shear reinforcement did not exceed d/2 or 24 inches.

Table 16: Transverse Deep Beam Factored Shear Capacity

Span No.	Factored Shear Capacity (k)
IV	266
V	237
VI	213

3.4.2.2 Transverse Floor Beams

All transverse floor beams have stirrups that are ¾-inch-diameter round bars. The typical sections from the beam drawings provided by AHD (1929) shows that Spans IV and V along with Spans VI and VII have the same stirrup spacing configuration. However, the spacings among the two groups, Spans IV and V and Spans VI and VII, are different.

The factored nominal shear strength was calculated using Eq. (5). A plot of the factored shear capacities for Spans IV and V is shown in Figure 25. The capacities were calculated for all stirrup spacings and cross section depths throughout half of the beam. The beam is symmetrical about midspan. The shear capacity along the beam was discretized into three distinct zones for rating: Zone 1, Zone 2, and Zone 3. Each plateau of shear capacity corresponds to a zone. Qualitatively, these zones can be seen in Figure 25.

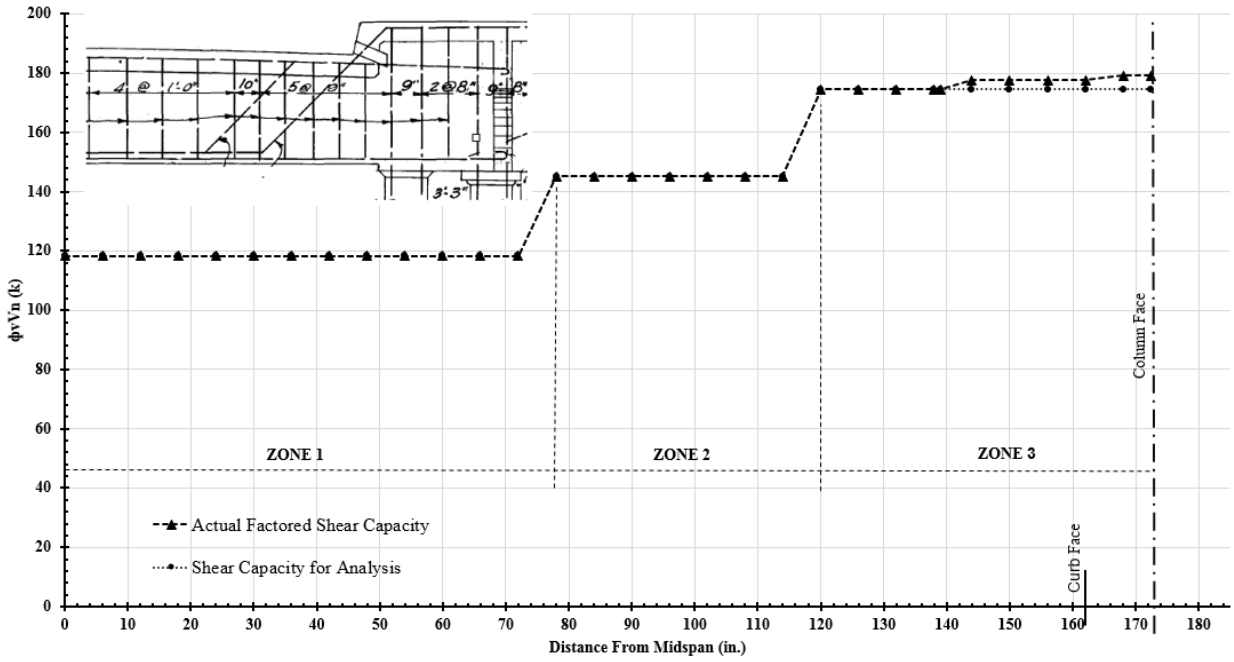

Figure 25: Shear Capacities for Spans IV and V

As shown by the line with triangular markers in Figure 25, the shear capacity increases slightly at a distance around 145 in. from midspan due to an increase in depth to the tension reinforcement. The increase in depth results from the top layer of the bottom reinforcement

being bent up across the web. The small increase in shear capacity to the increase in depth and the shear capacity associated with the longitudinal reinforcement being bent up near the end of the beam were neglected in the rating calculations. So, the shear capacity used in the rating calculations for Zone 3 was the value determined at the beginning of that zone around 120 in. from midspan.

The same procedure was used in calculating the shear capacity for Spans VI and VII. The factored shear capacity for the transverse floor beams for all spans is listed in Table 17.

Table 17: Transverse Floor Beams Factored Shear Capacity

	Factored Shear Capacity (k)		
Span No.	Zone 1	Zone 2	Zone 3
IV and V	118	145	175
VI and VII	109	134	161

3.4.2.3 Arch Rib

The drawings provided by AHD (1929) shows that the arch ribs for Spans IV, V, and VI have 3/8-in. diameter hoops that are spaced at 2 ft 0 in. For Span IV, the sections within 4 ft 0 in. of the arch base have hoop spacing of 1 ft 6 in. For Span VII, the hoops are 3/8-inch diameter bar spaced at 1 ft 6 in.

The arch rib factored shear capacity was calculated using Eq. (5). Section 8.16.6.2 of AASHTO (2002) allows for the contribution of axial load to be added to V_c for shear in compression members. For the arch rib factored shear capacity, Eq. (6) was replaced with the following.

$$V_c = 2\left(1 + \frac{N_u}{2000A_g}\right)\sqrt{f'_c}\,b_w d \qquad (8)$$

Where:

A_g = gross area of section (in.^{2})

N_u = factored axial load normal to the cross section (lbs)

For Spans IV, V, and VI, the arch rib shear ratings did not control, and the axial effects were only considered from dead loads. However, for arch sections near midspan of Span VII, the arch rib shear rating did control. To capture the full factored shear capacity for this section the axial effects were considered from dead and live loads. For all spans, the axial effect from dead loads were larger than the axial effect from live loads.

3.4.3 Tension

All hangers are reinforced by 1-in. square reinforcing bars as shown in AHD (1929). Each hanger per pair has four reinforcing bars. The hangers were rated as axial tension members. The axial tension capacity was found by

$$\phi P_n = \phi A_s f_y \tag{9}$$

Where ϕ equals 0.9.

The hangers were rated as axial tension members because the limit state for these hangers is when the concrete has cracked and the steel reinforcing bars have yielded. As a result, the axial tension capacity of the hangers was found for each, individual hanger. For Spans IV, V, and VI, the tension capacity for each hanger is 119 kips.

3.4.4 Axial Load and Bending Moment

The capacity for the beam-column members such as arch ribs and columns were determined from the axial load-moment interaction diagram, referred to here as load-moment interaction diagram.

All Column 2s are 14 in. by 15 in. with four 1-in.-square reinforcing bars positioned in the corners as shown in Figure 13. All Column 3s are as labeled in Figure 15. For all spans, the arch ribs have eight reinforcing bars in the top layer and eight reinforcing bars in the bottom layers. The bars are both round and square reinforcing bars ranging from 3/4-in.-diameter round bars in Span VII to 1-1/4-in-square bars in Span IV. For all spans, Section 2.2 of this report provides the geometry and reinforcements for the arch rib sections. In addition, the drawings from AHD (1929) have more details about the bar shapes, sizes, and layout configuration.

3.4.4.1 Load-Moment Interaction Diagram

Strength design method, or load factor design, was used in accordance with AASHTO (2002) Section 8.16.2 to develop a spreadsheet that plots a load-moment interaction diagram for a rectangular cross section with specified area of reinforcement. For Column 2s, the cross section is shown along with the properties in Figure 26. All values in the second column are user inputs.

d =	11.63	in.
d' =	2.375	in.
ε_{cu} =	0.003	
A_s =	2	$in.^2$
A'_s =	2	$in.^2$
f_y =	33	ksi
E_s =	29000	ksi
f'_c =	3	ksi
β_1 =	0.85	
b =	15	in.
h =	14	in.
A_g =	210	$in.^2$
ϕ_{column} =	0.7	

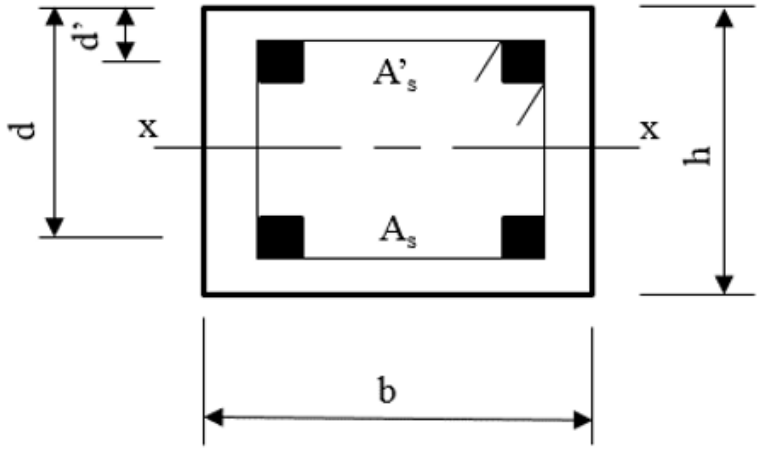

Figure 26: Load-Moment Interaction User Inputs

The spreadsheet calculations, shown in Figure 27 , were set up by varying the distance from the extreme compression fiber to the neutral axis, c, which is the first column in the spreadsheet. For each cross section, the "solver" application in Excel was used to find the value of c for the case when the axial load is zero. Per Section 8.16.1.2 in AASHTO (2002), the spreadsheet does account for the linear increase in the strength reduction factor, φ, as the factored nominal axial strength, ϕP_n, decreased from $0.10f'_cA_g$ to zero.

	Tension Steel				Compression (top) Steel						Concrete							
c (in)	ε_s	f_s (ksi)	A_s Yield?	T (ksi)	ε'_s	$\varepsilon'_{s\ control}$	f'_s (ksi)	$f'_{s\_control}$ (ksi)	A'_s Yield?	C'_s (kips)	a (in)	C_c (kips)	Net Force (kips)	M_n (k-ft)	ϕ	ϕM_n (k-ft)	Net Force (kips)	ϕP_n
														0		0.0	657	460.1
12.5	-0.00021	-6.1	N	-12.1	-0.0024	0.0024	33.00	33.0	Y	-60.9	10.63	-406.4	-479	76	0.7	53.2	479	335.6
11.5	0.00003	1.0	N	2.0	-0.0024	0.0024	33.00	33.0	Y	-60.9	9.78	-373.9	-433	90	0.7	63.0	433	303.0
10.5	0.00032	9.4	N	18.7	-0.0023	0.0023	33.00	33.0	Y	-60.9	8.93	-341.4	-384	103	0.7	72.0	384	268.5
9.5	0.00067	19.5	N	39.0	-0.0023	0.0023	33.00	33.0	Y	-60.9	8.08	-308.9	-331	115	0.7	80.3	331	231.5
8.5	0.00110	32.0	N	64.1	-0.0022	0.0022	33.00	33.0	Y	-60.9	7.23	-276.4	-273	126	0.7	88.3	273	191.2
7.5	0.00165	33.0	Y	66.0	-0.0021	0.0021	33.00	33.0	Y	-60.9	6.38	-243.8	-239	126	0.7	88.5	239	167.1
6.5	0.00237	33.0	Y	66.0	-0.0019	0.0019	33.00	33.0	Y	-60.9	5.53	-211.3	-206	124	0.7	86.5	206	144.4
5.5	0.00334	33.0	Y	66.0	-0.0017	0.0017	33.00	33.0	Y	-60.9	4.68	-178.8	-174	118	0.7	82.9	174	121.6
4.5	0.00475	33.0	Y	66.0	-0.0014	0.0014	33.00	33.0	Y	-60.9	3.83	-146.3	-141	111	0.7	77.7	141	98.8
3.5	0.00697	33.0	Y	66.0	-0.0010	0.0010	27.96	28.0	N	-50.8	2.98	-113.8	-99	97	0.7	68.1	99	69.0
2.5	0.01096	33.0	Y	66.0	-0.0002	0.0002	4.35	4.4	N	-8.7	2.13	-81.3	-24	69	0.836	57.7	24	20.1
2.272	0.01236	33	Y	66.0	0.0001	-0.0001	-3.94	-3.9	N	7.9	1.93	-73.9	**0.000**	60	0.900	53.6	0	0.0
2	0.01445	33	Y	66.0	0.0006	-0.0006	-16.31	-16.3	N	32.6	1.70	-65.0	34	46	0.9	41.6	-34	-30.2
1.5	0.02026	33	Y	66.0	0.0018	-0.0018	-50.75	-33.0	Y	66.0	1.28	-48.8	83	26	0.9	23.3	-83	-74.9
1	0.03189	33	Y	66.0	0.0041	-0.0041	-119.63	-33.0	Y	66.0	0.85	-32.5	99	18	0.9	16.1	-99	-89.5
0.5	0.06678	33	Y	66.0	0.0113	-0.0113	-326.25	-33.0	Y	66.0	0.43	-16.3	116	9	0.9	8.3	-116	-104.2

Figure 27: Spreadsheet for Plotting Load-Moment Interaction Diagram

The spreadsheet plots the load-moment interaction diagram shown in Figure 28. The capacity curve is shown by the line with round markers. Also plotted on the interaction diagram is the applied load effect line, or the factored loading line, for the tri-axle truck at the operating level. This line is shown with the square markers. The maximum factored axial strength is limited by the maximum axial strength defined in Section 8.16.4 of AASHTO (2002). This limit was drawn in as a horizontal line by the user for each cross section.

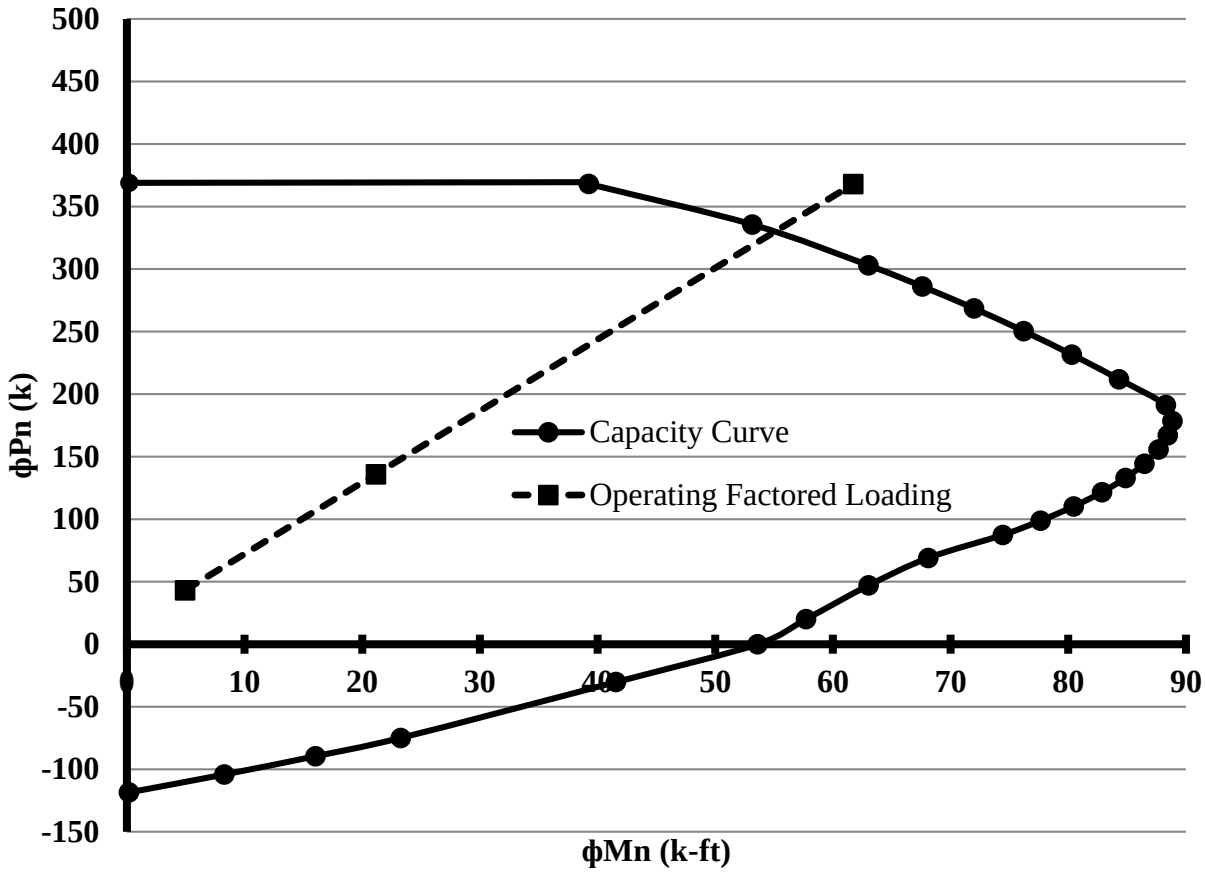

Figure 28: Load-Moment Interaction Diagram for Interior Column 2

3.4.4.2 Finding the Rating Factor

A rating factor can be determined from the load-moment interaction diagram shown in Figure 28 for a given combination of applied axial load and bending moment. To determine the rating factor, an applied load effect line was plotted on the interaction diagram. The applied load effect line comes from the bending moment and axial load equations shown below:

$$M_u = (RF \cdot A_2 \cdot M_{LL+I}) + (A_1 \cdot M_{DL}) \quad (10)$$

$$P_u = (RF \cdot A_2 \cdot P_{LL+I}) + (A_1 \cdot P_{DL}) \quad (11)$$

Where:

RF = rating factor

A_1 = dead load factor, 1.3

A_2 = live load factor, 1.3 for operating level and 2.17 for inventory level

M_{DL} = moment due to applied dead loads (k-ft)

M_{LL+I} = moment due to applied live loads with impact (k-ft)

P_{DL} = axial load due to applied dead loads (k)

P_{LL+I} = axial load due to applied live loads with impact (k)

The first point on the applied load effect line, which is the square marker nearest the origin, corresponds to a case where there is only applied dead load, which means the rating factor, RF, equals zero in Eq. (10) and Eq. (11). The other values along the factored loading lines include both the dead loads and truck loads as the RF was varied. The RF is strategically chosen so that the factored loading line crosses the capacity curve.

The true RF is determined by identifying the intersection of the factored loading line with the capacity curve. Identifying the intersection is simplified by assuming the capacity curve is linear between the nearest points above and below the intersection. The coordinates of the nearest two points on the capacity curve are x_1, y_1, x_2, and y_2. The slope between these two points is called m_{12}. In addition, the slope of the factored loading line is m_3, and the coordinates of a point along the factored loading line are x_3 and y_3. The abscissa of the intersection can be found using Eq. (12). The ordinate of the intersection can be found using Eq. (13). .

$$x = \frac{(m_3 \cdot x_3) - y_3 - (m_{12} \cdot x_1) + y_1}{m_3 - m_{12}} \tag{12}$$

$$y = \frac{\frac{y_3}{m_3} - x_3 - \frac{y_1}{m_{12}} + x_1}{\frac{1}{m_3} - \frac{1}{m_{12}}} \tag{13}$$

Once the intersection is found, the bending moment value is substituted back into Eq. (10) to find the RF. Similarly, the RF can be obtained by substituting the axial load value into Eq. (11). A routine was created as shown in Figure 29 for each truck loading to combine the applied dead and live loads from the structural analysis to plot the applied load effect line.

Also, another routine was created to find the intersection of two line segments in a plane shown in Figure 30. Once the intersection was identified, the RF was calculated for the particular cross section.

Tri-Axle Truck										
Axial and Moment LFR - Operating Case - Interior Columns - Highest Bending Moment										
A_1	M_{DL} (k-ft)	P_{DL} (k)	A_{2O}	IM	M_{LL} (k-ft)	P_{LL} (k)	RF	M_u (k-ft)	P_U (k)	Slope
1.3	3.8	33.2	1.3	1.3	9.89	54.80	0	4.94	43.16	5.54
1.3	3.8	33.2	1.3	1.3	9.89	54.80	1	21.65	135.77	5.54
1.3	3.8	33.2	1.3	1.3	9.89	54.80	3.5	63.44	367.30	
1.3	3.8	33.2	1.3	1.3	9.89	54.80	**3.05**	**56.00**	**326.06**	

Figure 29: Example Routine for Applied Load Effect Line

Intersection of Two Lines					
Applied Load Eqn.		**Capacity Eqn.**		**Intersection**	
m =	5.54	x_1 =	63	x =	56.00
x_1 =	21.65	y_1 =	303	y =	326.06
y_1 =	135.77	x_2 =	53.1		
$P_{column2}$ (k)	23.045	y_2 =	335.6		
		m =	-3.29		

Figure 30: Routine Finding Intersection of Capacity and Applied Load Effect Lines

Ratings were provided for the interior and exterior column. An example load-moment interaction diagram with the factored loading line for an interior Column 2 is shown in Figure 28. An example load-moment interaction diagram with the factored loading line for an exterior Column 2 is shown in Figure 31. The applied loads resulted in different combinations of axial load and bending moment for each column. Initially, it was ambiguous as to which load case would control the rating. Therefore, a rating was provided for the load case combination with the highest axial load effect and the load case combination with the highest bending moment. The lower RF controlled the rating for that particular column.

The position of the factored loading line describes the state of loading in the member. In Figure 28, the factored loading line lies above the horizontal axis, this column is in compression

for the applied loadings. In Figure 31, the factored loading line lies above and below the horizontal axis. This column is in compression under applied dead loads and in tension under applied live loads. Due to this phenomenon, the exterior columns resulted in lower RFs than the interior columns.

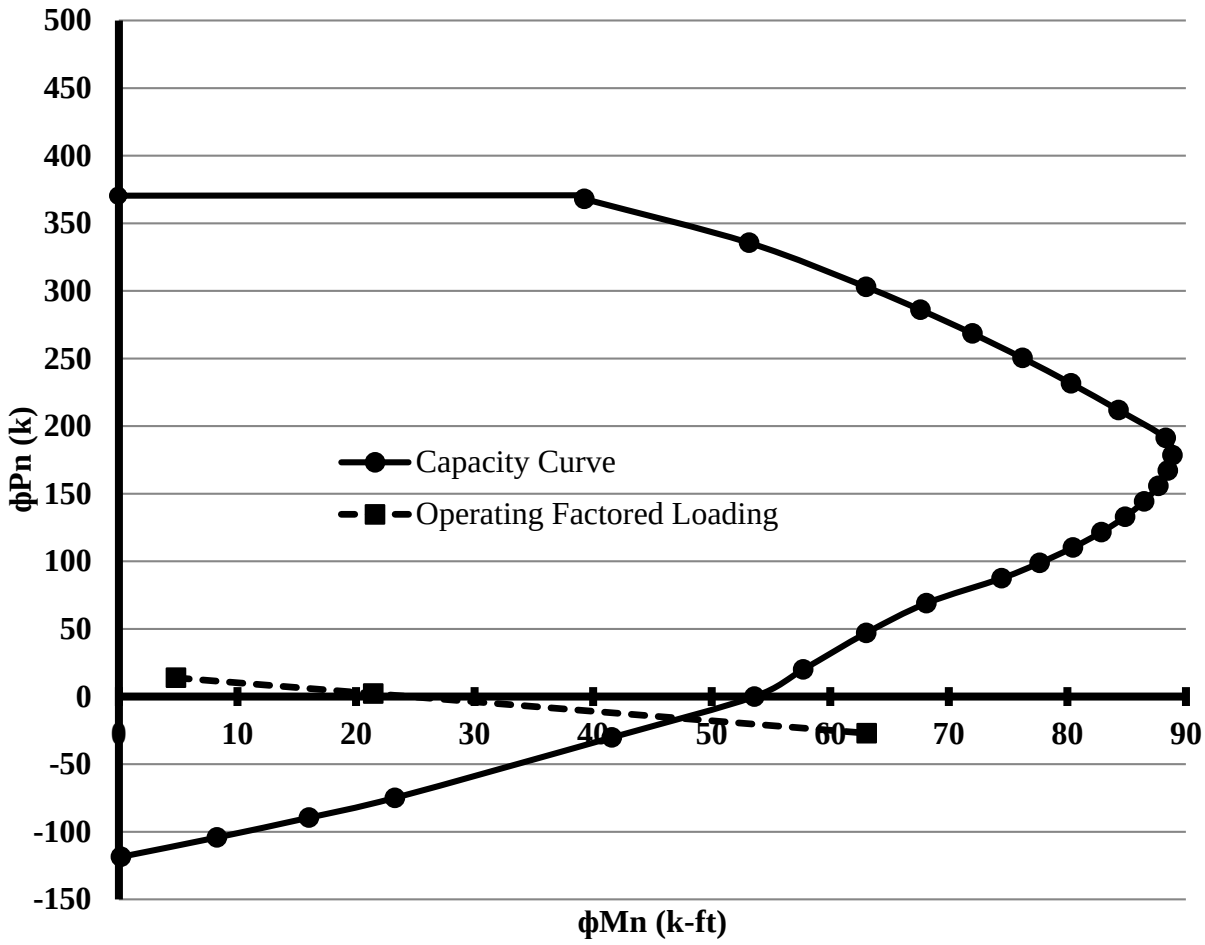

Figure 31: Axial Load-Interaction Diagram for Exterior Column 2

3.4.4.3 Load-Moment Interaction Diagram for Column 3

A spreadsheet routine was generated to plot the load-moment interaction diagram for the interior Column 3 with the 1-ft 2-in by 1-ft 6-in cross section as shown in Figure 15. For the exterior Column 3, which has the geometrically varied T-shaped cross section as illustrated in Figure 14, a lower bound capacity was used in the rating. The web width of the exterior T-shaped column

is the same as the width of the interior column at 1-ft 6-in. The capacity of the exterior Column 3 was determined by neglecting the flanges and using the load-moment interaction diagram for the same cross section as the interior Column 3.

3.5 TRANSVERSE FRAMES AND MEMBERS MODELS

Transverse frame models were built in SAP2000 and analyzed to obtain ratings for the transverse beams, columns, and hangers. Transverse frame models considered are: Beam and Column 2, Beam and Column 3, Beam and Hanger 1, and Transverse Deep Beam models. The loads placed on these models included dead loads from the bridge components and live loads from the truck loadings. The bridge components were discretized into various parts for convenience in the structural analysis. Appurtenances' weights such as side railings and pillars were accounted for.

3.5.1 Dead Loads

Dead loads for each transverse beam were resolved into uniformly distributed loads and concentrated loads. They were calculated based on a tributary width, equal to the spacing of the transverse beams. Dead loads were discretized into various parts for convenience. As shown in Figure 9, these parts are: roadway or slab, transverse beam, curb, and bracket. The dead loads for each part of the transverse beam were applied in the structural analysis models as uniformly distributed loads over their respective lengths.

The bracket section was simplified into a trapezoidal section. In Figure 32, the image on the left is the bracket section as shown in the bridge drawings. The image on the right, is the simplified bracket section used for analyses. Dimensional properties for all brackets are listed in Table 18. Dimension t_1 was scaled from the drawing. Dimensions t_2 and $L_{bracket}$ were obtained from the drawings.

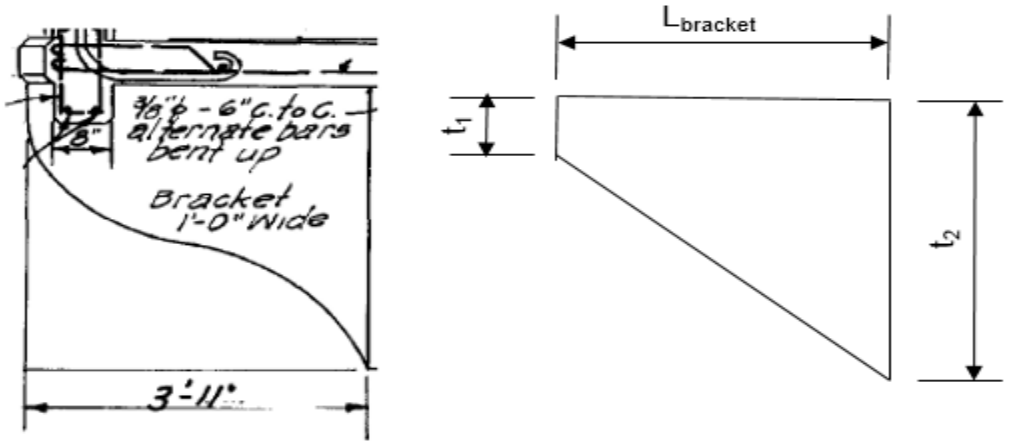

Figure 32: Bracket Section (Left image, AHD 1929)

Table 18: Brackets Dimensional Properties

	t_1	t_2	$L_{bracket}$	$W_{bracket}$
Spans IV and V	6 in.	3 ft 11 in.	3 ft 11 in.	1 ft 0 in.
Spans VI and VII	6 in.	3 ft 8 in.	3 ft 11 in.	1 ft 0 in.

On either side of the bridge (north and south sides), there are railings that are made up of steel sections and concrete pillars shown in Figure 33. By looking at close-up images of the railings and scaling dimensions, the top and bottom longitudinal railings are assumed to be a WT 4 x 12 section. The vertical plates are taken as ¼ in. x 2 in. x 36 in. steel. The weight of the railings was calculated and applied as a concentrated load five inches inward from the outer edge of the bracket section in all transverse models.

Figure 33: Side Railings on the Bridge

3.5.2 Live Loads

The live loads are the eight trucks specified by ALDOT and the lane load required by AASHTO (2002). The magnitude of the axle weights of ALDOT trucks are shown in Figure 34. Simple graphics of ALDOT trucks are shown in Figure 20. For the lane load shown in Figure 35, AASHTO (2002) required a uniformly distributed load of 0.640 kip/ft along with concentrated loads of 18 kips positioned for maximum moment and 26 kips positioned for maximum shear.

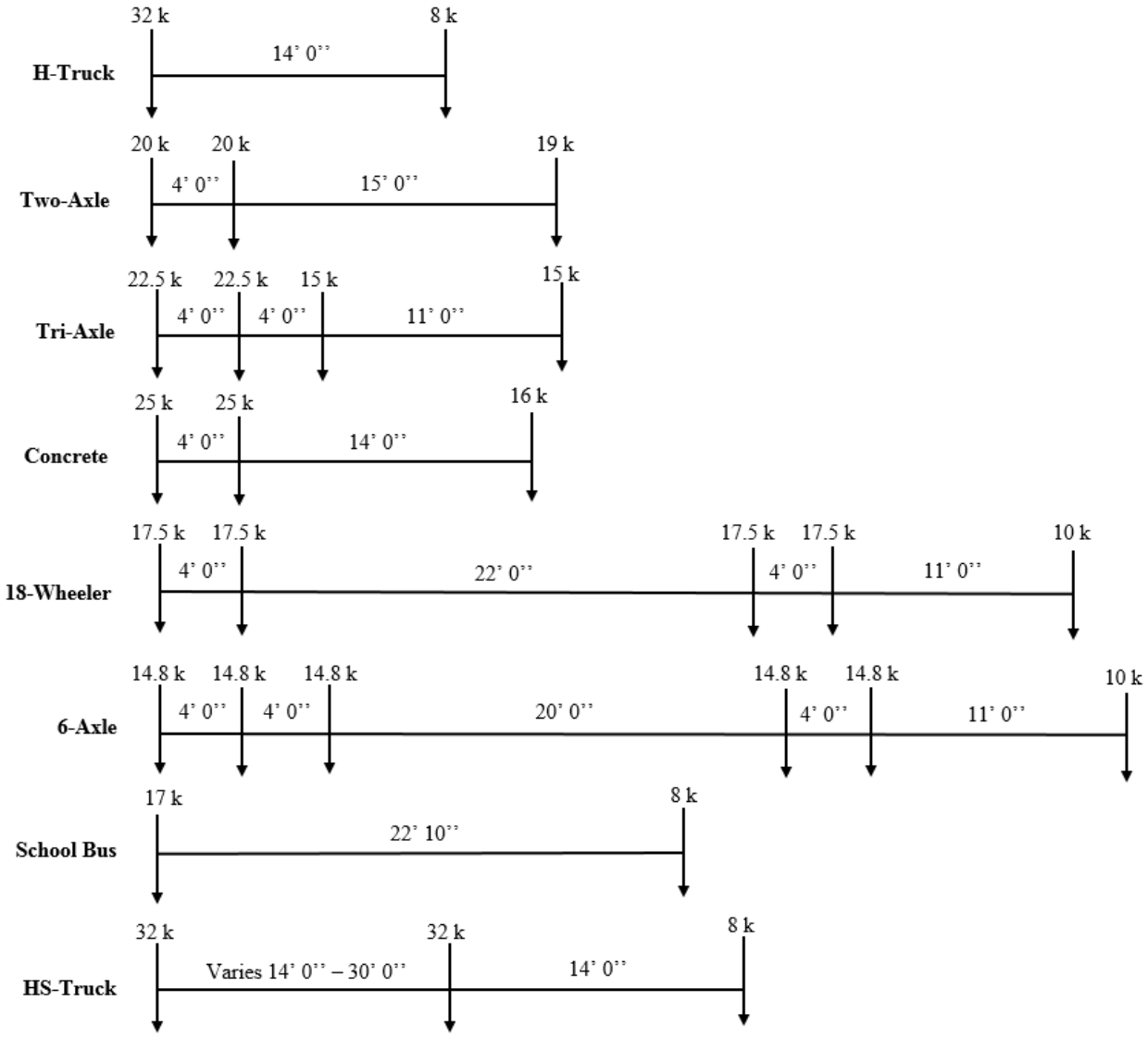

Figure 34: Axle Weights and Spacings of Standard ALDOT Trucks

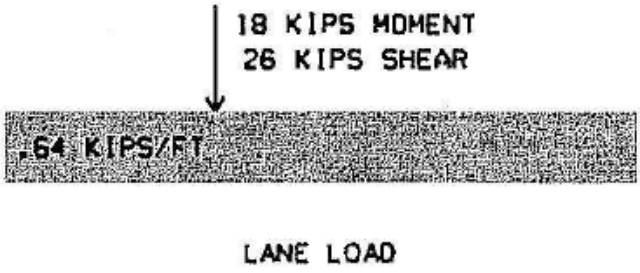

Figure 35: AASHTO (2002) Lane Load

3.5.2.1 Transverse Load Positions/Cases

To create the worst-case effects on the bridge, the live loads consisting of truck loads are strategically positioned across the 27-ft roadway width as shown in Figure 36 and Figure 37 per the requirements of Section 3.6 in AASHTO (2002). Truck loads are a pair of wheel line concentrated loads called W. Using a 10-ft truck width, the wheel line concentrated loads were placed in 12-ft design lanes and were moved transversely across the roadway width. A 1-ft transverse increment was used, which resulted in eight live load cases.

Per the traffic lane loading requirements stated in Section 3.6.4 of AASHTO (2002), two trucks were placed in their lanes as far left as possible as shown by LC1 in Figure 36. The left truck shifted to the right 1 ft at a time in its lane while the right truck remained stationary as shown by LCs 2 and 3. Once the left truck could no longer shift to the right, both trucks remained stationary in their respective lanes, and the lanes were shifted to the right 1 ft at a time shown by LCs 4, 5, and 6 in Figure 36 and Figure 37. Once the lanes have shifted to the right as far as possible, the right truck shifted to the right 1 ft at a time while the left truck remained stationary shown by LCs 7 and 8.

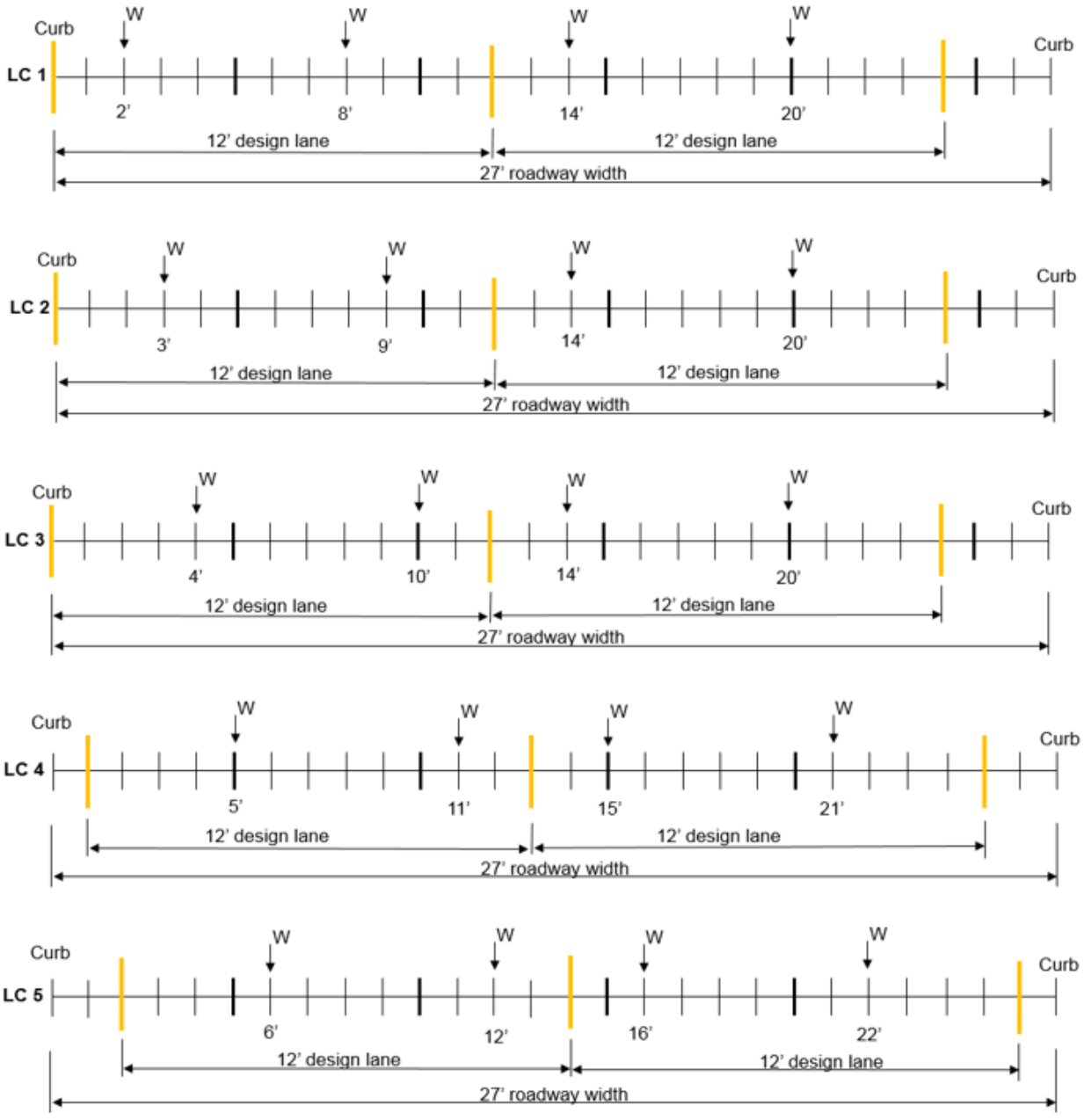

Figure 36: Live Load Cases 1 - 5

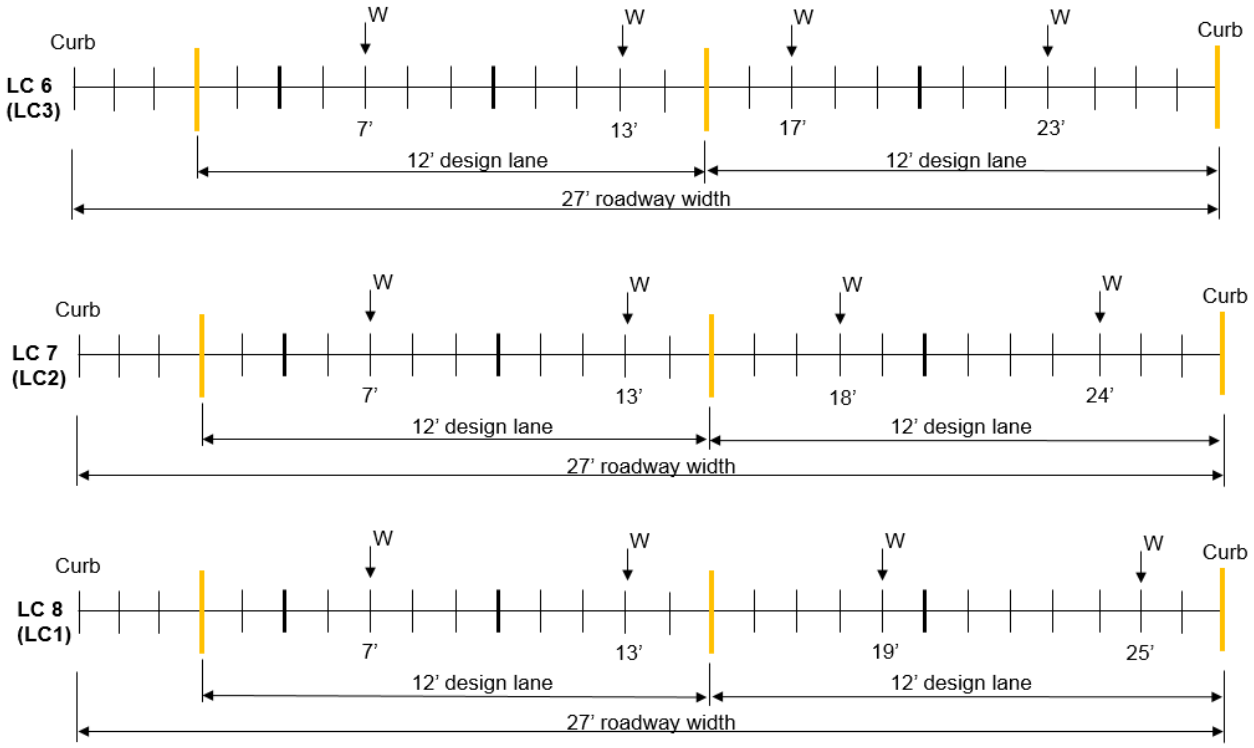

Figure 37: Live Load Cases 6 – 8

Of these eight load cases, the first five are unique and generate the worst-case effects on the left side of the bridge. In Figure 37, LC 6 mirrored LC 3; LC 7 mirrored LC 2; and LC 8 mirrored LC 1. Since the transverse beam is symmetric about midspan, the worst effects on the left half apply to the right half. The magnitude of these wheel line concentrated loads, W, came from a longitudinal beam analysis as required by Section 3.23.3.2 of AASHTO (2002).

3.5.2.2 Longitudinal Beam Analysis

For the longitudinal beam analysis, the length of the longitudinal beam was chosen to span between the expansion joints that encompass the hangers, columns, and transverse deep beam of interest as shown in Figure 38. For Span V, a longitudinal beam was created from the finger joint at midspan and extended eastward to the first expansion joint in Span IV.

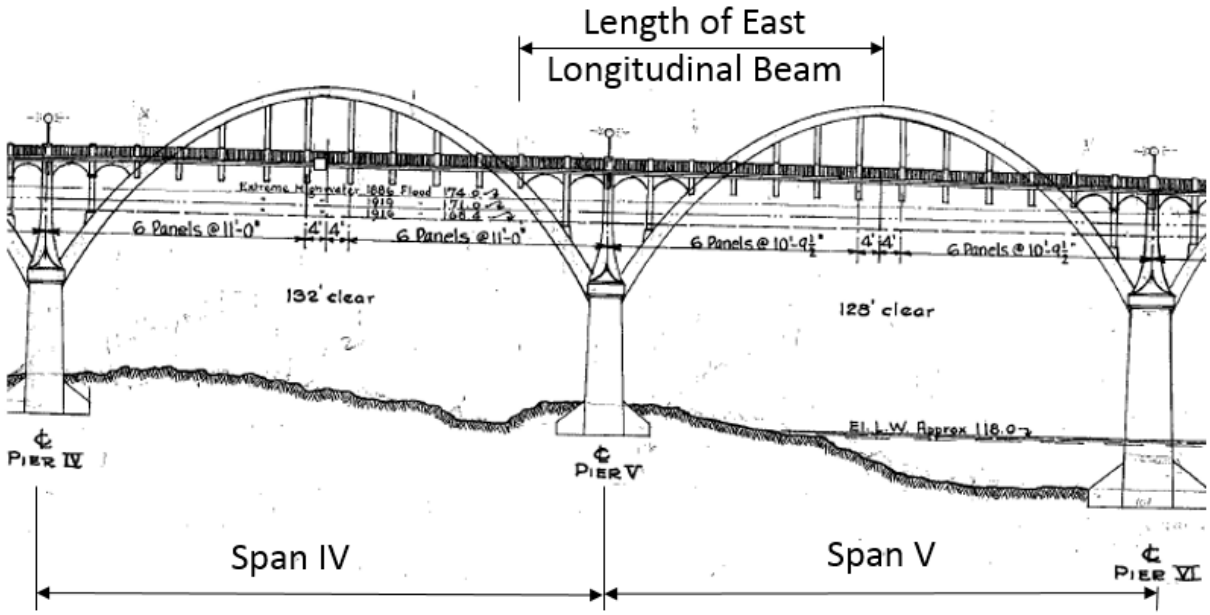

Figure 38: East Longitudinal Beam (AHD 1929)

Using this length of longitudinal beam, a structural analysis model was created as shown in Figure 39. Locations of transverse beams were represented by simple support reactions. In Table 3.23.3.1 of AASHTO (2002), for a concrete floor with a spacing of floor beams greater than 6 ft, the beams between the flooring shall be assumed to act as a simple beam. So, the bending moments were released at one end of each longitudinal beam span. At midspan of Span V, there is a finger joint in the bridge deck. Thus, the bending moment was not released at the simple support at the Hanger 1 shown in Figure 39. Once the longitudinal beam model was built, each truck was applied to the defined travel path as a moving load with no eccentricity. Being defined as a moving load, the truck travelled in both directions. A detailed discussion about moving loads is provided in Section 3.6.2.2.

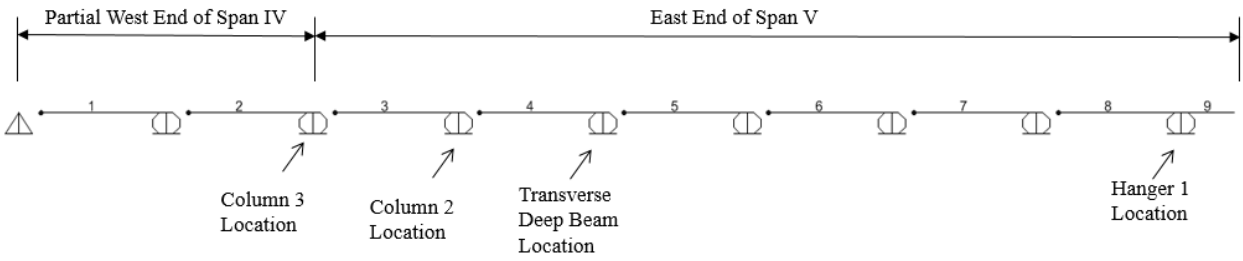

Figure 39: East Longitudinal Beam Model (SAP 2013)

The longitudinal beam model for Span V was extended into the adjacent spans, Spans IV and VI as shown in Figure 40. The extent of the west longitudinal beam is shown in relation to the east longitudinal beam. The transverse beam spacings of Spans IV and VI are different. Since the magnitude of the reactions from the truck loads on the longitudinal beam model is a function of the transverse beam spacings, another longitudinal beam model was analyzed in the opposite direction to capture the largest support reaction.

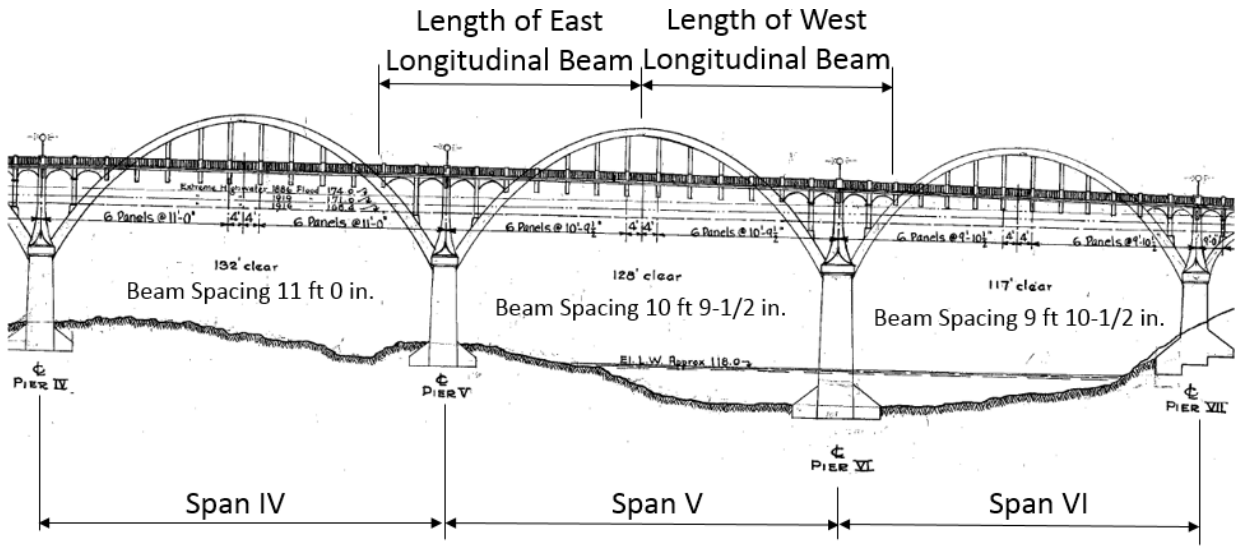

Figure 40: West Longitudinal Beam in Relation to East Longitudinal Beam (AHD 1929)

The west longitudinal beam started at the finger joint at midspan in Span V, the same start location as the previous model, and extended in the opposite direction, westward. Using this length of longitudinal beam, another structural analysis model was created as shown in Figure 41.

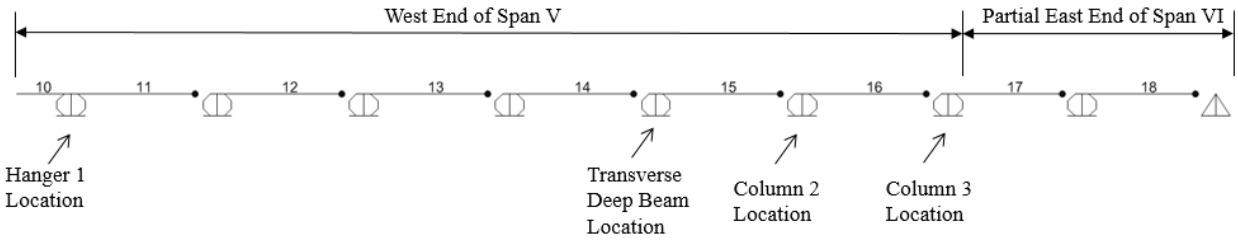

Figure 41: West Longitudinal Beam Model (SAP 2013)

The reaction envelope for each longitudinal beam model for each truck represented the worst reaction exerted to the hangers, columns, and transverse deep beam. One-half the magnitude of the reactions on the longitudinal beam model are the wheel line load, W, on the transverse beam. On the longitudinal beam for Spans IV, V, and VI, the largest reaction at the hanger locations is at the Hanger 1 location. For Span VII, the longitudinal beam model is shown in Figure 42, the largest reaction at the column locations is at the Column 4 location.

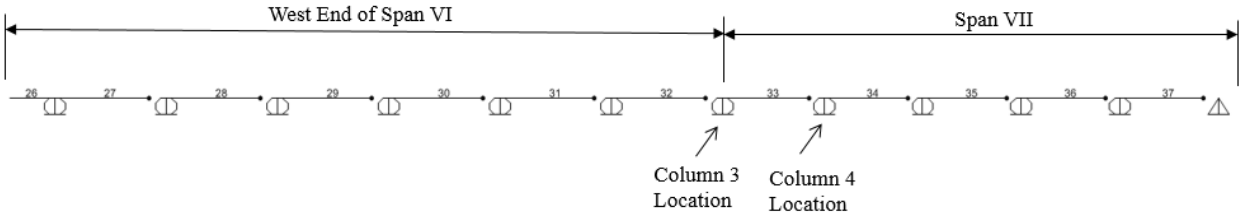

Figure 42: Span VII Longitudinal Beam Model (SAP 2013)

The magnitude of these wheel line loads are shown in Appendix A1 for Span IV, Appendix B1 for Span V, Appendix C1 for Span VI, and Appendix D1 for Span VII.

3.5.3 Beam and Column 2 Modeling

An example Beam and Column 2 model from SAP2000 is shown in Figure 43 for Spans IV, V, and VI. The columns were modeled as a pair of concrete columns. They were modeled as frame members. The model was restrained from sidesway to account for the diaphragm action that exists from the presence of the deck. Sidesway was inhibited by restricting motion in the lateral direction at the level of the transverse beam and is important since there are unsymmetrical live loadings. The transverse beam consisted of two sections, roadway and curb, with the bracket section connecting to the ends as shown in Figure 9.

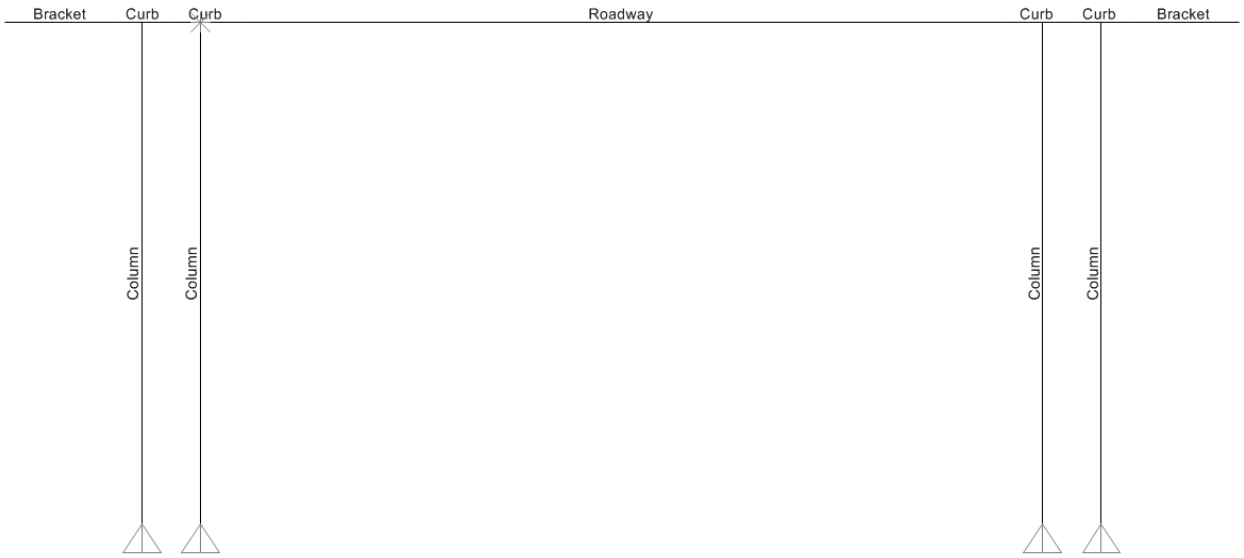

Figure 43: Beam and Column 2 Model (SAP 2013)

The length of the column was determined from the dimensional scaling of the column in the elevation drawing by using AutoCAD and is shown in Table 19. For modeling purposes, its length is from the mid-thickness of the slab to the centerline of arch rib. Column locations are at the centerlines of columns from the drawings provided by AHD (1929).

Table 19: Column 2 Lengths for Modeling

Span No.	Length (ft)
IV	18.1
V	17.8
VI	16.9
VII	14.5*

*For Span VII, the column is named Column 4.

The columns in the Beam and Column 2 model were rated for the case with the highest combination of axial load and for the case with the highest combination of bending moment.

The lower of the two RFs control the rating. The transverse beam was rated for bending moment and shear.

Cross sectional properties for the Beam and Column 2 model are located in Appendix A3 for Span IV, Appendix B3 for Span V, and Appendix C3 for Span VI. The parts comprising up of the transverse beam at Column 2, Column 3, and Hanger 1 have the same cross sectional properties.

3.5.3.1 Slenderness Effects

Column 2s were checked for slenderness. However, slenderness effect is insignificant in all of Column 2s as the inequality given in Eq. (14) is true.

3.5.4 Beam and Column 3 Modeling

An example Beam and Column 3 model is shown in Figure 44 for Spans IV, V, and VI. The columns were modeled as frame members. The exterior columns were discretized into a top and a bottom section at mid-height as discussed previously in Section 2.4.2. Like the Beam and Column 2 model, this model was restrained from sidesway.

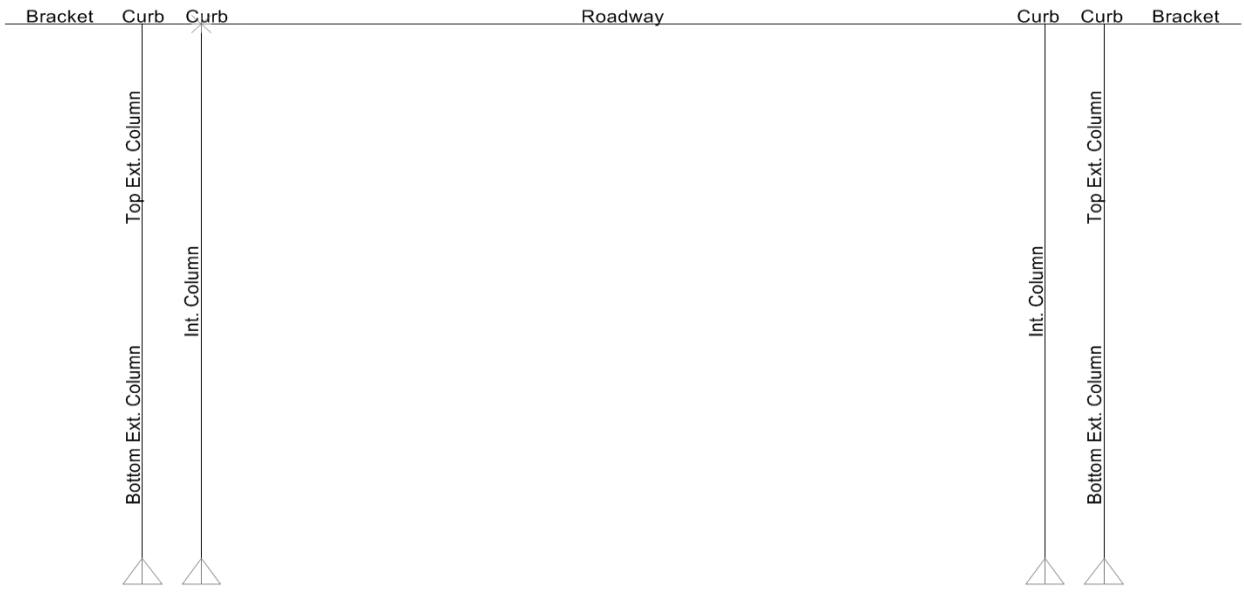

Figure 44: Beam and Column 3 Model (SAP 2013)

The length of Column 3 was found from the dimensional scaling of Column 3 from the elevation drawing using AutoCAD and are shown in Table 20. For modeling purposes, the length is from the mid-thickness of the slab to the arch extrados curve. Column locations are at the centerlines of columns from the drawings provided by AHD (1929).

Table 20: Column 3 Lengths for Modeling

	Length (ft)
Column 3 at Pier V	24.42
Column 3 at Pier VI	23.92
Column 3 at Pier VII	22.30

The columns in the Beam and Column 3 model were rated for the case with the highest combination of axial load and for the case with the highest combination of bending moment. The lower of the two RFs control the rating. The transverse beam was rated for bending moment and shear.

Cross sectional properties for the Beam and Column 3 model are located in Appendix A4 for Span IV, Appendix B4 for Span V, Appendix C4 for Span VI, and Appendix D3 for Span VII.

3.5.4.1 Slenderness Effects

Column 3s were assessed for slenderness in accordance with Section 8.16.5 of AASHTO (2002). For compression members braced against sidesway, effects of slenderness may be neglected if the following inequality is true.

$$\frac{kl_u}{r} \leq 34 - 12\frac{M_{1b}}{M_{2b}} \qquad (14)$$

Where:

k = effective length factor

l_u = unsupported length of compression member (ft)

r = radius of gyration; 0.30 times the overall dimension in the direction in which stability is being considered for rectangular sections (ft)

M_{1b} = value of smaller end moment on compression member from conventional elastic frame analysis with applied dead load and live load plus impact (k-ft). It is zero for all columns in this report, since one end is pinned.

M_{2b} = value of larger end moment on compression member from conventional elastic frame analysis with applied dead load and live load plus impact (k-ft)

Column 3 must resist the factored axial load P_u and a magnified factored bending moment, M_c, given by

$$M_c = \delta_b M_{2b} \tag{15}$$

Where:

δ_b = the braced frame moment magnifier

The braced frame moment magnifier is given by

$$\delta_b = \frac{C_m}{1 - \frac{P_u}{\phi P_c}} \geq 1.0 \tag{16}$$

Where:

C_m = factor relating the actual moment diagram to an equivalent uniform moment diagram. It is taken as 1.0 according to Section 8.14.3 (AASHTO 2002)

P_u = factored axial load (kip)

P_c = critical load (kip)

ϕ = stiffness reduction factor taken as 0.85 according to Section 8.14.3 (AASHTO 2002)

The critical load for Column 3 can be calculated from

$$P_c = \frac{\pi^2 EI}{(kl_u)^2} \tag{17}$$

The flexural rigidity, EI, can be calculated from the following equation.

$$EI = \frac{\frac{E_c I_g}{5} + E_s I_s}{1 + \beta_d} \tag{18}$$

Where:

β_d = absolute value of the ratio of maximum factored dead load moment to maximum factored total load moment

E_c = modulus of elasticity of concrete (ksi)

E_s = modulus of elasticity of steel (ksi)

I_g = moment of inertia of the gross concrete cross section (in^4)

I_s = moment of inertia of the reinforcement about the centroidal axis of the gross concrete cross section (in^4)

Table 21 lists the kl_u/r values in determining slenderness effects for all Column 3s. Slenderness effects were considered for all Column 3s as all of the kl_u/r values are larger than 46, which is the maximum that the right hand side of the inequality in Eq. (14) can be.

Table 21: Column 3s kl_u/r

	Column 3 at					
	Pier V		Pier VI		Pier VII	
	Interior	Exterior	Interior	Exterior	Interior	Exterior
k	1.0	1.0	1.0	1.0	1.0	1.0
l_u (ft)	21.0	21.0	19.6	19.6	17.3	17.3
r (ft)	0.35	0.33	0.35	0.33	0.35	0.33
kl_u/r	60.1	64.3	56.0	60.0	49.4	52.7

3.5.4.2 Slenderness Calculations

Column 3 slenderness was calculated based on an iterative procedure. β_d and P_u are both a function of the product of the rating factor and live load factor, A_2RF, as shown in the following equations.

$$\beta_d = \frac{A_1 \cdot M_{DL}}{A_1 \cdot M_{DL} + A_2 \cdot I \cdot M_{LL} \cdot RF} \tag{19}$$

$$P_u = \left(RF \cdot A_2 \cdot P_{LL+I}\right) + \left(A_1 \cdot P_{DL}\right) \tag{20}$$

Since P_u is a function of A_2RF, the moment magnifier, δ_b, shown in Eq. (16) is also a function of A_2RF. The rating factor is unknown prior to the analysis. A spreadsheet routine was set up like the one in Figure 45 to find δ_b corresponding with the final rating factor. A δ_b was assumed which yielded a rating factor. Then, the rating factor was substituted into Eq. (19) and (20), which outputted a δ_b in the process. The process was repeated until the two δ_b's were equal. The δ_b's that yielded the final rating factor are shown in Table 22 for all Column 3s. Since the product A_2RF is the same for the operating and inventory cases, the δ_b's value are the same for these cases.

Slenderness			
l_u (ft)	19.59	**C_m**	1.0
k	1.0	**$E_cI_g/5$ (k-in^2)**	2570046
P_u (k)	262.68	**E_sI_s (k-in^2)**	1954512
P_c (k)	727.49	**β_d**	0.1108
RF	2.47	**EI (k-in^2)**	4073388
δ_b	2.07	**δ_b**	2.07

Figure 45: Spreadsheet for Finding δ_b

Table 22: Column 3 Moment Magnifiers

	δ_b	
	Interior	Exterior
Column 3 at Pier V	2.30	1.11
Column 3 at Pier VI	2.07	1.11
Column 3 at Pier VII	1.75	1.08

3.5.5 Span VII Beam and Column Models

For the Beam and Columns 4 and 7 models in Span VII, the cross sectional parts for modeling them are the same as the parts for the Beam and Column 2 model presented in Section 3.5.3. For the Beam and Columns 5 and 6 in Span VII, the transverse beams and columns have the same cross section geometry and reinforcements; thus, only the Beam and Column 5 was modeled.

The Beam and Column 4 of Span VII was modeled the same in terms of joint restraints and no frame release as the Beam and Column 2 model presented in Section 3.5.3. However, the Beam and Columns 5 and 7 of Span VII were modeled slightly different due to an interesting phenomenon that arises in these two models.

3.5.5.1 Span VII Beam and Columns 5 and 7 Models

Two models were created and utilized for ratings for Beam and Columns 5 and 7 of Span VII. The first model is called Case A, and the second model is called Case B. Models for Cases A and B of the Beam and Column 5 model are shown in Figure 46 and Figure 47, respectively. Case A has a moment release on the exterior columns at the end connecting to the transverse beam. This is an appropriate way of modeling the exterior columns since they are in tension for

both dead and live load effects. The exterior columns are strictly tension members from applied load effects and are thus modeled to reflect that condition. Case B has the exterior columns modeled as frame members with axial and bending stiffness.

The exterior Column 7s of the Beam and Column 7 model were in compression for dead load effects and tension for live load effects. However, the extent in which it is in compression for dead load is minimal and insignificant. Therefore, the exterior columns are essentially tension members. As a result, the Beam and Column 7 was modeled the same as Beam and Column 5 with ratings for Cases A and B.

The interior columns in the Beam and Column 5 and 7 models were rated for the highest combination of axial load and the highest combination of bending moment like any other columns. The lower rating controls. The exterior columns were rated for axial tension using the Case A model shown in Figure 46. This model yields the most appropriate rating factor for the exterior columns. However, for comparison purposes, ratings using Case B shown in Figure 47 is also provided in Appendix D2.2. Ratings obtained from Case B, in which the exterior columns were modeled as frame members, severely penalized the exterior columns since they are tension members under applied load effects. Ratings for Case B are not representative of the most appropriate ratings for the columns. For the transverse beam, it was rated for bending moment and shear.

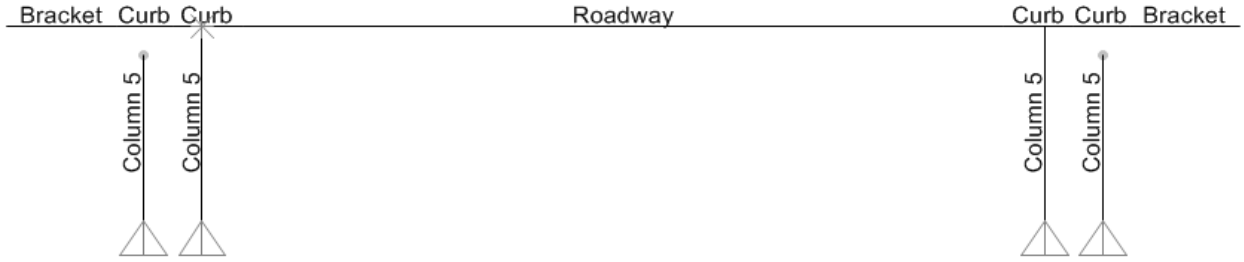

Figure 46: Span VII Beam and Column 5 Model – Case A (SAP 2013)

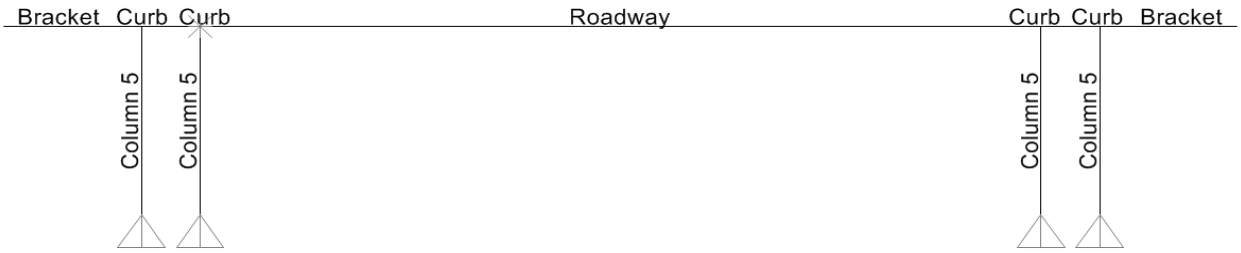

Figure 47: Span VII Beam and Column 5 Model - Case B (SAP 2013)

The lengths of the columns in Span VII were from the dimensional scaling of the columns from the elevation drawing and are shown in Table 23. Cross sectional properties for the Beam and Column 4, 5, and 7 models are located in Appendix D4.

Table 23: Span VII Column Lengths for Modeling

	Length (ft)
Column 4	14.5
Column 5	7.13
Column 7	10.6

3.5.5.2 Slenderness Effects

Columns 4 – 7 in Span VII were checked for slenderness. However, slenderness effect is insignificant in these columns since the inequality given in Eq. (14) is true.

3.5.6 Beam and Hanger Models

Two beam and hanger models were analyzed. The first model was a beam and composite concrete hanger; a photo of a pair of hangers is shown in Figure 48. In this model, the pair of concrete hangers were assumed to act compositely because they are connected to the arch rib at the top and transverse beam and sidewalk slab at the bottom, and there are intermediate concrete braces. Ratings were obtained for this case in Appendix B8. However, operating ratings were significantly less than one, so an alternate modeling approach was taken.

Figure 48: Composite Concrete Hangers

Rating is based on member capacity. Before the hangers reach their potential capacity, they will go through a state where the concrete in a compression zone associated with the bending resistance has crushed and the steel has yielded. Once the concrete crushes, additional axial tension can be applied and the hangers lose bending moment strength and stiffness. Then, the once composite concrete hangers will only be left with the tension capacity of the steel reinforcements. As a result, the rating of the hangers was obtained from a beam and steel hanger model, also referred to as Beam and Hanger 1 Model.

3.5.6.1 Beam and Hanger 1 Model

In the Beam and Hanger 1 model, the cross sectional area of the steel is four square inches as shown in Figure 49. The dashed outer lines indicate the cracked concrete while the dashed inner lines indicating the stirrups.

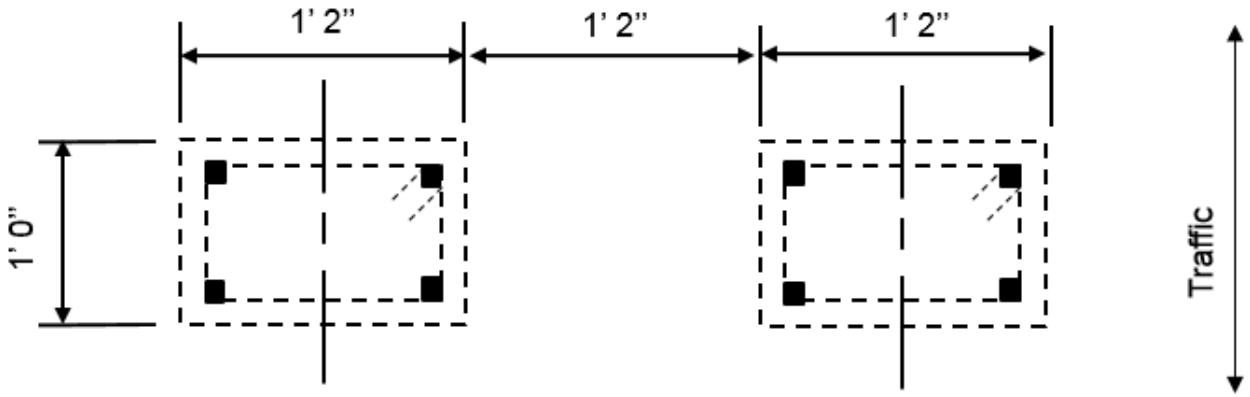

Figure 49: Steel Hanger Cross Section

The hanger with steel reinforcements was modeled as pair of steel hangers per side as frame members as shown in Figure 50. The hanger lengths for modeling were from the slab centerline to the arch rib centerline for Hanger 1 and are shown in Table 24. Its location was defined at the centroid of the hanger group. The steel hangers were assumed to have no flexural rigidity; thus, bending moment was released at the end connecting to the transverse beam. This model was restrained from sidesway at the level of the transverse beam. For the beam and steel hanger model, all hangers were under tension. A rating was determined for the hanger with the largest axial tension, which are the interior hangers. The transverse beam in the Beam and Hanger 1 model was rated for bending moment and shear. This model resulted in higher ratings for the hangers than the beam and composite concrete hanger model and provides a more appropriate rating.

Table 24: Hanger 1 Lengths for Modeling

Span No.	Length (ft)
IV	18.8
V	18.0
VI	16.4

Cross sectional properties for the Beam and Hanger 1 model are located in Appendix A5 for Span IV, Appendix B5 for Span V, and Appendix C5 for Span VI.

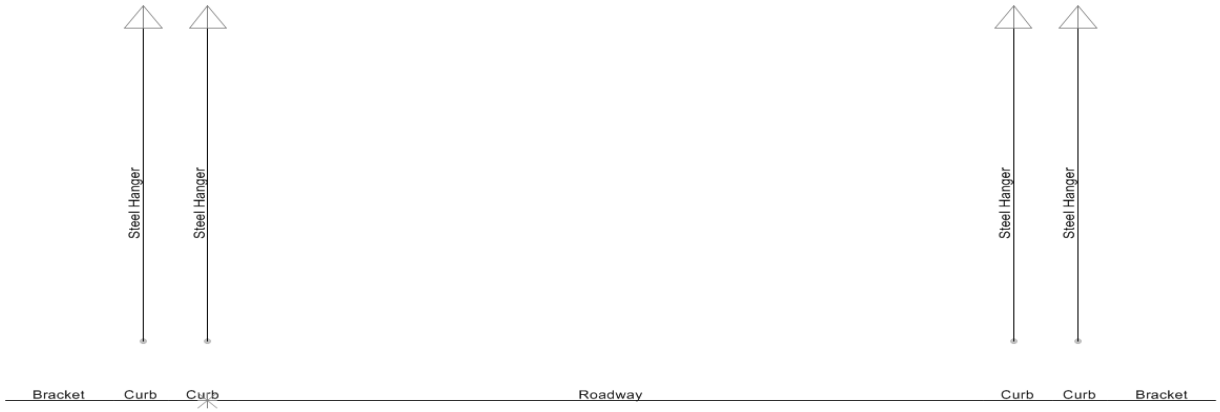

Figure 50: Beam and Steel Hanger 1 Model (SAP 2013)

3.5.7 Transverse Deep Beam Model

The Transverse Deep Beam model is shown in Figure 51. The beam was assumed to be simply connected to the arch rib since there was minimal reinforcement for negative moment. The width of the arch rib is 4 ft. The clear span of the transverse deep beam is 32 ft, from the center-to-center of arch rib. The length of the transverse deep beam is 36 ft from out-to-out of the arch. At either end of the transverse deep beam are the bracket sections.

The transverse deep beam was rated for bending moment and shear. Cross sectional properties for the Transverse Deep Beam models are located in Appendix A6 for Span IV, Appendix B6 for Span V, and Appendix C6 for Span VI.

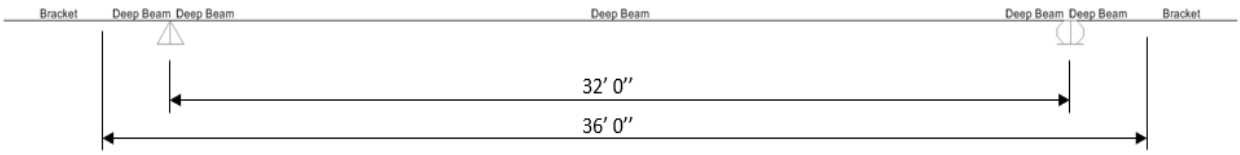

Figure 51: Transverse Deep Beam Model (SAP 2013)

3.6 ARCHES

Complete 2-D models of each arch span were built and analyzed to obtain ratings for the arch rib sections. The applied loads placed on the arch models included dead loads from the bridge components and live loads from the truck loadings.

3.6.1 Dead Loads

For each arch span, the dead loads consisted of dead weights from the arch ribs, hangers, transverse floor beams, transverse deep beams, columns, brackets, railings, decorative arch blocks connecting to arch rib at deck elevation, and the arches joining the transverse floor beams on the underside of the deck. The dead weights resulting from the hangers, transverse deep beam, and Column 2 were inputted manually. To not double count these dead weights, the properties for the hangers and Column 2 had a weight property modifier of zero. The dead weight of the decorative arch block was inputted as a concentrated load. The dead weights of the arches on the underside of the deck were inputted as uniformly distributed load. For all other sections, the dead weights were calculated by SAP2000 as self-weight based on the geometric properties entered in for each section.

3.6.2 Live Loads

The live loads considered are the eight trucks specified by ALDOT and the lane load specified by AASHTO (2002). The truck's axle weight and axle spacing were defined for each truck as a moving load case. More information on moving load is provided in Section 3.6.2.2.

The 0.64 k/ft uniformly distributed load was applied to all of the deck frames. The 18 kips for moment and 26 kips for shear were applied as a concentrated moving loads along the deck frames.

3.6.2.1 Lateral Truck Distribution

The 2-D arch model represents one side of the arch span. However, the set of wheel line loads from the trucks can be anywhere transversely across the roadway width. Therefore, an analysis

was performed to find the largest proportion of one truck that is supported by one arch. The largest proportion of the lane load and one truck carried by one arch is shown in Table 25. These factors apply to all spans. The factors shown in Table 25 were determined by applying the tri-axle truck's wheel line loads onto the Beam and Column 2 and Beam and Hanger 1 models and determining the largest proportion of one truck that gets carried by one side. The procedure for calculating this proportion using the Beam and Column 2 model is shown in Appendix B7.1. LC1, shown in Figure 36, was utilized in this analysis because it is the load case that created the largest proportion of one truck on one side.

Table 25: Lateral Truck Distribution Factors for All Arch Models

	Truck Loads	Lane Loads
Distribution Factor	1.160	1.156

3.6.2.2 Moving Load Analyses

The live loads, consisting of eight truck loads and the lane load, were added to the arch models as moving loads. The moving load analysis allows for the maximum value to be obtained for the shear, bending moment, and axial load at any cross section along the arch rib. Before the moving analysis could be applied, a path was defined directly on all of the deck frames from left to right or from right to left. The arches were analyzed for truck positions at every 6 in. along the travel path.

Next, the live loads were defined. The axle weights along with the axle spacings were defined for each truck. Once all axle weights were entered for all trucks, a load case was defined for each truck. Each load case was defined as a moving load traveling on the previously created path. For the first-order analysis, the moving loads were selected to be executed using the unstressed stiffness state. For the second-order analyses, the moving loads were selected to be executed using the stiffness after the end of the nonlinear dead load analysis. An explanation of the nonlinear analysis is provided in Section 3.6.5.1.

3.6.3 Load Factors

The load factor rating method utilized has load factors for the dead and live loads for the operating and inventory case as shown in Table 26. The dead load factor is the same for the operating and inventory case. The live load factors consisted of the A_2 factors as listed in Table 13, the live load distribution factor as listed in Table 25, and the impact factor for dynamic loading in Table 27. The impact fraction equation is Eq. (21). The maximum impact fraction required by AASHTO (2002) is 0.30. L is the length in feet of the portion of the span that is loaded to produce the maximum stress in the member and is taken as the horizontal distance between the pier centerlines.

$$I = \frac{50}{L + 125} \tag{21}$$

Table 26: Load Factors for Arch Loading Associated with LFR Method

		Operating		Inventory	
Span No.	Load Type	DL Factor	LL Factor	DL Factor	LL Factor
IV	Truck	1.3	1.793	1.3	2.993
	Lane	1.3	1.786	1.3	2.982
V	Truck	1.3	1.796	1.3	2.998
	Lane	1.3	1.789	1.3	2.987
VI	Truck	1.3	1.808	1.3	3.018
	Lane	1.3	1.802	1.3	3.007
VII	Truck	1.3	1.955	1.3	3.263
	Lane	1.3	1.948	1.3	3.251

Table 27: Impact Factors

Arch Span No.	Impact (1+I)
IV	1.189
V	1.191
VI	1.199
VII	1.296

3.6.4 Spans IV, V, VI, and VII Arch Models

Each arch span geometry was traced in AutoCAD (discussed in Section 2.2.1 for Spans IV, V, and VI and Sections 2.2.2 for VII) was imported into SAP2000 to allow for modifications and adjustments to the models to replicate the existing conditions. The number of sections for each full arch span is shown in Table 28.

Table 28: Arch Section Quantity

Span No.	Arch Section Quantity
IV	82
V	80
VI	72
VII	35

The boundary conditions and restraints for half of the arch span are shown in Figure 52. The arch base and Column 3 base are fixed. To prevent the 2-D model from translating in an unwanted direction, out-of-plane and in-plane motion were restrained as follows. At the east end of the deck slab, out-of-plane and in-plane motion were restrained. At the arch midspan and the deck slab midspan, out-of-plane motion was restrained. All hangers and columns except the

Column 3 have moment releases at both ends. The longitudinal deck slab served as a platform on which the applied truck loads were transmitted into the arch rib by transferring loads through the hangers and columns. As a result, each segment of the longitudinal deck beam had a moment release at one end.

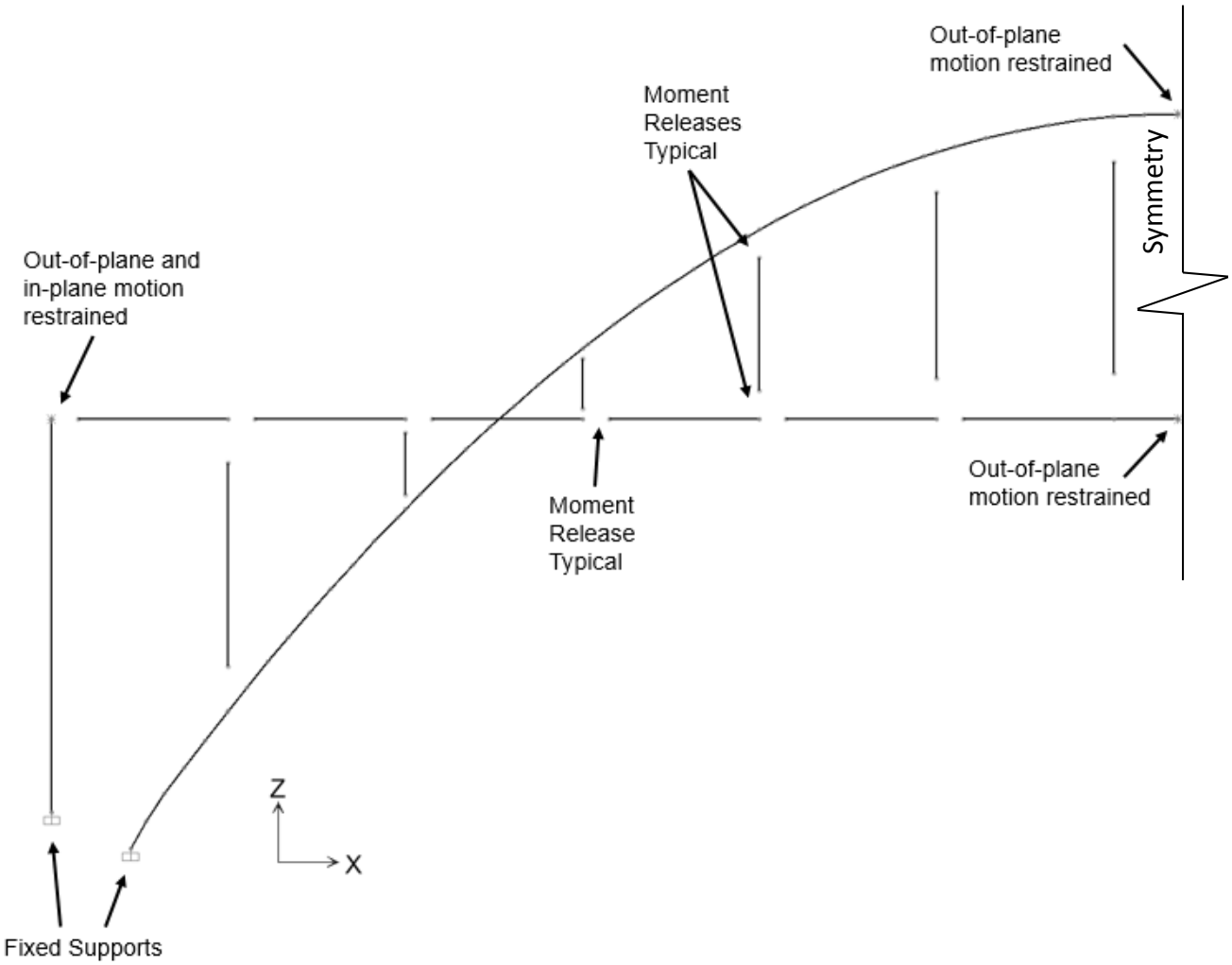

Figure 52: Boundary Conditions and Restraints for Half Spans IV, V, and VI (SAP 2013)

The boundary conditions and bending moment releases illustrated in Figure 52 result in all portions of the model being structurally determinate except the arch. There are two primary reasons that this approach was taken. First, the hangers are rated as tension members without flexural capacity, so using pin-pin links to represent the hangers is consistent. Secondly, the

longitudinal distribution of loading used for rating the transverse floor beams and frames assumes that the deck in a system of simple beams in accordance with AASHTO (2002) as discussed in Section 3.5.2.2 of this report. So, the modeling of the deck system shown in Figure 52 is consistent with the rating of the transverse floor beams and frames.

Also, it is important to note that by restraining in-plane motion at the top of the pier column as shown in Figure 52, in-plane sway of the deck system is prevented. Restraining sway motion of the deck system is necessary since all flexural resistance to sway has been removed by the moment releases at the ends of the columns, hangers, and longitudinal beams.

The properties for each frame element in the arch span models were entered. For the arch rib sections and the deck slab, the actual dimensions of each cross section were entered. The thickness of the deck slab was the actual thickness of the slab from AHD (1929) drawings provided. Since the arch model is a 2-D model and represents one side of the bridge, the width of the deck is half the full width. For the columns and hangers, the properties were calculated and entered due to them not being a standard SAP2000 preset section. The sections were assigned to the correct frame. The support to the deck provided by the Transverse Deep Beam was modeled with a column. The column at Transverse Deep Beam was set to have the same properties as the Column 2 in the model.

Once the dead loads and properties were entered for the half-span model, it was mirrored parallel to the y-axis. All properties of each member were replicated and mirrored automatically. A discussion of the dead loads is provided in Section 3.6.1.

To model the finger joint at midspan for Spans IV, V, and VI, the frame members were edited so that the deck slab frames on either side of midspan were not connected as shown in Figure 53. There is 0.2-inch of separation between the slabs in the middle. The 4-ft slab at midspan cantilevers out from the Hanger 1s.

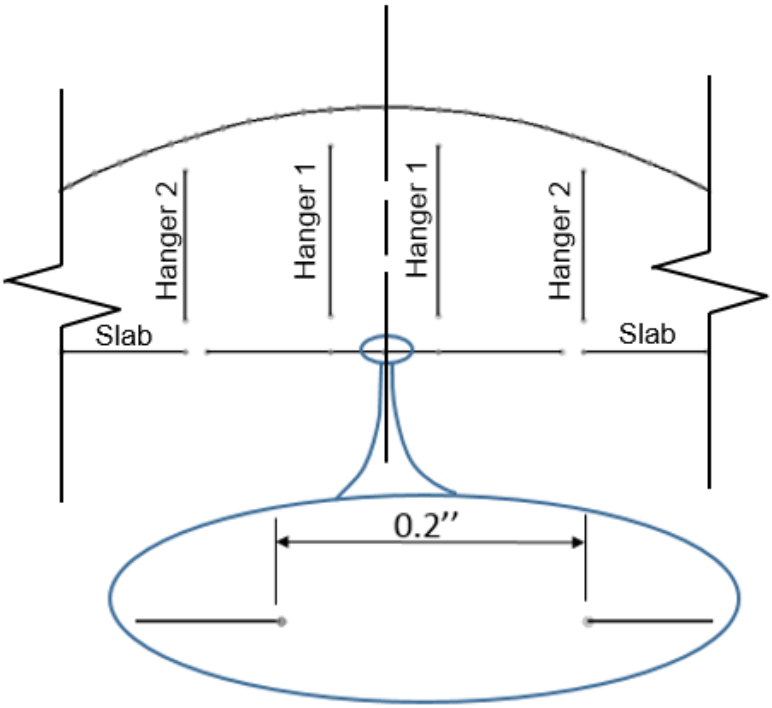

Figure 53: Deck Slab Showing Slabs at Midspan are Not Connected (SAP 2013)

For Span VII, a full arch geometry was defined using the full elevation drawing provided. Thus, this model did not need to be mirrored after the import. The boundary conditions for this model are shown in Figure 54.

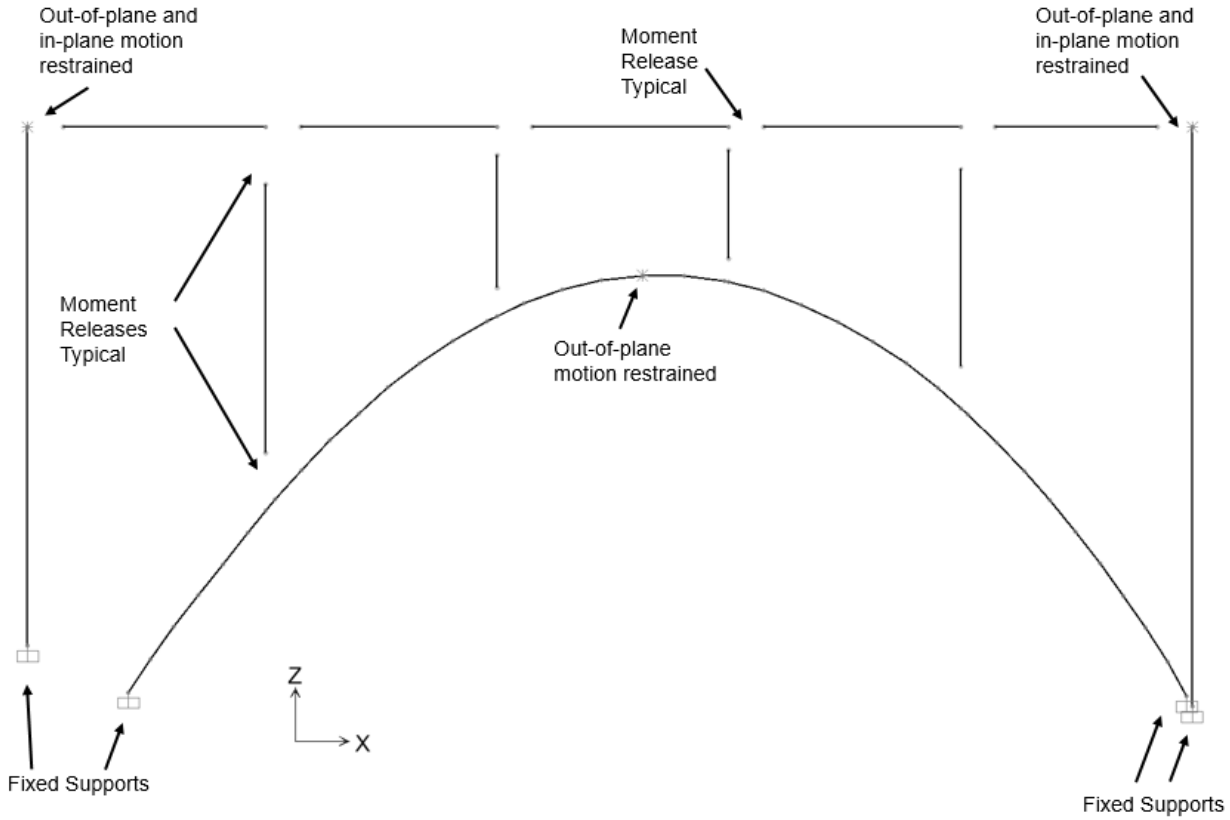

Figure 54: Boundary Conditions and Restraints for Span VII (SAP 2013)

For all arch spans, the arch sections were rated for shear and the combination of axial load and bending moment. Cross sectional properties for the arches are provided in Appendix A7 for Span IV, Appendix B7 for Span V, Appendix C7 for Span VI, and Appendix D5 for Span VII.

3.6.5 Slenderness Check

Section 8.14.3 in AASHTO (2002) provides a way of checking the slenderness ratio of compression members to evaluate whether or not is necessary to include slenderness effects through the calculation and use of a moment magnifier. A decision must be made regarding whether the compression member is braced or not braced against sidesway to perform the check. Since relative translation between the ends of the arch ribs is prevented, the arch ribs are assumed to be braced against sidesway. For members braced against sidesway, slenderness may be neglected if the inequality of Eq. (14) is true (see Section 3.5.4.1). According to the

Commentary to Section 10.10.1 of ACI 318-11, neglecting an increase in bending moments due to slenderness of up to five percent is acceptable through the use of Eq. (14).

The inequality of Eq. (14) was developed for columns in reinforced concrete frames. Whether the application of Eq. (14) to arch ribs such as those considered here is technically appropriate is not clear, even though AASHTO (2002) Section 8.14.3.1 points toward this equation. In the work reported here, it was assumed that slenderness effects were significant. For completeness, Table 29 provides a summary of the calculations of (kl_u/r) values for the arch ribs of each span.

The effective length factor, k, shown in Table 29 is based on the rise-to-span ratio and was taken from Table 8.14.3 of AASHTO (2002). The label h_{qs} is the height of the arch rib cross section at the quarter span and is used in determining the radius of gyration. The length l_u is one-half of the span length of the arch rib. For Spans IV, V, and VI, (kl_u/r) calculated are 62.00, 64.67, and 58.48, respectively, as shown in Table 29. However, looking at the right expression in Eq. (14), the largest value that this expression can be is 46. All of the kl_u/r magnitudes are larger than 46. For Span VII, the (kl_u/r) is 33.56, and the right expression in Eq. (14) can be as small as 22. Therefore, slenderness was considered for all of the concrete arches.

Table 29: Arch Properties and kl_u/r

	Span IV	Span V	Span VI	Span VII
Arch Rise (ft)	45.58	44.57	40.44	15.79
Arch Span (ft)	130.2	128.3	116.5	39.99
Rise/Span	0.35	0.35	0.35	0.39
k	0.72	0.72	0.72	0.72
l_u (ft)	65.10	64.13	58.24	19.99
h_{qs} (ft)	2.52	2.38	2.39	1.43
r (ft)	0.76	0.71	0.72	0.43
kl_u/r	62.00	64.67	58.48	33.56

3.6.5.1 Slenderness Effects using Combination of Second-Order and Linear Analyses

Chapter 4 provides an in-depth discussion of methods that may be used to account for in-plane slenderness effects for arches. One conclusion from Chapter 4 is that a combined analysis using second-order analysis for dead loads and a linear analysis for moving live loads is appropriate. The linear moving load analysis is performed using the structural stiffness matrix found at the end of the second-order analysis for dead loads. Below is a description of how that combined analysis was implemented.

In consideration of slenderness, the moment of inertia and concrete modulus of elasticity were modified to accurately represent the long-term condition of the concrete arches as shown in Table 30. According to Section 8.14.3.1 in AASHTO (2002), the stiffness reduction factor, ϕ, is 0.85 for concrete arches. This stiffness reduction factor is applied to the gross moment of inertia of all sections of the arch rib.

Table 30: Modifications on I_g and E_c

Span No.	Stiffness Reduction Factor	Long Term E_c (ksi)
IV	0.85	1517
V	0.85	1517
VI	0.85	1517
VII	0.85	1505

The modulus of elasticity for 3,000 psi concrete is 3,122,000 psi calculated based on the following equation.

$$E_c = 57000\sqrt{f'_c} \qquad (22)$$

The creep adjusted, long-term concrete modulus of elasticity, E_{c_LT}, (ACI 209R 1992) was calculated by

$$E_{c\_LT} = \frac{E_c}{1+\upsilon_u} \tag{23}$$

Where:

ν_u = the ultimate creep coefficient

The long-term modulus accounts for creep deformations in the arch. For the Bibb Graves Bridge, the ultimate creep coefficient was calculated to be 1.06 for Spans IV through VI, and 1.07 for Span VII. The ultimate creep coefficient was calculated using the procedure given by ACI 209R-92 (1992) and is shown for Span IV in Appendix A7 in Figure 79A.

Slenderness was incorporated into the arch models by a nonlinear analysis. A nonlinear load case for the dead loads was created with the appropriate load factors for P-delta effects plus large displacements. The load factors are in Table 26. Since this load case is for dead loads, the initial stiffness was from an unstressed initial condition. For the live loads, load cases were created for each truck as moving load cases. For these cases, the stiffness was from the stiffness at the end of the nonlinear dead load case. For the lane loads, slenderness was incorporated in a similar fashion as for the truck loads.

Due to the redistribution of internal forces and moments, it is possible that the internal forces and moments decrease at a given cross section relative to the values obtained in a first-order analysis. To ensure that the nonlinear analysis yielded the largest member forces and moments, those results were compared to the results from the conventional elastic, linear analysis. The larger forces and moments from these two analyses were utilized for ratings. This comparison is similar to checking the inequality in Eq. (16).

3.6.5.2 Slenderness Effects and Shear Rating of Span VII

The slenderness effects for Span VII were included using the combination of second-order and linear analyses. This is the same method applied to all other spans and is described in Section 3.6.5.1. Using this method yielded a shear rating for Span VII's arch Section A16 of less than 1.0 for the tri-axle and concrete truck as shown in Table 31. To ensure that the combination of second-order and linear analyses did not unnecessarily penalize the shear rating, an alternate rating was determined using results from first-order analysis. Those rating results are show in

Table 32. The ratings for shear are only slightly higher than the ratings found using the combination of second-order and linear analyses.

Table 31: Shear Ratings for Span VII Section A16 using Combination of Second-Order and Linear Analyses

	Shear	
Truck	Operating	Inventory
Tri-Axle	0.86	0.54
Concrete	0.90	0.57

Table 32: Shear Ratings for Span VII Section A16 using First-Order Analysis

	Shear	
Truck	Operating	Inventory
Tri-Axle	0.87	0.55
Concrete	0.91	0.57

Chapter 4

SLENDERNESS EFFECTS IN REINFORCED CONCRETE ARCHES

Early in the project, the procedures for rating the various bridge components were developed. During those initial analyses and preliminary ratings, it was found that moment magnifiers calculated using AASHTO procedures would be approximately 1.2 for some arch spans. This increase in bending moment results in significant reductions in the arch ratings. So, a detailed investigation of the methods available for including slenderness effects in the arch ratings was carried out. A description of the various methods and comparisons of results are presented in this chapter. The comparisons indicate that the combination of elastic second-order analysis for dead load and linear analysis using a reduced stiffness for truck loads is appropriate for use in calculating the arch ratings.

4.1 AASHTO MOMENT MAGNIFIER METHOD

AASHTO (2002) provides general requirements for reinforced concrete arches in Section 8.14.3. Slenderness effects in the plane of the arch rib may be accounted for in a load rating using the approximate moment magnifier method from Section 8.16.5.2 as summarized below. The equations regarding to slenderness in this section were presented in Section 3.5.4.1 for Column 3s, but are shown here again in the context of arches for convenience.

The arch rib must resist the factored axial load, P_u, and a magnified factored bending moment, M_c, given by

$$M_c = \delta_b M_{2b} \tag{24}$$

Where:

δ_b = braced frame moment magnifier

M_{2b} = value of the larger factored end moment on the member calculated by conventional elastic frame analysis with applied dead load and live load plus impact (k-ft)

In this study the arch ribs were modelled by subdividing each rib into a large number of short, straight frame members. For this type model, the moment magnifier is applied to the largest moment in each member along the length of the arch.

The braced frame moment magnifier is given by

$$\delta_b = \frac{C_m}{1 - \frac{P_u}{\phi P_c}} \geq 1.0 \qquad (25)$$

Where:

P_u = factored axial load (k)

P_c = critical load (k)

ϕ = 0.85

C_m = 1, according to AASHTO (2002) Section 8.14.3

The ϕ-value in this equation is a stiffness reduction factor not a resistance factor. Wight and MacGregor (2012) provide background on stiffness reduction factors in slenderness analyses for reinforced concrete members. The stiffness reduction factor accounts for variability introduced by the moment magnifier method and in the critical load, P_c.

The critical load for the arch rib can be calculated from

$$P_c = \frac{\pi^2 EI}{\left(kl_u\right)^2} \qquad (26)$$

Where:

k = an effective length factor listed in AASHTO (2002) Table 8.14.3

l_u = the unsupported length equal to one-half the length of the arch rib according to AASHTO (2002) Section 8.14.3.1 (ft)

AASHTO (2002) Section 8.14.3.1 also states, "the radius of gyration, r, (be taken) about an axis perpendicular to the plane of the arch at the quarter point of the arch span." This statement suggests that the cross section properties at the quarter point of the span should be used for calculation of the critical load. AASHTO (2002) Table 8.14.3 lists effective length factor values of 0.7 for fixed base arches with rise-to-span ratios of 0.1 to 0.3, and 0.72 when the rise-to-span ratio is 0.3 to 0.4.

Two equations for EI are given in AASHTO (2002) Section 8.16.5.2 as follows.

$$EI = \frac{\frac{E_c I_g}{5} + E_s I_s}{1 + \beta_d} \tag{27}$$

Or,

$$EI = \frac{\frac{E_c I_g}{2.5}}{1 + \beta_d} \tag{28}$$

Where:

β_d = absolute value of the ratio of the maximum factored dead load moment to the maximum factored total load moment

E_c = modulus of elasticity for concrete (ksf)

E_s = modulus of elasticity for steel (ksf)

I_g = moment of inertia of the gross concrete cross section (ft^4)

I_s = moment of inertia of the reinforcement about the centroidal axis of the gross concrete cross section (ft^4)

AASHTO (2002) allows the use of either Eqs. (36) or (34). These equations result in values of the flexural rigidity, EI, in units of ksf that are significantly reduced from the value calculated by simply using $E_c I_g$. The reduced EI values account for cracking of the member and creep deformations.

Values of the moment magnifier, δ_b, were calculated for each of the arch spans and are listed in Table 33 along with values for I_g, I_s, and β_d. For all cases, E_c = 3,122 ksi. Values for β_d were determined using factored moments at the quarter point in the span, and the live load moments were determined for the standard tri-axle truck.

Table 33: Moment Magnifiers δ_b from using AASHTO (2002)

		Value at Quarter-Span			
Span	Loading	I_g (in.^{4})	I_s (in.^{4})	β_d	δ_b
IV	Operating	110,600	2650	0.029	1.178
	Inventory	110,600	2650	0.018	1.205
V	Operating	90,850	2250	0.036	1.209
	Inventory	90,850	2250	0.022	1.243
VI	Operating	94,360	2100	1.153	1.153
	Inventory	94,360	2100	1.179	1.179
VII	Operating	19,790	260	0.128	1.039
	Inventory	19,790	260	0.081	1.050

4.2 AASHTO *LRFD* METHODS

AASHTO (2012) provides a moment magnifier procedure and guidance for an advanced, or refined, analysis for including slenderness effects in reinforced concrete arches.

4.2.1 Moment Magnifier

Moment magnification for arches is addressed in Section 4.5.3.2.2c. This procedure is essentially as described in the previous section with three differences pointed out here. First, the stiffness reduction factor, ϕ, in Eq. (25) has the value 0.75 instead of 0.85. Secondly, the terminology "maximum factored permanent load moment" is used instead of "maximum factored dead load moment" in the defining the numerator of the ratio β_d. And thirdly, the moment magnifier, δ_b, is applied only to live load plus impact moments from a standard small deflection analysis instead of the moments from combined dead load and live load plus impact.

The first two differences between the moment magnifier procedures provided in AASHTO (2002) and AASHTO (2012) are not fundamental differences in approach. Presumably the change is stiffness reduction factor is related to the overall differences between the design loads, load factors, and design philosophies. The purpose of dividing the flexural rigidity, EI, by the factor $(1+\beta_d)$ in Eqs. (27) and (28) is to account for the destabilizing effect of long-term transverse deflection of a compression member due to creep. Creep occurs over time as a result of sustained, or permanent, load. Typically the sustained load on a reinforced concrete arch is the dead load, but AASHTO (2012) require the engineer to make a decision about what part of the total load is sustained by use of the term "sustained load" instead of "dead load" in the definition of β_d. Additional information is provided later in this chapter regarding the third difference of applying, or not applying, the moment magnifier to the dead load moments.

4.3 ADVANCED ANALYSIS

Section 4.5.3.2 of the AASHTO (2012) provides general background on the topic of large deflection theory. Five primary factors must be considered in an advanced analysis to account for slenderness effects: (1) the effects of deformation of the structure on the equations of equilibrium, (2) the effects of deformation and out-of-straightness of the members, (3) time- and stress-dependent material properties, (4) interaction effects of tensile and compressive axial forces on member stiffness, and (5) the order of load application. An advanced analysis accounting for these factors will be a nonlinear analysis, so the analysis must be performed using factored loads. The five factors identified in the AASHTO (2012) and listed above can be accounted for with an elastic second-order analysis by making appropriate choices of cross section and material characteristics.

ACI's Building Code Requirements for Structural Concrete (ACI 318-11) and Commentary identifies the dominate effects that must be considered in selecting cross section properties for use in an elastic second-order analysis to account for slenderness effects: (1) influence of axial loads, (2) presence of cracked regions along the member length, and (3) duration of the loads.

For reinforced concrete arches, AASHTO (2012) Section 5.14.3.2 provides the following statement, "The in-plane stability of the arch rib(s) shall be investigated using a modulus of elasticity and moment of inertia appropriate for the combination of loads and moment in the rib(s)." Commentary to this section states, "Stability under long-term loads with a reduced modulus of elasticity may govern the stability." Commentary to Section 5.14.3.2 also provides insight regarding the selection of cross section and material properties appropriate for long-term loading and transient loading. For long-term loading, the transformed cross section properties and long-term modulus determined by dividing the short-term modulus by one plus the creep coefficient are appropriate. For transient loading, the cracked section properties including the effects of factored axial load and the short-term modulus are appropriate. The short-term modulus, E_c, in units of ksi can be estimated for normalweight concrete from

$$E_c = 1{,}820\sqrt{f'_c} \tag{29}$$

Where:

f'_c = specified concrete strength (ksi)

4.4 ELASTIC BUCKLING ANALYSIS

Many commercially available structural analysis software packages provide the capability of performing an elastic buckling analysis of an arch bridge span. The goal of using structural analysis software to model an arch and perform an elastic buckling analysis is to improve the accuracy of the critical load estimate beyond that determined from Eq. (26). The improved accuracy of the critical load will improve the moment magnifier determined from Eq. (25).

Application of an elastic buckling analysis in a bridge rating requires (1) use of proper cross section and material properties in modelling the structure, (2) use of the appropriate combination and position(s) of factored dead load and live load plus impact in the analysis, and (3) calculation of the moment magnifier, δ_b, from the eigenvalue results. The approach taken here for addressing these three topics is to replace the buckling load analysis represented by Eq. (26) with a more advanced buckling load analysis performed using SAP2000.

The curved arch geometry can be modeled with short, straight members the same as for static load analysis. The thickness of the arches studied here increased from the peak of the arch at midspan to the base. This change in cross section was modeled by assigning different cross

section properties to each member making up the arch model. Some structural analysis software may require compression members to be subdivided into several pieces to improve the accuracy of the calculated buckling load depending on the formulation of the member stiffness matrix used in the software. In arches such as those considered here, that requirement is easily met by the need to subdivide the arch to model the curved geometry and change in cross section.

Flexural rigidity, EI, calculated from Eqs. (27) or (28) is appropriate for use in elastic buckling analysis. Here Eq. (28) was used because of the convenience of incorporating it into the overall modeling and analysis processes. In this project, SAP2000 (2013) was used for all analyses. SAP2000 allows a multiplier to be input for multiplication by the cross section moment of inertia. At a given value of β_d, EI from Eq. (4.5) becomes a constant multiplier times the gross cross section moment of inertia times the modulus of elasticity of the concrete.

Here β_d was determined as the average of five values, one calculated at each base of the arch, each quarter-span, and at the peak. Due to the changes in cross section and bending moments along the arch, an average value for β_d is more appropriate than a single value. As an example, for the Span IV arch, the individual values of β_d at each base, quarter-span, and peak are 0.051, 0.029, and 0.193. There is symmetry in the values at each base and each quarter-span point because the geometry of the arch is symmetrical. The average value of β_d is 0.099 for Span IV.

The individual values of β_d were calculated as the absolute value of the ratio of the maximum factored dead load moment to the maximum factored total load moment. For the arches considered here, there were no sustained loads except for the dead load. Live load and dead load factors were 1.3 as appropriate for load factor for LFR's operating ratings according to The MBE (2011). The magnitudes of the moments were determined from a structural analysis of the arch using the flexural rigidity E_cI_g appropriate for each subdivision along the length of the arch. A moving load analysis was performed with the standard tri-axle truck to determine the maximum live load moment at the five sections of interest for calculation of β_d.

The output of an elastic buckling analysis from software such as SAP2000 is the buckled shapes (eigenvectors) and load multipliers (eigenvalues). A review of the buckled shapes provides information about the behavior of the structure and is very useful for identifying modeling errors. The load multipliers provide the buckling load as a multiple of the applied loading. For example, in a rating analysis, factored dead load and factored truck load plus

impact are applied. A buckling analysis is performed for a specific location of the truck loading; moving load analysis can only be accomplished by performing a buckling analysis for each possible truck position. Hence, the load multiplier is the factor that must be applied to the combination of all applied loads to find the total magnitude that causes buckling when the dead loading and truck loading are in specific locations. The load multiplier is equivalent to (P_c/P_u) in Eq. (25) for the combination of applied loads and truck position.

The moment magnifier can be calculated from buckling analysis results as

$$\delta_b = \frac{1}{1 - \frac{1}{\phi LM}} \geq 1.0 \qquad (30)$$

Where:

LM = the load multiplier

ϕ = stiffness reduction factor, 0.85 for LFR ratings

Since the load multiplier is dependent on the position of the truck loading, δ_b can take on an infinite number of values. Here a series buckling analyses was performed where the truck position was varied to determine the lowest value of the load multiplier. That lowest value was used to calculate a single value of the moment magnifier δ_b for use at all cross sections along the arch. The use of a single value of moment magnifier is consistent with the AASHTO approach.

4.5 ELASTIC SECOND-ORDER ANALYSIS

Elastic second-order analysis has become a popular means of directly determining the internal forces for use in design of reinforced concrete and steel structures because it makes the calculation of buckling loads and moment magnifiers unnecessary. Moment magnifier procedures are approximate second-order analysis procedures. Bending moments determined from first-order structural analysis are multiplied by a moment magnifier to estimate the bending moments that include second-order effects.

In classical first-order structural analysis, the geometry and stiffness of the structure is based on the initial configuration prior to deformation or deflection, and the influence of axial load on the stiffness of individual members is neglected. An elastic analysis assumes that no permanent deformation occurs, and this is a fundamental assumption in a first-order analysis. An elastic second-order analysis assumes that there is no permanent deformation, but includes the

effects of axial load on the stiffness of the members and enforces equilibrium in the deformed configuration of the structure. The second-order slenderness effects (P-Δ and P-δ effects) are captured by such an analysis. A goal of the work presented here is to identify how an elastic second-order analysis of reinforced concrete arches can be performed to accurately include slenderness effects in a load rating analysis to avoid the use of a moment magnifier.

Earlier, insights from the AASHTO (2012) Commentary regarding advanced analysis of reinforced concrete arches were summarized by the following: 1) For long-term loads, the transformed cross section properties and long-term modulus determined by dividing the short-term modulus by one plus the creep coefficient are appropriate. 2) For transient loads, the cracked section properties including the effects of factored axial load and the short-term modulus are appropriate. These two statements indicate that different modulus and cross section characteristics are appropriate for dead loads and truck loads. Carrying out a single second-order structural analysis with changes in the stiffness characteristics after the application of the dead load and before the application of the live loads is not practical. Performing a dead load analysis with one set of stiffness characteristics, a live load analysis with a different set of stiffness characteristics, and then adding the results together is not logical for nonlinear analysis given that load order effects can be significant.

There are two primary challenges to performing an elastic second-order analysis for use in the load rating of a concrete arch that carries moving traffic: 1) use of appropriate cross section and material characteristics to account for the effects of cracking and the long-term effects of creep while accurately predicting the response to live load, and 2) providing a practical means of performing moving load analysis so that the maximum forces in each member can be identified for use in the load rating. The SAP2000 reference manual (CSI 2011) suggests a combination of second-order analysis and linear moving load analysis for structures with challenges such as the two listed above. Specifically, a second-order analysis is performed for the factored dead load, and a linear moving load analysis is performed for the factored truck loading plus impact using the structural stiffness determined at the end of the dead load analysis. An investigation of the appropriateness of using that type analysis, referred to here as a combined analysis, for load rating of reinforced concrete arch bridges is presented later in this chapter. Since a second-order analysis for the dead load is a part of the combined analysis, the long-term structural model described below is used in that type analysis.

4.5.1 Long-Term Model

A model of the Span IV arch was created for use in elastic second-order analyses that is referred to here as the long-term model because the modulus of elasticity and cross section characteristics are as recommended by AASHTO (2012) for long-term loading.

The modulus of elasticity of the concrete is

$$E = \frac{E_c}{1 + \nu_u} \tag{31}$$

Where:

E_c = concrete modulus of elasticity, calculated using Eq. (29)

ν_u = the ultimate creep coefficient, determined from ACI 209 (1982) as 1.06

The moment of inertia for each cross section along the arch was

$$I = \phi I_g \tag{32}$$

Where:

ϕ = a stiffness reduction factor

I_g = gross section moment of inertia (in.^{4})

Use of the stiffness reduction factor in Eq. (32) is intended to account for the variability in cross section rigidity along the arch due to cracking. A value of 0.85 was used here for ratings by the load factor method because that is the value recommended by AASHTO (2012) for use in Eq. (25). Future research may identify a more appropriate value of stiffness reduction factor, but 0.85 is reasonable at the current time. The uncracked transformed section moment of inertia could be used instead of the gross moment of inertia in Eq. (32), but the longitudinal reinforcement in the arch is relatively light and the difference is small. A β_d factor is not used because the load duration effects resulting from creep are accounted for by using the long-term modulus given in Eq. (31).

4.5.2 Transient Model

A model of the Span IV arch was created for use in elastic second-order analyses that is referred to here as the transient model because the modulus of elasticity and cross section characteristics

are as recommended by AASHTO (2012) for transient loading. The properties of this model are the same as those used in the elastic buckling analyses described previously.

4.5.3 Comparison of the Models

A simple comparison of the long-term model and the transient model is possible by comparing the flexural rigidity, EI, used for each. Even though the thickness of each arch increases going from the peak to the base, the ratio (EI/E_cI_g) remains constant for each arch. For the long-term model of each arch, the ratio (E/E_c) = 0.485, (I/I_g) = 0.85, and (EI/E_cI_g) = 0.485. For the transient models, (E/E_c) = 1, and the ratio (I/I_g) varied based on the value of β_d so that (EI/E_cI_g) = 0.364, 0.364, 0.371 and 0.342 for Spans IV, V, VI, and VII, respectively. Hence, the difference in the flexural rigidities between the long-term and transient models used for each arch differed by 27 to 35 percent.

4.6 Results of Elastic Buckling Analyses

Elastic buckling analyses were performed using the transient model of each arch span. The applied loading included dead load plus the standard tri-axle truck loading as shown in Figure 34. Appropriate factors were used for dead load, live load and impact, and lateral distribution of loading between the two arches of each span as shown in Table 26. Separate analyses were performed for operating and inventory rating cases. The live load factors 1.3 and 2.17 were used for the operating and inventory rating cases, so the load multipliers, LM, determined through the buckling analyses correspond to a rating factor of one.

Through trial and error the location of the tri-axle truck that created the lowest buckling load was determined for each span. The critical truck locations are illustrated in Figure 55 and Figure 56. These truck locations create high axial load in the arch rib at the peak. Figure 55 illustrates the critical truck location for Spans IV, V and VI. These spans are very similar in geometry except for the overall span length. The spacing of the hangers and columns vary as the span length changes so that the number of hangers and columns in each span is the same. For Spans IV, V and VI, the critical truck location is when the center axle of the three rear axles is at midspan. There is a finger joint in the deck at midspan, so the axle at midspan was positioned

immediately to the left of the joint in the model. Span VII is not symmetric and the deck is above the arch over the entire span. The critical truck location is when the center axle of the rear three axles is above the column nearest midspan.

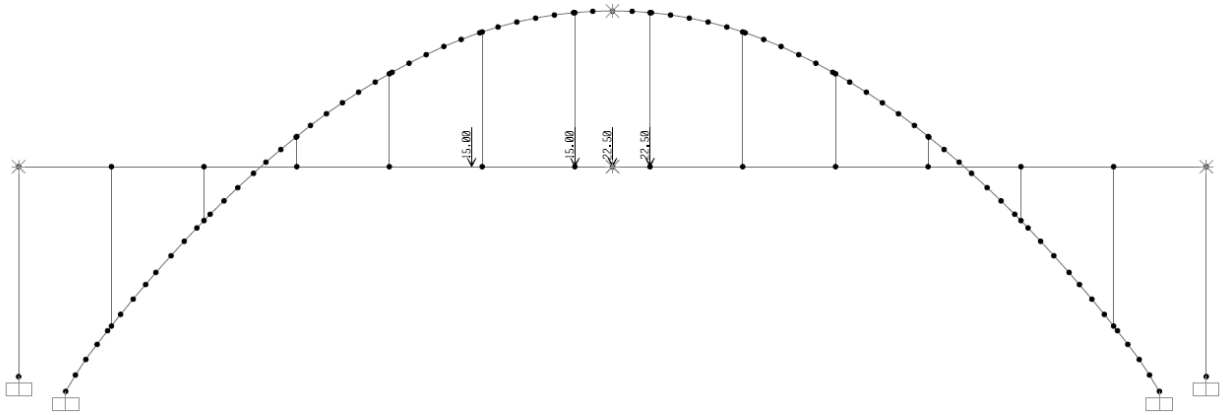

Figure 55: Critical Truck Location for Buckling of Spans IV, V, and VI

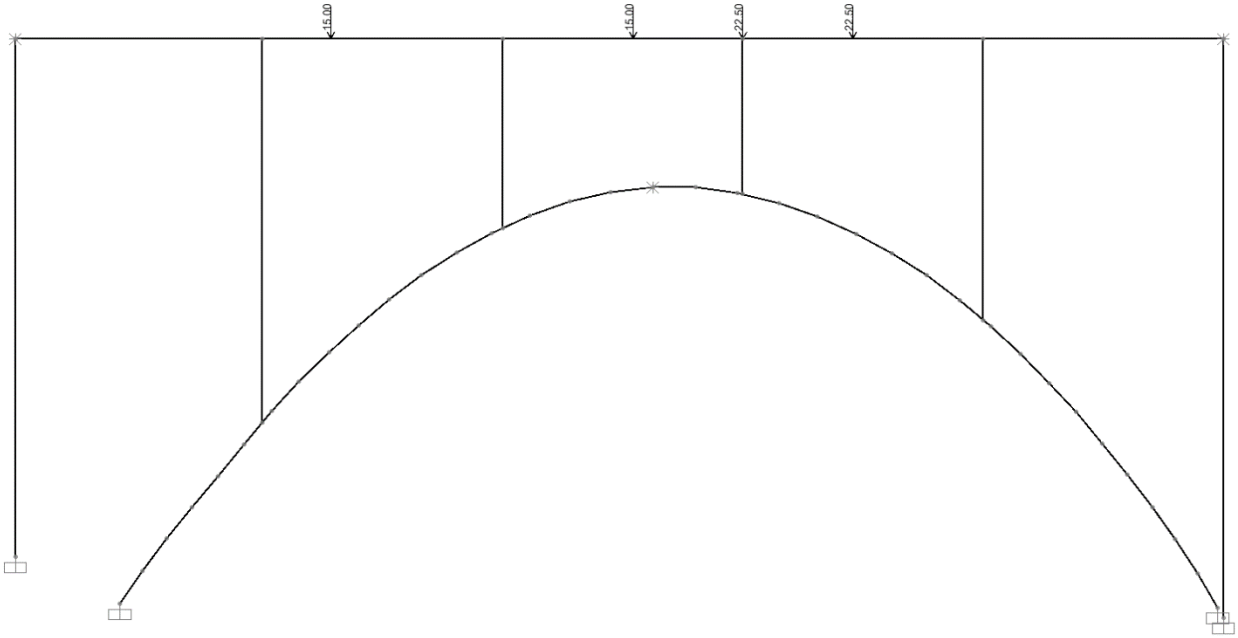

Figure 56: Critical Truck Location for Buckling of Span VII

Buckled shapes for the first (lowest) buckling mode for each arch are illustrated by Figure 57 and Figure 58. The buckled shapes for Span IV, V and VI appear identical as shown in Figure 57. The buckled shape of Span VII shown in Figure 58 is also very similar to that of the other spans.

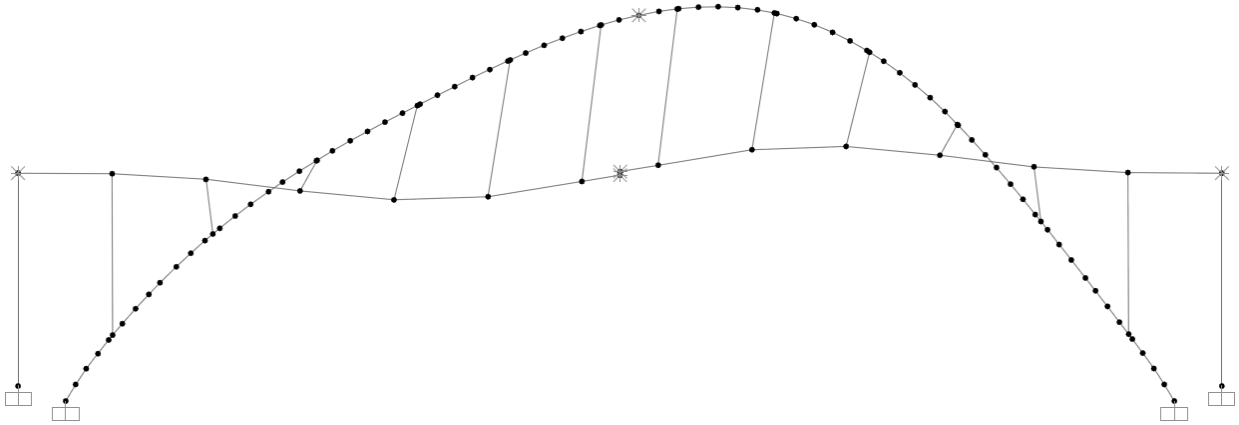

Figure 57: First Mode Buckled Shape for Spans IV, V, and VI

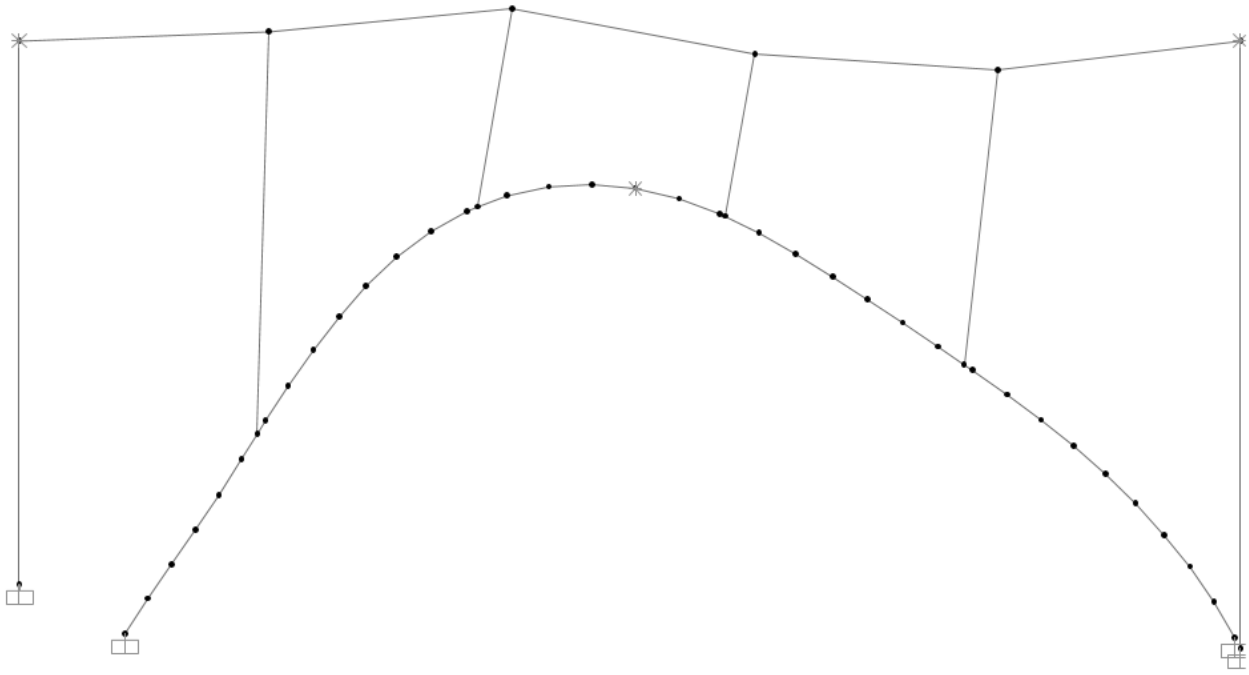

Figure 58: First Mode Buckled Shape for Span VII

Load multiplier values for the first buckling mode are listed in Table 34 along with the corresponding moment magnifier values determined from Eq. (4.7). Comparison of the moment magnifiers listed in Table 33 and Table 34 shows that the magnifiers determined through the elastic buckling analyses are smaller than those determined by the AASHTO procedure. But, the differences between the moment magnifiers are not huge.

Table 34: Moment Magnifiers δ_b from Elastic Buckling Analyses

Span	Loading	β_d	LM	δ_b
IV	Operating	0.099	9.6314	1.139
	Inventory	0.099	8.3492	1.164
V	Operating	0.098	9.2984	1.145
	Inventory	0.098	8.0208	1.172
VI	Operating	0.078	11.991	1.109
	Inventory	0.078	10.192	1.130
VII	Operating	0.170	26.113	1.047
	Inventory	0.170	20.162	1.062

4.7 Results of Elastic Second-Order Analyses

Elastic second-order analyses were performed for the purpose of identifying the best way to account for slenderness effects in the arches. The most convenient for use in load rating is a combined analysis which includes a second-order analysis for the factored dead load and then uses the structural stiffness at the end of that analysis in a linear moving load analysis for the factored truck loading. This is especially true for the project reported here where operating and inventory ratings are required for eight different standard trucks. So, analyses were performed to produce comparisons between second-order analyses, the combined analysis, and moment magnifier procedures. Three specific truck locations were chosen for each arch. These locations were chosen to maximize the load effects at three specific cross sections as illustrated in Figure

59 and Figure 60. The load ratings of the arches of Span IV, V and VI are controlled by the cross section at the hanger nearest midspan (Hanger 1). The next most critical location is at the third hanger from midspan (Hanger 3). And, the cross section at the base of the arch was considered important for comparisons. Similarly, the cross section which controlled the ratings (Column 6), the next most critical cross section (Column 5), and the base of the arch were selected for comparisons for Span VII.

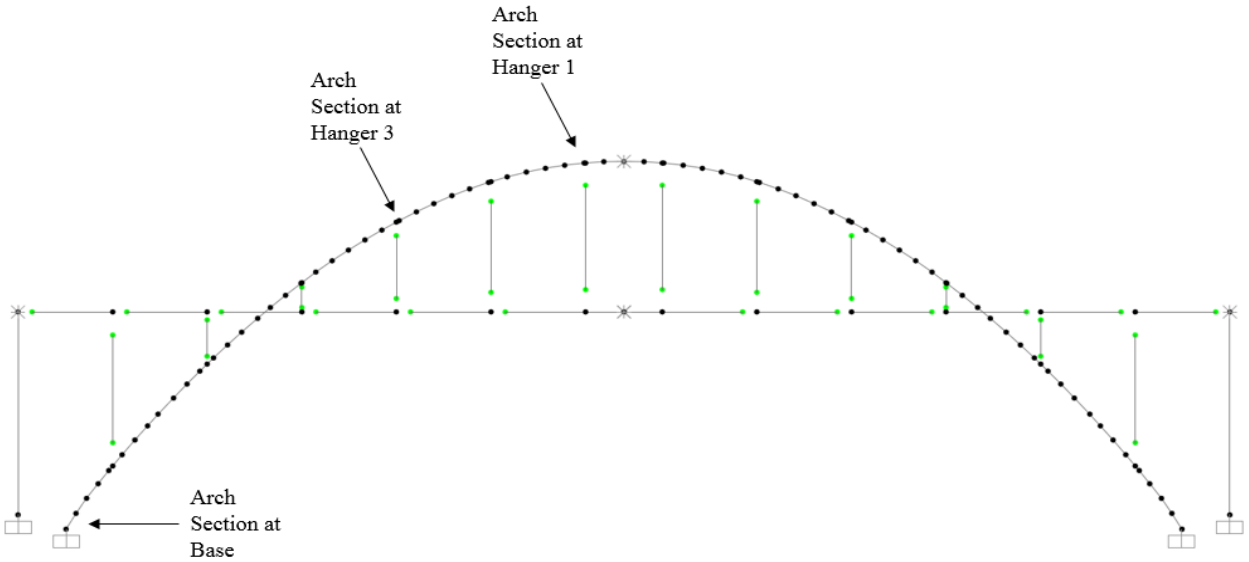

Figure 59: Critical Cross Sections for Spans IV, V, and VI

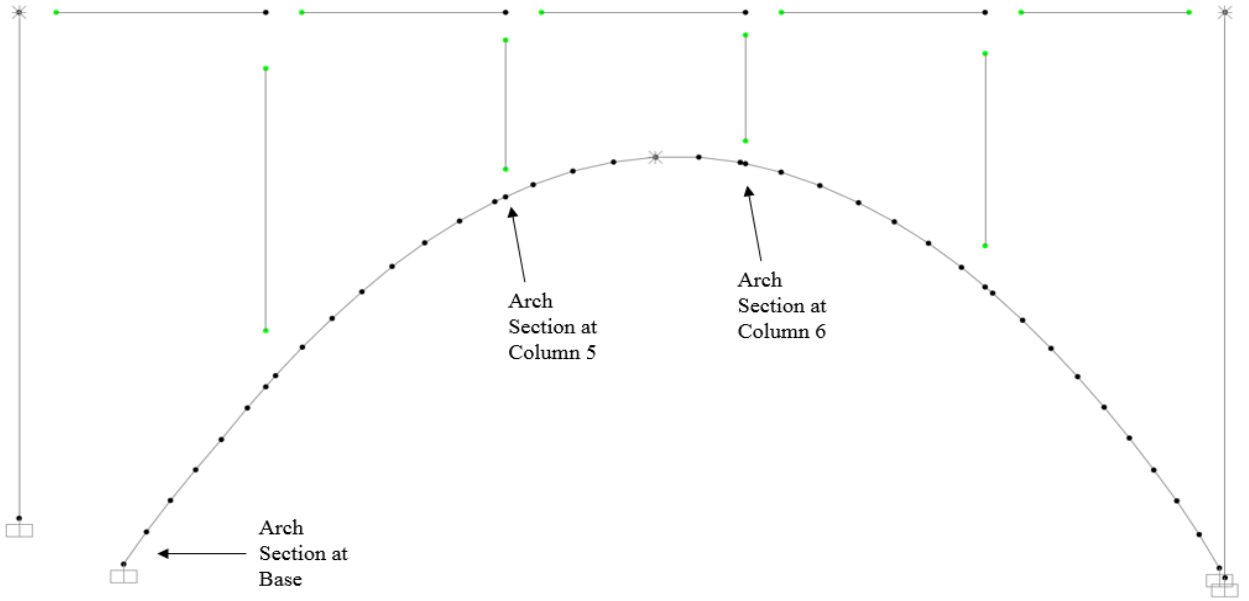

Figure 60: Critical Cross Sections for Span VII

Analyses for comparisons were performed using the tri-axle truck loading plus impact since that truck produced the lowest rating factors of all the eight standard trucks considered in this project. A first-order analysis was performed using the flexural rigidity E_cI_g for use with the moment magnifier procedures. Second-order analyses for full factored dead load plus live load were performed using both the transient model and the long-term model. And, the combined analysis was simulated by performing a second-order analysis for the dead load and then using the stiffness at the end of that analysis to perform a linear analysis for one of the three critical truck positions described above. Analyses of each type were repeated for each of the three critical truck locations. A summary of the resulting factored axial loads and bending moments at the critical cross sections in each span is provided in Table 35 through Table 38. The moment magnifiers listed in Table 33 and Table 34 were used with the first order analysis to produce results shown in rows labeled AASHTO (2002), AASHTO (2012), and Buckling Analysis.

Some observations are justified by the results shown in Table 35 through Table 38. The axial load values are not significantly affected by second-order effects. This is seen by comparing the axial loads found by the first-order analyses to those found by the second-order analyses for either the long-term or transient model. This observation is consistent with the moment magnifier procedures in most structural design codes since the axial loads used in design are the values from first-order analysis without modification by a magnifier.

The second-order analysis results from the transient model and the long-term model are very similar. The percent difference between bending moments obtained from these models is less than 2.2 percent for all cases shown in Table 35 and Table 38. Based on the guidance provided by the AASHTO (2012) as previously discussed, the transient model is most appropriate for the live loads and the long-term model is most appropriate for the dead loads and inclusion of the effects of creep on the shape of the arch. The good agreement between the results from these two models may or may not occur for other arches. Since it is not possible to state which model produces the best results for dead load plus live load, the average of the results from these two models is used as the standard of comparison below. These average second-order analysis results are the best estimates of the internal forces in the arches including second-order, slenderness, effects.

Table 35: Span IV – Factored Axial Loads and Bending Moments

Analysis	Loading	Hanger 1		Hanger 3		Base	
		P (k)	M (k-ft)	P (k)	M (k-ft)	P (k)	M (k-ft)
First-Order	1.3 D	-375	62	-437	52	-672	-235
	1.3 (L+I)	-95	677	-86	723	-122	-1313
	2.17 (L+I)	-159	1131	-144	1207	-204	-2191
	Operating	-470	740	-524	774	-795	-1547
	Inventory	-534	1193	-582	1258	-876	-2426
Second-Order, Long-Term	Operating	-472	773	-527	815	-796	-1621
	Inventory	-538	1262	-588	1327	-879	-2546
Second-Order, Transient	Operating	-473	766	-528	817	-797	-1608
	Inventory	-539	1259	-589	1332	-880	-2539
Average Second-Order	Operating	-473	769	-527	816	-797	-1614
	Inventory	-539	1260	-588	1330	-880	-2542
Combined Analysis	Operating	-472	764	-526	815	-796	-1612
	Inventory	-536	1236	-585	1326	-879	-2522
AASHTO (2002), $\delta_b(1.3D + A_2(L + I))$	Operating	-470	871	-524	912	-795	-1830
	Inventory	-534	1437	-582	1516	-876	-2923
AASHTO (2012), $1.3D + \delta_b A_2(L + I)$	Operating	-470	860	-524	903	-795	-1781
	Inventory	-534	1425	-582	1505	-876	-2875
Buckling Analysis, $\delta_b(1.3D + A_2(L + I))$	Operating	-470	842	-524	882	-795	-1769
	Inventory	-534	1388	-582	1464	-876	-2824
Buckling Analysis, $1.3D + \delta_b A_2(L + I)$	Operating	-470	834	-524	875	-795	-1730
	Inventory	-534	1378	-582	1456	-876	-2785

Table 36: Span V – Factored Axial Loads and Bending Moments

		Hanger 1		Hanger 3		Base	
		P	M	P	M	P	M
Analysis	Loading	(k)	(k-ft)	(k)	(k-ft)	(k)	(k-ft)
First-Order	1.3 D	-364	68	-429	41	-654	-243
	1.3 (L+I)	-89	673	-87	699	-122	-1319
	2.17 (L+I)	-149	1123	-145	1166	-204	-2202
	Operating	-453	741	-516	740	-776	-1562
	Inventory	-512	1191	-574	1207	-858	-2445
Second-Order, Long-Term	Operating	-454	778	-519	780	-778	-1623
	Inventory	-515	1267	-580	1275	-862	-2555
Second-Order, Transient	Operating	-455	772	-520	781	-779	-1610
	Inventory	-516	1264	-582	1280	-862	-2548
Average Second-Order	Operating	-455	775	-520	780	-779	-1616
	Inventory	-515	1266	-581	1278	-862	-2552
Combined Analysis	Operating	-454	768	-518	779	-778	-1616
	Inventory	-515	1238	-578	1274	-861	-2536
AASHTO (2002), $\delta_b(1.3D + A_2(L + I))$	Operating	-453	896	-516	894	-776	-1888
	Inventory	-512	1481	-574	1498	-858	-3039
AASHTO (2012), $1.3D + \delta_b A_2(L + I)$	Operating	-453	882	-516	886	-776	-1838
	Inventory	-512	1464	-574	1490	-858	-2980
Buckling Analysis, $\delta_b(1.3D + A_2(L + I))$	Operating	-453	848	-516	847	-776	-1788
	Inventory	-512	1396	-574	1412	-858	-2865
Buckling Analysis, $1.3D + \delta_b A_2(L + I)$	Operating	-453	839	-516	841	-776	-1753
	Inventory	-512	1385	-574	1408	-858	-2824

Table 37: Span VI – Factored Axial Loads and Bending Moments

		Hanger 1		Hanger 3		Base	
		P	M	P	M	P	M
Analysis	Loading	(k)	(k-ft)	(k)	(k-ft)	(k)	(k-ft)
First-Order	1.3 D	-327	41	-383	56	-584	-163
	1.3 (L+I)	-96	608	-86	638	-123	-1149
	2.17 (L+I)	-161	1014	-144	1065	-205	-1918
	Operating	-423	648	-469	694	-707	-1312
	Inventory	-488	1055	-527	1122	-789	-2081
Second-Order, Long-Term	Operating	-425	672	-472	721	-709	-1344
	Inventory	-492	1106	-532	1166	-793	-2136
Second-Order, Transient	Operating	-426	664	-473	721	-710	-1328
	Inventory	-493	1099	-533	1167	-794	-2121
Average Second-Order	Operating	-426	668	-473	721	-709	-1336
	Inventory	-492	1103	-533	1167	-793	-2129
Combined Analysis	Operating	-425	664	-472	722	-709	-1343
	Inventory	-490	1084	-530	1167	-792	-2133
AASHTO (2002), $\delta_b(1.3D + A_2(L + I))$	Operating	-423	748	-469	801	-707	-1513
	Inventory	-488	1244	-527	1322	-789	-2454
AASHTO (2012), $1.3D + \delta_b A_2(L + I)$	Operating	-423	741	-469	792	-707	-1488
	Inventory	-488	1236	-527	1312	-789	-2425
Buckling Analysis, $\delta_b(1.3D + A_2(L + I))$	Operating	-423	719	-469	770	-707	-1456
	Inventory	-488	1192	-527	1267	-789	-2352
Buckling Analysis, $1.3D + \delta_b A_2(L + I)$	Operating	-423	715	-469	764	-707	-1438
	Inventory	-488	1187	-527	1260	-789	-2331

Table 38: Span VII – Factored Axial Loads and Bending Moments

		Hanger 1		Hanger 3		Base	
		P	M	P	M	P	M
Analysis	Loading	(k)	(k-ft)	(k)	(k-ft)	(k)	(k-ft)
First-Order	1.3 D	-95	33	-107	39	-171	-91
	1.3 (L+I)	-77	141	-79	165	-90	-330
	2.17 (L+I)	-129	236	-132	275	-150	-550
	Operating	-172	175	-186	204	-261	-421
	Inventory	-224	269	-239	314	-321	-641
Second-Order, Long-Term	Operating	-172	175	-186	206	-261	-423
	Inventory	-224	271	-238	320	-321	-647
Second-Order, Transient	Operating	-173	171	-187	204	-261	-417
	Inventory	-225	266	-239	318	-321	-641
Average Second-Order	Operating	-173	173	-186	205	-261	-420
	Inventory	-225	269	-239	319	-321	-644
Combined Analysis	Operating	-172	174	-186	205	-261	-422
	Inventory	-224	269	-239	316	-321	-644
AASHTO (2002), $\delta_b(1.3D + A_2(L + I))$	Operating	-172	182	-186	212	-261	-437
	Inventory	-224	283	-239	330	-321	-673
AASHTO (2012), $1.3D + \delta_b A_2(L + I)$	Operating	-172	180	-186	210	-261	-434
	Inventory	-224	281	-239	328	-321	-669
Buckling Analysis, $\delta_b(1.3D + A_2(L + I))$	Operating	-172	183	-186	213	-261	-440
	Inventory	-224	286	-239	333	-321	-681
Buckling Analysis, $1.3D + \delta_b A_2(L + I)$	Operating	-172	181	-186	211	-261	-436
	Inventory	-224	284	-239	331	-321	-675

4.8 COMPARISONS OF SECOND-ORDER ANALYSIS METHODS

As stated earlier, moment magnifier procedures are approximate second-order analyses that are used to estimate values of bending moment that include slenderness effects. An appropriate comparison of the various second-order analysis methods can be made by comparing the ratios of bending moment determined at the critical cross sections by second-order analysis to first-order analysis. These ratios (M_{2nd}/M_{1st}) were obtained from the bending moments listed in Table 34 through Table 38 and are listed in Table 39 through Table 42. The ratios are indicators of the amount of magnification of the total factored moment resulting from slenderness effects as predicted by the individual methods of analysis.

Table 39: Span IV – Values of (M_{2nd}/M_{1st})

Analysis	Loading	Hanger 1	Hanger 3	Base
Average Second-Order	Operating	1.04	1.05	1.04
	Inventory	1.06	1.06	1.05
Combined Analysis	Operating	1.03	1.05	1.04
	Inventory	1.04	1.05	1.04
AASHTO (2002), $\delta_b(1.3D + A_2(L + I))$	Operating	1.18	1.18	1.18
	Inventory	1.21	1.21	1.21
AASHTO (2012), $1.3D + \delta_b A_2(L + I)$	Operating	1.16	1.17	1.15
	Inventory	1.19	1.20	1.19
Buckling Analysis, $\delta_b(1.3D + A_2(L + I))$	Operating	1.14	1.14	1.14
	Inventory	1.16	1.16	1.16
Buckling Analysis, $1.3D + \delta_b A_2(L + I)$	Operating	1.13	1.13	1.11
	Inventory	1.16	1.16	1.15

Table 40: Span V – Values of (M_{2nd}/M_{1st})

Analysis	Loading	Hanger 1	Hanger 3	Base
Average Second-Order	Operating	1.05	1.06	1.03
	Inventory	1.06	1.06	1.04
Combined Analysis	Operating	1.04	1.05	1.03
	Inventory	1.04	1.06	1.04
AASHTO (2002), $\delta_b(1.3D + A_2(L + I))$	Operating	1.21	1.21	1.21
	Inventory	1.24	1.24	1.24
AASHTO (2012), $1.3D + \delta_b A_2(L + I)$	Operating	1.19	1.20	1.18
	Inventory	1.23	1.24	1.22
Buckling Analysis, $\delta_b(1.3D + A_2(L + I))$	Operating	1.15	1.15	1.15
	Inventory	1.17	1.17	1.17
Buckling Analysis, $1.3D + \delta_b A_2(L + I)$	Operating	1.13	1.14	1.12
	Inventory	1.16	1.17	1.15

Table 41: Span VI – Values of (M_{2nd}/M_{1st})

Analysis	Loading	Hanger 1	Hanger 3	Base
Average Second-Order	Operating	1.03	1.04	1.02
	Inventory	1.05	1.04	1.02
Combined Analysis	Operating	1.02	1.04	1.02
	Inventory	1.03	1.04	1.03
AASHTO (2002), $\delta_b(1.3D + A_2(L + I))$	Operating	1.15	1.15	1.15
	Inventory	1.18	1.18	1.18
AASHTO (2012), $1.3D + \delta_b A_2(L + I)$	Operating	1.14	1.14	1.13
	Inventory	1.17	1.17	1.16
Buckling Analysis, $\delta_b(1.3D + A_2(L + I))$	Operating	1.11	1.11	1.11
	Inventory	1.13	1.13	1.13
Buckling Analysis, $1.3D + \delta_b A_2(L + I)$	Operating	1.10	1.10	1.10
	Inventory	1.12	1.12	1.12

Table 42: Span VII – Values of (M_{2nd}/M_{1st})

Analysis	Loading	Hanger 1	Hanger 3	Base
Average Second-Order	Operating	0.99	1.01	1.00
	Inventory	1.00	1.01	1.00
Combined Analysis	Operating	1.00	1.01	1.00
	Inventory	1.00	1.01	1.00
AASHTO (2002), $\delta_b(1.3D + A_2(L + I))$	Operating	1.04	1.04	1.04
	Inventory	1.05	1.05	1.05
AASHTO (2012), $1.3D + \delta_b A_2(L + I)$	Operating	1.03	1.03	1.03
	Inventory	1.04	1.04	1.04
Buckling Analysis, $\delta_b(1.3D + A_2(L + I))$	Operating	1.05	1.05	1.05
	Inventory	1.06	1.06	1.06
Buckling Analysis, $1.3D + \delta_b A_2(L + I)$	Operating	1.04	1.04	1.04
	Inventory	1.05	1.05	1.05

Values listed in Table 39 through Table 42 in rows labeled "Average Second-Order" indicate that increase in bending moments due to slenderness effects is six percent or less at the critical locations in each of the arches. In one case, Span VII at Column 6 for operating loading, the second-order analysis result is 0.99 which indicates that the moment is less than the moment determined by first-order analysis. This is possible since the bending moment is redistributed along the arch span by the second-order effects.

The increase in bending moments predicted by the AASHTO moment magnifier procedures is significantly higher than that predicted by second-order analysis as shown in Table 39 through Table 42. Use of structural analysis software to perform buckling analyses for use in the moment magnifier procedures does produce improved results.

The combined analysis produces results that are the closest to the second-order analysis results. The combined analysis predicts increases in bending moment due to slenderness effects in some cases that are less than predicted by the second-order analysis. The increase in bending moment predicted by the combined analysis is less than that predicted by the second-order

analysis because a linear analysis at a reduced stiffness is used for the live load component of the total loading. The reduction in stiffness associated with the axial load due to live load is not accounted for in the combined analysis.

The amount by which the combined analysis underestimates the increase in bending moment due to slenderness effects is acceptably small for use in determining bridge ratings in light of the potential for error in the comparisons resulting from modeling error, concrete modulus of elasticity, ultimate creep coefficient, stiffness reduction factor, variations in flexural rigidity (EI) along the arch, and calculation of the cross section capacities.

4.9 SLENDERNESS EFFECTS IN REINFORCED CONCRETE ARCHES SUMMARY AND CONCLUSION

A summary of procedures available for including slenderness effects in analyses for the load rating of reinforced concrete arches was presented. These procedures included the use of elastic second-order analysis, moment magnifiers calculated from elastic buckling analyses, and moment magnifiers defined by AASHTO (2002) and the AASHTO (2012). When rating factors for several standard trucks are required for multiple arch spans, the repetition of second-order analyses to simulate moving truck loading can be impractical. A combined analysis was investigated where a second-order analysis is performed for the factored dead load and the resulting structural stiffness is used to perform a linear analysis for truck loading. Since the analysis for truck loading is linear, moving load analysis procedures commonly available in structural analysis software can be used to greatly simplify the analysis required for load rating of the arch. Comparisons of the increase in bending moment resulting from slenderness effects at critical locations in four different arches were made with results from second-order analyses. The combined analysis was found to be sufficiently accurate for use in the load rating of reinforced concrete arch bridges.

Chapter 5

RATING RESULTS

This chapter presents the rating results for Spans IV, V, VI, and VII. Ratings are shown for the operating and inventory case for the eight ALDOT trucks and the AASHTO lane load. The bridge components for rating include: columns, hangers, transverse deep beams, transverse floor beams, and arch ribs. For Spans IV, V, and VI, the ratings performed and listed here are for: Columns 2 and 3, Hanger 1, Transverse Deep Beam, transverse floor beams at Columns 2, 3, and Hanger 1, and arch rib sections. For Span VII, the ratings performed and listed here are for: Columns 4, 5, and 7, transverse floor beams at Columns 4 and 5, and arch rib sections.

5.1 SPAN IV RATING RESULTS

The naming convention for Spans IV, V, and VI is shown here again in Figure 61 for convenience. For Span IV, the ratings are presented for Column 2, Column 3, Hanger 1, Transverse Deep Beam, transverse floor beams at Column 2, Column 3, and at Hanger 1, and arch rib sections.

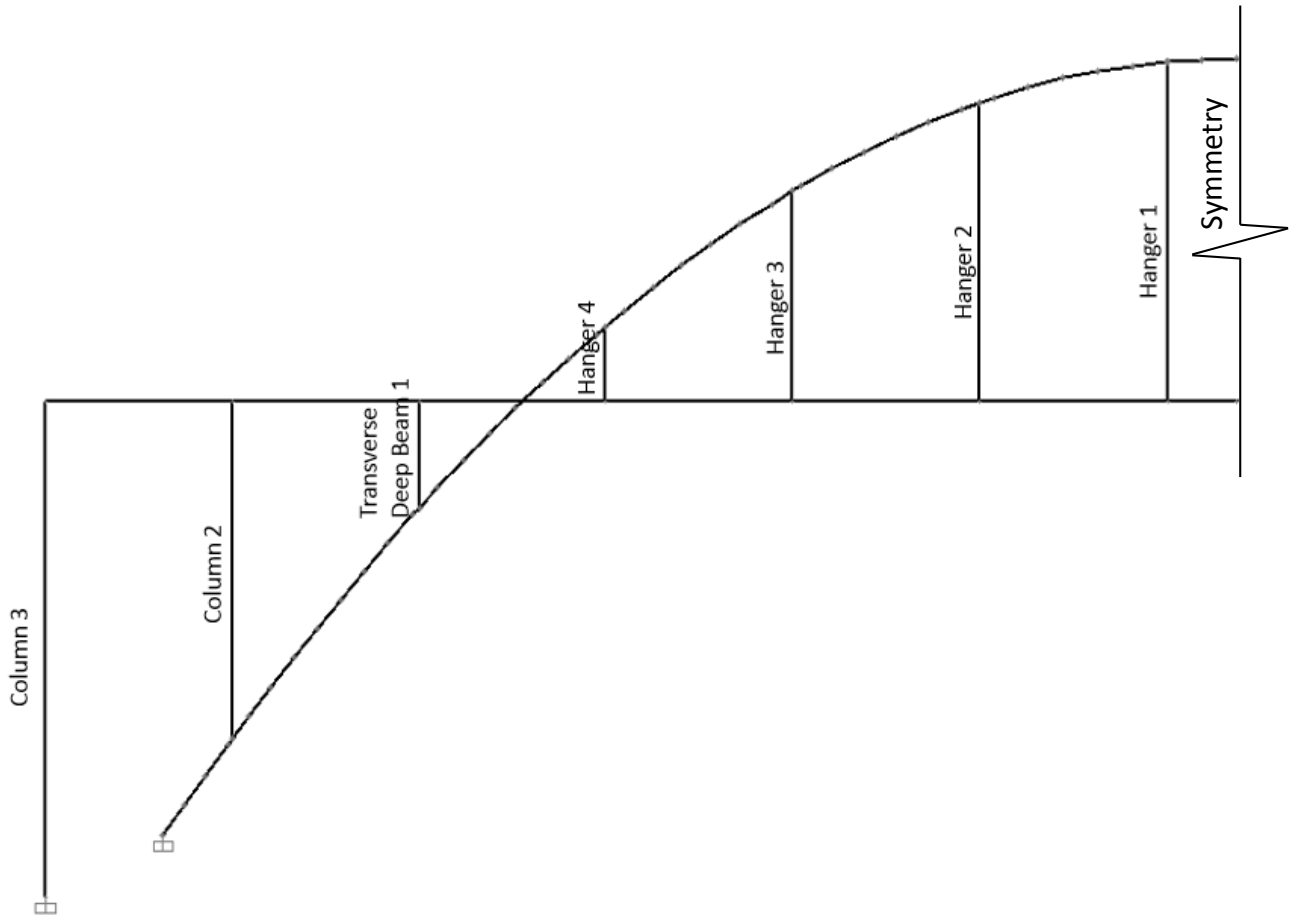

Figure 61: Spans IV, V, and VI East End Naming Convention (SAP 2013) (Duplicate - Figure 5)

5.1.1 Column 2

Ratings are provided for the interior and exterior Column 2s as shown in Table 43 and Table 44, respectively. Ratings were calculated using the Beam and Column 2 model presented in Section 3.5.3. The interior columns are under axial compression for dead and live loads. The exterior columns are in tension under live loads. As a result, rating factors for the exterior columns are lower than the interior columns.

Table 43: Span IV - Interior Column 2 Rating Factors

Trucks	Rating Factors	
	Operating	Inventory
Tri-Axle	3.06	1.83
H-Truck	4.43	2.66
Two-Axle	4.33	2.60
Concrete	3.47	2.08
18-Wheeler	4.95	2.97
6-Axle	4.22	2.53
School Bus	8.35	5.00
HS-Truck	4.43	2.66

Table 44: Span IV - Exterior Column 2 Rating Factors

Trucks	Rating Factors	
	Operating	Inventory
Tri-Axle	2.58	1.55
H-Truck	3.75	2.24
Two-Axle	3.66	2.19
Concrete	2.93	1.75
18-Wheeler	4.18	2.51
6-Axle	3.56	2.13
School Bus	7.05	4.22
HS-Truck	3.75	2.24

5.1.2 Column 3

Ratings are provided for the interior and exterior Column 3s as shown in Table 45 and Table 46, respectively. Ratings were calculated using the Beam and Column 3 model presented in Section 3.5.4. Unlike Column 2, where the exterior Column 2 was in tension under live loads, both the interior and exterior Column 3s are under compression for dead and live loads. Rating factors for the exterior columns are lower than for the interior columns.

Table 45: Span IV - Interior Column 3 Rating Factors

Trucks	Rating Factors	
	Operating	Inventory
Tri-Axle	2.31	1.38
H-Truck	3.34	2.00
Two-Axle	3.27	1.96
Concrete	2.61	1.57
18-Wheeler	3.73	2.24
6-Axle	3.19	1.91
School Bus	6.29	3.77
HS-Truck	3.34	2.00

Table 46: Span IV - Exterior Column 3 Rating Factors

Trucks	Rating Factors	
	Operating	Inventory
Tri-Axle	1.86	1.12
H-Truck	2.69	1.61
Two-Axle	2.63	1.58
Concrete	2.10	1.26
18-Wheeler	3.01	1.80
6-Axle	2.57	1.54
School Bus	5.07	3.04
HS-Truck	2.69	1.61

5.1.3 Hanger 1

Ratings are provided for the hangers as shown in Table 47. Ratings were calculated using the Beam and Hanger 1 model presented in Section 3.5.6.1. It was decided from the longitudinal beam analysis that Hanger 1 carries the highest tension axial load from the truck loadings. Thus, only Hanger 1 was rated for axial tension since all hangers have the same capacity.

Table 47: Span IV - Hanger 1 Rating Factors

Trucks	Rating Factors	
	Operating	Inventory
Tri-Axle	1.13	0.68
H-Truck	1.60	0.96
Two-Axle	1.50	0.90
Concrete	1.20	0.72
18-Wheeler	1.71	1.03
6-Axle	1.59	0.96
School Bus	3.05	1.83
HS-Truck	1.52	0.91

5.1.4 Transverse Deep Beam

Ratings are provided for the Transverse Deep Beam as shown in Table 48. Ratings were calculated using the Transverse Deep Beam model presented in Section 3.5.7. The Transverse Deep Beam was rated for bending moment and shear; and, the bending moment controls the rating.

Table 48: Span IV - Transverse Deep Beam Rating Factors

Trucks	Rating Factors			
	Bending Moment		Shear	
	Operating	Inventory	Operating	Inventory
Tri-Axle	1.21	0.72	2.36	1.41
H-Truck	1.75	1.05	3.42	2.05
Two-Axle	1.71	1.03	3.34	2.00
Concrete	1.37	0.82	2.67	1.60
18-Wheeler	1.96	1.17	3.82	2.29
6-Axle	1.67	1.00	3.25	1.95
School Bus	3.30	1.98	6.44	3.86
HS-Truck	1.75	1.05	3.42	2.05

5.1.5 Transverse Floor Beams

The transverse floor beams were rated for bending moment and shear. For shear ratings, transverse floor beams were discretized into three zones. The transverse floor beams at column locations were rated for positive bending moment, negative bending moment, and shear. The transverse floor beams at hanger locations were rated for positive bending moment and shear. Negative bending moment in the hanger is not rated because the hangers are assumed to have no flexural rigidity. The controlling positive bending moment and shear ratings are at the transverse floor beam at Hanger 1 location and are shown in Section 5.1.5.3. The controlling negative bending moment rating is at the transverse floor beam at Column 2 location and is shown in the following section. For completeness, full rating results are provided for transverse beam at Columns 2 and 3 are in Appendix A2.1 and A2.2.

5.1.5.1 Transverse Floor Beam at Column 2

The transverse floor beam at Column 2 controls the rating for negative bending moment and is shown in Table 49. Ratings were calculated using the transverse floor beam model presented in Section 3.5.3. For completeness, full rating results are provided for the transverse floor beam at Column 2 in Appendix A2.1.

Table 49: Span IV - Transverse Floor Beam at Column 2 Rating Factors

Trucks	Rating Factors	
	Negative Moment	
	Operating	Inventory
Tri-Axle	7.44	4.46
H-Truck	10.78	6.46
Two-Axle	10.53	6.31
Concrete	8.43	5.05
18-Wheeler	12.04	7.21
6-Axle	10.25	6.14
School Bus	20.29	12.15
HS-Truck	10.78	6.46

5.1.5.2 Transverse Floor Beam at Column 3

Full rating results are provided for completeness for the transverse floor beam at Column 3 in Appendix A2.2.

5.1.5.3 Transverse Floor Beam at Hanger 1

Rating factors are provided for the transverse floor beam at Hanger 1 as shown in Table 50 for bending moment and Table 51 for shear. Ratings were calculated using the transverse floor beam presented in Section 3.5.6.1. The transverse floor beam at Hanger 1 was rated for positive bending moment and shear; however, the transverse floor beam was discretized into three zones for shear ratings. All of the transverse floor beams at the hanger locations have no negative bending moment because the hangers were modeled as axial tension members. Positive bending moment controls the rating. For the tri-axle truck, it is 0.98 at the operating level.

Table 50: Span IV - Transverse Floor Beam at Hanger 1 Rating Factors: Part 1

Trucks	Rating Factors	
	Bending Moment	
	Operating	Inventory
Tri-Axle	**0.98**	0.59
H-Truck	1.39	0.83
Two-Axle	1.30	0.78
Concrete	1.04	0.63
18-Wheeler	1.49	0.89
6-Axle	1.39	0.83
School Bus	2.66	1.59
HS-Truck	1.32	0.79

Table 51: Span IV - Transverse Floor Beam at Hanger 1 Rating Factors: Part 2

Trucks	Rating Factors					
	V_{zone1}		V_{zone2}		V_{zone3}	
	Operating	Inventory	Operating	Inventory	Operating	Inventory
Tri-Axle	1.48	0.89	1.05	0.63	1.17	0.70
H-Truck	2.10	1.26	1.49	0.89	1.65	0.99
Two-Axle	1.97	1.18	1.40	0.84	1.55	0.93
Concrete	1.58	0.94	1.12	0.67	1.24	0.74
18-Wheeler	2.25	1.35	1.60	0.96	1.77	1.06
6-Axle	2.10	1.26	1.49	0.89	1.65	0.99
School Bus	4.01	2.40	2.85	1.71	3.17	1.90
HS-Truck	2.00	1.20	1.42	0.85	1.58	0.95

5.1.6 Arch Rib

Rating factors are provided for the arch rib at seven locations as pointed out in Figure 62. Critical sections were determined by looking at the qualitative and quantitative output diagrams for the shear, bending moment, and axial load from SAP2000. Ratings were provided for one-half of the arch rib since the span is symmetrical. Ratings were calculated using the arch rib model presented in Section 3.6.4. The arch rib sections were rated for shear and the combination of axial load and bending moment. Ratings for the lane loading are provided in addition to ratings for the eight standard trucks.

Rating factors for Sections A1, A2, A3, A8, A14, A21, and A41 are shown in Table 52 through Table 58. All operating ratings are greater than 1.0. The combination of axial load and bending moment controlled the ratings. The lowest rating factor is for the tri-axle truck, and it is at arch Section A2.

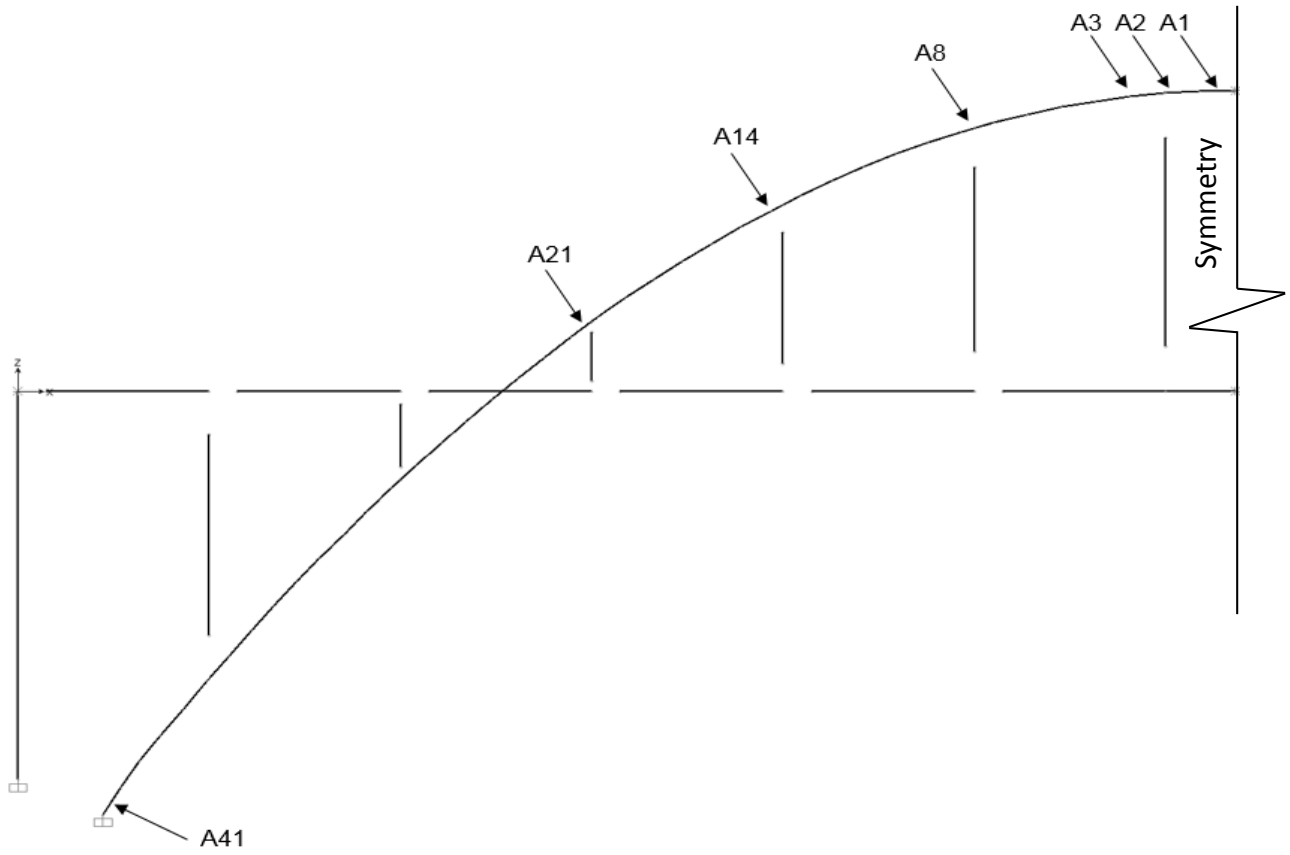

Figure 62: Span IV – Arch Rib with Rated Sections Labeled (SAP 2013)

Table 52: Span IV - Arch Section A1 Rating Factors

Trucks	Rating Factors			
	Axial and Moment		Shear	
	Operating	Inventory	Operating	Inventory
Tri-Axle	1.31	0.79	2.06	1.24
H-Truck	1.87	1.12	3.48	2.09
Two-Axle	1.77	1.06	2.69	1.61
Concrete	1.40	0.84	2.30	1.38
18-Wheeler	2.08	1.24	2.78	1.67
6-Axle	1.97	1.18	2.58	1.55
School Bus	3.78	2.27	6.29	3.77
HS-Truck	1.68	1.01	2.33	1.40
HS Lane - M	3.86	2.31	6.75	4.04
HS Lane - V	2.61	1.56	4.77	2.86

Table 53: Span IV - Arch Section A2 Rating Factors

Trucks	Rating Factors			
	Axial and Moment		Shear	
	Operating	Inventory	Operating	Inventory
Tri-Axle	1.03	0.62	1.14	0.69
H-Truck	1.51	0.91	1.61	0.96
Two-Axle	1.38	0.83	1.44	0.87
Concrete	1.11	0.66	1.21	0.73
18-Wheeler	1.62	0.97	1.52	0.91
6-Axle	1.55	0.93	1.48	0.89
School Bus	3.05	1.83	2.96	1.77
HS-Truck	1.29	0.77	1.26	0.75
HS Lane - M	3.06	1.83	2.36	1.41
HS Lane - V	2.08	1.25	1.76	1.06

Table 54: Span IV - Arch Section A3 Rating Factors

Trucks	Rating Factors			
	Axial and Moment		Shear	
	Operating	Inventory	Operating	Inventory
Tri-Axle	1.06	0.64	1.47	0.88
H-Truck	1.57	0.94	2.03	1.22
Two-Axle	1.42	0.85	1.85	1.11
Concrete	1.14	0.69	1.55	0.93
18-Wheeler	1.68	1.01	1.97	1.18
6-Axle	1.60	0.96	1.93	1.15
School Bus	3.16	1.89	3.76	2.25
HS-Truck	1.34	0.80	1.62	0.97
HS Lane - M	3.17	1.90	3.18	1.91
HS Lane - V	2.16	1.29	2.34	1.40

Table 55: Span IV - Arch Section A8 Rating Factors

Trucks	Rating Factors			
	Axial and Moment		Shear	
	Operating	Inventory	Operating	Inventory
Tri-Axle	1.23	0.74	1.95	1.17
H-Truck	1.94	1.16	2.82	1.69
Two-Axle	1.70	1.02	2.56	1.53
Concrete	1.40	0.84	2.16	1.29
18-Wheeler	2.02	1.21	2.82	1.69
6-Axle	1.81	1.08	2.60	1.56
School Bus	3.82	2.29	5.34	3.20
HS-Truck	1.60	0.96	2.25	1.35
HS Lane - M	4.19	2.51	4.76	2.85
HS Lane - V	2.81	1.69	3.62	2.17

Table 56: Span IV - Arch Section A14 Rating Factors

Trucks	Rating Factors			
	Axial and Moment		Shear	
	Operating	Inventory	Operating	Inventory
Tri-Axle	1.12	0.67	2.10	1.26
H-Truck	1.78	1.06	3.37	2.02
Two-Axle	1.54	0.92	2.76	1.65
Concrete	1.27	0.76	2.31	1.38
18-Wheeler	1.81	1.08	3.25	1.95
6-Axle	1.64	0.98	2.99	1.79
School Bus	3.51	2.10	6.41	3.84
HS-Truck	1.43	0.86	2.46	1.47
HS Lane - M	3.92	2.35	5.06	3.03
HS Lane - V	2.61	1.56	3.80	2.28

Table 57: Span IV - Arch Section A21 Rating Factors

Trucks	Rating Factors			
	Axial and Moment		Shear	
	Operating	Inventory	Operating	Inventory
Tri-Axle	1.46	0.87	2.03	1.22
H-Truck	2.28	1.36	3.28	1.97
Two-Axle	2.03	1.22	2.68	1.60
Concrete	1.65	0.99	2.24	1.34
18-Wheeler	2.48	1.48	3.16	1.89
6-Axle	2.24	1.34	2.89	1.73
School Bus	4.60	2.75	6.25	3.75
HS-Truck	1.95	1.17	2.37	1.42
HS Lane - M	4.90	2.93	5.25	3.14
HS Lane - V	3.29	1.97	3.90	2.34

Table 58: Span IV - Arch Section A41 Rating Factors

Trucks	Rating Factors			
	Axial and Moment		Shear	
	Operating	Inventory	Operating	Inventory
Tri-Axle	1.31	0.78	3.34	2.00
H-Truck	2.33	1.39	5.68	3.41
Two-Axle	1.73	1.04	4.42	2.65
Concrete	1.49	0.89	3.75	2.25
18-Wheeler	1.84	1.10	4.01	2.40
6-Axle	1.80	1.08	3.85	2.30
School Bus	4.31	2.58	10.69	6.40
HS-Truck	1.47	0.88	3.85	2.31
HS Lane - M	7.08	4.24	8.53	5.11
HS Lane - V	4.49	2.69	6.79	4.07

5.2 SPAN V RATING RESULTS

For Span V, the ratings are presented for Columns 2 and 3, Hanger 1, Transverse Deep Beam, transverse floor beams at Column 2 and 3 and at Hanger 1, and arch rib sections.

5.2.1 Column 2

Ratings are provided for the interior and exterior Column 2s as shown in Table 59 and Table 60, respectively. Ratings were calculated using the Beam and Column 2 model presented in Section 3.5.3. The interior columns are under axial compression for dead and live loads. The exterior columns are in tension under live loads.

Table 59: Span V - Interior Column 2 Rating Factors

Trucks	Rating Factors	
	Operating	Inventory
Tri-Axle	3.05	1.83
H-Truck	4.40	2.64
Two-Axle	4.32	2.59
Concrete	3.46	2.07
18-Wheeler	4.94	2.96
6-Axle	4.21	2.52
School Bus	8.29	4.96
HS-Truck	4.40	2.64

Table 60: Span V - Exterior Column 2 Rating Factors

Trucks	Rating Factors	
	Operating	Inventory
Tri-Axle	2.55	1.53
H-Truck	3.67	2.20
Two-Axle	3.61	2.16
Concrete	2.88	1.73
18-Wheeler	4.12	2.47
6-Axle	3.52	2.11
School Bus	6.92	4.14
HS-Truck	3.67	2.20

5.2.2 Column 3

Ratings are provided for the interior and exterior Column 3s as shown in Table 61 and Table 62, respectively. Ratings were calculated using the Beam and Column 3 model presented in Section 3.5.4. Unlike Column 2, where the exterior Column 2 was in tension under live loads, both the interior and exterior Column 3s are under compression for dead and live loads. Rating factors for the exterior columns are lower than for the interior columns.

Table 61: Span V - Interior Column 3 Rating Factors

Trucks	Rating Factors	
	Operating	Inventory
Tri-Axle	2.47	1.48
H	3.58	2.14
Two-Axle	3.50	2.09
Concrete	2.80	1.68
18-Wheeler	4.00	2.39
6-Axle	3.41	2.05
School Bus	6.74	4.04
HS-Truck	3.58	2.14

Table 62: Span V - Exterior Column 3 Rating Factors

Trucks	Rating Factors	
	Operating	Inventory
Tri-Axle	1.83	1.10
H	2.64	1.58
Two-Axle	2.58	1.55
Concrete	2.07	1.24
18-Wheeler	2.95	1.77
6-Axle	2.52	1.51
School Bus	4.98	2.98
HS-Truck	2.64	1.58

5.2.3 Hanger 1

Ratings are provided for the hangers as shown in Table 63. Ratings were calculated using the Beam and Hanger 1 model presented in Section 3.5.6.1. It was decided from the longitudinal beam analysis that Hanger 1 carries the highest tension axial load from the truck loadings. Thus, only Hanger 1 was rated for axial tension since all hangers have the same capacity.

Table 63: Span V - Hanger 1 Rating Factors

Trucks	Rating Factors	
	Operating	Inventory
Tri-Axle	1.12	0.67
H-Truck	1.59	0.95
Two-Axle	1.49	0.89
Concrete	1.19	0.71
18-Wheeler	1.70	1.02
6-Axle	1.59	0.95
School Bus	3.02	1.81
HS-Truck	1.53	0.91

5.2.4 Transverse Deep Beam

Ratings are provided for the Transverse Deep Beam as shown in Table 64. Ratings were calculated using the Transverse Deep Beam model presented in Section 3.5.7. The Transverse Deep Beam was rated for bending moment and shear; and, the bending moment controls the rating.

Table 64: Span V - Transverse Deep Beam Rating Factors

Trucks	Rating Factors			
	Bending Moment		Shear	
	Operating	Inventory	Operating	Inventory
Tri-Axle	1.06	0.64	2.16	1.30
H-Truck	1.53	0.92	3.12	1.87
Two-Axle	1.50	0.90	3.06	1.83
Concrete	1.20	0.72	2.45	1.47
18-Wheeler	1.72	1.03	3.49	2.09
6-Axle	1.47	0.88	2.98	1.79
School Bus	2.88	1.73	5.86	3.51
HS-Truck	1.53	0.92	3.12	1.87

5.2.5 Transverse Floor Beams

The transverse floor beams were rated for bending moment and shear. For shear ratings, transverse floor beams were discretized into three zones. The transverse floor beams at column locations were rated for positive and negative bending moment and shear. The transverse floor beams at hanger locations were rated for positive bending moment and shear. Negative bending moment in the hanger is not rated because the hangers are assumed to have no flexural rigidity. The controlling positive bending moment and shear ratings are at the transverse floor beam at Hanger 1 location and are shown in Section 5.2.5.3. The controlling negative bending moment rating is at the transverse floor beam at Column 2 location and is shown in the following section. For completeness, full rating results are provided for transverse beam at Columns 2 and 3 in Appendix B2.1 and B2.2.

5.2.5.1 Transverse Floor Beam at Column 2

The transverse floor beam at Column 2 controls the rating for negative bending moment for all transverse floor beams and is shown in Table 65. Ratings were calculated using the transverse floor beam model presented in Section 3.5.3. For completeness, full rating results are provided for the transverse floor beam at Column 2 in Appendix B2.1.

Table 65: Span V - Transverse Floor Beam at Column 2 Rating Factors

Trucks	Rating Factors	
	Negative Moment	
	Operating	Inventory
Tri-Axle	7.30	4.37
H-Truck	10.52	6.30
Two-Axle	10.33	6.19
Concrete	8.26	4.95
18-Wheeler	11.80	7.07
6-Axle	10.07	6.03
School Bus	19.81	11.87
HS-Truck	10.52	6.30

5.2.5.2 Transverse Floor Beam at Column 3

Full rating results are provided for completeness for the transverse floor beam at Column 3 in Appendix B2.2.

5.2.5.3 Transverse Floor Beam at Hanger 1

The positive bending moment and shear at Hanger 1 location controls the rating for all transverse floor beams. Full rating results are provided for the transverse floor beam at Hanger 1 as shown in Table 66 for bending moment and Table 67 for shear. Ratings were calculated using the transverse floor beam presented in Section 3.5.6.1. For the tri-axle truck, the positive bending moment operating rating factor is 0.99.

Table 66: Span V - Transverse Floor Beam at Hanger 1 Rating Factors: Part 1

Trucks	Rating Factors	
	Bending Moment	
	Operating	Inventory
Tri-Axle	**0.99**	0.59
H-Truck	1.39	0.83
Two-Axle	1.31	0.78
Concrete	1.04	0.63
18-Wheeler	1.49	0.89
6-Axle	1.39	0.84
School Bus	2.66	1.59
HS-Truck	1.34	0.80

Table 67: Span V - Transverse Floor Beam at Hanger 1 Rating Factors: Part 2

Trucks	Rating Factors					
	V_{zone1}		V_{zone2}		V_{zone3}	
	Operating	Inventory	Operating	Inventory	Operating	Inventory
Tri-Axle	1.48	0.89	1.06	0.63	1.17	0.70
H-Truck	2.10	1.26	1.49	0.89	1.66	0.99
Two-Axle	1.97	1.18	1.40	0.84	1.55	0.93
Concrete	1.57	0.94	1.12	0.67	1.24	0.74
18-Wheeler	2.25	1.35	1.60	0.96	1.77	1.06
6-Axle	2.10	1.26	1.49	0.89	1.66	0.99
School Bus	4.00	2.40	2.84	1.70	3.16	1.89
HS-Truck	2.02	1.21	1.43	0.86	1.59	0.95

5.2.6 Arch Rib

Rating factors are provided for the arch rib at seven locations as pointed out in Figure 63. Critical sections were determined by looking at the qualitative and quantitative output diagrams for the shear, bending moment, and axial load from SAP2000. Ratings were provided for one-half of the arch rib since the span is symmetrical. Ratings were calculated using the arch rib model presented in Section 3.6.4. The arch rib sections were rated for shear and the combination

of axial load and bending moment. Ratings for the lane loading are provided in addition to ratings for the eight standard trucks.

Rating factors for Sections A1, A2, A3, A8, A14, A20, and A40 are shown in Table 68 through Table 74. All operating ratings are 1.0 and above except for arch Section A2 where the combination of axial load and bending moment has an operating rating of 0.96. The combination of axial load and bending moment controlled the ratings. The tri-axle truck has the lowest rating factor, and it is at arch Section A2.

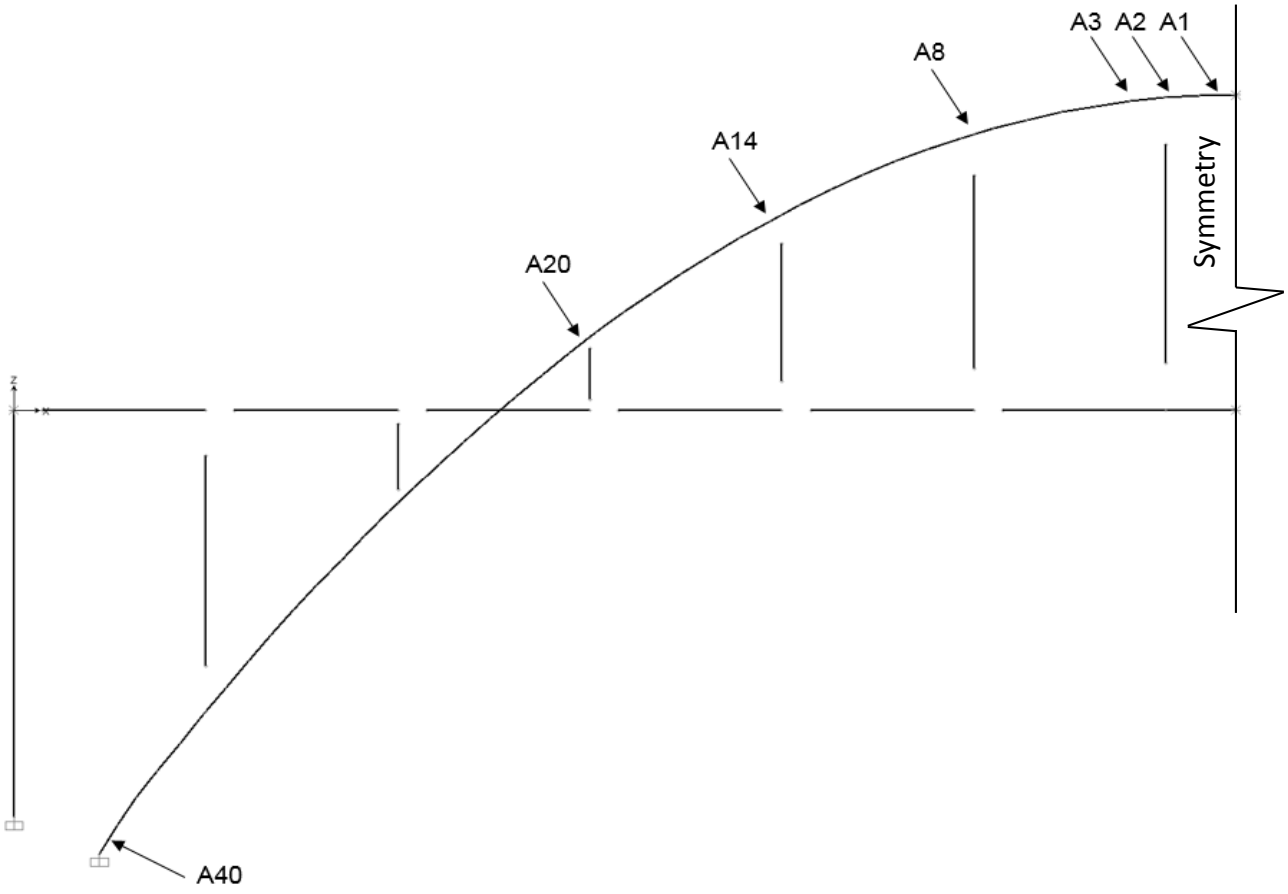

Figure 63: Span V - Arch Rib with Rated Sections Labeled (SAP 2013)

Table 68: Span V - Arch Section A1 Rating Factors

Trucks	Rating Factors			
	Axial and Moment		Shear	
	Operating	Inventory	Operating	Inventory
Tri-Axle	1.24	0.74	2.03	1.22
H-Truck	1.75	1.05	3.42	2.05
Two-Axle	1.66	1.00	2.65	1.59
Concrete	1.31	0.79	2.26	1.35
18-Wheeler	1.94	1.16	2.77	1.66
6-Axle	1.84	1.10	2.57	1.54
School Bus	3.53	2.11	6.20	3.71
HS-Truck	1.58	0.95	2.30	1.38
HS Lane - M	3.56	2.13	6.70	4.02
HS Lane - V	2.41	1.45	4.72	2.83

Table 69: Span V - Arch Section A2 Rating Factors

Trucks	Rating Factors			
	Axial and Moment		Shear	
	Operating	Inventory	Operating	Inventory
Tri-Axle	**0.96**	0.58	1.06	0.63
H-Truck	1.41	0.85	1.48	0.89
Two-Axle	1.29	0.77	1.34	0.80
Concrete	1.04	0.62	1.12	0.67
18-Wheeler	1.52	0.91	1.42	0.85
6-Axle	1.45	0.87	1.38	0.83
School Bus	2.86	1.71	2.74	1.64
HS-Truck	1.22	0.73	1.17	0.70
HS Lane - M	2.83	1.70	2.17	1.30
HS Lane - V	1.93	1.16	1.63	0.97

Table 70: Span V - Arch Section A3 Rating Factors

Trucks	Rating Factors			
	Axial and Moment		Shear	
	Operating	Inventory	Operating	Inventory
Tri-Axle	1.00	0.60	1.41	0.85
H-Truck	1.46	0.88	1.94	1.16
Two-Axle	1.34	0.80	1.78	1.07
Concrete	1.07	0.64	1.49	0.89
18-Wheeler	1.57	0.94	1.91	1.14
6-Axle	1.50	0.90	1.87	1.12
School Bus	2.97	1.78	3.61	2.16
HS-Truck	1.26	0.75	1.56	0.93
HS Lane - M	2.95	1.77	3.05	1.83
HS Lane - V	2.01	1.20	2.24	1.34

Table 71: Span V - Arch Section A8 Rating Factors

Trucks	Rating Factors			
	Axial and Moment		Shear	
	Operating	Inventory	Operating	Inventory
Tri-Axle	1.16	0.69	2.01	1.20
H-Truck	1.81	1.08	3.29	1.97
Two-Axle	1.60	0.96	2.63	1.57
Concrete	1.32	0.79	2.22	1.33
18-Wheeler	1.92	1.15	2.87	1.72
6-Axle	1.71	1.02	2.65	1.59
School Bus	3.58	2.14	6.06	3.63
HS-Truck	1.52	0.91	2.32	1.39
HS Lane - M	3.85	2.31	4.86	2.91
HS Lane - V	2.60	1.55	3.68	2.20

Table 72: Span V - Arch Section A14 Rating Factors

Trucks	Rating Factors			
	Axial and Moment		Shear	
	Operating	Inventory	Operating	Inventory
Tri-Axle	1.09	0.65	2.22	1.33
H-Truck	1.73	1.04	3.56	2.13
Two-Axle	1.50	0.90	2.93	1.75
Concrete	1.24	0.74	2.44	1.46
18-Wheeler	1.77	1.06	3.44	2.06
6-Axle	1.60	0.96	3.19	1.91
School Bus	3.42	2.05	6.80	4.07
HS-Truck	1.40	0.84	2.61	1.56
HS Lane - M	3.72	2.23	5.38	3.22
HS Lane - V	2.50	1.50	4.03	2.42

Table 73: Span V - Arch Section A20 Rating Factors

Trucks	Rating Factors			
	Axial and Moment		Shear	
	Operating	Inventory	Operating	Inventory
Tri-Axle	1.47	0.88	2.07	1.24
H-Truck	2.27	1.36	3.34	2.00
Two-Axle	2.04	1.22	2.74	1.64
Concrete	1.66	1.00	2.28	1.37
18-Wheeler	2.49	1.49	3.22	1.93
6-Axle	2.24	1.34	2.97	1.78
School Bus	4.57	2.74	6.38	3.82
HS-Truck	1.97	1.18	2.43	1.46
HS Lane - M	5.50	3.29	5.35	3.20
HS Lane - V	3.28	1.96	3.97	2.38

Table 74: Span V - Arch Section A40 Rating Factors

Trucks	Rating Factors			
	Axial and Moment		Shear	
	Operating	Inventory	Operating	Inventory
Tri-Axle	1.25	0.75	3.30	1.98
H-Truck	2.23	1.34	5.63	3.37
Two-Axle	1.66	1.00	4.37	2.62
Concrete	1.43	0.85	3.71	2.22
18-Wheeler	1.79	1.07	4.23	2.54
6-Axle	1.74	1.04	4.07	2.44
School Bus	4.16	2.49	10.57	6.33
HS-Truck	1.41	0.85	3.81	2.28
HS Lane - M	6.55	3.92	9.53	5.71
HS Lane - V	4.22	2.53	7.50	4.49

5.3 SPAN VI RATING RESULTS

For Span VI, the ratings are presented for Column 2, Column 3, Hanger 1, Transverse Deep Beam, transverse floor beams at Column 2, at Column 2, and at Hanger 1, and arch rib sections.

5.3.1 Column 2

Ratings are provided for the interior and exterior Column 2s as shown in Table 75 and Table 76, respectively. Ratings were calculated using the Beam and Column 2 model presented in Section 3.5.3. The interior columns are under axial compression for dead and live loads. The exterior columns are in tension under live loads.

Table 75: Span VI - Interior Column 2 Rating Factors

Trucks	Rating Factors	
	Operating	Inventory
Tri-Axle	2.73	1.64
H-Truck	3.83	2.29
Two-Axle	3.84	2.30
Concrete	3.07	1.84
18-Wheeler	4.39	2.63
6-Axle	3.78	2.26
School Bus	7.20	4.32
HS-Truck	3.83	2.29

Table 76: Span VI - Exterior Column 2 Rating Factors

Trucks	Rating Factors	
	Operating	Inventory
Tri-Axle	1.88	1.13
H-Truck	2.64	1.58
Two-Axle	2.64	1.58
Concrete	2.11	1.27
18-Wheeler	3.02	1.81
6-Axle	2.60	1.56
School Bus	4.96	2.97
HS-Truck	2.64	1.58

5.3.2 Column 3

Ratings are provided for the interior and exterior Column 3s as shown in Table 77 and Table 78, respectively. Ratings were calculated using the Beam and Column 3 model presented in Section 3.5.4. Unlike Column 2s, where the exterior columns are in tension under live loads, both the interior and exterior Column 3s are under compression for dead and live loads. Rating factors for the exterior columns are lower than for the interior columns.

Table 77: Span VI - Interior Column 3 Rating Factors

Trucks	Rating Factors	
	Operating	Inventory
Tri-Axle	2.73	1.64
H-Truck	3.89	2.33
Two-Axle	3.82	2.29
Concrete	3.06	1.83
18-Wheeler	4.37	2.62
6-Axle	3.78	2.27
School Bus	7.33	4.39
HS-Truck	3.89	2.33

Table 78: Span VI - Exterior Column 3 Rating Factors

Trucks	Rating Factors	
	Operating	**Inventory**
Tri-Axle	1.89	1.13
H-Truck	2.70	1.62
Two-Axle	2.65	1.59
Concrete	2.12	1.27
18-Wheeler	3.03	1.81
6-Axle	2.62	1.57
School Bus	5.08	3.04
HS-Truck	2.70	1.62

5.3.3 Hanger 1

Ratings are provided for the hangers as shown in Table 79. Ratings were calculated using the Beam and Hanger 1 model presented in Section 3.5.6.1. It was decided from the longitudinal beam analysis that Hanger 1 carries the highest tension axial load from the truck loadings. Thus, only Hanger 1 was rated for axial tension since all hangers have the same capacity.

Table 79: Span VI - Hanger 1 Rating Factors

Trucks	Rating Factors	
	Operating	**Inventory**
Tri-Axle	1.08	0.64
H-Truck	1.51	0.90
Two-Axle	1.41	0.84
Concrete	1.13	0.68
18-Wheeler	1.61	0.96
6-Axle	1.53	0.91
School Bus	2.84	1.70
HS-Truck	1.51	0.90

5.3.4 Transverse Deep Beam

Ratings are provided for the Transverse Deep Beam as shown in Table 80. Ratings were calculated using the Transverse Deep Beam model presented in Section 3.5.7. The Transverse Deep Beam was rated for bending moment and shear. The bending moment controls the rating with a 0.98 operating rating for the tri-axle truck.

Table 80: Span VI - Transverse Deep Beam Rating Factors

Trucks	Rating Factors			
	Bending Moment		Shear	
	Operating	Inventory	Operating	Inventory
Tri-Axle	**0.98**	0.59	1.94	1.16
H-Truck	1.38	0.82	2.72	1.63
Two-Axle	1.38	0.83	2.73	1.63
Concrete	1.10	0.66	2.18	1.31
18-Wheeler	1.58	0.94	3.12	1.87
6-Axle	1.36	0.81	2.68	1.61
School Bus	2.59	1.55	5.12	3.07
HS-Truck	1.38	0.82	2.72	1.63

5.3.5 Transverse Floor Beams

The transverse floor beams were rated for bending moment and shear. For shear ratings, transverse floor beams were discretized into three zones. The transverse floor beams at column locations were rated for positive bending moment, negative bending moment, and shear. The transverse floor beams at hanger locations were rated for positive bending moment and shear. Negative bending moment in the hanger is not rated because the hangers are assumed to have no flexural rigidity. The controlling positive bending moment and shear ratings are at the transverse floor beam at Hanger 1 location and are shown in Section 5.3.5.3. The controlling negative bending moment rating is at the transverse floor beam at Column 2 location and is shown in the following section. For completeness, full rating results are provided for transverse beam at Columns 2 and 3 are in Appendix C2.1 and C2.2.

5.3.5.1 Transverse Floor Beam at Column 2

The transverse floor beam at Column 2 controls the rating for negative bending moment for all transverse floor beams and is shown in Table 81. Ratings were calculated using the transverse floor beam model presented in Section 3.5.3. For completeness, full rating results are provided for the transverse floor beam at Column 2 in Appendix C2.1.

Table 81: Span VI - Transverse Floor Beam at Column 2 Rating Factors

Trucks	Rating Factors	
	Negative Moment	
	Operating	Inventory
Tri-Axle	4.65	2.79
H-Truck	6.52	3.90
Two-Axle	6.53	3.91
Concrete	5.23	3.13
18-Wheeler	7.47	4.47
6-Axle	6.43	3.85
School Bus	12.27	7.35
HS-Truck	6.52	3.90

5.3.5.2 Transverse Floor Beam at Column 3

Full rating results are provided for completeness for the transverse floor beam at Column 3 in Appendix C2.2.

5.3.5.3 Transverse Floor Beam at Hanger 1

Rating factors are provided for the transverse floor beam at Hanger 1 as shown in Table 82 for bending moment and Table 83 for shear. Ratings were calculated using the transverse floor beam presented in Section 3.5.6.1. The transverse floor beam at Hanger 1 was rated for positive bending moment and shear; however, the transverse floor beam was discretized into three zones for shear ratings. All of the transverse floor beams at the hanger locations have no negative

bending moment because the hangers were modeled as axial tension hangers only. Bending moment controls the rating. For the tri-axle truck and concrete truck, the bending moment operating rating factor is 0.93 and 0.97, respectively.

Table 82: Span VI - Transverse Floor Beam at Hanger 1 Rating Factors: Part 1

Trucks	Rating Factors	
	Bending Moment	
	Operating	Inventory
Tri-Axle	**0.93**	0.55
H-Truck	1.30	0.78
Two-Axle	1.21	0.73
Concrete	**0.97**	0.58
18-Wheeler	1.39	0.83
6-Axle	1.31	0.79
School Bus	2.44	1.46
HS-Truck	1.30	0.78

Table 83: Span VI - Transverse Floor Beam at Hanger 1 Rating Factors: Part 2

Trucks	Rating Factors					
	V_{zone1}		V_{zone2}		V_{zone3}	
	Operating	Inventory	Operating	Inventory	Operating	Inventory
Tri-Axle	1.37	0.82	1.05	0.63	1.09	0.65
H-Truck	1.92	1.15	1.47	0.88	1.52	0.91
Two-Axle	1.80	1.08	1.37	0.82	1.43	0.85
Concrete	1.44	0.86	1.10	0.66	1.14	0.68
18-Wheeler	2.05	1.23	1.57	0.94	1.63	0.98
6-Axle	1.95	1.17	1.49	0.89	1.54	0.93
School Bus	3.62	2.17	2.76	1.65	2.87	1.72
HS-Truck	1.92	1.15	1.47	0.88	1.52	0.91

5.3.6 Arch Rib

Rating factors are provided for the arch rib at seven locations as pointed out in Figure 64. Critical sections were determined by looking at the qualitative and quantitative output diagrams

for the shear, bending moment, and axial load from SAP2000. Ratings were provided for one-half of the arch rib since the span is symmetrical. Ratings were calculated using the arch rib model presented in Section 3.6.4. The arch rib sections were rated for shear and the combination of axial load and bending moment. Ratings for the lane loading are provided in addition to ratings for the eight standard trucks.

Rating factors for Sections A1, A2, A3, A7, A13, A18, and A36 are shown in Table 84 through Table 90, respectively. All operating ratings are 1.0 and above except for arch Sections A2 and A3 where the combination of axial load and bending moment are 0.96 and 0.99, respectively, for the tri-axle truck. The combination of axial load and bending moment controlled the ratings.

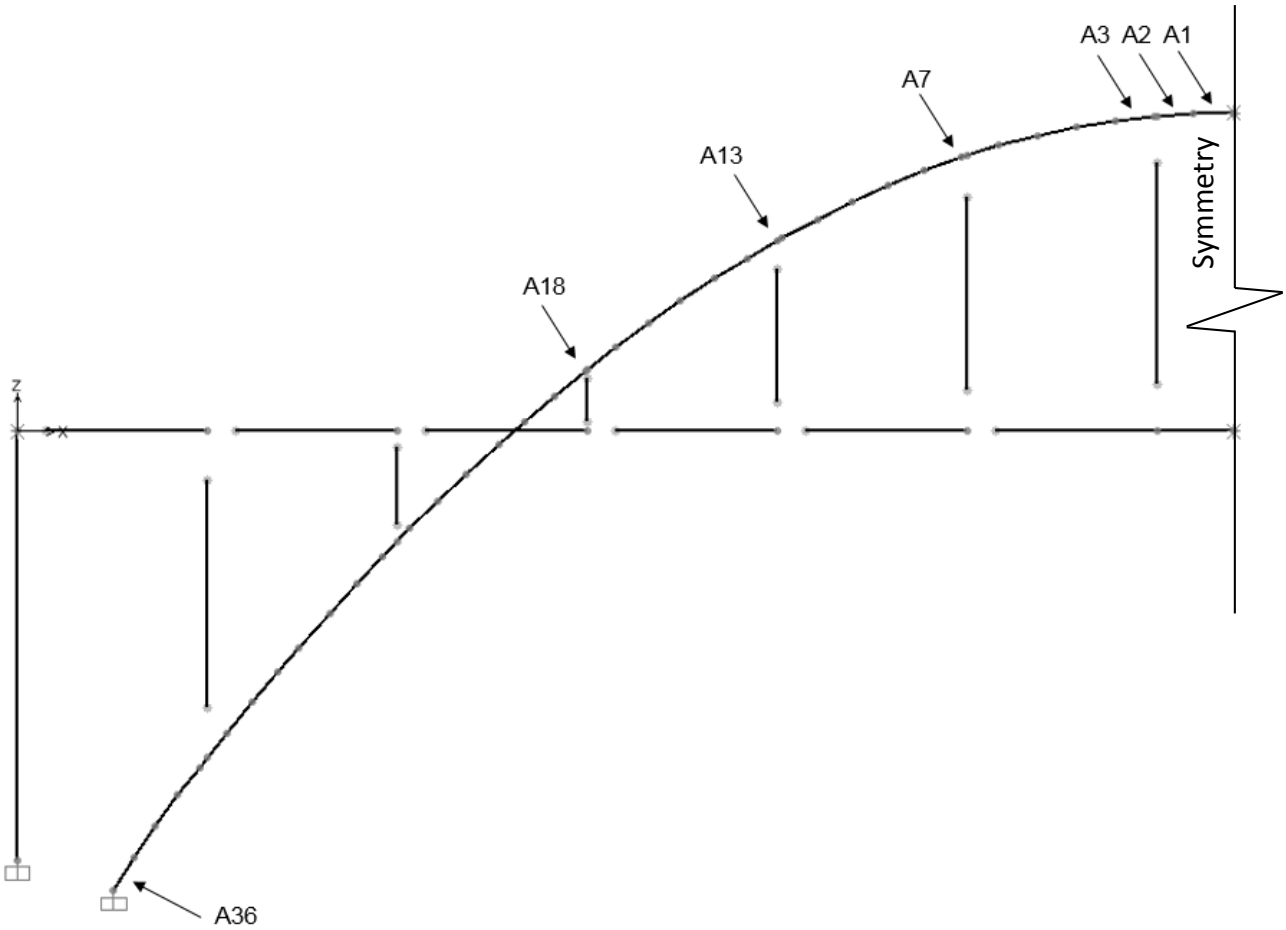

Figure 64: Span VI - Arch Rib with Rated Sections Labeled (SAP 2013)

Table 84: Span VI - Arch Section A1 Rating Factors

Trucks	Rating Factors			
	Axial and Moment		Shear	
	Operating	Inventory	Operating	Inventory
Tri-Axle	1.22	0.73	1.98	1.19
H-Truck	1.70	1.02	3.30	1.98
Two-Axle	1.65	0.99	2.59	1.55
Concrete	1.29	0.77	2.20	1.32
18-Wheeler	1.90	1.14	2.77	1.66
6-Axle	1.81	1.08	2.57	1.54
School Bus	3.36	2.01	6.05	3.62
HS-Truck	1.60	0.96	2.26	1.35
HS Lane - M	3.47	2.08	6.52	3.91
HS Lane - V	2.32	1.39	4.57	2.74

Table 85: Span VI - Arch Section A2 Rating Factors

Trucks	Rating Factors			
	Axial and Moment		Shear	
	Operating	Inventory	Operating	Inventory
Tri-Axle	**0.96**	0.57	1.12	0.67
H-Truck	1.38	0.83	1.54	0.92
Two-Axle	1.28	0.77	1.42	0.85
Concrete	1.02	0.61	1.19	0.71
18-Wheeler	1.49	0.89	1.53	0.92
6-Axle	1.43	0.86	1.50	0.90
School Bus	2.79	1.67	2.86	1.72
HS-Truck	1.23	0.74	1.24	0.74
HS Lane - M	2.76	1.65	2.31	1.38
HS Lane - V	1.87	1.12	1.71	1.03

Table 86: Span VI - Arch Section A3 Rating Factors

Trucks	Rating Factors			
	Axial and Moment		Shear	
	Operating	Inventory	Operating	Inventory
Tri-Axle	**0.99**	0.59	1.38	0.83
H-Truck	1.43	0.85	1.85	1.11
Two-Axle	1.32	0.79	1.74	1.04
Concrete	1.05	0.63	1.45	0.87
18-Wheeler	1.54	0.92	1.89	1.13
6-Axle	1.47	0.88	1.86	1.11
School Bus	2.89	1.73	3.47	2.08
HS-Truck	1.26	0.75	1.52	0.91
HS Lane - M	2.89	1.73	2.94	1.76
HS Lane - V	1.95	1.17	2.15	1.29

Table 87: Span VI - Arch Section A7 Rating Factors

Trucks	Rating Factors			
	Axial and Moment		Shear	
	Operating	Inventory	Operating	Inventory
Tri-Axle	1.10	0.66	1.82	1.09
H-Truck	1.68	1.01	2.41	1.45
Two-Axle	1.53	0.91	2.39	1.43
Concrete	1.25	0.75	2.01	1.20
18-Wheeler	1.84	1.10	2.64	1.58
6-Axle	1.63	0.98	2.44	1.46
School Bus	3.32	1.99	4.59	2.75
HS-Truck	1.44	0.86	2.14	1.28
HS Lane - M	3.67	2.20	4.29	2.57
HS Lane - V	2.44	1.46	3.26	1.95

Table 88: Span VI - Arch Section A13 Rating Factors

Trucks	Rating Factors			
	Axial and Moment		Shear	
	Operating	Inventory	Operating	Inventory
Tri-Axle	1.02	0.61	2.06	1.24
H-Truck	1.57	0.94	3.24	1.94
Two-Axle	1.41	0.84	2.73	1.63
Concrete	1.15	0.69	2.25	1.35
18-Wheeler	1.72	1.03	3.16	1.90
6-Axle	1.53	0.92	3.03	1.81
School Bus	3.13	1.87	6.32	3.79
HS-Truck	1.33	0.80	2.44	1.46
HS Lane - M	3.42	2.05	5.00	3.00
HS Lane - V	2.28	1.36	3.72	2.23

Table 89: Span VI - Arch Section A18 Rating Factors

Trucks	Rating Factors			
	Axial and Moment		Shear	
	Operating	Inventory	Operating	Inventory
Tri-Axle	1.56	0.93	1.93	1.16
H-Truck	2.36	1.41	3.06	1.83
Two-Axle	2.19	1.31	2.56	1.54
Concrete	1.76	1.05	2.12	1.27
18-Wheeler	2.69	1.61	2.98	1.78
6-Axle	2.40	1.44	2.86	1.72
School Bus	4.73	2.84	5.94	3.56
HS-Truck	2.14	1.28	2.30	1.38
HS Lane - M	4.97	2.98	4.90	2.94
HS Lane - V	3.35	2.01	3.62	2.17

Table 90: Span VI - Arch Section A36 Rating Factors

Trucks	Rating Factors			
	Axial and Moment		Shear	
	Operating	Inventory	Operating	Inventory
Tri-Axle	1.30	0.78	3.14	1.88
H-Truck	2.32	1.39	5.30	3.18
Two-Axle	1.74	1.04	4.18	2.51
Concrete	1.48	0.89	3.52	2.11
18-Wheeler	2.01	1.21	4.10	2.46
6-Axle	1.93	1.16	3.94	2.36
School Bus	4.45	2.67	10.18	6.10
HS-Truck	1.50	0.90	3.70	2.22
HS Lane - M	7.00	4.19	9.18	5.50
HS Lane - V	4.41	2.64	7.16	4.29

5.4 SPAN VII RATING RESULTS

For Span VII, the naming convention is presented in Figure 65 for convenience. Columns 4, 5, 6, and 7 have the same cross sectional geometry; however, the reinforcements are different as discussed in Section 2.4. Since the columns have different reinforcements, they have different capacities. Therefore, each column was rated. For the columns, the ratings are presented for Columns 4, 5, and 7. Column 3 in Span VII is the same as Column 3 in Span VI; therefore, ratings for Column 3 are in the Span VI section. Columns 5 and 6 have the same reinforcing bars and transverse truck loadings, thus ratings are provided for Column 5 only. In addition, ratings are provided for the transverse floor beams and arch rib sections.

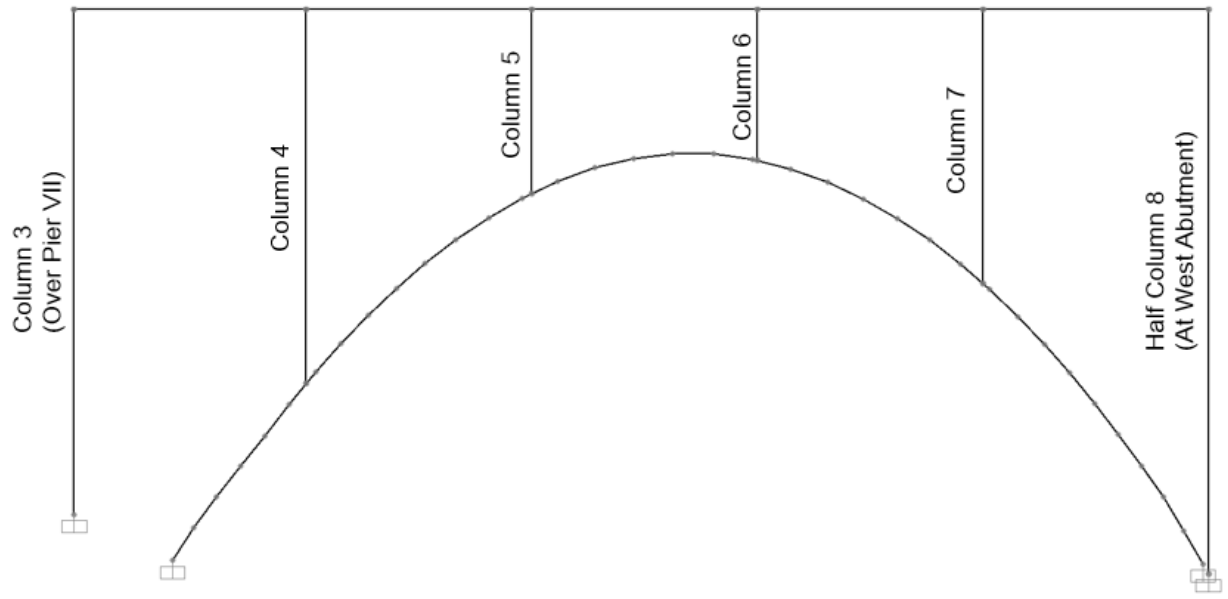

Figure 65: Span VII Naming Convention (SAP 2013) (Duplicate - Figure 6)

5.4.1 Column 4

Ratings are provided for the interior and exterior Column 4s as shown in Table 91 and Table 92, respectively. Ratings were calculated using the Beam and Column 4 model presented in Section 3.5.5. The interior columns are under axial compression for dead and live loads. The exterior columns are in tension under live loads.

Table 91: Span VII - Interior Column 4 Rating Factors

Trucks	Rating Factors	
	Operating	Inventory
Tri-Axle	2.61	1.56
H-Truck	3.52	2.11
Two-Axle	3.62	2.17
Concrete	2.90	1.74
18-Wheeler	4.14	2.48
6-Axle	3.63	2.17
School Bus	6.63	3.97
HS-Truck	3.52	2.11

Table 92: Span VII - Exterior Column 4 Rating Factors

Trucks	Rating Factors	
	Operating	Inventory
Tri-Axle	1.63	0.98
H-Truck	2.21	1.32
Two-Axle	2.27	1.36
Concrete	1.81	1.09
18-Wheeler	2.59	1.55
6-Axle	2.27	1.36
School Bus	4.15	2.49
HS-Truck	2.21	1.32

5.4.2 Column 5

Ratings are provided for the interior and exterior Column 5s using two separate model cases. Ratings from Case A, shown in Figure 46, are shown in Table 93 for the interior column and Table 94 for the exterior column. Ratings were calculated using the Beam and Column 5 model presented in Section 3.5.5.1. The interior columns are under compression for dead and live loads while the exterior columns are under tension for the same applied loads. Ratings from Case B, shown in Figure 47, are in Appendix D4.1.

Table 93: Span VII - Interior Column 5 Rating Factors – Case A

Trucks	Rating Factors	
	Operating	Inventory
Tri-Axle	1.45	0.87
H-Truck	1.94	1.16
Two-Axle	2.01	1.20
Concrete	1.61	0.96
18-Wheeler	2.30	1.38
6-Axle	2.01	1.20
School Bus	3.65	2.19
HS-Truck	1.94	1.16

Table 94: Span VII - Exterior Column 5 Rating Factors – Case A

Trucks	Rating Factors	
	Operating	Inventory
Tri-Axle	**0.99**	0.59
H-Truck	1.32	0.79
Two-Axle	1.37	0.82
Concrete	1.10	0.66
18-Wheeler	1.57	0.94
6-Axle	1.37	0.82
School Bus	2.49	1.49
HS-Truck	1.32	0.79

5.4.3 Column 7

Ratings are provided for the interior and exterior Column 7s using two separate model cases. Ratings from Case A, shown in Figure 46, are shown in Table 95 for the interior columns and Table 96 for the exterior columns. Ratings were calculated using the Beam and Column 7 model presented in Section 3.5.5.1. The interior columns are under compression for dead and live loads, while the exterior columns are essentially in tension for the same load effects. Ratings from Case B, shown in Figure 47, are in Appendix D4.1.

Table 95: Span VII - Interior Column 7 Rating Factors – Case A

Trucks	Rating Factors	
	Operating	Inventory
Tri-Axle	2.02	1.21
H-Truck	2.71	1.62
Two-Axle	2.81	1.68
Concrete	2.25	1.35
18-Wheeler	3.21	1.92
6-Axle	2.81	1.68
School Bus	5.10	3.06
HS-Truck	2.71	1.62

Table 96: Span VII - Exterior Column 7 Rating Factors – Case A

Trucks	Rating Factors	
	Operating	Inventory
Tri-Axle	2.59	1.55
H-Truck	3.47	2.08
Two-Axle	3.59	2.15
Concrete	2.87	1.72
18-Wheeler	4.10	2.46
6-Axle	3.59	2.15
School Bus	6.53	3.91
HS-Truck	3.47	2.08

5.4.4 Transverse Floor Beams

The transverse floor beams were rated for positive bending moment, negative bending moment, and shear. The controlling positive bending moment is at the transverse beam at Column 4 location as shown in the next section. The controlling negative bending moment is at the transverse beam at Column 5 location as shown in the next section. For shear ratings, transverse floor beams were discretized into three zones. The controlling shear rating is at the transverse beam at Column 4 location as shown in Section 5.4.6.

5.4.4.1 Transverse Floor Beam Bending Moment Rating

The controlling positive bending moment rating for the transverse floor beam are at the Column 4 locations and are shown in Table 97. The controlling negative bending moment ratings for the transverse floor beam are at Column 5 locations. Remember that there were two model cases for the Beam and Column 5. The negative bending moment ratings for the transverse beam using Case A are shown here in Table 98. For Case B, the ratings are shown in Appendix D2.2 for results presentation consistency. However, the absolute lowest negative bending moment rating is 2.13, which is Case B.

For completeness, negative bending moment ratings for the transverse beam at column 4 are provided in Appendix D2.1. The shear ratings for this transverse beam are shown in the next section because it is the controlling transverse beam for shear ratings. Also, for completeness, shear and positive bending moment ratings for the transverse floor beam at Column 5 location – Case A are in Appendix D2.2. None of the transverse beam rating factors at Column 5 are less than 1.0 for Case A or Case B.

Table 97: Span VII - Transverse Floor Beam at Column 4 Positive Bending Moment Rating Factors

Trucks	Rating Factors	
	Positive Moment	
	Operating	Inventory
Tri-Axle	1.64	0.98
H-Truck	2.22	1.33
Two-Axle	2.28	1.36
Concrete	1.82	1.09
18-Wheeler	2.60	1.56
6-Axle	2.28	1.37
School Bus	4.17	2.50
HS-Truck	2.22	1.33

Table 98: Span VII - Transverse Floor Beam at Column 5 Negative Bending Moment Rating Factors – Case A

Trucks	Rating Factors	
	Negative Moment	
	Operating	Inventory
Tri-Axle	2.49	1.49
H-Truck	3.33	2.00
Two-Axle	3.45	2.07
Concrete	2.76	1.65
18-Wheeler	3.94	2.36
6-Axle	3.45	2.07
School Bus	6.27	3.76
HS-Truck	3.33	2.00

5.4.4.2 Transverse Floor Beam Shear Rating

The transverse floor beam at Column 4 controls the rating for shear and is shown in Table 99. Ratings were calculated using the transverse floor beam model presented in Section 3.5.5.

Table 99: Span VII - Transverse Floor Beam at Column 4 Rating Factors

Trucks	Rating Factors					
	V_{zone1}		V_{zone2}		V_{zone3}	
	Operating	Inventory	Operating	Inventory	Operating	Inventory
Tri-Axle	2.01	1.20	1.42	0.85	1.48	0.89
H-Truck	2.71	1.62	1.92	1.15	2.00	1.20
Two-Axle	2.79	1.67	1.98	1.18	2.06	1.23
Concrete	2.23	1.34	1.58	0.95	1.65	0.99
18-Wheeler	3.18	1.91	2.26	1.35	2.35	1.41
6-Axle	2.79	1.67	1.98	1.19	2.06	1.24
School Bus	5.10	3.06	3.62	2.17	3.77	2.26
HS-Truck	2.71	1.62	1.92	1.15	2.00	1.20

5.4.5 Arch Rib

Rating factors are provided for the arch rib at eight locations as pointed out in Figure 66. Critical sections were determined by looking at the qualitative and quantitative output diagrams for the shear, bending moment, and axial load from SAP2000. Ratings were calculated using the arch rib model presented in Section 3.6.4. The arch rib sections were rated for shear and the combination of axial load and bending moment. Ratings for the lane loading are provided in addition to ratings for the eight standard trucks.

Rating factors for Sections A1, A10, A14, A16, A18, A22, A30, and A35 are shown in Table 100 through Table 107, respectively. For all sections except those at the ends, the shear controls the rating. All operating ratings are 1.0 and above except for arch Section A16 where the shear rating is 0.86 for the tri-axle truck and 0.90 for the concrete truck.

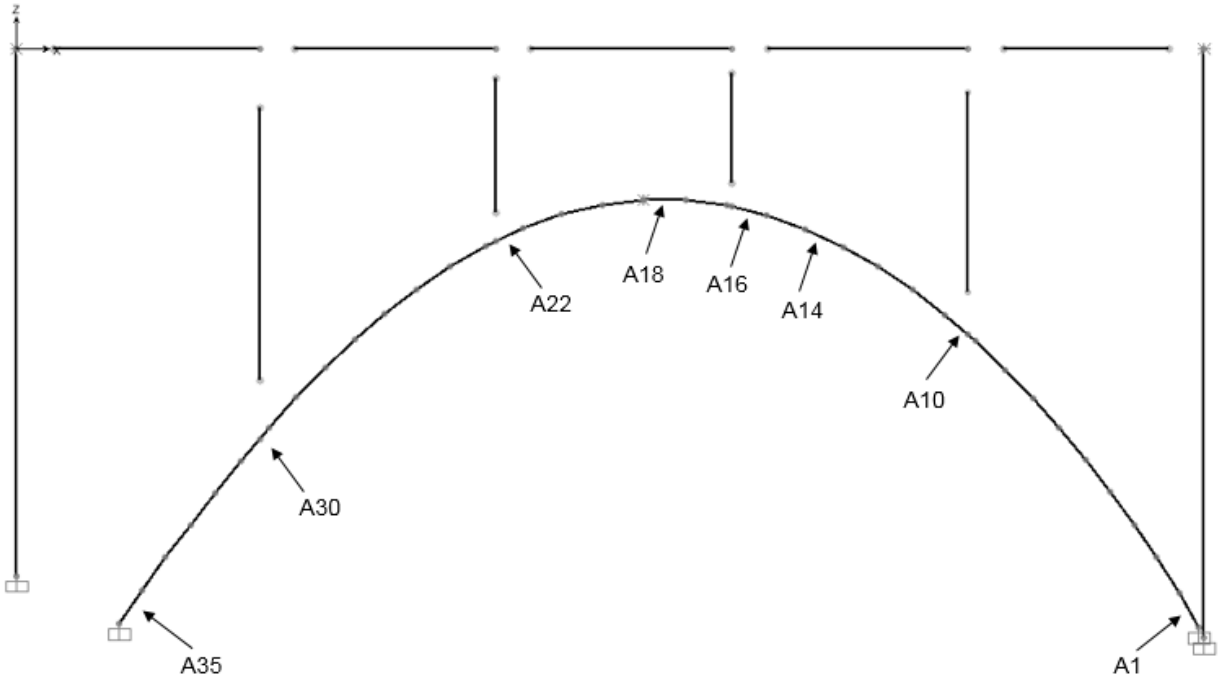

Figure 66: Span VII - Arch Rib with Rated Sections Labeled (SAP 2013)

Table 100: Span VII - Arch Section A1 Rating Factors

Trucks	Rating Factors			
	Axial and Moment		Shear	
	Operating	Inventory	Operating	Inventory
Tri-Axle	2.92	1.75	3.16	1.89
H-Truck	3.40	2.03	5.30	3.17
Two-Axle	3.87	2.32	4.45	2.66
Concrete	3.04	1.82	3.56	2.14
18-Wheeler	4.39	2.63	5.01	3.00
6-Axle	4.05	2.43	4.38	2.62
School Bus	6.31	3.78	10.18	6.10
HS-Truck	3.90	2.33	4.25	2.54
HS Lane - M	7.77	4.65	7.01	4.20
HS Lane - V	5.08	3.04	5.30	3.18

Table 101: Span VII - Arch Section A10 Rating Factors

Trucks	Rating Factors			
	Axial and Moment		Shear	
	Operating	Inventory	Operating	Inventory
Tri-Axle	1.95	1.17	1.12	0.67
H-Truck	2.25	1.35	1.55	0.93
Two-Axle	2.56	1.53	1.55	0.93
Concrete	2.01	1.20	1.24	0.74
18-Wheeler	2.89	1.73	1.77	1.06
6-Axle	2.70	1.62	1.56	0.94
School Bus	4.20	2.51	2.91	1.74
HS-Truck	2.56	1.53	1.55	0.93
HS Lane - M	4.06	2.43	2.21	1.32
HS Lane - V	2.78	1.66	1.63	0.98

Table 102: Span VII - Arch Section A14 Rating Factors

Trucks	Rating Factors			
	Axial and Moment		Shear	
	Operating	Inventory	Operating	Inventory
Tri-Axle	3.78	2.26	2.74	1.64
H-Truck	4.71	2.82	3.33	2.00
Two-Axle	4.84	2.90	3.38	2.03
Concrete	3.86	2.31	2.71	1.62
18-Wheeler	5.42	3.25	3.87	2.32
6-Axle	5.36	3.21	3.99	2.39
School Bus	8.97	5.38	6.29	3.77
HS-Truck	4.64	2.78	3.30	1.98
HS Lane - M	8.71	5.22	5.35	3.21
HS Lane - V	6.03	3.61	3.83	2.29

Table 103: Span VII - Arch Section A16 Rating Factors

Trucks	Rating Factors			
	Axial and Moment		Shear	
	Operating	Inventory	Operating	Inventory
Tri-Axle	1.79	1.07	**0.86**	0.54
H-Truck	2.10	1.26	1.13	0.70
Two-Axle	2.31	1.38	1.11	0.69
Concrete	1.85	1.11	**0.90**	0.57
18-Wheeler	2.66	1.59	1.23	0.76
6-Axle	2.53	1.52	1.20	0.74
School Bus	3.93	2.35	2.13	1.30
HS-Truck	2.19	1.31	1.05	0.66
HS Lane - M	3.52	2.11	1.55	0.96
HS Lane - V	2.48	1.48	1.18	0.73

Table 104: Span VII - Arch Section A18 Rating Factors

Trucks	Rating Factors			
	Axial and Moment		Shear	
	Operating	Inventory	Operating	Inventory
Tri-Axle	4.08	2.45	1.69	1.01
H-Truck	4.17	2.50	2.16	1.29
Two-Axle	5.27	3.16	2.14	1.28
Concrete	4.20	2.51	1.71	1.02
18-Wheeler	6.08	3.64	2.38	1.43
6-Axle	5.71	3.42	2.43	1.46
School Bus	7.73	4.63	4.16	2.49
HS-Truck	4.52	2.71	2.01	1.21
HS Lane - M	8.17	4.89	3.39	2.03
HS Lane - V	5.39	3.23	2.45	1.47

Table 105: Span VII - Arch Section A22 Rating Factors

Trucks	Rating Factors			
	Axial and Moment		Shear	
	Operating	Inventory	Operating	Inventory
Tri-Axle	1.45	0.87	1.01	0.60
H-Truck	1.76	1.06	1.37	0.82
Two-Axle	1.88	1.12	1.36	0.81
Concrete	1.49	0.89	1.09	0.65
18-Wheeler	2.13	1.28	1.54	0.92
6-Axle	2.06	1.23	1.41	0.85
School Bus	3.31	1.98	2.62	1.57
HS-Truck	1.83	1.10	1.33	0.79
HS Lane - M	2.99	1.79	1.88	1.13
HS Lane - V	2.09	1.25	1.41	0.84

Table 106: Span VII - Arch Section A30 Rating Factors

Trucks	Rating Factors			
	Axial and Moment		Shear	
	Operating	Inventory	Operating	Inventory
Tri-Axle	7.10	4.25	1.37	0.82
H-Truck	7.99	4.79	1.92	1.15
Two-Axle	9.13	5.47	1.89	1.13
Concrete	7.42	4.44	1.51	0.91
18-Wheeler	6.51	3.90	2.16	1.29
6-Axle	7.24	4.34	1.90	1.14
School Bus	13.55	8.12	3.62	2.17
HS-Truck	8.03	4.81	1.92	1.15
HS Lane - M	12.72	7.62	2.93	1.75
HS Lane - V	9.50	5.69	2.12	1.27

Table 107: Span VII - Arch Section A35 Rating Factors

Trucks	Rating Factors			
	Axial and Moment		Shear	
	Operating	Inventory	Operating	Inventory
Tri-Axle	2.18	1.30	3.05	1.83
H-Truck	3.02	1.81	4.14	2.48
Two-Axle	3.00	1.79	4.25	2.54
Concrete	2.34	1.40	3.40	2.04
18-Wheeler	3.35	2.00	4.85	2.91
6-Axle	3.01	1.80	4.23	2.54
School Bus	5.68	3.40	7.80	4.67
HS-Truck	3.59	2.15	4.14	2.48
HS Lane - M	5.76	3.45	7.18	4.30
HS Lane - V	3.86	2.31	5.01	3.00

5.5 SUMMARY OF RATING RESULTS

A summary of the rating results is shown in Table 108. The limiting components along with the limit state and truck are shown. The results shown in the column labeled "Operating RF" were calculated for a concrete compressive strength of 3,000 psi. The results shown in the column labeled "Higher Operating RF in Ch. 6" are calculated using the concrete compressive strength shown. The column labeled "Ch. 6 Section" indicates the section number in Chapter 6 where additional results are presented.

Table 108: Components with Operating Factor Less Than 1.0

Span	Component	Limit State	Truck	Operating RF	Higher Operating RF in Ch. 6	Ch. 6 Section
IV	Trans. Floor Bm. at Hanger 1	Positive Bending	Tri-Axle	0.98	No	6.6
V	Trans. Floor Bm. at Hanger 1	Positive Bending	Tri-Axle	0.99	No	6.6
V	Arch Rib Section A2	Axial Compr. and Moment	Tri-Axle	0.96	1.00 for f'_c 3,500 psi	6.5
VI	Trans. Deep Beam	Positive Bending	Tri-Axle	0.98	No	6.7
VI	Trans. Floor Bm. at Hanger 1	Positive Bending	Tri-Axle	0.93	No	6.6
VI	Trans. Floor Bm. at Hanger 1	Positive Bending	Concrete	0.97	No	
VI	Arch Rib Section A2	Axial Compr. and Moment	Tri-Axle	0.96	1.02 for f'_c 4,000 psi	6.5
VI	Arch Rib Section A3	Axial Compr. and Moment	Tri-Axle	0.99	> 1.0 for f'_c 4,000 psi	
VII	Exterior Column 5 - Case A	Axial Tension	Tri-Axle	0.99	No	
VII	Arch Rib Section A16	Shear	Tri-Axle	0.86	1.10 for f'_c 4,000 psi	6.5
VII	Arch Rib Section A16	Shear	Concrete	0.90	> 1.0 for f'_c 4,000 psi	

Chapter 6

SENSITIVITY ANALYSES

Literature cited by Johnson et al. (2014) indicates that without restraint or applied stress, ASR will result in free expansion of concrete in all directions similar to that caused by a temperature increase in most common engineering materials. Expansion due to a temperature change in an indeterminate structure causes both internal forces and displacements. In this chapter, ASR-expansion in the arch rib of Span V is simulated using a uniform temperature increase for the purpose of investigating the internal forces and displacements that may result from ASR-expansion. Specifically, three questions are addressed: 1) Do the internal forces resulting from expansion add to or counteract those resulting from gravity loads? 2) What magnitudes of expansion are required to produce transverse flexural cracking at critical sections along the arch? And, 3) what magnitudes of deflection of the arch may result from expansion? Analyses that address these questions are presented in Section 6.1 and 6.2.

As illustrated by the compressive strengths of core samples listed in Table 11 and the discussion of that table, there is significant variation in the strength of the concrete in the arches. A compressive strength of 3,000 psi, and the corresponding modulus of elasticity from Eq. (22), was used in the analysis and ratings of all arch ribs. Rating factors less than one were calculated for the arch ribs of Spans V, VI and VII. The effects of assuming different values for the concrete compressive strength on the internal forces due to dead load and live loads, and the resulting rating factors and arch deflections, are investigated in Sections 6.3, 6.4 and 6.5. Values of compressive strength above 3,000 psi are assumed because higher values of compressive strength may be justified by the core test results of Table 11 or by additional sampling and testing. Higher compressive strengths result in rating factors greater than one for all the arch ribs as shown in Table 108. Values of compressive strength below 3,000 psi are assumed because deterioration due to ASR may result in reductions in cross section capacity. The effects of ASR-expansion on cross section capacity are not well understood, so it is not clear that simple reductions in compressive strength accurately reflect the reductions in cross section capacity that

may result from ASR. But, results for reductions in compressive strength are presented for future reference.

As summarized in Table 108, some of the transverse floor beams and transverse deep beams have rating factors less than one when the concrete compressive strength is assumed to be 3,000 psi. Since ASR may cause reductions in these cross section capacities in the future, concrete strengths below 3,000 psi are used to calculate rating factors in Section 6.6 and 6.7. These results illustrate that the beam ratings are controlled by flexure and are not sensitive to the concrete strength.

The live load utilized for all sensitivity analyses reported in this chapter is the tri-axle truck. From the LFR results shown in Chapter 5, the tri-axle truck is the controlling truck out of the eight standard trucks used in this project.

6.1 Effects of ASR-Expansion on Arch Internal Forces

The ASR-expansion of the arch rib of Span V was simulated by applying a uniform temperature increase to the arch rib. According to crack mappings provided by Johnson et al. (2014), ASR-cracks are present only in the arch sections above the deck. As a result, the uniform temperature increase used to model the ASR-expansion was only applied to sections above the deck. The model used for this analysis was the linear model, in which $E = E_c$ and $I = I_g$. Doing so, the effects of ASR-expansion were evaluated without being confounded by slenderness and creep effects. In addition, the model did not include the LFR's dead and live load factors since these analyses were used to estimate the serviceability effects of ASR-expansion on arch deflection and the potential for transverse flexural cracking. The lateral truck distribution factor, 1.160, and impact factor, 1.191, for Span V shown in Table 25 and Table 27, respectively, were included for live load cases.

The amount of ASR-expansion in the arch ribs was estimated from data and information reported by Johnson et al. (2014) in an earlier investigation of ASR in the Bibb Graves Bridge. Johnson reported that the first observations of ASR damage in the Bibb Graves Bridge were in 1956. He also reported transverse strain measurements made on the arches of Span 4 and Span 5 that indicate an average ASR-expansion of approximately 200 microstrain/year. By assuming

this rate of expansion has been constant since the 1950's, the total ASR-expansion to date is on the order of 10,000 microstrain (0.010 in./in.). This magnitude of total expansion is very large and is probably an overestimate of the actual amount. But, it is impossible to estimate the amount of total expansion with a high degree of confidence.

The uniform temperature increase required to produce a longitudinal free expansion of 10,000 microstrain in the arch model is 1,440°F. This temperature change was calculated from the following equation.

$$\Delta T_c = \frac{\varepsilon_l}{\alpha_t} \tag{33}$$

Where:

ε_l = longitudinal strain (in./in.)

α_t = coefficient of thermal expansion, 6.95×10^{-6} in./in./°F for concrete made with Alabama river gravel (Johnson's Master's Thesis 2014)

The effects of ASR-expansion on arch internal forces were assessed at three critical locations determined from the ratings in the previous Chapter. These arch sections are A2, A14, and A40 for Span V. These arch sections are at Hanger 1, Hanger 3, and base, respectively. These sections are shown in Figure 63. At each section, the bending moment, axial load, and shear were compared for various levels of ASR-expansion that will be used later. The comparisons were made for concrete strengths of 3,000 psi and 4,740 psi. The latter concrete strength is equal to the equivalent specified concrete strength shown in Table 11 determined from all core samples taken from the arch ribs.

Table 109 and Table 110 list the internal forces corresponding to the uniform temperature change for each section associated with four levels of longitudinal strain. For both concrete strengths, the bending moment, axial compression, and shear increase as the longitudinal strain increases.

Table 109: Effects of ASR-Expansion on Arch Internal Forces on 3,000 psi Model

Longitudinal Strain (με)	Section	Internal Force		
		M (k-ft)	P (k)	V (k)
10,000	A2	-1190	-100.	5.70
	A14	-498	-87.7	-49.0
	A40	3280	-52.2	85.8
3,447	A2	-409	-34.6	1.96
	A14	-172	-30.2	-16.9
	A40	1130	-18.0	29.6
1,814	A2	-215	-18.2	1.03
	A14	-90.0	-15.9	-8.88
	A40	594	-9.47	15.6
1,223	A2	-145	-12.3	0.690
	A14	-61.0	-10.7	-5.99
	A40	401	-6.38	10.5

Table 110: Effects of ASR-Expansion on Arch Internal Forces on 4,740 psi Model

Longitudinal Strain (με)	Section	Internal Force		
		M (k-ft)	P (k)	V (k)
10,000	A2	-1490	-126	7.10
	A14	-627	-110.	-61.6
	A40	4120	-65.6	108
1,897	A2	-283	-23.9	1.40
	A14	-119	-20.9	-11.7
	A40	781	-12.4	20.5
1,807	A2	-269	-22.8	1.29
	A14	-113	-19.9	-11.1
	A40	744	-11.9	19.5
1,341	A2	-200.	-16.9	-0.960
	A14	-84.0	-14.8	-8.26
	A40	552	-8.80	14.5

6.1.1 Bending Moment Sign Resulting from ASR-Expansion

When the uniform temperature increase simulating the ASR-expansion was applied to the model, it resulted in positive and negative bending distributed along the arch as shown in Figure 67. From the arch center to approximately the arch rib location between Hangers 3 and 4, the

uniform temperature change resulted in negative bending, tension on the top side. Then, from the location between Hangers 3 and 4 to the arch base, the uniform temperature increase resulted in positive bending. For comparison, a diagram of the arch half-span with the bending moment distribution for dead load is shown in Figure 68. In terms of stresses, the bending from the uniform temperature increase and the bending from the dead load are opposite in sign; so they counteract each other. The stress from axial load is additive, since it is in compression for all cases. For thoroughness, the bending moment, axial load, and shear resulting from dead and live load corresponding to the ASR-expansion model are presented in Appendix E1.

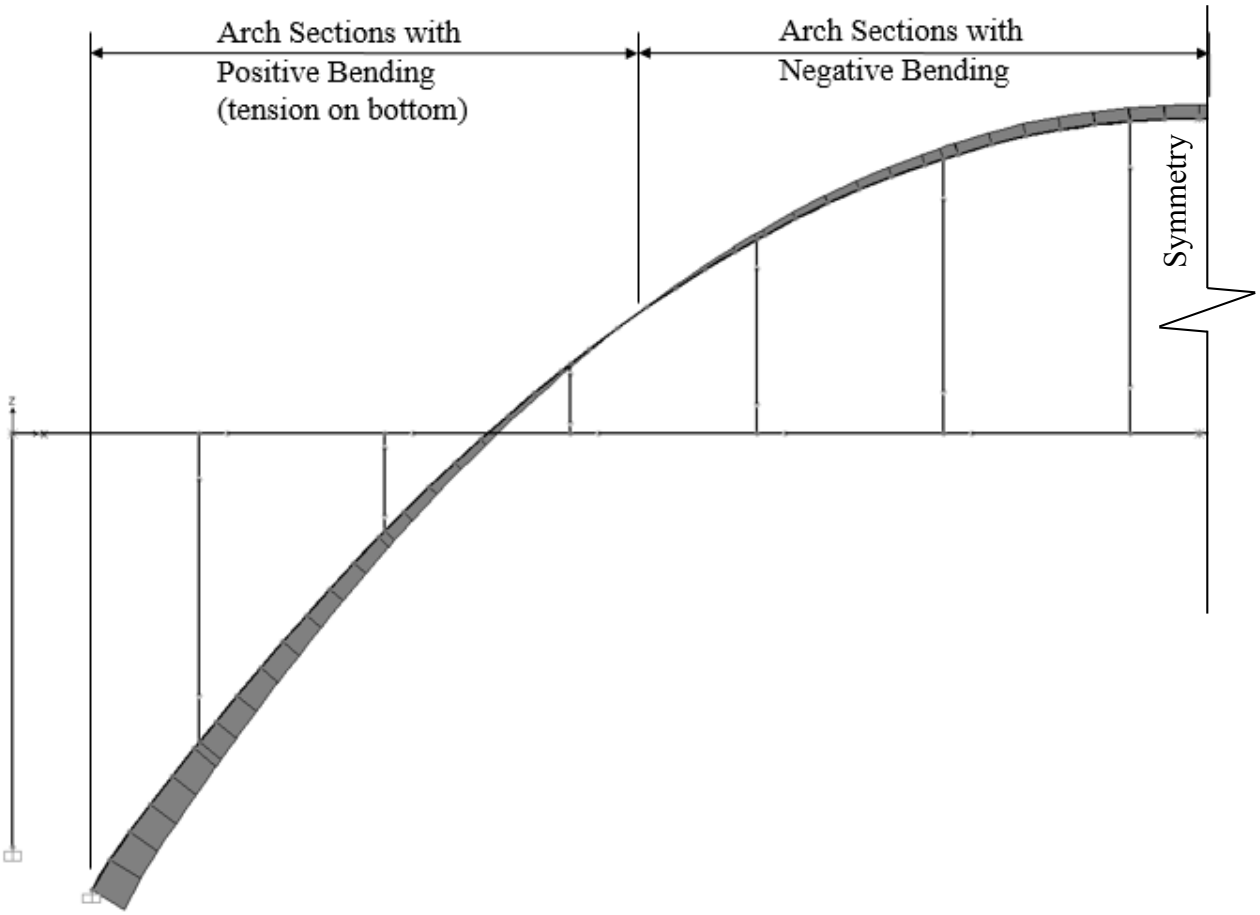

Figure 67: Positive and Negative Bending Distribution Resulting from Uniform Temperature Increase (SAP 2013)

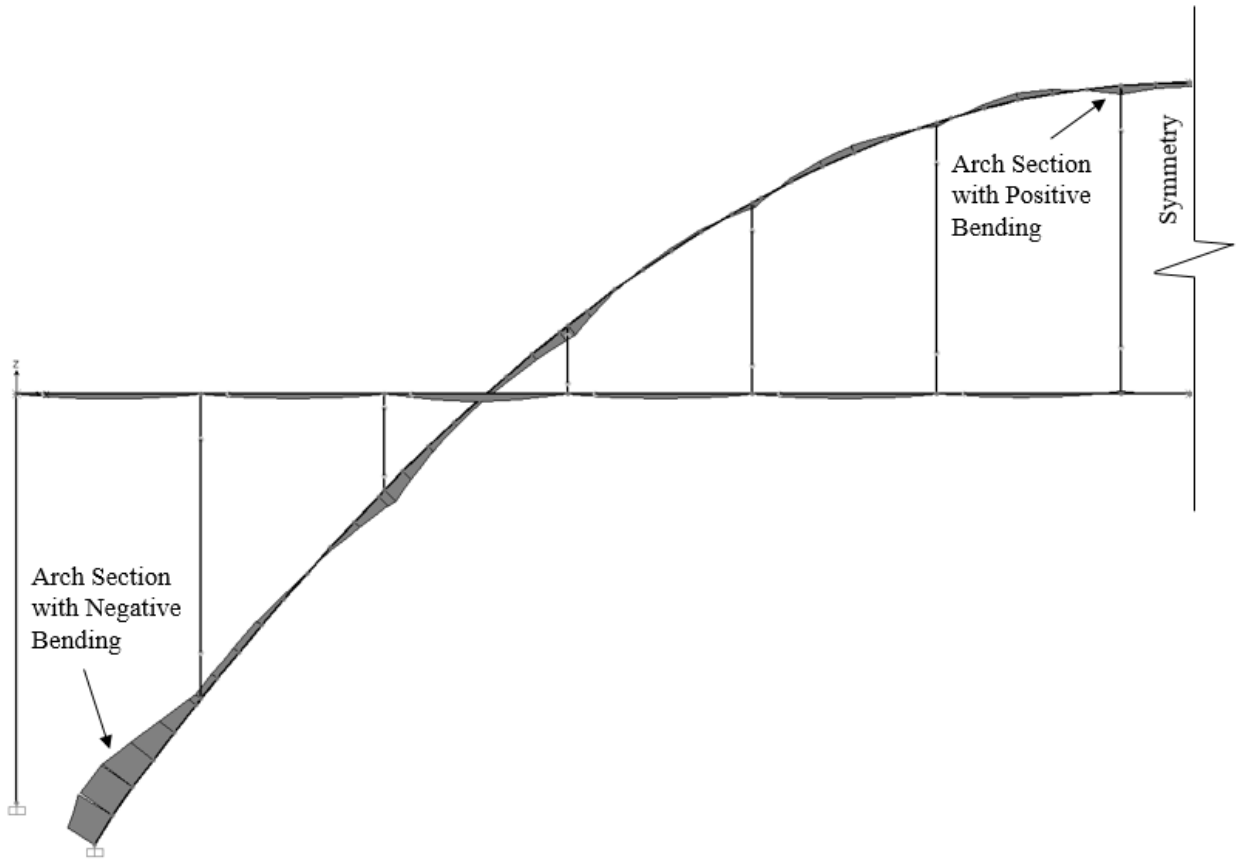

Figure 68: Positive and Negative Bending Distribution Resulting from Dead Load (SAP 2013)

6.1.2 Potential for Transverse Flexural Cracking due to ASR-Expansion Along With Dead and Live Load Effects

A question of interest is whether the internal forces due to ASR-expansion will result in transverse cracking of the arch cross sections. This is investigated by calculating extreme fiber stresses due to dead and live loads plus the internal bending moment and axial load due to ASR-expansion.

Using the bending moment and axial load from Table 109 and Table 110 for ASR-expansion internal forces, and Tables in Appendix E1 for dead and live load internal forces, stresses were computed at the top and bottom fiber for each section. Bending stresses and axial load stresses were computed using the following equations, respectively.

$$f_b = \frac{-M \cdot y}{I_g} \quad (34)$$

$$f_a = \frac{P}{A} \quad (35)$$

Where:

M = bending moment (k-in.), positive if tension is on the bottom

y = distance from the centroid to the fiber in which stress is being computed (in.)

I_g = gross section moment of inertia about the axis of bending ($in.^4$)

P = axial load (k), positive if tension

A = cross sectional area of section ($in.^4$)

The resultant stress at the cross section was found by combining the Eqs. (34) and (35). The stresses at the top and bottom fiber are shown in Table 111 and Table 112, where negative indicates compressive stress. The temperature change, calculated using Eq. (33), necessary to create each longitudinal strain is also shown in each Table. The longitudinal strains were selected so that the resulting stress equaled the modulus of rupture at either the top or bottom of each cross section. The modulus of rupture was found using the following equation from AASHTO (2002) Section 8.15.2.

$$f_r = 7.5\sqrt{f'_c} \quad (36)$$

Using the above equation, f_r for 3,000 and 4,740 psi concrete are 411 and 516 psi, respectively.

Table 111: Longitudinal Strains at the Rupture Stress on 3,000 psi Model

Longitudinal Strain (με)	Temperature Change (˚F)	Section	Location	DL Stress (psi)	ASR Stress (psi)	LL Stress (psi)	Combined Stress (psi)
1814	261	A2	Top	-324	425	310	**411**
			Bottom	-110	-453	-427	-990
3447	496	A14	T	-302	299	-1072	-1080
			B	-184	-344	938	**411**
1223	176	A40	T	-65	-280	-607	-950
			B	-386	274	521	**411**

Table 112: Longitudinal Strains at the Rupture Stress on 4,740 psi Model

Longitudinal Strain (με)	Temperature Change (˚F)	Section	Location	DL Stress (psi)	ASR Stress (psi)	LL Stress (psi)	Combined Stress (psi)
1807	260	A2	Top	-324	532	310	**516**
			Bottom	-110	-567	-427	-110
1897	273	A14	T	-302	207	-1072	-1170
			B	-184	-238	938	**516**
1341	193	A40	T	-65	-386	-607	-1060
			B	-386	378	521	**516**

The results shown in Table 111 and Table 112 indicate that transverse flexural cracking should occur first at the bottom fibers at the base of the arch under the combined action of ASR-expansion, dead load, and heavy live loading from side-by-side tri-axle trucks. The results shown in Table 111 and Table 112 indicate that the modulus of rupture will be reached at the extreme fibers of the arch at longitudinal strain levels that are significantly below the 10,000 microstrain value estimated to have occurred over the life of the structure. In the next section, a similar investigation is made that includes stresses due to dead load and ASR-expansion only.

6.1.3 Potential for Transverse Flexural Cracking due to ASR-Expansion Along With Dead Load Effects Only

An investigation was made to find the longitudinal strain required to produce the rupture stress at the arch extreme fibers when live load effects are neglected. This is necessary to find at what strain the arch will begin to show signs of transverse cracking from ASR-expansion and self-weight only.

The combined stresses from ASR-expansion and dead load are shown in Table 113 and Table 114. The results from these Tables indicate an interesting trend related to the strength of the concrete in the arches. Currently there are limited signs of transverse cracking of the arches of Span V that might have resulted from longitudinal ASR-expansion. Is this due to the concrete strength in the arches being significantly higher than expected? Tables 106 and 107 indicate that as the concrete strength increases, the potential for transverse cracking also increases. This results because the modulus of elasticity of the concrete increases with increasing concrete

strength, and the forces due to ASR-expansion increase. Overall, the longitudinal strain levels due to ASR that are required to produce the rupture stress at the extreme fibers of the arch are higher when the live load stresses are not included, but the longitudinal strain levels are less than the 10,000 microstrain estimated to have occurred over the life of the structure. Since transverse cracking has not occurred, it is likely that the 10,000 microstrain is an overestimate of the total ASR-expansion or that ASR-expansion is not correctly modeled as a uniform increase in temperature. Table 111 through Table 114 show that transverse flexural cracking should be expected at the top surface of the arch at A2 (Hanger 1) and the bottom at A40 (Base). This is true with or without including the effects of live load. Future inspections of the arches should include observations regarding the presence or absence of transverse cracking at these two locations.

Table 113: Longitudinal Strains at the Rupture Stress on 3,000 psi Model without Live Load

Longitudinal Strain (με)	Temperature Change (˚F)	Section	Location	DL Stress (psi)	ASR Stress (psi)	Combined Stress (psi)
3141	452	A2	Top	-324	735	**411**
			Bottom	-110	-784	-894
8208	1181	A14	T	-302	712	**411**
			B	-184	-818	-1002
3551	511	A40	T	-65.0	-813	-878
			B	-386	797	**411**

Table 114: Longitudinal Strains at the Rupture Stress on 4,740 psi Model without Live Load

Longitudinal Strain (με)	Temperature Change (˚F)	Section	Location	DL Stress (psi)	ASR Stress (psi)	Combined Stress (psi)
2856	411	A2	Top	-324	841	**516**
			Bottom	-110.	-896	-1006
7492	1078	A14	T	-302	817	**516**
			B	-184	-939	-1120
3204	461	A40	T	-65.0	-922	-987
			B	-386	903	**516**

6.2 EFFECTS OF ASR-EXPANSION ON ARCH DEFLECTIONS

Vertical deflection at the center point of the arch span, Point A in Figure 69, was calculated for four values of longitudinal strain. The deflection was calculated for the arch model with 3,000 psi concrete and the model with 4,740 psi concrete. The vertical deflection due to ASR-expansion was the maximum at Point A, and it was upward. In this Chapter, all references to deflection are to vertical deflection.

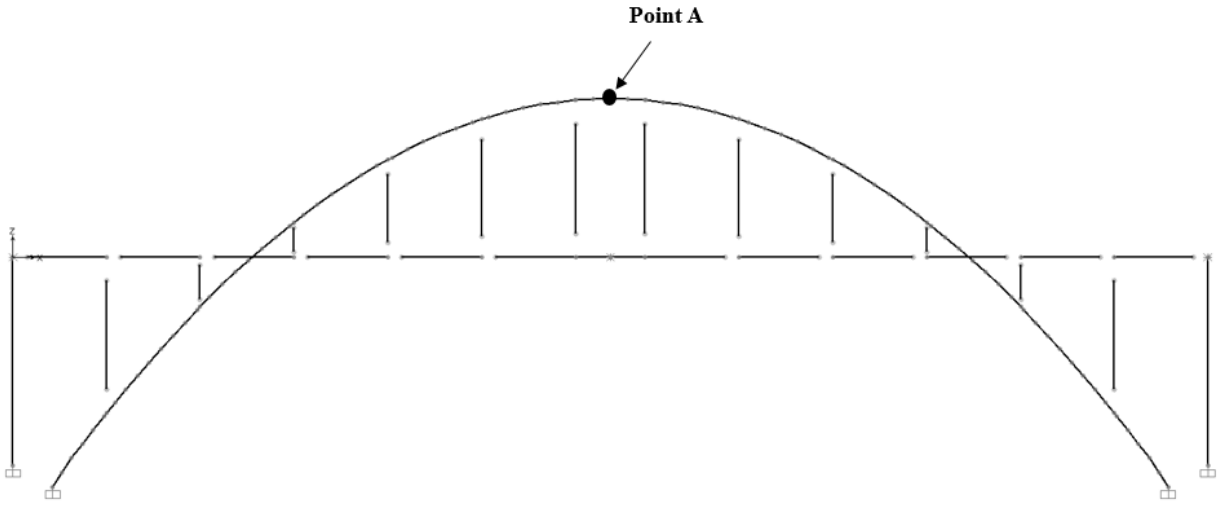

Figure 69: Deflection at Arch Center Span (Point A)

Table 115 lists the dead and live load deflection at Point A for the 3,000 psi and the 4,740 psi models. This Table shows that the deflection at Point A using the short term E_c, from Eq.

(22), is equaled to or less than 0.10 inch and 0.41 inch for the dead and live load, respectively. These deflections are rather small when compared with the deflection resulting from ASR-expansion.

Table 115: Dead and Live Load Deflection at Point A

Property		Deflection (in.)	
f'_c (psi)	E_c (ksi)	Dead Load	Live Load
3000	3122	-0.10	-0.41
4740	3924	-0.08	-0.33

For various longitudinal strains, Table 116 and Table 117 list the deflection at Point A resulting from ASR-expansion only for the 3,000 psi and 4,740 psi concrete models, respectively. Column 2 of each Table lists the deflection in inches resulting from different levels of ASR-expansion. Based on the longitudinal strain of 10,000 microstrain, the arch center at Point A has deflected 9.4 inches upward over the past 50 years. The deflection from ASR-expansion is significantly larger than the deflection resulting from dead and live load, shown in Table 115.

Column 3 of Table 116 and Table 117 display the number of years it takes to develop the deflection corresponding to the given longitudinal strains. Column 3 is calculated by taking the longitudinal strain and dividing it by the longitudinal strain rate per year presented in Section 6.1. Column 4 is the number of years it takes to develop one inch of deflection resulting from ASR-expansion. This is found by taking Column 3 and dividing by Column 2.

Table 116: Vertical Deflection at Point A Resulting from ASR-Expansion for 3,000 psi Model

Longitudinal Strain (με)	Vertical Deflection (in.)	Years	Years / in.
1223	1.15	6.1	5.3
1814	1.70	9.1	5.3
3447	3.24	17.2	5.3
10000	9.39	50.0	5.3

Table 117: Vertical Deflection at Point A Resulting from ASR-Expansion for 4,740 psi Model

Longitudinal Strain (με)	Vertical Deflection (in.)	Years	Years / in.
1341	1.26	6.7	5.3
1807	1.70	9.0	5.3
1897	1.78	9.5	5.3
10000	9.39	50.0	5.3

The data from Table 116, longitudinal strain and vertical deflection, are plotted in Figure 70. This plot shows that the deflection at the arch center increases linearly with increasing longitudinal strain. The same plot results from the data in Table 117.

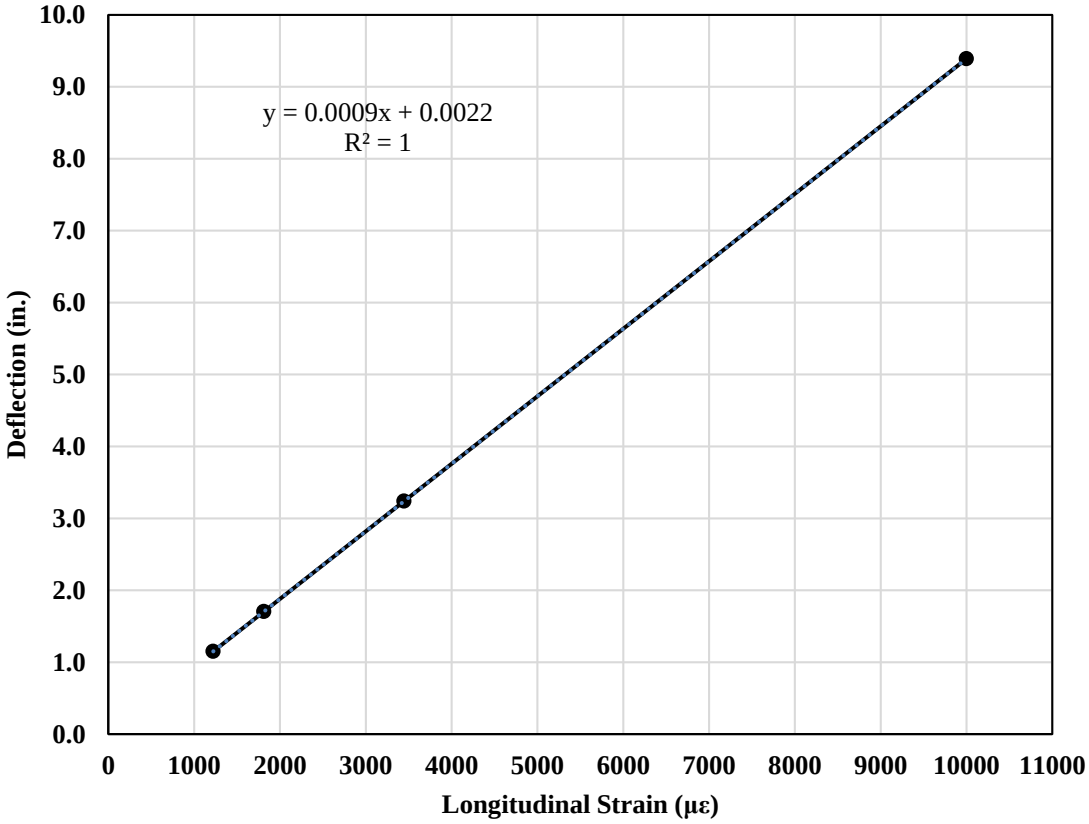

Figure 70: Deflection Plot Resulting from ASR-Expansion for 3,000 psi Model

From the analysis of effects of ASR-expansion on arch deflection, it takes approximately 5.3 years to see one inch of upward vertical deflection at the arch center. This vertical deflection is only dependent on the time it takes for ASR-expansion to occur and is independent of f'_c and E_c.

6.3 Effects of Changes in Concrete Modulus of Elasticity on Arch Internal Forces

The arch ratings reported in Chapter 5 were based on a concrete compressive strength of 3,000 psi and the corresponding modulus of elasticity determined from Eq. (22) and (23). The effects of varying the modulus of elasticity on the internal forces in the arch ribs were investigated. The accuracy of the internal forces predicted through the structural analysis of the arches affect the accuracy of the load ratings. There are two primary reasons to consider changes in the modulus

of elasticity: 1) the core test results in Table 11 suggest that the concrete strength and corresponding modulus of elasticity in the arches may be higher than 3,000 psi, and 2) one potential effect of ASR is to reduce the modulus of elasticity of the concrete (Pantazopoulou and Thomas 1999).

The E_c selected for analysis was based on a range of f'_c from 4,740 psi to 2,000 psi. The upper limit of f'_c was chosen from Table 11 where the equivalent concrete compressive strength from core samples was presented. Therefore, internal forces in the arch models were assessed at concrete compressive strengths of 4,740; 4,000; 3,500; 3,000; 2,500; and 2,000 psi.

Since these changes in E_c were used to obtain ratings also, the sensitivity analysis was performed using the combination of second-order and linear analysis arch model to yield a true comparison. Therefore, the long-term modulus given by Eq. (23) was used in the arch model, and the I in the model was $0.85I_g$. Table 118 lists the long-term E_c used in the arch models.

Table 118: Long-Term E_c Used in Arch Models

f'_c (psi)	4740	4000	3500	3000	2500	2000
E_c (ksi)	3924	3605	3372	3122	2850	2549
E_{c_LT} (ksi)	1907	1752	1639	1517	1385	1239

The effects of changes in concrete modulus of elasticity on arch internal forces were assessed at the most critical section along the arch. That section is Section A2 for Spans IV, V, and VI, and Section A16 for Span VII. Table 119 through Table 122 lists the capacity and arch internal forces for arch Span IV through VII, respectively. This analysis shows that the arch internal forces are essentially independent of the concrete modulus of elasticity. The most change in internal forces from changes in E_c can be seen in the live load bending moment; even then, the largest percent change is less than 2 % for Spans IV, V, and VI, and no change for Span VII.

Table 119: Span IV - Arch Capacity and Internal Forces at Section A2

	E_{c_LT} (ksi)	1907	1752	1639	1517	1385	1239
Capacity	ϕV_n (k)	160	147	138	127	116	104
	ϕP_n (k)	489	484	481	478	474	468
	ϕM_n (k-ft)	860	826	807	782	756	719
Applied	V_{DL} (k)	45.6	45.6	45.6	45.6	45.6	45.6
	P_{DL} (k)	375	375	375	375	375	375
	M_{DL} (k-ft)	58.2	58.0	57.9	57.8	57.7	57.4
	V_{LL} (k)	71.5	71.5	71.5	71.5	71.5	71.4
	P_{LL} (k)	100	100	100	100	100	100
	M_{LL} (k-ft)	698	700	702	704	707	711

Table 120: Span V - Arch Capacity and Internal Forces at Section A2

	E_{c_LT} (ksi)	1907	1752	1639	1517	1385	1239
Capacity	ϕV_n (k)	155	142	133	123	112	100
	ϕP_n (k)	475	471	467	464	460	455
	ϕM_n (k-ft)	815	785	764	741	717	684
Applied	V_{DL} (k)	46.5	46.5	46.5	46.5	46.5	46.5
	P_{DL} (k)	367	367	367	367	367	367
	M_{DL} (k-ft)	65.2	65.1	65.1	65.0	65.0	64.9
	V_{LL} (k)	72.3	72.2	72.2	72.2	72.2	72.2
	P_{LL} (k)	100	100	100	101	101	101
	M_{LL} (k-ft)	696	698	700	703	706	710

Table 121: Span VI - Arch Capacity and Internal Forces at Section A2

	E_{c_LT} (ksi)	1907	1752	1639	1517	1385	1239
Capacity	ϕV_n (k)	150	138	129	120	109	98
	ϕP_n (k)	435	431	428	424	420	416
	ϕM_n (k-ft)	698	675	656	636	611	585
Applied	V_{DL} (k)	38.5	38.5	38.5	38.5	38.5	38.5
	P_{DL} (k)	327	327	327	327	327	327
	M_{DL} (k-ft)	37.1	37.0	37.0	36.8	36.7	36.5
	V_{LL} (k)	72.2	72.2	72.2	72.2	72.2	72.1
	P_{LL} (k)	101	101	101	102	102	102
	M_{LL} (k-ft)	622	623	624	626	628	631

Table 122: Span VII - Arch Capacity and Internal Forces at Section A16

	E_{c_LT} (ksi)	1907	1752	1639	1517	1385	1239
Capacity	ϕV_n (k)	86.3	79.3	74.2	68.7	62.7	56.1
	ϕP_n (k)	222	214	208	202	196	189
	ϕM_n (k-ft)	266	251	242	230	219	206
Applied	V_{DL} (k)	28.9	28.9	28.9	28.9	28.9	28.9
	P_{DL} (k)	94.9	94.9	94.9	94.9	94.9	94.9
	M_{DL} (k-ft)	32.6	32.6	32.6	32.6	32.6	32.6
	V_{LL} (k)	46.0	46.0	46.0	46.0	46.0	46.0
	P_{LL} (k)	79.6	79.6	79.6	79.6	79.6	79.6
	M_{LL} (k-ft)	147	147	147	147	147	147

The changes in concrete modulus of elasticity did not affect the arch internal forces significantly; however, it did affect the dead and live load deflection as expected. This is presented in the next section.

6.4 Effects of Changes in Concrete Modulus of Elasticity on Arch Deflections

The effects of changes in concrete modulus of elasticity on arch deflections were analyzed at the same levels of f'_c and long-term E_c from the previous section. The arch models utilized were the

same arch models from the previous section. Deflections were obtained at the single location for Spans IV through VII, where the combined effect of dead and live load deflection was the largest. That location is on the arch rib at the Hanger 3 location for Spans IV, V, and VI, and at Column 5 for Span VII. Drawings with these vertical components pointed out are in Figure 61 and Figure 65, respectively.

Figure 71 through Figure 74 shows the deflection plot of the dead and live loads for Spans IV through Span VII, respectively, as the long-term modulus of elasticity is varied. Accompanying these plots are Table 123 through Table 126 that list the magnitudes of the dead and live load deflection along with the total deflection.

The plots show that as the long-term E_c decreases from 1,907 ksi to 1,239 ksi, corresponding to a decrease in f'_c from 4,740 psi to 2,000 psi the dead and live load defection increases. However, the live load deflection is more sensitive to the decrease in long-term E_c. When comparing the smallest long-term E_c, 1,239 ksi, the largest total deflection is seen in Span V on the arch rib at Hanger 3 with a downward displacement of 3.19 in. On the other hand, the smallest total deflection is seen in Span VII on the arch rib at Column 5 with a downward displacement of 0.34 in.

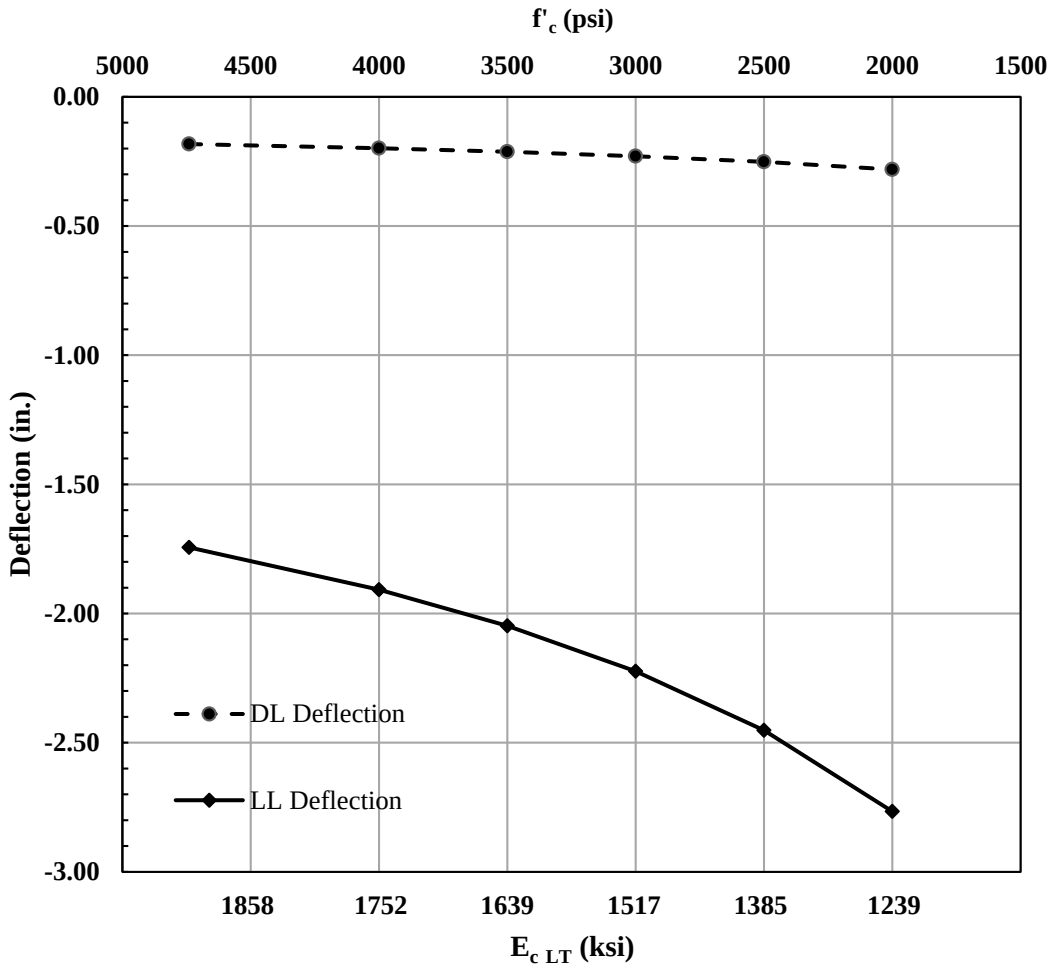

Figure 71: Span IV - Effects of Changes in E_c on Deflection

Table 123: Span IV – Effects of Changes in E_c on Total Deflection

	f'_c (psi)	4740	4000	3500	3000	2500	2000
	$E_{c\,LT}$ (ksi)	1907	1752	1639	1517	1385	1239
Arch Deflection at Hanger 3	**DL (in.)**	-0.18	-0.20	-0.21	-0.23	-0.25	-0.28
	LL (in.)	-1.74	-1.91	-2.05	-2.22	-2.45	-2.77
	Δ_{total} (in.)	-1.93	-2.11	-2.26	-2.45	-2.70	-3.05

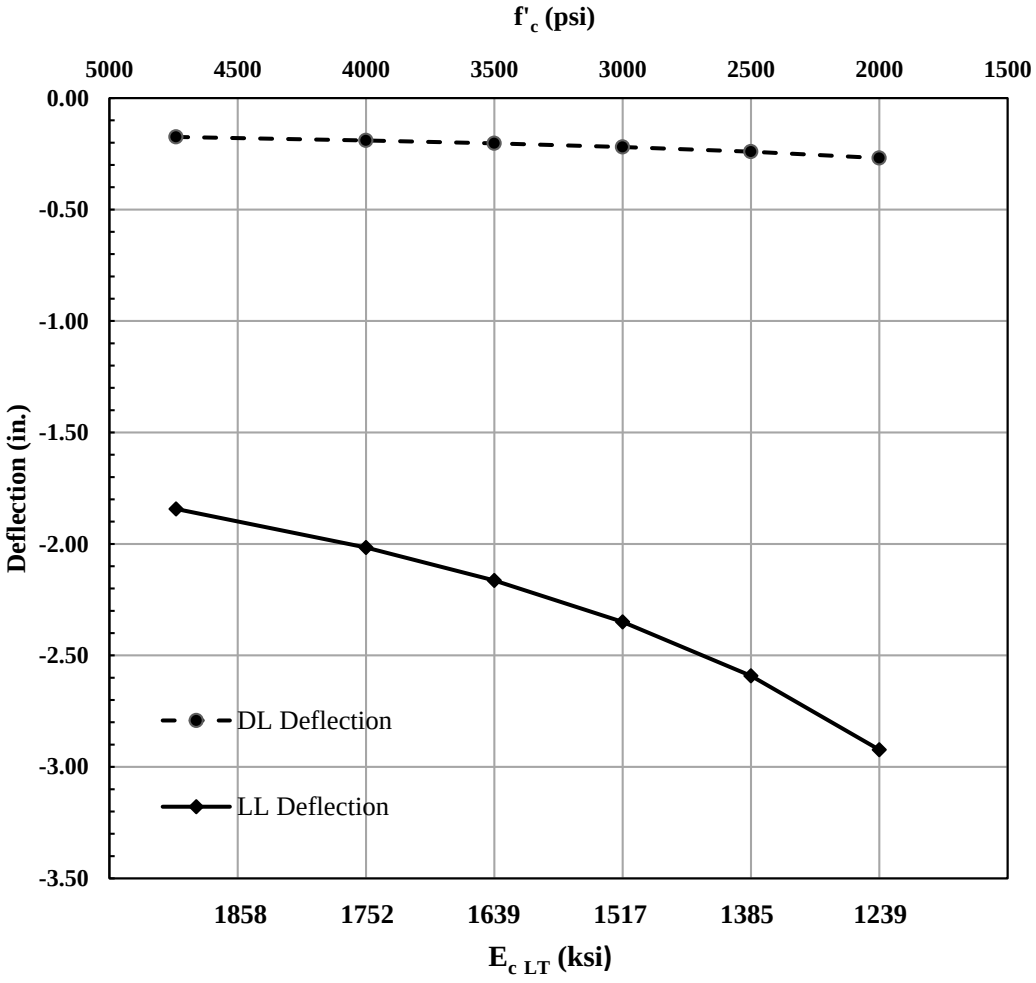

Figure 72: Span V - Effects of Changes in E_c on Deflection

Table 124: Span V – Effects of Changes in E_c on Total Deflection

	f'_c (psi)	4740	4000	3500	3000	2500	2000
	$E_{c\,LT}$ (ksi)	1907	1752	1639	1517	1385	1239
Arch Deflection at Hanger 3	**DL (in.)**	-0.17	-0.19	-0.20	-0.22	-0.24	-0.27
	LL (in.)	-1.84	-2.02	-2.16	-2.35	-2.59	-2.92
	Δ_{total} (in.)	-2.02	-2.21	-2.37	-2.57	-2.83	-3.19

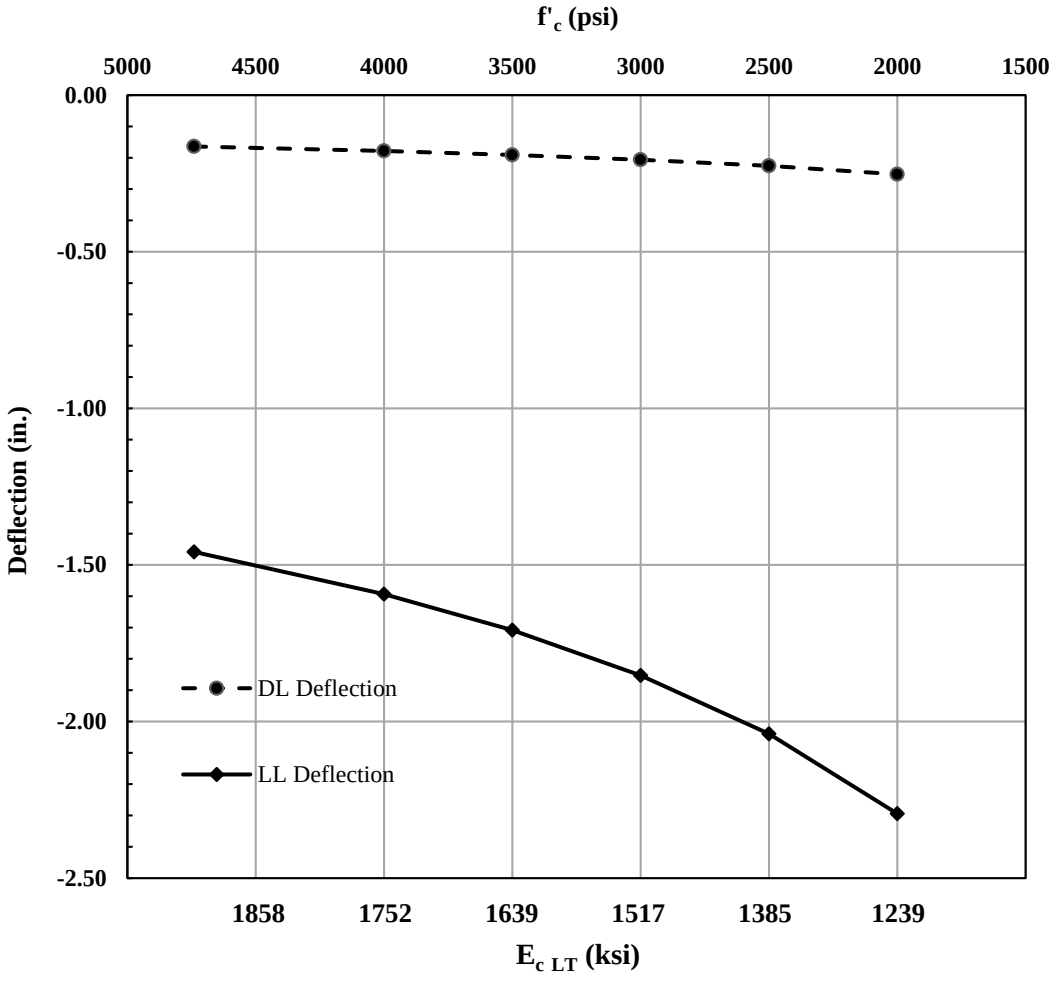

Figure 73: Span VI - Effects of Changes in E_c on Deflection

Table 125: Span VI – Effects of Changes in E_c on Total Deflection

	f'_c (psi)	4740	4000	3500	3000	2500	2000
	$E_{c\,LT}$ (ksi)	1907	1752	1639	1517	1385	1239
Arch Deflection at Hanger 3	**DL (in.)**	-0.16	-0.18	-0.19	-0.21	-0.23	-0.25
	LL (in.)	-1.46	-1.59	-1.71	-1.85	-2.04	-2.29
	Δ_{total} (in.)	-1.62	-1.77	-1.90	-2.06	-2.27	-2.55

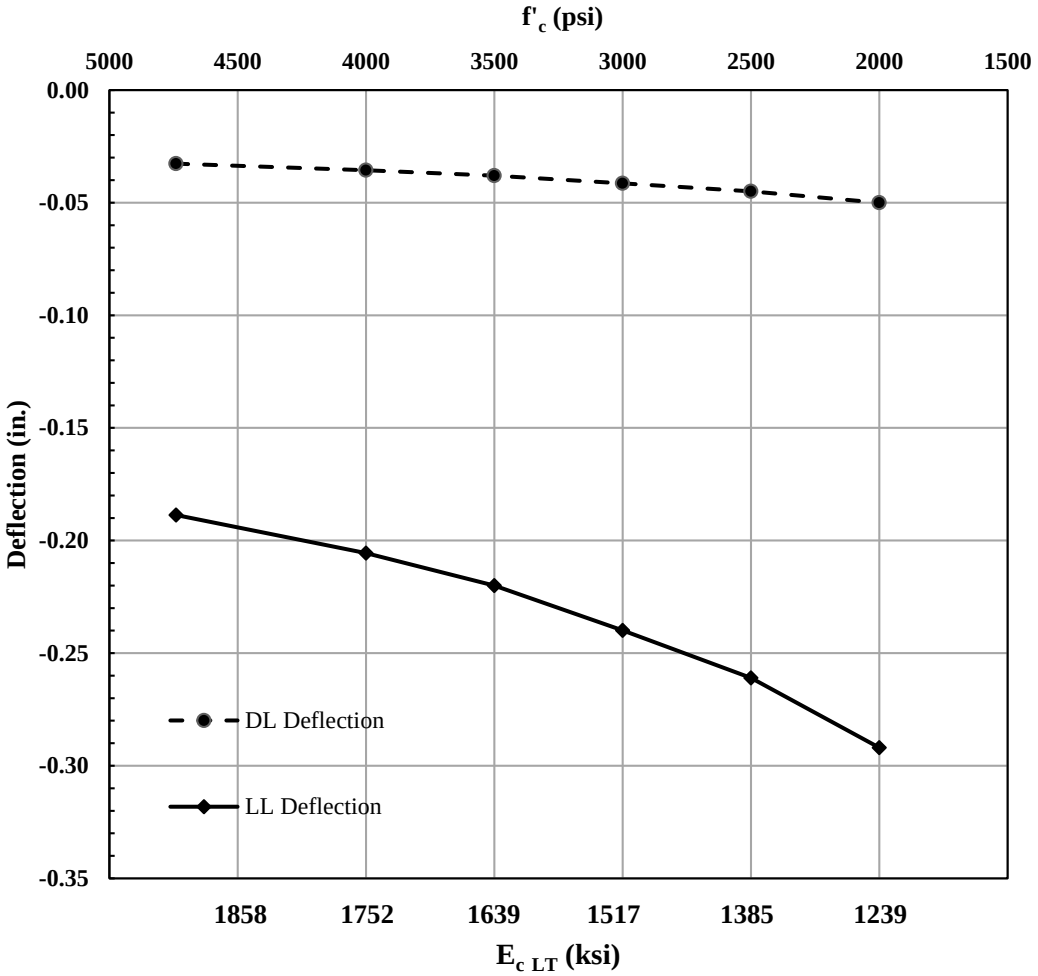

Figure 74: Span VII - Effects of Changes in E_c on Deflection

Table 126: Span VII – Effects of Changes in E_c on Total Deflection

	f'_c (psi)	4740	4000	3500	3000	2500	2000
	$E_{c\,LT}$ (ksi)	1907	1752	1639	1517	1385	1239
Arch Deflection at Column 5	**DL (in.)**	-0.03	-0.04	-0.04	-0.04	-0.05	-0.05
	LL (in.)	-0.19	-0.21	-0.22	-0.24	-0.26	-0.29
	Δ_{total} (in.)	-0.22	-0.24	-0.26	-0.28	-0.31	-0.34

6.5 Effects of Changes in Concrete Compressive Strength on Arch Ratings

The effects of changes in concrete compressive strength on arch ratings were analyzed at a range of f'_c from 4,740 psi to 2,000 psi. The upper limit of f'_c was chosen from Table 11 where the equivalent concrete compressive strength from core samples was presented for the arch. Therefore, effects of changes in f'_c on arch ratings were assessed at concrete strengths of 4,740; 4,000; 3,500; 3,000; 2,500; and 2,000 psi.

The model utilized for analyzing the effects of f'_c on arch ratings was the combination of second-order and linear analysis arch model. This model was used to obtain the ratings reported in Chapter 5 of this report. The modulus of elasticity used was the long-term E_c, and the I in the model was $0.85I_g$. Table 118 lists the f'_c and long-term E_c used in this sensitivity analysis.

Arch ratings were obtained at the most critical location on the arch for the tri-axle truck. For Spans IV through VI, the most critical arch section is A2. For Span VII, it is A16. Drawings with these sections pointed out are in Figure 62, Figure 63, Figure 64, and Figure 66 for Spans IV, V, VI, and VII, respectively.

Figure 75 through Figure 78 are the plots of operating rating factor as a function of f'_c for shear and combined axial load and bending moment for Spans IV through VII, respectively. Accompanying theses plots are Table 127 through Table 130 that show both the operating and inventory rating factors for each level of concrete compressive strength analyzed.

For Spans IV through VII, as the concrete compressive strength decreases from 4,740 psi to 2,000 psi, the rating factors decrease also. However, the shear rating factors are more sensitive to the decrease in f'_c than the combination of axial load and bending moment rating factors.

At the 3,000 psi f'_c level, Spans V and VI have an operating rating factor for combined axial load and bending moment of 0.96. At the same f'_c, Span VII has an operating shear rating of 0.86. However, this sensitivity analysis shows that at f'_c of 4,000 psi, all the arch ratings are above 1.0.

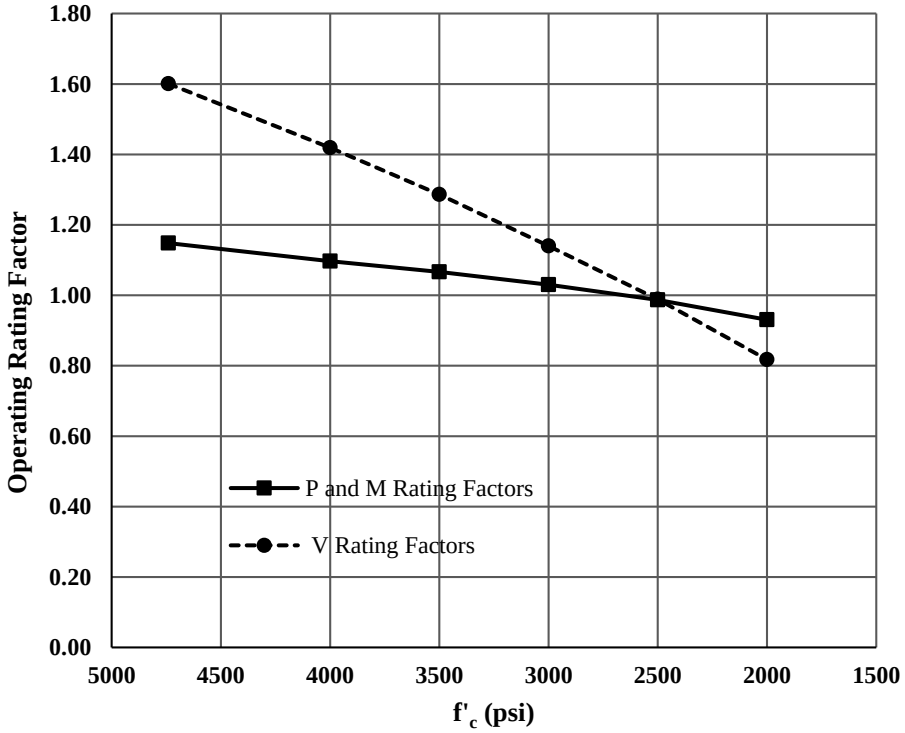

Figure 75: Span IV - Effect of f'$_c$ on Arch Operating Ratings

Table 127: Span IV – Effect of f'$_c$ on Arch Ratings

f'$_c$ (psi)	4740		4000		3500		3000		2500		2000	
LFR	Oper.	Inv.	Oper.	Inv.	Oper.	Inv.	Oper.	Inv.	Oper.	Inv.	Oper.	Inv.
P and M	1.15	0.69	1.10	0.66	1.07	0.64	1.03	0.62	0.99	0.59	0.93	0.56
V	1.60	0.96	1.42	0.85	1.29	0.77	1.14	0.69	0.99	0.59	0.82	0.49

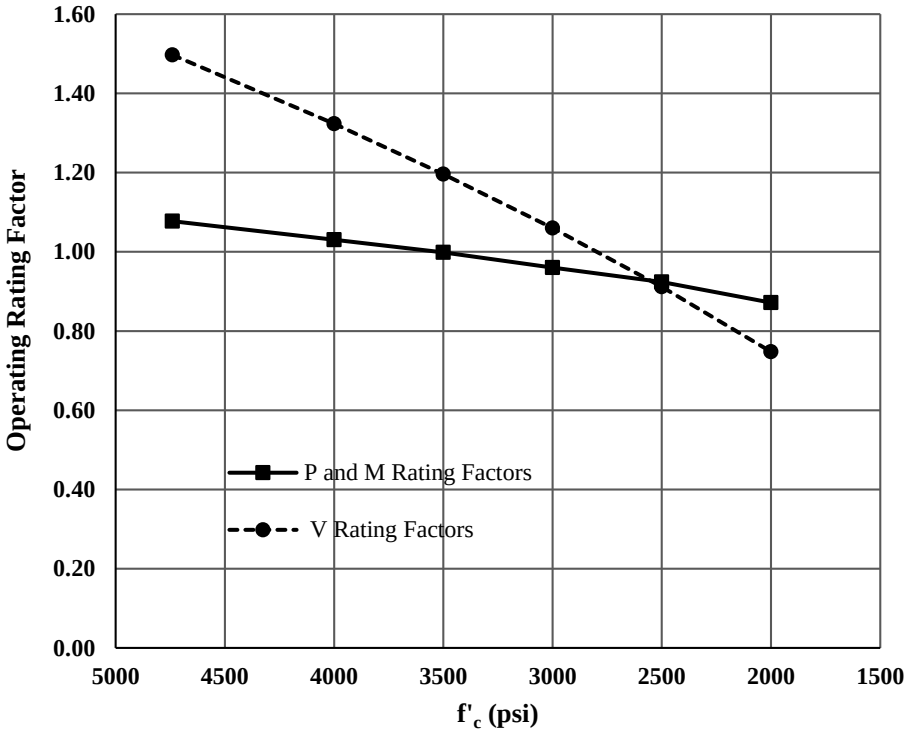

Figure 76: Span V - Effect of f'$_c$ on Arch Operating Ratings

Table 128: Span V – Effect of f'$_c$ on Arch Ratings

f'$_c$ (psi)	4740		4000		3500		3000		2500		2000	
LFR	Oper.	Inv.	Oper.	Inv.	Oper.	Inv.	Oper.	Inv.	Oper.	Inv.	Oper.	Inv.
P and M	1.08	0.65	1.03	0.62	1.00	0.60	0.96	0.58	0.92	0.55	0.87	0.52
V	1.50	0.90	1.32	0.79	1.20	0.72	1.06	0.63	0.91	0.55	0.75	0.45

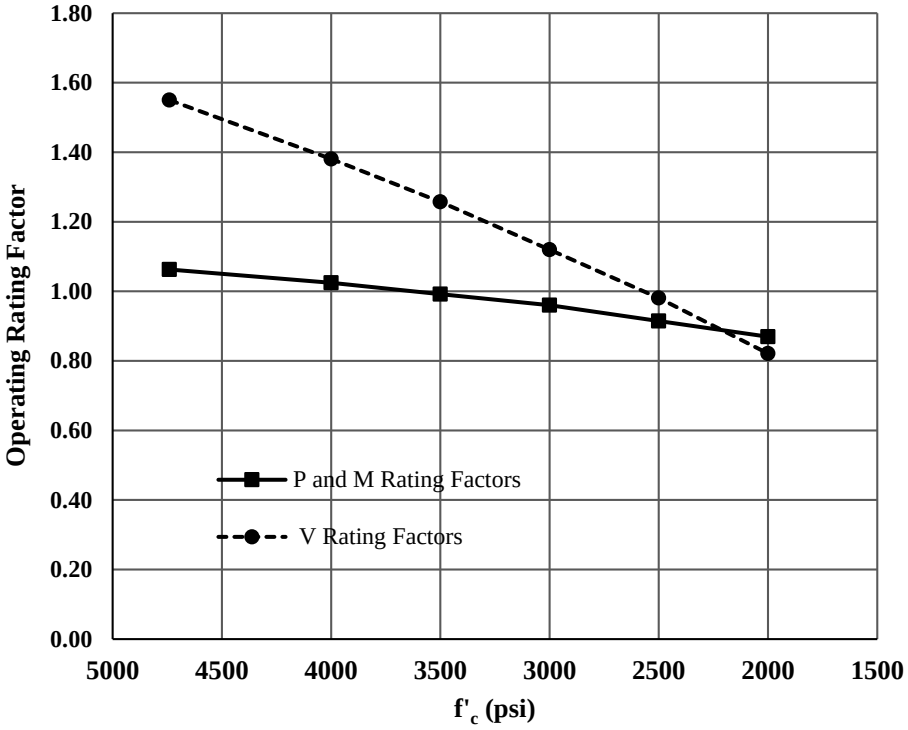

Figure 77: Span VI - Effect of f'$_c$ on Arch Operating Ratings

Table 129: Span VI – Effect of f'$_c$ on Arch Ratings

f'$_c$ (psi)	4740		4000		3500		3000		2500		2000	
LFR	Oper.	Inv.	Oper.	Inv.	Oper.	Inv.	Oper.	Inv.	Oper.	Inv.	Oper.	Inv.
P and M	1.06	0.64	1.02	0.61	0.99	0.59	0.96	0.57	0.91	0.55	0.87	0.52
V	1.55	0.93	1.38	0.83	1.26	0.75	1.12	0.67	0.98	0.59	0.82	0.49

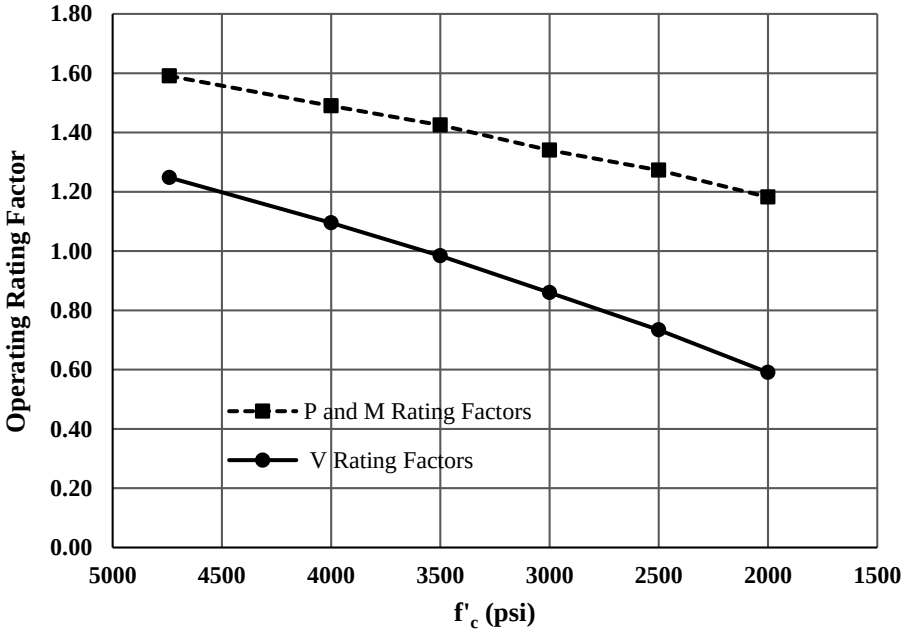

Figure 78: Span VII - Effect of f'$_c$ on Arch Operating Ratings

Table 130: Span VII – Effect of f'$_c$ on Arch Ratings

f'$_c$ (psi)	4740		4000		3500		3000		2500		2000	
LFR	Oper.	Inv.	Oper.	Inv.	Oper.	Inv.	Oper.	Inv.	Oper.	Inv.	Oper.	Inv.
P and M	1.59	0.95	1.49	0.89	1.42	0.85	1.34	0.80	1.27	0.76	1.18	0.71
V	1.25	0.75	1.10	0.66	0.98	0.59	0.86	0.48	0.73	0.44	0.59	0.35

6.6 EFFECTS OF CHANGES IN CONCRETE COMPRESSIVE STRENGTH ON TRANSVERSE BEAM RATINGS

The effects of changes in concrete compressive strength on transverse beam ratings were analyzed at f'_c intervals of 3,000, 2,500, and 2,000 psi. The corresponding E_c's are listed in Table 131. The analysis was performed on transverse beams with an operating rating of 1.15 or less for the tri-axle truck for either the shear or bending moment. This included transverse beams at Hanger 1 for Spans IV, V, and VI. The models used to perform the sensitivity analysis are the transverse frame models that were used to obtain the ratings in Chapter 5.

Table 131: f'_c and E_c for Transverse Beam Sensitivity Analysis

f'_c (psi)	3000	2500	2000
E_c (ksi)	3122	2850	2549

For Spans IV through VI, Table 132 through Table 134 show the bending moment and shear capacities, internal forces from dead and live loads, along with the rating factors for the three levels of f'_c for the transverse beams at Hanger 1. As f'_c decreases, the bending moment capacity along with the bending moments from applied load effects decrease at approximately the same rate. As a result, the bending moment ratings are not greatly affected by changes in f'_c for the transverse beams at Hanger 1 for Spans IV through VI. In addition as f'_c decreases, the shear capacities in the three zones decrease, however, the shear from applied load effects are unaffected by changes in f'_c. As a result, the shear rating factors decrease when the f'_c decreases for the transverse beams at Hanger 1 for Spans IV through VI.

Table 132 through Table 134 show that bending moment controls the ratings of the transverse beams. Also, the ratings are essentially unchanged over the range of concrete strengths considered. These trends would also be true for modest increase in concrete strength. Therefore, it is unlikely that additional information about the concrete strength that might be obtained through core testing will result in significant improvements in the transverse beam ratings.

Table 132: Span IV – Transverse Beam at Hanger 1 Sensitivity Analysis Results

	f'_c (psi)	3000		2500		2000	
	E_c (ksi)	3122		2850		2550	
Capacity	**ϕM_n (k-ft)**	1324		1317		1307	
	ϕV_{n_zone1} (k)	118.4		112.7		106.5	
	ϕV_{n_zone2} (k)	145.1		139.4		133.2	
	ϕV_{n_zone3} (k)	174.5		168.7		162.4	
Applied Dead Load	**Moment (k-ft)**	183.3		182.7		182.0	
	V_{zone1} (k)	11.4		11.4		11.4	
	V_{zone2} (k)	17.6		17.6		17.6	
	V_{zone3} (k)	23.7		23.7		23.7	
Applied Live Load	**Moment (k-ft)**	653.6		651.6		649.0	
	V_{zone1} (k)	41.3		41.3		41.3	
	V_{zone2} (k)	68.7		68.7		68.7	
	V_{zone3} (k)	72.6		72.7		72.7	
		Oper.	**Inv.**	**Oper.**	**Inv.**	**Oper.**	**Inv.**
LFR	**Moment**	0.98	0.59	0.98	0.59	0.98	0.58
	V_{zone1}	1.48	0.89	1.40	0.84	1.31	0.79
	V_{zone2}	1.05	0.63	1.00	0.60	0.95	0.57
	V_{zone3}	1.17	0.70	1.12	0.67	1.07	0.64

Table 133: Span V – Transverse Beam at Hanger 1 Sensitivity Analysis Results

	f'_c (psi)	3000		2500		2000	
	E (ksi)	3122		2850		2550	
Capacity	**ϕM_n (k-ft)**	1324		1317		1307	
	ϕV_{n_zone1} (k)	118.4		112.7		106.5	
	ϕV_{n_zone2} (k)	145.1		139.4		133.2	
	ϕV_{n_zone3} (k)	174.5		168.7		162.4	
Applied Dead Load	**Moment (k-ft)**	180.8		180.3		179.5	
	V_{zone1} (k)	11.3		11.3		11.3	
	V_{zone2} (k)	17.4		17.4		17.4	
	V_{zone3} (k)	23.4		23.4		23.4	
Applied Live Load	**Moment (k-ft)**	653.3		651.2		648.4	
	V_{zone1} (k)	41.3		41.3		41.4	
	V_{zone2} (k)	68.7		68.7		68.7	
	V_{zone3} (k)	72.7		72.7		72.7	
		Oper.	**Inv.**	**Oper.**	**Inv.**	**Oper.**	**Inv.**
LFR	**Moment**	0.99	0.59	0.98	0.59	0.98	0.59
	V_{zone1}	1.48	0.89	1.40	0.84	1.31	0.79
	V_{zone2}	1.06	0.63	1.01	0.60	0.95	0.57
	V_{zone3}	1.15	0.69	1.13	0.67	1.07	0.64

Table 134: Span VI – Transverse Beam at Hanger 1 Sensitivity Analysis Results

	f'_c (psi)	3000		2500		2000	
	E (ksi)	3122		2850		2550	
Capacity	**ϕM_n (k-ft)**	1219		1212		1202	
	ϕV_{n_zone1} (k)	109.2		104.0		98.2	
	ϕV_{n_zone2} (k)	133.9		128.7		122.9	
	ϕV_{n_zone3} (k)	161.2		155.9		150.0	
Applied Dead Load	**Moment (k-ft)**	157.2		156.5		155.6	
	V_{zone1} (k)	10.0		10.0		10.0	
	V_{zone2} (k)	14.6		14.6		14.6	
	V_{zone3} (k)	20.7		20.7		20.7	
Applied Live Load	**Moment (k-ft)**	648.6		645.9		642.4	
	V_{zone1} (k)	41.5		41.5		41.5	
	V_{zone2} (k)	65.0		65.0		65.0	
	V_{zone3} (k)	73.0		73.0		73.0	
		Oper.	**Inv.**	**Oper.**	**Inv.**	**Oper.**	**Inv.**
LFR	**Moment**	0.93	0.55	0.92	0.55	0.92	0.55
	V_{zone1}	1.37	0.82	1.30	0.78	1.21	0.73
	V_{zone2}	1.05	0.63	1.00	0.60	0.95	0.57
	V_{zone3}	1.09	0.65	1.05	0.63	1.00	0.60

6.7 EFFECTS OF CHANGES IN CONCRETE COMPRESSIVE STRENGTH ON TRANSVERSE DEEP BEAM RATINGS

The effects of changes in concrete compressive strength on transverse deep beam ratings were analyzed at the same f'$_c$ values of 3,000, 2,500, and 2,000 psi from the previous section. The analysis was performed on transverse deep beams with an operating rating of 1.15 or less for the tri-axle truck for bending moment. This included Transverse Deep Beam of Spans V and VI. The models used to perform the sensitivity analysis are the transverse deep beam models that were used to obtain the ratings in Chapter 5.

Table 135 and Table 136 show the bending moment capacity and bending moment from applied load effects along with the rating factors for the three levels of f'_c for the Transverse Deep Beam of Spans V and VI. As f'_c decreases, the bending moment capacity decreases, but the bending moment from applied load is unaffected because the beam is assumed to be simply supported. However, the rating factors are not greatly affected by the decrease in f'_c.

Table 135: Span V – Transverse Deep Beam Sensitivity Analysis Results

	f'_c (psi)	3000		2500		2000	
	E_c (ksi)	3122		2850		2550	
Capacity	ϕM_n (k-ft)	1270		1257		1238	
Applied	M_{DL} (k-ft)	273.5		273.5		273.5	
	M_{LL} (k-ft)	509.2		509.2		509.2	
		Oper.	**Inv.**	**Oper.**	**Inv.**	**Oper.**	**Inv.**
LFR	**Moment**	1.06	0.64	1.05	0.63	1.05	0.63

Table 136: Span VI – Transverse Deep Beam Sensitivity Analysis Results

	f'_c (psi)	3000		2500		2000	
	E_c (ksi)	3122		2850		2550	
Capacity	ϕM_n (k-ft)	1219		1212		1202	
Applied	M_{DL} (k-ft)	240.4		240.4		240.4	
	M_{LL} (k-ft)	494.9		494.9		494.9	
		Oper.	**Inv.**	**Oper.**	**Inv.**	**Oper.**	**Inv.**
LFR	**Moment**	0.98	0.59	0.97	0.58	0.97	0.58

6.8 SENSITIVITY ANALYSES CONCLUSIONS

Analyses presented in the chapter provide some useful conclusions regarding the "as-designed" ratings of the Bibb Graves Bridge. The two most critical elements are the transverse floor beams at Hanger 1 locations in Span VI and Span II, and the arch rib cross section at the Column 6 locations in Span VII and Span I. The rating factors for these locations for the tri-axle truck for a concrete compressive strength of 3,000 psi are 0.93 and 0.86, respectively. The transverse beam

ratings are controlled by flexure and are not significantly affected by changes in concrete compressive strength. So, additional information that may be gained from core testing of the concrete in those beams is not likely to significantly improve the rating factor beyond 0.93. The rating factor of 0.86 for the arch rib of Span VII and Span I is controlled by shear. Results presented in Table 130 show that this rating factor can be increased to 0.93 by the use of a concrete compressive strength of approximately 3,300 psi. The use of 3,300 psi appears reasonable for an "as-designed" rating based on the core test results of Table 11. So, the rating factors listed in Table 82 for the transverse floor beam at Hanger 1 locations in Span VI (and Span II) are recommended for use as the controlling ratings of the bridge.

ASR-expansion was simulated using a uniform temperature increase in the portions of the arch rib above the roadway deck in Span V. Based on those analyses the following conclusions are made. Transverse flexural cracking on the top surface of the arch rib at the Hanger 1 locations and on the bottom surface of the arch rib at the base of the arch was predicted to result from large magnitudes of ASR-expansion. Upward vertical deflection at the peak of the arch of Span V was predicted to increase at a rate of approximately one inch in 5 or 6 years due to expansion. If ASR-expansion is creating internal forces in the arch ribs similar to those resulting from a uniform temperature increase, it may be possible to monitor the resulting deflections to gain insight about the changing condition of the bridge. Also, the locations where transverse flexural cracking was predicted to occur should be monitored for signs of distress as part of future bridge inspections.

Applied bending moments, shears, and axial forces at cross sections in the arch ribs were found to be only mildly affected by changes in concrete modulus of elasticity. If future ASR-expansion causes moderate reductions in the modulus of elasticity of the arch rib concrete, the applied forces used in the ratings reported here will not change significantly. But, the cross section capacities may be significantly reduced by ASR. The reductions in cross section capacity may not be accurately predicted by simple reductions in the assumed concrete compressive strength. Predictions of the loss in cross section capacity due to ASR were outside the scope of this project but are worthy of future study.

Chapter 7

SUMMARY AND CONCLUSIONS

7.1 PROJECT SUMMARY

The historic Bibb Graves Bridge is a reinforced concrete bridge that was constructed from 1929 to 1931 in Wetumpka, Alabama. The bridge is 44 feet wide by approximately 800 feet long and crosses the Coosa River in Elmore County. It consists of seven arched spans that support the roadway deck, with the center five spans being through arches while the arches at either end are below the roadway deck.

The arches of Span V of the bridge have significant longitudinal cracks resulting from alkali-silica reactivity. As a result, there are plans to mitigate the ASR-cracks to preserve the strength of the bridge. Before these plans are implemented, a load rating of the Bibb Graves Bridge was executed during this project to identify what the design capacity of the bridge is. An evaluation of the impact of deterioration due to ASR was outside the scope of this project.

Since the bridge is essentially symmetric about midspan, load ratings were provided for Spans IV, V, VI, and VII. In each span, components including columns, hangers, transverse beams, and the arch rib were rated. Load ratings were for eight standard ALDOT trucks and the AASHTO lane load. Load ratings were performed in accordance with AASHTO's 2011 second edition The Manual for Bridge Evaluation, which defines the Load Factor Rating method and references AASHTO's 2002 seventeenth edition the Standard Specifications for Highway Bridges. As required by ALDOT, all structural analysis models were executed using SAP2000 version 15.

Preliminary ratings of the arches of Span V resulted in an operating rating factor of 0.81 for the tri-axle truck. Slenderness effects calculated using the moment magnifier method from AASHTO (2002) resulted in significant increases in the bending moments. An investigation was conducted to identify a more accurate method for including slenderness effects in the arch rating calculations. An analysis that combines an elastic second-order analysis for dead loads and a linear analysis for moving live loads was found to be very practical and sufficiently accurate for

determining the load ratings of the arches. Using this combined analysis approach resulted in significant increases in the arch ratings beyond those calculated using the AASHTO moment magnifier method. The resulting operating rating factor for the Span V arches increased from 0.81 to 0.96 for a concrete compressive strength of 3,000 psi.

In addition to the bridge ratings, a series of analyses was performed to estimate the effects of ASR-expansion on the internal forces and deflections of the arches of Span V. ASR-expansion was simulated as a uniform thermal expansion in the portion of the arch rib that is above the deck since that is the area where the arches exhibit the most significant ASR-induced longitudinal cracking. The annual amount of longitudinal ASR-expansion was estimated from field measurements of transverse ASR strain reported by Johnson et al. (2014).

The effects of changes in concrete compressive strength and modulus of elasticity on arch internal forces, ratings and deflections were examined. And, the effects of changes in concrete compressive strength on transverse beam ratings were examined.

7.2 PROJECT CONCLUSIONS

From the eight standard ALDOT trucks for ratings, the tri-axle truck controls all ratings for all rated components. Presented below by span are components of the bridge where load postings may be necessary if load ratings are based on the 3,000 psi concrete compressive strength. All critical ratings mentioned below are for the tri-axle truck except as noted. Based on the symmetry of the bridge, the conclusions stated below for Span V also apply to Span III, conclusions for Span VI apply to Span II, and conclusions for Span VII apply to Span I.

For Span IV, all operating rating factors for the rated components are 1.0 and above except for the transverse beam at the midspan hanger, Hanger 1, location where the rating factor is 0.98 for bending moment.

For Span V, all operating rating factors for the rated components are 1.0 and above except for two components. The first component is the arch rib at the midspan hanger, Section A2, which has a rating factor of 0.96 for combined axial load and bending moment. The second component is the transverse beam at the midspan hanger, Hanger 1, location where the rating factor is 0.99 for bending moment.

For Span VI, all operating rating factors for the rated components are 1.0 and above except for three components. The first component is the arch rib which has rating factors of 0.96 and 0.99 for combined axial load and bending at the midspan hanger, Section A2 and Section A3, respectively. The second component is the transverse beam at the midspan hanger, Hanger 1, location where the rating factor is 0.93 for bending moment for the tri-axle truck and 0.97 for the concrete truck. The third component is the transverse deep beam where the bending moment rating factor is 0.98.

For Span VII, all operating rating factors for the rated components are 1.0 and above except for two components. The first component is the arch rib at the section nearest the midspan column, Section A16, which has rating factors for shear of 0.86 and 0.90 for the tri-axle and concrete truck, respectively. The second component is the exterior column near midspan, exterior Column 5, where the rating factor is 0.99 for axial tension.

The two most critical elements of the Bibb Graves Bridge are the transverse floor beams at Hanger 1 locations in Span VI and the arch rib cross section at the Column 6 locations in Span VII. The rating factors for these locations for the tri-axle truck for a concrete compressive strength of 3,000 psi are 0.93 and 0.86, respectively. The transverse beam ratings are controlled by flexure and are not significantly affected by changes in concrete compressive strength. So, additional information that may be gained from core testing of the concrete in those beams is not likely to significantly improve the rating factor beyond 0.93. The rating factor of 0.86 for the arch rib of Span VII is controlled by shear. Results presented in Table 130 show that this rating factor can be increased to 0.93 by the use of a concrete compressive strength of approximately 3,300 psi. The use of 3,300 psi appears reasonable for an “as-designed” rating based on the core test results of Table 11. So, the rating factors listed in Table 82 for the transverse floor beam at Hanger 1 locations in Span VI are recommended for use as the controlling ratings of the bridge.

ASR-expansion was simulated using a uniform temperature increase in the portions of the arch rib above the roadway deck in Span V. Based on those analyses the following conclusions are made. Transverse flexural cracking on the top surface of the arch rib at the Hanger 1 locations and on the bottom surface of the arch rib at the base of the arch was predicted to result from large magnitudes of ASR-expansion. Upward vertical deflection at the peak of the arch of Span V was predicted to increase at a rate of approximately one inch in 5 or 6 years due to expansion. If ASR-expansion is creating internal forces in the arch ribs similar to those resulting

from a uniform temperature increase, it may be possible to monitor the resulting deflections to gain insight about the changing condition of the bridge. Also, the locations where transverse flexural cracking was predicted to occur should be monitored for signs of distress as part of future bridge inspections.

Applied bending moments, shears, and axial forces at cross sections in the arch ribs were found to be only mildly affected by changes in concrete modulus of elasticity. If future ASR-expansion causes moderate reductions in the modulus of elasticity of the arch rib concrete, the applied forces used in the ratings reported here will not change significantly. But, the cross section capacities may be significantly reduced by ASR. The reductions in cross section capacity may not be accurately predicted by simple reductions in the assumed concrete compressive strength. Predictions of the loss in cross section capacity due to ASR were outside the scope of this project but are worthy of future study.

References

AASHTO. 2002. *Standard Specifications for Highway Bridges.* American Association of State Highway and Transportation Officials, 17th Edition, Washington, DC. 829 pages.

AASHTO. 2011. *The Manual for Bridge Evaluation.* American Association of State Highway and Transportation Officials, 2nd Edition, Washington, DC.

AASHTO. 2012. *AASHTO LRFD Bridge Design Specifications.* American Association of State Highway and Transportation Officials, Washington, DC.

ACI Committee 209. 1992. *Prediction of Creep, Shrinkage and Temperature Effects in Concrete Structures.* ACI209R-92. American Concrete Institute, Farmington Hills, MI.

ACI Committee 318. 2011. *Building Code Requirements for Structural Concrete (ACI 318-11) and Commentary*. American Concrete Institute (ACI), Farmington Hills, MI.

ACI Committee 562. 2013. *Code Requirements for Evaluation, Repair, and Rehabilitation of Concrete Buildings (ACI 562-13) and Commentary.* American Concrete Institute (ACI), Farmington Hills, MI.

ACI Manual of Concrete Practice. 2013. *Part 1 – ACI 117-10 to 225R-99.* American Concrete Institute (ACI), Farmington Hills, MI.

AHD. 1928 – 1929. "Plan and Profile of Proposed State Bridge: Over Coosa River - Elmore County at Wetumpka State Aid Project S-327." State of Alabama Highway Department of Alabama (AHD).

AISC. 2005. *Steel Construction Manual.* American Institute of Steel Construction, 13th Edition, United States of America.

AutoCAD. 2014. *AutoCAD 2014 – English.* Autodesk, Inc.

CSI Analysis Reference Manual. 2011. *For SAP2000, ETABS, SAFE and CSiBridge.* Computers and Structures, Inc. California.

Geoscience News and Information. 2005. "Map of Alabama Cities – Alabama Road Map." Geology.com. Accessed April 26, 2014. http://geology.com/cities-map/alabama.shtml

Johnson, D. K., R. L. Warnock, A. K. Schindler, R. W. Barnes. 2014. *Effectiveness of Silane in Mitigating Alkali-Silica Reaction in the Bibb Graves Bridge.* FHWA/ALDOT 930-802. Alabama Department of Transportation. 243p.

Mathcad 14. 2014. *Mathcad 14.* PTC Inc. Massachusetts.

Miller, E. 2013. *Live-Load Response of In-Service Bridge Constructed with Precast, Prestressed Self-Consolidating Concrete Girders.* Masters Thesis. Auburn, Alabama: Auburn University.

Pantazopoulou, S. J. and M. D. A. Thomas. Modeling Stress-Strain Behavior of Concrete Damaged by Alkali-Aggregate Reaction (AAR). *ACI Structural Journal,* Vol. 96, No. 5, pp. 790, 1999.

SAP2000 v15. 2013. *CSi Watch & Learn.* Computers and Structures, Inc. California. http://www.csiamerica.com/sap2000/watch-and-learn (accessed April 23, 2014).

SAP2000 v15. 2013. *SAP2000 15*. Computers and Structures, Inc. California.

Taylor, V. L. 1930. "A New Type of Highway Bridge." *The Auburn Engineer,* November: 34-35.

TranSystems 2009. "Evaluation Report." *Bibb Graves Bridge AL Route 111 Over Coosa River,* June: 1-10 and 15-19.

Wight, James and James MacGregor. 2012. Reinforced Concrete: Mechanincs and Design, 6th Edition. New Jersey: Prentice Hall.

Appendix A: Span IV

A1: Longitudinal Beam Analysis Results

Table 137A: Wheel Line Load Magnitudes

Truck	Wheel Line Load, W, at			
	Hanger 1 (k)	Transverse Deep Beam (k)	Column 2 (k)	Column 3 (k)
Tri-Axle	31.34	23.18	23.18	23.13
H-Truck	22.17	15.99	15.99	15.99
Two-Axle	23.62	16.37	16.37	16.37
Concrete	29.53	20.46	20.46	20.46
18-Wheeler	20.67	14.32	14.32	14.32
6-Axle	22.19	16.82	16.82	16.76
School Bus	11.59	8.50	8.50	8.50
HS-Truck	23.25	15.99	15.99	15.99

A2: TRANSVERSE FLOOR BEAMS

Cross sectional properties listed within this section applies to all transverse floor frames for Span IV unless specified differently in the following sections.

Table 138A: Transverse Floor Beam Cross Sectional Properties

	Roadway	Curb	Bracket
A_g (ft^2)	9.708	9.625	5.708
I_x (ft^4)	11.01	18.75	3.453
I_y (ft^4)	29.27	18.68	14.48

Table 139A: Transverse Floor Beam Dead Loads

W_{slab} (k/ft)	1.100
$W_{trans.\ beam}$ (k/ft)	0.656
$W_{elev.\ beam}$ (k/ft)	0.225
$W_{sidewalk}$ (k/ft)	0.825
$W_{bracket}$ (k/ft)	0.331
$P_{rail\ tot}$ (k)	0.702

A2.1: Transverse Floor Beam at Column 2 Ratings

Transverse floor beam at Column 2 rating results are listed in Table 140A and Table 141A.

Table 140A: Span IV - Transverse Floor Beam at Column 2 Rating Factors: Part 1

Trucks	Rating Factors			
	Positive Moment		Negative Moment	
	Operating	Inventory	Operating	Inventory
Tri-Axle	1.51	0.90	7.44	4.46
H-Truck	2.19	1.31	10.78	6.46
Two-Axle	2.14	1.28	10.53	6.31
Concrete	1.71	1.02	8.43	5.05
18-Wheeler	2.44	1.46	12.04	7.21
6-Axle	2.08	1.25	10.25	6.14
School Bus	4.12	2.47	20.29	12.15
HS-Truck	2.19	1.31	10.78	6.46

Table 141A: Span IV - Transverse Floor Beam at Column 2 Rating Factors: Part 2

Trucks	Rating Factors					
	V_{zone1}		V_{zone2}		V_{zone3}	
	Operating	Inventory	Operating	Inventory	Operating	Inventory
Tri-Axle	2.00	1.20	1.42	0.85	1.58	0.95
H-Truck	2.90	1.74	2.06	1.24	2.29	1.37
Two-Axle	2.84	1.70	2.02	1.21	2.24	1.34
Concrete	2.27	1.36	1.61	0.97	1.79	1.07
18-Wheeler	3.24	1.94	2.30	1.38	2.56	1.53
6-Axle	2.76	1.65	1.96	1.18	2.18	1.31
School Bus	5.46	3.27	3.88	2.33	4.31	2.58
HS-Truck	2.90	1.74	2.06	1.24	2.29	1.37

A2.2: Transverse Floor Beam at Column 3 Ratings

For completeness, transverse floor beam at Column 3 rating results are listed in Table 142A for bending moment and Table 143A for shear. Ratings were calculated using the transverse floor beam model presented in Section 3.5.4.

Table 142A: Span IV - Transverse Floor Beam at Column 3 Rating Factors: Part 1

Trucks	Rating Factors			
	Positive Moment		Negative Moment	
	Operating	Inventory	Operating	Inventory
Tri-Axle	1.50	0.90	7.73	4.63
H-Truck	2.17	1.30	11.18	6.70
Two-Axle	2.12	1.27	10.92	6.54
Concrete	1.69	1.02	8.74	5.24
18-Wheeler	2.42	1.45	12.48	7.48
6-Axle	2.07	1.24	10.67	6.39
School Bus	4.08	2.44	21.04	12.61
HS-Truck	2.17	1.30	11.18	6.70

Table 143A: Span IV - Transverse Floor Beam at Column 3 Rating Factors: Part 2

Trucks	Rating Factors					
	V_{zone1}		V_{zone2}		V_{zone3}	
	Operating	Inventory	Operating	Inventory	Operating	Inventory
Tri-Axle	2.01	1.20	1.43	0.86	1.59	0.95
H-Truck	2.91	1.74	2.06	1.24	2.29	1.37
Two-Axle	2.84	1.70	2.02	1.21	2.24	1.34
Concrete	2.27	1.36	1.61	0.97	1.79	1.07
18-Wheeler	3.25	1.95	2.30	1.38	2.56	1.53
6-Axle	2.78	1.66	1.97	1.18	2.19	1.31
School Bus	5.47	3.28	3.89	2.33	4.32	2.59
HS-Truck	2.91	1.74	2.06	1.24	2.29	1.37

A3: COLUMN 2

Table 144A: Column 2 Cross Sectional Properties and Dead Load

A_g (ft^2)	1.458
I_x (ft^4)	0.165
I_y (ft^4)	0.190
$P_{column\ 2}$ (k)	3.955

Properties and load listed for Column 2 are for each interior and exterior column.

A4: COLUMN 3

Table 145A: Column 3 Cross Sectional Properties and Dead Load

		Exterior	
	Interior	Top	Bottom
A_g (ft^2)	1.750	2.400	3.742
I_x (ft^4)	0.198	0.305	0.401
I_y (ft^4)	0.328	0.860	5.234
$P_{column\ 3}$ (k)	6.410	4.396	6.853

A5: HANGER 1

Table 146A: Hanger 1 Cross Sectional Properties and Dead Load

A_s (ft^2)	0.0278
I_x (ft^4)	0.00414
I_y (ft^4)	0.00255
$P_{hanger\ 1}$ (k)	3.280

Properties and load listed for Hanger 1 are for each interior and exterior hanger.

A6: TRANSVERSE DEEP BEAM

Table 147A: Transverse Deep Beam Cross Sectional Properties

A_g (ft^2)	9.390
I_x (ft^4)	30.66
I_y (ft^4)	1.761

Table 148A: Transverse Deep Beam Dead Loads

W_{slab} (k/ft)	1.100
$W_{trans.\ deep\ beam}$ (k/ft)	1.409
$W_{elev.\ beam}$ (k/ft)	0.225
$W_{sidewalk}$ (k/ft)	0.825
$W_{bracket}$ (k/ft)	0.331
$P_{rail\ tot}$ (k)	0.702
$P_{support\ tot}$ (k)	4.196

A7: ARCH

The hanger and column cross sectional properties in the arch model combines the properties of the individual hanger and column properties from the transverse frame models. For Column 3s, the interior column cross sectional properties is combined with the top exterior column cross sectional properties.

Table 149A: Arch Cross Sectional Properties

	Column 2	Column 3	Hangers
A_g (ft^2)	2.917	4.150	0.0556
I_x (ft^4)	0.331	0.503	0.00828
I_y (ft^4)	0.380	1.188	0.0051

Table 150A: Arch Dead Loads

$P_{\text{hanger 1 total}}$ (k)	28.23
$P_{\text{hanger 2 total}}$ (k)	27.46
$P_{\text{hanger 3 total}}$ (k)	25.77
$P_{\text{hanger 4 total}}$ (k)	23.19
$P_{\text{TDB 1 total}}$ (k)	35.20
$P_{\text{column 2 total}}$ (k)	29.57
$P_{\text{column 3 total}}$ (k)	21.66
$P_{\text{arch post total}}$ (k)	7.604
$W_{\text{arch 1 total}}$ (k/ft)	0.073
$W_{\text{arch 2 total}}$ (k/ft)	0.074

$W_{\text{arch 1 total}}$ is a distributed load that represents the self-weight of the arch beneath the deck slab that is nearest the transverse deep beam. $W_{\text{arch 2 total}}$ is the same but for the arch nearest the Column 3.

Estimation of Creep Coefficient using ACI 209R-92:

Correction Factors:

Loading age:

$\gamma_{la} := 0.84$ *Table 2.5.1, for 28-days, moist cured*

Relative humidity:

$\gamma_{\lambda} := 0.80$ *Table 2.5.4, 70% RH*

Volume-surface ratios:

$$top := \frac{28 \cdot 48}{2 \cdot 28 + 2 \cdot 48} = 8.842$$

$$base := \frac{47.76 \cdot 48}{2 \cdot 47.76 + 2 \cdot 48} = 11.97$$

$$\gamma_{vs\_top} := \frac{2}{3} \cdot (1 + 1.13 \cdot \exp(-0.54 \cdot top)) = 0.673$$

$$\gamma_{vs\_base} := \frac{2}{3} \cdot (1 + 1.13 \cdot \exp(-0.54 \cdot base)) = 0.668$$

$\gamma_{vs} := 0.67$

Product of applicable correction factors:

$\gamma_c := \gamma_{la} \cdot \gamma_{\lambda} \cdot \gamma_{vs} = 0.45$

Ultimate Creep Coefficient:

$v_u := 2.35 \cdot \gamma_c = 1.06$

Figure 79A: MathCAD (2014) Sheet Showing Ultimate Creep Coefficient Calculations for Span IV

Appendix B: Span V

B1: Longitudinal Beam Analysis Results

Table 151B: Wheel Line Load Magnitudes

Truck	Wheel Line Load, W, at			
	Hanger 1 (k)	Transverse Deep Beam (k)	Column 2 (k)	Column 3 (k)
Tri-Axle	31.37	23.05	23.05	23.13
H-Truck	22.21	15.99	15.99	15.99
Two-Axle	23.69	16.30	16.30	16.37
Concrete	29.62	20.37	20.37	20.46
18-Wheeler	20.73	14.26	14.26	14.32
6-Axle	22.19	16.71	16.71	16.76
School Bus	11.65	8.50	8.50	8.50
HS-Truck	23.08	15.99	15.99	15.99

B2: TRANSVERSE FLOOR BEAMS

Cross sectional properties listed within this section applies to all transverse floor frames for Span V unless specified differently in the following sections.

Table 152B: Transverse Floor Beam Cross Sectional Properties

	Roadway	Curb	Bracket
A_g (ft^2)	9.708	9.625	5.708
I_x (ft^4)	11.01	18.75	3.453
I_y (ft^4)	29.27	18.68	14.48

Table 153B: Transverse Floor Beam Dead Loads

W_{slab} (k/ft)	1.079
$W_{trans.\ beam}$ (k/ft)	0.656
$W_{elev.\ beam}$ (k/ft)	0.225
$W_{sidewalk}$ (k/ft)	0.809
$W_{bracket}$ (k/ft)	0.331
$P_{rail\ tot}$ (k)	0.697

B2.1: Transverse Floor Beam at Column 2 Ratings

Transverse floor beam at Column 2 rating results are listed in Table 154B and Table 155B.

Table 154B: Span V - Transverse Floor Beam at Column 2 Rating Factors: Part 1

Trucks	Rating Factors			
	Positive Moment		Negative Moment	
	Operating	Inventory	Operating	Inventory
Tri-Axle	1.52	0.91	7.30	4.37
H-Truck	2.20	1.32	10.52	6.30
Two-Axle	2.16	1.29	10.33	6.19
Concrete	1.73	1.03	8.26	4.95
18-Wheeler	2.46	1.48	11.80	7.07
6-Axle	2.10	1.26	10.07	6.03
School Bus	4.14	2.48	19.81	11.87
HS-Truck	2.20	1.32	10.52	6.30

Table 155B: Span V - Transverse Floor Beam at Column 2 Rating Factors: Part 2

Trucks	Rating Factors					
	V_{zone1}		V_{zone2}		V_{zone3}	
	Operating	Inventory	Operating	Inventory	Operating	Inventory
Tri-Axle	2.02	1.21	1.43	0.86	1.59	0.95
H-Truck	2.91	1.74	2.07	1.24	2.30	1.38
Two-Axle	2.85	1.71	2.03	1.22	2.25	1.35
Concrete	2.28	1.37	1.62	0.97	1.80	1.08
18-Wheeler	3.26	1.95	2.32	1.39	2.58	1.54
6-Axle	2.78	1.67	1.98	1.19	2.20	1.32
School Bus	5.47	3.28	3.89	2.33	4.32	2.59
HS-Truck	2.91	1.74	2.07	1.24	2.30	1.38

B2.2: Transverse Floor Beam at Column 3 Ratings

For completeness, transverse floor beam at Column 3 rating results are listed in Table 156B for bending moment and Table 157B for shear. Ratings were calculated using the transverse floor beam model presented in Section 3.5.4.

Table 156B: Span V - Transverse Floor Beam at Column 3 Rating Factors: Part 1

Trucks	Rating Factors			
	Positive Moment		Negative Moment	
	Operating	Inventory	Operating	Inventory
Tri-Axle	1.51	0.90	7.45	4.46
H-Truck	2.18	1.31	10.77	6.45
Two-Axle	2.13	1.28	10.52	6.30
Concrete	1.70	1.02	8.42	5.04
18-Wheeler	2.44	1.46	12.03	7.20
6-Axle	2.08	1.25	10.28	6.16
School Bus	4.11	2.46	20.27	12.14
HS-Truck	2.18	1.31	10.77	6.45

Table 157B: Span V - Transverse Floor Beam at Column 3 Rating Factors: Part 2

Trucks	Rating Factors					
	V_{zone1}		V_{zone2}		V_{zone3}	
	Operating	Inventory	Operating	Inventory	Operating	Inventory
Tri-Axle	2.01	1.21	1.43	0.86	1.59	0.95
H-Truck	2.91	1.75	2.07	1.24	2.30	1.38
Two-Axle	2.85	1.71	2.02	1.21	2.25	1.35
Concrete	2.28	1.36	1.62	0.97	1.80	1.08
18-Wheeler	3.25	1.95	2.31	1.38	2.57	1.54
6-Axle	2.78	1.67	1.97	1.18	2.19	1.31
School Bus	5.48	3.29	3.89	2.33	4.33	2.59
HS-Truck	2.91	1.75	2.07	1.24	2.30	1.38

B3: COLUMN 2

Table 158B: Column 2 Cross Sectional Properties and Dead Load

A_g (ft^2)	1.458
I_x (ft^4)	0.165
I_y (ft^4)	0.190
$P_{column\ 2}$ (k)	3.894

Properties and load listed for Column 2 are for each interior and exterior column.

B4: COLUMN 3

Table 159B: Column 3 Cross Sectional Properties and Dead Load

		Exterior	
	Interior	Top	Bottom
A_g (ft^2)	1.750	2.415	3.678
I_x (ft^4)	0.198	0.306	0.397
I_y (ft^4)	0.328	0.881	4.888
$P_{column\ 3}$ (k)	6.279	4.332	6.597

B5: HANGER 1

Table 160B: Hanger 1 Cross Sectional Properties and Dead Load

A_s (ft^2)	0.0278
I_x (ft^4)	0.00414
I_y (ft^4)	0.00255
$P_{hanger\ 1}$ (k)	3.150

Properties and load listed for Hanger 1 are for each interior and exterior hanger.

B6: TRANSVERSE DEEP BEAM

Table 161B: Transverse Deep Beam Cross Sectional Properties

A_g (ft^2)	8.445
I_x (ft^4)	22.307
I_y (ft^4)	1.583

Table 162B: Transverse Deep Beam Dead Loads

W_{slab} (k/ft)	1.079
$W_{trans.\ deep\ beam}$ (k/ft)	1.267
$W_{elev.\ beam}$ (k/ft)	0.225
$W_{sidewalk}$ (k/ft)	0.809
$W_{bracket}$ (k/ft)	0.331
$P_{rail\ tot}$ (k)	0.697
$P_{support\ tot}$ (k)	4.196

B7: ARCH

The hanger and column cross sectional properties in the arch model combines the properties of the individual hanger and column properties from the transverse frame models. For Column 3s, the interior column cross sectional properties is combined with the top exterior column cross sectional properties.

Table 163B: Arch Cross Sectional Properties

	Column 2	Column 3	Hangers
A_g (ft^2)	2.917	4.165	0.0556
I_x (ft^4)	0.331	0.504	0.00828
I_y (ft^4)	0.380	1.209	0.00510

B7.1: LATERAL TRUCK DISTRIBUTION

The largest proportion that gets carried by one side of the arch depends on the transverse position of the trucks. Analysis was performed using the Beam and Column 2 model shown in Figure 80B to find that largest proportion.

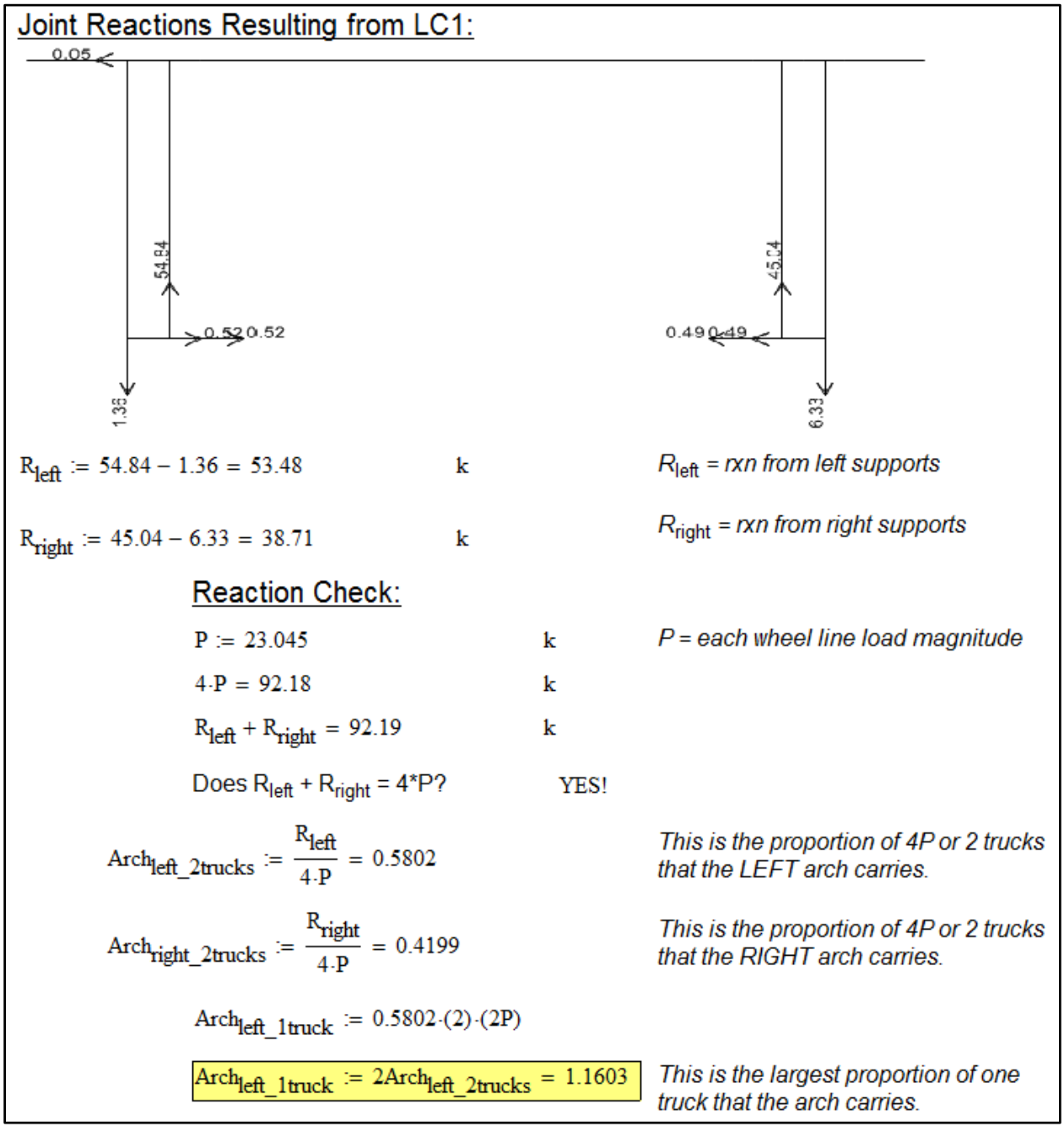

Figure 80B: Lateral Truck Distribution using Beam and Column 2 Model

Table 164B: Arch Dead Loads

$P_{\text{hanger 1 total}}$ (k)	27.82
$P_{\text{hanger 2 total}}$ (k)	27.07
$P_{\text{hanger 3 total}}$ (k)	25.44
$P_{\text{hanger 4 total}}$ (k)	22.93
$P_{\text{TDB 1 total}}$ (k)	32.51
$P_{\text{column 2 total}}$ (k)	29.31
$P_{\text{column 3 total}}$ (k)	21.52
$P_{\text{arch post total}}$ (k)	7.604
$W_{\text{arch 1 total}}$ (k/ft)	0.073
$W_{\text{arch 2 total}}$ (k/ft)	0.074

$W_{\text{arch 1 total}}$ is a distributed load that represents the self-weight of the arch beneath the deck slab that is nearest the transverse deep beam. $W_{\text{arch 2 total}}$ is the same but for the arch nearest the Column 3.

B8: BEAM AND COMPOSITE CONCRETE HANGER

An example beam and composite Hanger 1 model is shown in Figure 81B. The composite concrete hanger was modeled in SAP2000 as a frame member. Its location was defined at the centroid of the hanger group. The model was restrained from sidesway at the level of the transverse beam. This transverse beam consisted of the same sections as the transverse beam in the Beam and Column 2 model, with a bracket section at each end. The hanger length is shown Table 24.

Figure 81B: Beam and Composite Hanger 1 Model

These composite concrete hangers have no flexural rigidity under dead loads. The properties of these hangers are listed in Table 165B. In accordance with Taylor (1930), the roadway slabs were casted before the steel reinforcements were encapsulated in concrete to allow normal elongation of the bars under dead loads. Thus, the interaction diagram shown in Figure 82B was adjusted to reflect this condition. The dead load strain in each of the composite concrete hangers was calculated using the applied axial load acting on the total area of steel in the hanger. This dead load strain was added to the live load steel strains in tension and subtracted from the live load steel strains in compression. To reflect this in the factored loading line, shown in Figure 82B, there was no moment resulting from dead loads. Therefore, the first point of the factored loading line was from axial tension only. However, there was moment under live loads. All parts of the factored loading line was below the horizontal axis meaning the composite concrete hangers are in the tension.

Table 165B: Composite Concrete Hanger 1 Cross Sectional Properties and Dead Load

A_g (ft^2)	2.333
I_x (ft^4)	3.441
I_y (ft^4)	0.194
$P_{hanger\ 1}$ (k)	6.3

Analogous to the beam and column model, the composite concrete hanger case was rated for the case with the highest combination of axial load and for the case with the highest combination of bending moment. However, the highest bending moment case controls and the results for the tri-axle truck is shown in Table 166B. For both of these cases, the ratings were significantly less than one for the operating case.

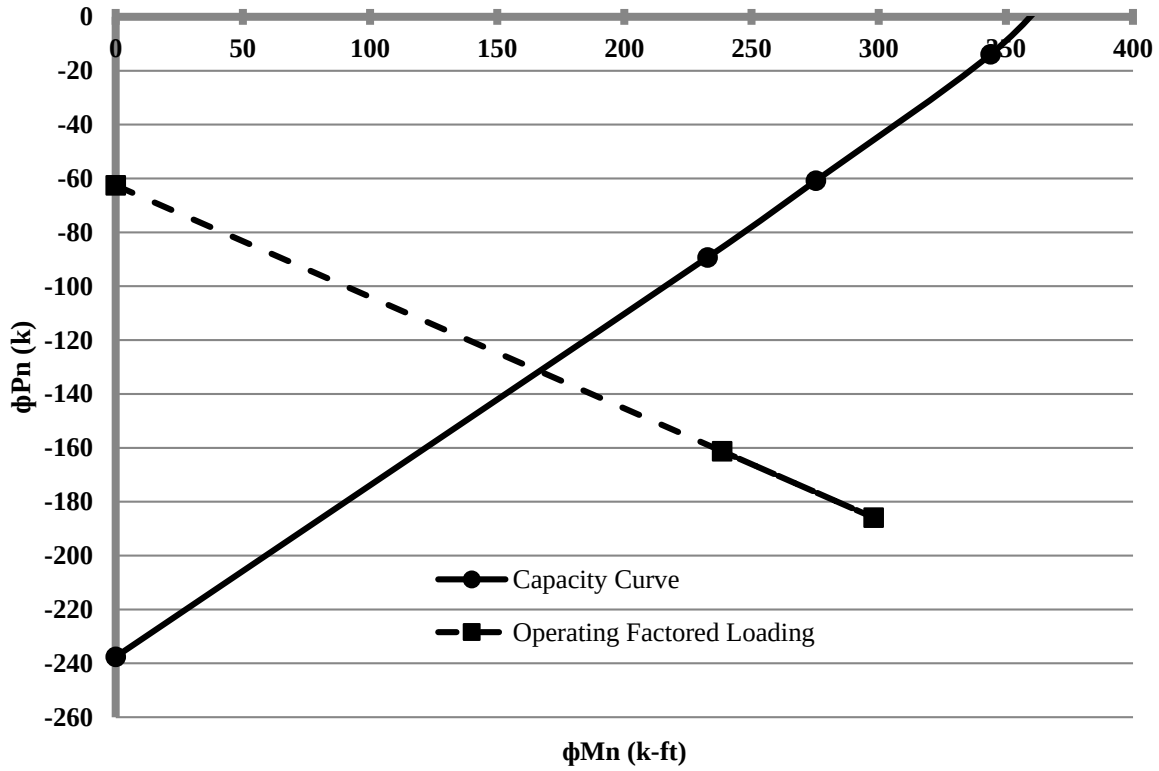

Figure 82B: Composite Hanger Interaction Diagram

Table 166B: LFR for Composite Concrete Hanger

ALDOT Posting Vehicle	Axial and Moment	
	Operating	Inventory
Tri-Axle	0.55	0.33

Appendix C: Span VI

C1: Longitudinal Beam Analysis Results

Table 167C: Wheel Line Load Magnitudes

Truck	Wheel Line Load, W, at			
	Hanger 1 (k)	Transverse Deep Beam (k)	Column 2 (k)	Column 3 (k)
Tri-Axle	31.50	22.40	22.40	22.79
H-Truck	22.47	15.99	15.99	15.99
Two-Axle	24.04	15.95	15.95	16.30
Concrete	30.04	19.94	19.94	20.37
18-Wheeler	21.03	13.96	13.96	14.26
6-Axle	22.18	16.20	16.20	16.46
School Bus	11.94	8.50	8.50	8.50
HS-Truck	22.47	15.99	15.99	15.99

C2: Transverse Floor Beams

Cross sectional properties listed within this section applies to all transverse floor frames for Span VI unless specified differently in the following sections.

Table 168C: Transverse Floor Beam Cross Sectional Properties

	Roadway	Curb	Bracket
A_g (ft^2)	9.063	9.250	5.583
I_x (ft^4)	8.872	15.92	3.005
I_y (ft^4)	27.43	18.61	14.47

Table 169C: Transverse Floor Beam Dead Loads

W_{slab} (k/ft)	0.926
$W_{trans.\ beam}$ (k/ft)	0.609
$W_{elev.\ beam}$ (k/ft)	0.216
$W_{sidewalk}$ (k/ft)	0.741
$W_{bracket}$ (k/ft)	0.313
$P_{rail\ tot}$ (k)	0.675

C2.1: Transverse Floor Beam at Column 2 Ratings

Transverse floor beam at Column 2 rating results are listed in Table 170C and Table 171C.

Table 170C: Span VI - Transverse Floor Beam at Column 2 Rating Factors: Part 1

Trucks	Rating Factors			
	Positive Moment		Negative Moment	
	Operating	Inventory	Operating	Inventory
Tri-Axle	1.52	0.91	4.65	2.79
H-Truck	2.13	1.28	6.52	3.90
Two-Axle	2.14	1.28	6.53	3.91
Concrete	1.71	1.03	5.23	3.13
18-Wheeler	2.45	1.47	7.47	4.47
6-Axle	2.11	1.26	6.43	3.85
School Bus	4.02	2.41	12.27	7.35
HS-Truck	2.13	1.28	6.52	3.90

Table 171C: Span VI - Transverse Floor Beam at Column 2 Rating Factors: Part 2

Trucks	Rating Factors					
	V_{zone1}		V_{zone2}		V_{zone3}	
	Operating	Inventory	Operating	Inventory	Operating	Inventory
Tri-Axle	1.92	1.15	1.47	0.88	1.53	0.91
H-Truck	2.69	1.61	2.06	1.23	2.14	1.28
Two-Axle	2.70	1.62	2.06	1.24	2.14	1.28
Concrete	2.16	1.29	1.65	0.99	1.72	1.03
18-Wheeler	3.09	1.85	2.36	1.41	2.45	1.47
6-Axle	2.66	1.59	2.03	1.22	2.11	1.27
School Bus	5.07	3.04	3.88	2.32	4.03	2.41
HS-Truck	2.69	1.61	2.06	1.23	2.14	1.28

C2.2: Transverse Floor Beam at Column 3 Ratings

For completeness, transverse floor beam at Column 3 rating results are listed in Table 172C for bending moment and Table 173C for shear. Ratings were calculated using the transverse floor beam model presented in Section 3.5.4.

Table 172C: Span VI - Transverse Floor Beam at Column 3 Rating Factors: Part 1

Trucks	Rating Factors			
	Positive Moment		Negative Moment	
	Operating	Inventory	Operating	Inventory
Tri-Axle	1.44	0.86	6.23	3.73
H-Truck	2.05	1.23	8.87	5.31
Two-Axle	2.01	1.20	8.70	5.21
Concrete	1.61	0.96	6.96	4.17
18-Wheeler	2.30	1.38	9.95	5.96
6-Axle	1.99	1.19	8.62	5.16
School Bus	3.86	2.31	16.70	10.00
HS-Truck	2.05	1.23	8.87	5.31

Table 173C: Span VI - Transverse Floor Beam at Column 3 Rating Factors: Part 2

Trucks	Rating Factors					
	V_{zone1}		V_{zone2}		V_{zone3}	
	Operating	Inventory	Operating	Inventory	Operating	Inventory
Tri-Axle	1.90	1.14	1.45	0.87	1.50	0.90
H-Truck	2.70	1.62	2.06	1.23	2.14	1.28
Two-Axle	2.65	1.59	2.02	1.21	2.10	1.26
Concrete	2.12	1.27	1.62	0.97	1.68	1.01
18-Wheeler	3.03	1.82	2.31	1.38	2.40	1.44
6-Axle	2.63	1.57	2.00	1.20	2.08	1.25
School Bus	5.09	3.05	3.88	2.32	4.03	2.42
HS-Truck	2.70	1.62	2.06	1.23	2.14	1.28

C3: COLUMN 2

Table 174C: Column 2 Cross Sectional Properties and Dead Load

A_g (ft^2)	1.458
I_x (ft^4)	0.165
I_y (ft^4)	0.190
$P_{column\ 2}$ (k)	3.703

Properties and load listed for Column 2 are for each interior and exterior column.

C4: COLUMN 3

Table 175C: Column 3 Cross Sectional Properties and Dead Load

		Exterior	
	Interior	Top	Bottom
A_g (ft^2)	1.750	2.350	3.701
I_x (ft^4)	0.198	0.300	0.399
I_y (ft^4)	0.328	0.791	5.012
$P_{column\ 3}$ (k)	5.854	3.931	6.190

C5: HANGER 1

Table 176C: Hanger 1 Cross Sectional Properties and Dead Load

A_s (ft^2)	0.0278
I_x (ft^4)	0.00414
I_y (ft^4)	0.00255
$P_{hanger\ 1}$ (k)	2.870

Properties and load listed for Hanger 1 are for each interior and exterior hanger.

C6: TRANSVERSE DEEP BEAM

Table 177C: Transverse Deep Beam Cross Sectional Properties

A_g (ft^2)	7.635
I_x (ft^4)	16.484
I_y (ft^4)	1.432

Table 178C: Transverse Deep Beam Dead Loads

W_{slab} (k/ft)	0.926
$W_{trans.\ deep\ beam}$ (k/ft)	1.145
$W_{elev.\ beam}$ (k/ft)	0.216
$W_{sidewalk}$ (k/ft)	0.741
$W_{bracket}$ (k/ft)	0.313
$P_{rail\ tot}$ (k)	0.675
$P_{support\ tot}$ (k)	4.196

C7: ARCH

The hanger and column cross sectional properties in the arch model combines the properties of the individual hanger and column properties from the transverse frame models. For Column 3s, the interior column cross sectional properties is combined with the top exterior column cross sectional properties.

Table 179C: Arch Cross Sectional Properties

	Column 2	Column 3	Hangers
A_g (ft^2)	2.917	4.100	0.0556
I_x (ft^4)	0.331	0.498	0.00828
I_y (ft^4)	0.380	1.119	0.00510

Table 180C: Arch Dead Loads

$P_{\text{hanger 1 total}}$ (k)	25.70
$P_{\text{hanger 2 total}}$ (k)	24.98
$P_{\text{hanger 3 total}}$ (k)	23.42
$P_{\text{hanger 4 total}}$ (k)	21.09
$P_{\text{TDB 1 total}}$ (k)	29.61
$P_{\text{column 2 total}}$ (k)	27.37
$P_{\text{column 3 total}}$ (k)	19.96
$P_{\text{arch post total}}$ (k)	7.604
$W_{\text{arch 1 total}}$ (k/ft)	0.073
$W_{\text{arch 2 total}}$ (k/ft)	0.074

$W_{\text{arch 1 total}}$ is a distributed load that represents the self-weight of the arch beneath the deck slab that is nearest the transverse deep beam. $W_{\text{arch 2 total}}$ is the same but for the arch nearest the Column 3.

Appendix D: Span VII

D1: Longitudinal Beam Analysis Results

Table 181D: Wheel Line Load Magnitudes

Truck	Wheel Line Load, W, at	
	Column 3 (k)	Column 4 (k)
Tri-Axle	22.10	21.57
H-Truck	15.99	15.99
Two-Axle	15.95	15.56
Concrete	19.94	19.45
18-Wheeler	13.96	13.61
6-Axle	15.91	15.52
School Bus	8.50	8.49
HS-Truck	15.99	15.99

D2: TRANSVERSE FLOOR BEAMS

Cross sectional properties listed within this section applies to all transverse floor frames for Span VII unless specified differently in the following sections.

Table 182D: Transverse Floor Beam Cross Sectional Properties

	Roadway	Curb	Bracket
A_g (ft^2)	9.063	9.250	5.583
I_x (ft^4)	8.872	15.92	3.005
I_y (ft^4)	27.43	18.61	14.47

Table 183D: Transverse Floor Beam Dead Loads

W_{slab} (k/ft)	0.844
$W_{trans.\ beam}$ (k/ft)	0.609
$W_{elev.\ beam}$ (k/ft)	0.216
$W_{sidewalk}$ (k/ft)	0.675
$W_{bracket}$ (k/ft)	0.313
$P_{rail\ tot}$ (k)	0.654

D2.1: Transverse Beam at Column 4 Ratings

Negative bending moment ratings for the transverse beam at Column 4 location are listed in Table 184D.

Table 184D: Span VII – Transverse Beam at Column 4 Negative Bending Moment Rating Factors

Trucks	Rating Factors	
	Negative Moment	
	Operating	Inventory
Tri-Axle	4.03	2.41
H-Truck	5.43	3.26
Two-Axle	5.58	3.35
Concrete	4.47	2.68
18-Wheeler	6.38	3.82
6-Axle	5.60	3.35
School Bus	10.23	6.13
HS-Truck	5.43	3.26

D2.2: Transverse Beam at Column 5 Ratings

Bending moment ratings for the transverse beam at Column 5 location Case B are listed in Table 185D. For completeness, the shear ratings for the same transverse beam are listed in Table 186D.

In addition, bending moment rating factors for the transverse beam at Column 5 location – Case A are listed in Table 187D. Shear rating factors for the same beam are shown in Table 188D.

Table 185D: Span VII - Transverse Floor Beam at Column 5 Bending Moment Rating Factors – Case B

Trucks	Rating Factors			
	Positive Moment		Negative Moment	
	Operating	Inventory	Oper.	Inv.
Tri-Axle	1.90	1.14	2.13	1.28
H-Truck	2.55	1.53	2.86	1.71
Two-Axle	2.64	1.58	2.96	1.77
Concrete	2.12	1.27	2.37	1.42
18-Wheeler	3.02	1.81	3.38	2.03
6-Axle	2.64	1.58	2.96	1.77
School Bus	4.80	2.88	5.38	3.22
HS-Truck	2.55	1.53	2.86	1.71

Table 186D: Span VII - Transverse Floor Beam at Column 5 Shear Rating Factors – Case B

Trucks	Rating Factors					
	V_{zone1}		V_{zone2}		V_{zone3}	
	Operating	Inventory	Operating	Inventory	Operating	Inventory
Tri-Axle	2.01	1.20	1.43	0.86	1.49	0.89
H-Truck	2.69	1.61	1.92	1.15	2.00	1.20
Two-Axle	2.79	1.67	1.99	1.19	2.07	1.24
Concrete	2.23	1.34	1.59	0.95	1.65	0.99
18-Wheeler	3.19	1.91	2.27	1.36	2.36	1.42
6-Axle	2.79	1.67	1.99	1.19	2.07	1.24
School Bus	5.07	3.04	3.61	2.16	3.76	2.25
HS-Truck	2.69	1.61	1.92	1.15	2.00	1.20

Table 187D: Span VII - Transverse Floor Beam at Column 5 Bending Moment Rating Factors - Case A

Trucks	Rating Factors			
	Positive Moment		Negative Moment	
	Operating	Inventory	Operating	Inventory
Tri-Axle	1.83	1.09	2.49	1.49
H-Truck	2.45	1.47	3.33	2.00
Two-Axle	2.54	1.52	3.45	2.07
Concrete	2.03	1.22	2.76	1.65
18-Wheeler	2.90	1.74	3.94	2.36
6-Axle	2.54	1.52	3.45	2.07
School Bus	4.61	2.76	6.27	3.76
HS-Truck	2.45	1.47	3.33	2.00

Table 188D: Span VII - Transverse Floor Beam at Column 5 Shear Rating Factors – Case A

Trucks	Rating Factors					
	V_{zone1}		V_{zone2}		V_{zone3}	
	Operating	Inventory	Operating	Inventory	Operating	Inventory
Tri-Axle	2.01	1.21	1.43	0.86	1.49	0.89
H-Truck	2.70	1.62	1.92	1.15	2.00	1.20
Two-Axle	2.80	1.67	1.99	1.19	2.07	1.24
Concrete	2.24	1.34	1.59	0.95	1.66	0.99
18-Wheeler	3.20	1.91	2.27	1.36	2.36	1.42
6-Axle	2.80	1.68	1.99	1.19	2.07	1.24
School Bus	5.08	3.04	3.61	2.16	3.76	2.25
HS-Truck	2.70	1.62	1.92	1.15	2.00	1.20

D3: COLUMN 3

Table 189D: Column 3 Cross Sectional Properties and Dead Load

		Exterior	
	Interior	Top	Bottom
A_g (ft^2)	1.750	2.350	3.701
I_x (ft^4)	0.198	0.300	0.399
I_y (ft^4)	0.328	0.791	5.012
$P_{column\ 3}$ (k)	5.854	3.931	6.190

D4: COLUMNS 4 - 7

Table 190D: Columns 4 - 7 Cross Sectional Properties and Dead Load

A_g (ft^2)	1.458
I_x (ft^4)	0.165
I_y (ft^4)	0.190
$P_{column\ 4}$ (k)	3.163
$P_{column\ 5}$ (k)	1.560
$P_{column\ 6}$ (k)	1.278
$P_{column\ 7}$ (k)	2.321

Properties and load listed for Columns 4 – 7 are for each interior and exterior column.

D4.1: Column 5 Ratings – Case B

Ratings are listed in Table 191D and Table 192D for the columns from the Beam and Column 5 – Case B model. This model in which the exterior columns were modeled as frame members yields an operating rating factor of 0.32 for the exterior column for the tri-axle truck. This model does not provide the most appropriate ratings for the exterior columns.

Table 191D: Span VII – Interior Column 5 Rating Factors – Case B

Trucks	Rating Factors	
	Operating	Inventory
Tri-Axle	1.54	0.92
H-Truck	2.06	1.24
Two-Axle	2.14	1.28
Concrete	1.71	1.02
18-Wheeler	2.44	1.46
6-Axle	2.14	1.28
School Bus	3.88	2.33
HS-Truck	2.06	1.24

Table 192D: Span VII – Exterior Column 5 Rating Factors – Case B

Trucks	Rating Factors	
	Operating	Inventory
Tri-Axle	0.32	0.19
H-Truck	0.43	0.26
Two-Axle	0.45	0.27
Concrete	0.36	0.21
18-Wheeler	0.51	0.31
6-Axle	0.45	0.27
School Bus	0.81	0.49
HS-Truck	0.43	0.26

D4.2: Column 7 Ratings – Case B

Ratings are listed in Table 193D and Table 194D for the columns from the Beam and Column 7 – Case B model. This model in which the exterior columns were modeled as frame members yields an operating rating factor of 0.95 for the exterior column for the tri-axle truck. This model does not provide the most appropriate ratings for the exterior columns.

Table 193D: Span VII – Interior Column 7 Rating Factors – Case B

Trucks	Rating Factors	
	Operating	Inventory
Tri-Axle	2.11	1.26
H-Truck	2.83	1.69
Two-Axle	2.93	1.76
Concrete	2.34	1.40
18-Wheeler	3.35	2.01
6-Axle	2.93	1.76
School Bus	5.32	3.19
HS-Truck	2.83	1.69

Table 194D: Span VII – Exterior Column 7 Rating Factors – Case B

Trucks	Rating Factors	
	Operating	Inventory
Tri-Axle	0.95	0.57
H-Truck	1.27	0.76
Two-Axle	1.31	0.79
Concrete	1.05	0.63
18-Wheeler	1.50	0.90
6-Axle	1.32	0.79
School Bus	2.39	1.43
HS-Truck	1.27	0.76

D5: ARCH

The hanger and column cross sectional properties in the arch model combines the properties of the individual hanger and column properties from the transverse frame models. For Column 3s, the interior column cross sectional properties is combined with the top exterior column cross sectional properties.

Table 195D: Arch Cross Sectional Properties

	Column 3	Column 4 - 8
A_g (ft^2)	4.100	2.917
I_x (ft^4)	0.498	0.331
I_y (ft^4)	1.119	0.380

Table 196D: Arch Dead Loads

$P_{column\ 3\ total}$ (k)	19.39
$P_{column\ 4\ total}$ (k)	19.39
$P_{column\ 5\ total}$ (k)	19.39
$P_{column\ 6\ total}$ (k)	19.39
$P_{column\ 7\ total}$ (k)	19.39
$P_{column\ 8\ total}$ (k)	19.39
$W_{arch\ total}$ (k/ft)	0.074

$W_{arch\ total}$ is a distributed load that represents the self-weight of the arch beneath the deck slab that is present along the length of Span VII.

Appendix E: Sensitivity Analyses

E1: Span V Arch Internal Forces

Table 197E: Internal Forces Resulting from Dead Load on 3,000 psi Model

Longitudinal Strain (με)	Section	Dead Load		
		M (k-ft)	P (k)	V (k)
10,000	A2	52.5	-282	35.7
	A14	31.5	-330	16.8
	A40	-232	-503	23.8
3,447	A2	52.5	-282	35.7
	A14	31.5	-330	16.8
	A40	-232	-503	23.8
1,814	A2	52.5	-282	35.7
	A14	31.5	-330	16.8
	A40	-232	-503	23.8
1,223	A2	52.5	-282	35.7
	A14	31.5	-330	16.8
	A40	-232	-503	23.8

Table 198E: Internal Forces Resulting from Dead Load on 4,740 psi Model

Longitudinal Strain (με)	Section	Dead Load		
		M (k-ft)	P (k)	V (k)
10,000	A2	52.5	-282	35.7
	A14	31.5	-330	16.8
	A40	-232	-503	23.8
1,897	A2	52.5	-282	35.7
	A14	31.5	-330	16.8
	A40	-232	-503	23.8
1,807	A2	52.5	-282	35.7
	A14	31.5	-330	16.8
	A40	-232	-503	23.8
1,341	A2	52.5	-282	35.7
	A14	31.5	-330	16.8
	A40	-232	-503	23.8

Table 199E: Internal Forces Resulting from Live Load on 3,000 psi Model

Longitudinal Strain (με)	Section	Live Load		
		M (k-ft)	P (k)	V (k)
10,000	A2	-181	-76.2	55.7
	A14	537	-91.6	37.8
	A40	815	-96.2	44.7
3,447	A2	-181	-76.2	55.7
	A14	537	-91.6	37.8
	A40	815	-96.2	44.7
1,814	A2	-181	-76.2	55.7
	A14	537	-91.6	37.8
	A40	815	-96.2	44.7
1,223	A2	-181	-76.2	55.7
	A14	537	-91.6	37.8
	A40	815	-96.2	44.7

Table 200E: Internal Forces Resulting from Live Load on 4,740 psi Model

Longitudinal Strain (με)	Section	Live Load		
		M (k-ft)	P (k)	V (k)
10,000	A2	-181	-76.2	55.7
	A14	537	-91.6	37.8
	A40	815	-96.2	44.7
1,897	A2	-181	-76.2	55.7
	A14	537	-91.6	37.8
	A40	815	-96.2	44.7
1,807	A2	-181	-76.2	55.7
	A14	537	-91.6	37.8
	A40	815	-96.2	44.7
1,341	A2	-181	-76.2	55.7
	A14	537	-91.6	37.8
	A40	815	-96.2	44.7